

GAS-PHASE ELECTROCHEMICAL DETECTION OF TRACE ARSENIC IN  
DRINKING WATER

by

Jinsoo Hong  
A Dissertation  
Submitted to the  
Graduate Faculty  
of  
George Mason University  
in Partial Fulfillment of  
The Requirements for the Degree  
of  
Doctor of Philosophy  
Department of Chemistry and Biochemistry

Committee:

_____	Dr. Abul Hussam, Dissertation Director
_____	Dr. Nathalia Peixoto, Committee Member
_____	Dr. Paul D. Cooper, Committee Member
_____	Dr. John A. Schreifels, Committee Member
_____	Dr. John A. Schreifels, Department Chairperson
_____	Dr. Timothy L. Born, Associate Dean for Student and Academic Affairs, College of Science
_____	Dr. Vikas Chandhoke, Dean, College of Science
Date: _____	Fall Semester 2012 George Mason University Fairfax, VA

Gas-Phase Electrochemical Detection of Trace Arsenic in Drinking Water

A dissertation submitted in partial fulfillment of the requirements for the degree of  
Doctor of Philosophy at George Mason University

by

Jinsoo Hong  
Master of Science  
George Mason University, 2009

Abul Hussam, Professor  
Center for Clean Water and Sustainable Technologies  
Department of Chemistry and Biochemistry

Fall Semester 2012  
George Mason University  
Fairfax, VA



This work is licensed under a [creative commons attribution-noncommercial 3.0 unported license](https://creativecommons.org/licenses/by-nc/3.0/).

## **DEDICATION**

This work is dedicated to the people in Bangladesh and all nations suffering from arsenic crisis, and my family, friends, and colleagues.

## ACKNOWLEDGEMENTS

First of all, I would like to say EBEN EZER. I thank God who has led me thus far. I greatly thank my father and my mother who prayed for me before the dawn every day all throughout their lives. I acknowledge there are people who supported my research with constant and fervent prayers in mission group in Korean Central Presbyterian Church. My family, especially my mother, my wife, and my two sons with their sacrifices, have always supported me. They have endured all my negligence of family duties and lack of the presence with them. Most importantly, I would like to express my sincere gratitude to my mentor, Professor Abul Hussam who taught me critically important key concept of scientific research. Innovation and creative thinking is my slogan due to him. He has contributed profoundly to the design of electrochemical experiments and offered invaluable support and guidance throughout the Ph.D. studies. His clear intuition to scientific matters and spiritual and emotional encouragement are the keys to this research. Above of all, he has the heart of love which bears this fruit of an electrochemical sensor.

I would like to thank professors in GMU chemistry department, Dr. George Mushrush, Dr. Wayne Stalick, Dr. John Schreifels, Dr. Gerald L. Roberts Weatherspoon, Dr. Shahamat U. Khan, Dr. Paul Cooper and Dr. Robert Honeychuck for their spiritual and emotional support. I express sincere gratitude to my supervisor, Dr. Victor Pike at NIH who have taught me how to conduct scientific research and write up scientific papers. I would also like to thank my colleagues, Doug Mays, Kirubel Assegid, and Farhan Ahmed for receiving me and entertaining me wholeheartedly. I am grateful to the Department of Chemistry and Biochemistry at George Mason University for providing space, time, and materials for my Ph.D. researches. I respectfully appreciate the unconditional love and support of my entire family and I praise God, who gave me strength and made me to do all things. To all problems of the world, God is the only and the final solution.

At this moment, my only wish is that this sensor will be developed further and bear fruits in the field, saving many people from drinking water with harmful level of arsenic.

## TABLE OF CONTENTS

	Page
List of Tables .....	viii
List of Figures .....	ix
List of Equations .....	xii
List of Abbreviations and Symbols.....	xv
Abstracts .....	xvii
1. CHAPTER ONE.....	1
1.1. Introduction .....	1
1.2. General aspects of arsenic detection methodology and challenges associated with current methods .....	5
1.3. Review of electrochemical techniques for arsenic detection and measurement ..	9
1.3.1. Anodic stripping voltammetry .....	10
1.3.2. Cathodic stripping voltammetry (CSV).....	16
1.4. Electrochemical gas sensors: general overview .....	18
1.4.1. Kinetically controlled vs. diffusion controlled system .....	20
1.4.2. Electrochemical arsine gas sensor .....	24
1.4.3. Thermodynamic of direct oxidation of arsine in electrochemical cells .....	28
1.5. Redox reactions of halide in determination of As(III) and arsine.....	31
1.5.1. Analytical methods for As(III) and arsine using iodine as oxidant: Early work .....	31
1.5.2. Measurement of AsH <sub>3</sub> by chronoamperometry with iodine/iodide redox couple .....	34
1.6. Amperometry using iodine and iodide redox couple .....	40
1.7. The use of nonaqueous electrolytes for gas sensor .....	42
2. CHAPTER TWO.....	47
2.1. Motivation and purpose.....	47
2.2. Purpose of generating arsine gas from aqueous sample.....	47
2.3. Arsine sensor based on I <sup>-</sup> /I <sub>2</sub> redox couple .....	49

2.4.	Filter paper matrix-electrolyte based sensor .....	51
2.5.	Insights gained from a commercial sensor .....	53
2.6.	The use of Zn as reducing agent.....	57
2.7.	Motivation for use of organic salts as electrolytes .....	58
3.	CHAPTER THREE.....	60
3.1.	General Instrumentation.....	60
3.2.	Fabrication of Potentiostat .....	60
3.3.	General experimental procedure .....	68
3.3.1.	Chemicals.....	68
3.3.2.	Materials .....	70
3.3.3.	Electrochemical characterization of silver fabric electrode with Ag/AgI system .....	72
3.3.4.	General amperometric experimental procedure with thin layer cell.....	76
4.	CHAPTER FOUR .....	78
4.1.	Direct oxidation of arsine to arsenious acid on modified commercial cells .....	80
4.1.1.	Chronoamperometry response from cell A.....	83
4.1.2.	Chronoamperometry response from cell B.....	85
4.1.3.	Chronoamperometry response from cell C.....	88
4.2.	CA and OCP on silver-arsine complex formation. ....	94
4.2.1.	CA with cell D with silver wire .....	96
4.2.2.	Cell E: Plexiglass with silver fabric.....	103
4.3.	Development of pulse chronoamperometric technique for arsine detection....	105
4.3.1.	Conductometry with silver fabric electrodes with cylindrical chamber ..	110
4.3.2.	Conductometry with silver foil on a syringe filter.....	112
4.3.3.	Conductometry with silver fabric on a syringe filter .....	114
4.4.	Development of arsine sensor based on potentiometry.....	118
4.4.1.	Potentiometry with Ag/AgNO <sub>3</sub> system for arsine detection.....	118
4.4.1.1.	Materials and methods .....	119
4.4.1.2.	Results and discussion.....	120
4.5.	Amperometric arsine sensor .....	123
4.5.1.	Origins and characteristics of signals .....	124
4.5.2.	A model for signal response .....	130
4.5.3.	Mass transfer of arsine during continuous addition of NaBH <sub>4</sub> .....	130
4.6.	A thin layer cell with Au electrode on a syringe filter .....	136
4.6.1.	Materials and Methods.....	137
4.6.2.	Results and discussion .....	139
4.6.3.	Cyclic voltammetry (CV) of iodide to iodine .....	142
4.6.4.	Results and discussion .....	144

4.6.4.1.	Characterization of cell A: .....	144
4.6.4.2.	Characterization of cell B:.....	145
4.7.	Amperometry using Pt as working electrode on Plexiglass cell body. ....	146
4.7.1.	Material and method .....	147
4.7.2.	Results and Discussion .....	148
4.8.	Pt electrode on flat surface of Plexiglass with Ag/AgCl reference electrode. .	149
4.8.1.	Materials and method.....	150
4.8.2.	Results and Discussion .....	151
4.9.	Design and fabrication of pressure insensitive gas sensor .....	155
4.9.1.	Fabrication of the cell. ....	156
4.9.2.	Results and discussion .....	158
4.10.	Pt electrode on the surface of grooved surface of syringe filter .....	161
4.11.	Thin carbon fiber as working electrode .....	165
4.11.1.	Materials and Methods .....	166
4.11.2.	Results and discussion.....	167
4.11.2.1.	Amperometric response from cell A .....	167
4.11.2.2.	Amperometric response from cell B. ....	168
4.11.3.	Effect of iodine concentration .....	170
4.11.4.	Description of sensor.....	171
4.11.5.	Results and Discussion.....	174
4.12.	Amperometric detection of arsine on carbon fiber electrode in filter paper cell. 175	
4.12.1.	Data fitting with the theoretical model.....	181
4.12.2.	Sensitivity study with increased volume of sample: Method B .....	185
4.12.3.	Real sample analysis with Method B .....	186
4.12.4.	Conclusion.....	188
5.	Appendices .....	191
5.1.	Appendix A: Operation Instruction.....	191
5.2.	Appendix B: Potentiostat circuit .....	193
5.3.	Appendix C: Diffusion equation of iodide on a filter paper .....	201
	Index .....	203
	References.....	204
	Curriculum Vitae.....	210

## LIST OF TABLES

Table	Page
Table 1.4.1 Electrochemical Arsine Gas Sensor.....	26
Table 1.4.2 Standard reduction potential of half reactions involving direct oxidation of arsine. ....	28
Table 1.7.1 Electrochemical cells employing nonaqueous electrolytes .....	44
Table 3.2.1 Table of electronic components used for the potentiostat circuit .....	63
Table 3.2.2 Bit of PORTA to select different gain of i/v converter.....	65
Table 3.3.1 Calculated vs. theoretical potential of.....	74
Table 4.1.1 Electrochemical cell configuration of modified commercial electrode.....	81
Table 4.1.2 Standard reduction potential of half reactions of gold species. ....	92
Table 4.4.1 Measured potential vs. calculated potential change.....	121
Table 4.6.1 the results of comparison studies using different electrolytes and addition time of NaBH <sub>4</sub> .....	140
Table 4.6.2 Configuration of electrochemical cells.....	143
Table 4.7.1 Cell components in the Plexiglass cell. ....	147
Table 4.8.1 Amperometric responses obtained from this sensor .....	153
Table 4.9.1 Components of the cell .....	158
Table 4.10.1 Cell configuration .....	163
Table 4.11.1 Iodine solution preparation. ....	171
Table 4.11.2 Amperometric signal and background dependence on integration time and reductant addition timing .....	172
Table 4.12.1 Sensitivity and limit of detection based on calibration curve .....	177
Table 4.12.2 Table of 200 µg/L [As(III)] EPA standard containing interfering ions....	178
Table 4.12.3 Table of 50 µg/L [As(III)] EPA standard containing interfering ions.....	178
Table 4.12.4 Results of measurement of EPA standards containing other competing species. ....	178
Table 4.12.5 Computed characteristics of the electrochemical cell obtained from curve fitting to the model.....	184
Table 4.12.6 Error analysis of the characteristics of the carbon fiber cell.....	184
Table 4.12.7 Computed parameters for bi-exponential function .....	185
Table 4.12.8 Average and standard deviation of rate constants, k <sub>1</sub> and k <sub>2</sub> .....	185
Table 4.12.9 Measurement results of As(III) of real samples.....	187

## LIST OF FIGURES

Figure	Page
Figure 1.1.1 Diseases caused by chronic exposure to arsenic .....	5
Figure 1.3.1 Schematic representation of LSASV ( linear scan anodic stripping voltammetry).....	11
Figure 1.3.2 Overlay of LSV(linear sweep voltammograms) of cells containing different amount of arsine.....	16
Figure 1.4.1 Schematic of typical electrochemical oxygen gas sensor.....	18
Figure 1.4.2 Schematic of a stop-and-go electrolyte renewal system for a gas sensor.....	20
Figure 1.5.1 Flow injection system used by Lolic in flow injection system.. ..	37
Figure 1.5.2 CV of the flow injection system. ....	38
Figure 2.5.1 Schematic of a commercial sensor. ....	55
Figure 2.5.2 Schematic of typical gas sensor experiments for arsine.....	57
Figure 3.2.1 Schematics of potentiostat circuit.....	61
Figure 3.2.2 Potentiostat circuit board used in this work. ....	62
Figure 3.2.3 Analog Switch(AS), ADG441, used on our board.....	64
Figure 3.2.4 Voltage scan on 10 k $\Omega$ resistor with the potentiostat. ....	67
Figure 3.3.1 Open circuit potential between silver fabric vs. SSC.....	73
Figure 3.3.2 Plot of potential vs. log[KI].....	74
Figure 3.3.3 Measurement of open circuit potential of silver fabric vs. SSC.....	75
Figure 4.1.1 DPCA of the unmodified commercial sensor and modified sensor. ....	82
Figure 4.1.2 Signal response of 680 $\mu$ L of hydrogen gas into the cell A.. ..	84
Figure 4.1.3 CV of cell B in the presence of H <sub>2</sub> (g) and in the absence of H <sub>2</sub> (g).....	85
Figure 4.1.4 Overlay of double potential step chronoamperometry with cell B of three different experiments with increasing potential steps.....	86
Figure 4.1.5 Double potential step chronoamperometry in the absence of H <sub>2</sub> . ....	87
Figure 4.1.6 CA of cell B at 1.1 V in the presence of H <sub>2</sub> (g).....	88
Figure 4.1.7 CVs of the cell C in the presence and absence of H <sub>2</sub> (g).....	89
Figure 4.1.8 Amperometric response of the cell C.. ..	90
Figure 4.1.9 CV of cell C immediately after CA with 1.1 V.....	93
Figure 4.2.1 Diagram of mass transfer of silver ion in the cell. ....	96
Figure 4.2.2 Silver wire on a filter paper. ....	97
Figure 4.2.3 Schematic of system with the cell D. ....	98
Figure 4.2.4 CV of cell D.....	99
Figure 4.2.5 MPCA of cell D. ....	100
Figure 4.2.6 Single pulse CA of cell D:.....	100
Figure 4.2.7 Potential measurements of the cell D before and after arsine exposure.....	102

Figure 4.2.8 Setup of cell E. ....	104
Figure 4.2.9 CA from blank (left panel) and CA from 3 mL of 100 $\mu\text{g/L}$ As(III). ....	105
Figure 4.3.1 Excitation waveform for pulse chronoamperometry and the current at the end of each pulse.....	110
Figure 4.3.2 Signal response of the cell in section 4.3.1. ....	111
Figure 4.3.3 Cell with silver foil electrode for conductance measurement. ....	112
Figure 4.3.4 Comparison of arsenic standard (left panel) and blank (right panel). ....	113
Figure 4.3.5 Filter paper stained with blank and arsenic standard.....	114
Figure 4.3.6 Inside of cell 4.3.3 with two pieces of silver fabric.....	115
Figure 4.3.7 Typical current response profile of PCA from the cell 3.3.3. ....	115
Figure 4.3.8 A calibration curve constructed from cell 4.3.3. ....	116
Figure 4.3.9 A picture of filter paper from cell 3.3.3 after various amount of arsine from the generator vial.....	117
Figure 4.4.1 Plot of the magnitude of potential drop vs. [As(III)]......	121
Figure 4.5.1 An equivalent circuit of electrochemical cell. ....	124
Figure 4.5.2 Gradient generated from $\Gamma$ from AgI reduction on the surface of Ag electrode.....	126
Figure 4.5.3 A sketch of a typical amperometric signal ....	129
Figure 4.6.1 A typical amperometric signal response.....	140
Figure 4.6.2 A schematic diagram of the syringe filter cell (cell B) ....	143
Figure 4.6.3 Cyclic voltammetry of the cell A ....	144
Figure 4.6.4 Cyclic voltammetry of gold wire electrode. ....	146
Figure 4.7.1 Schematic diagram of Pt electrode on syringe filter ....	148
Figure 4.7.2 An amperometric signal from Pt foil electrode on a syringe filter.....	149
Figure 4.8.1 Internal structure of the cell.....	150
Figure 4.8.2 A completely assembled cell ....	151
Figure 4.8.3 Comparison experiments with blank and 50 $\mu\text{g/L}$ standard.....	152
Figure 4.8.4 A current signal with 2 mL of 100 $\mu\text{g/L}$ As(III). ....	152
Figure 4.8.5 Amperometry data while the sensor was held by hand and pressure was applied by squeezing the cell ....	154
Figure 4.9.1 Cell fabricated with four bolts and nuts to remove the pressure pulse.....	157
Figure 4.9.2 A signal from 2 mL of 400 $\mu\text{g/L}$ arsenite in 2.5 sulfuric acid.....	159
Figure 4.9.3 Signals from the two runs from 400 $\mu\text{g/L}$ standard.....	159
Figure 4.9.4 Signal response from two different standards. ....	160
Figure 4.10.1 Two parallel Pt electrodes as working electrode on the top unit.....	162
Figure 4.10.2 Silver fabric electrode on the bottom unit. ....	162
Figure 4.10.3 The internal structure of Pt foil cell.....	163
Figure 4.10.4 Amperometric signal response from 2 mL of 400 $\mu\text{g/L}$ .....	164
Figure 4.11.1 Carbon fiber electrode and silver fabric electrode ....	167
Figure 4.11.2 Comparison experiments of the same cell.....	168
Figure 4.11.3 Signal from cell B.....	169
Figure 4.11.4 Amperometric signal dependence on $[\text{I}_2]$ on the filter paper. ....	173
Figure 4.11.5 Background current vs. $[\text{I}_2]$ . ....	173

Figure 4.11.6 Background charge dependence on $[I_2]$ on the filter paper with various conditions.....	174
Figure 4.12.1 Calibration curve constructed from carbon fiber electrode.....	177
Figure 4.12.2 Linear curve fittings with exponential baselines.....	181
Figure 4.12.3 Curve fitting to the proposed model.....	183
Figure 4.12.4 Calibration curve constructed from Method B.....	186
Figure 5.2.1 Schematic of the potentiostat fabricated.....	193
Figure 5.2.2 Quadrant A of potentiostat circuit.....	194
Figure 5.2.3 Quadrant B.....	195
Figure 5.2.4 Quadrant C.....	196
Figure 5.2.5 Quadrant D.....	196
Figure 5.2.6 Schematic of a multiplexer (ADG1208) U6.1 that selects different gain from different resistor.....	198
Figure 5.3.1 Concentration gradient of the thin layer cell.....	201

## LIST OF EQUATIONS

Equation	Page
Equation 1.1.1 .....	2
Equation 1.3.1 .....	15
Equation 1.3.2 .....	15
Equation 1.3.3 .....	16
Equation 1.3.4 .....	17
Equation 1.4.1 .....	21
Equation 1.4.2 .....	22
Equation 1.4.3 .....	23
Equation 1.4.4 .....	23
Equation 1.4.5 .....	23
Equation 1.4.6 .....	25
Equation 1.4.7 .....	25
Equation 1.4.8 .....	25
Equation 1.4.9 .....	25
Equation 1.4.10 .....	28
Equation 1.4.11 .....	28
Equation 1.4.12 .....	28
Equation 1.4.13 .....	28
Equation 1.4.14 .....	28
Equation 1.4.15 .....	29
Equation 1.4.16 .....	29
Equation 1.5.1 .....	32
Equation 1.5.2 .....	32
Equation 1.5.3 .....	32
Equation 1.5.4 .....	33
Equation 1.5.5 .....	33
Equation 1.5.6 .....	33
Equation 1.5.7 .....	34
Equation 1.5.8 .....	34
Equation 1.7.1 .....	43
Equation 1.7.2 .....	43
Equation 1.7.3 .....	43
Equation 1.7.4 .....	43
Equation 2.3.1 .....	49
Equation 3.2.1 .....	61

Equation 3.3.1 .....	72
Equation 3.3.2 .....	72
Equation 3.3.3 .....	72
Equation 3.3.4 .....	75
Equation 3.3.5 .....	75
Equation 3.3.6 .....	75
Equation 4.1.1 .....	80
Equation 4.1.2 .....	80
Equation 4.1.3 .....	90
Equation 4.1.4 .....	92
Equation 4.1.5 .....	92
Equation 4.1.6 .....	92
Equation 4.1.7 .....	92
Equation 4.1.8 .....	92
Equation 4.1.9 .....	92
Equation 4.1.10 .....	92
Equation 4.2.1 .....	95
Equation 4.2.2 .....	95
Equation 4.2.3 .....	95
Equation 4.2.4 .....	95
Equation 4.2.5 .....	96
Equation 4.2.6 .....	96
Equation 4.2.7 .....	96
Equation 4.2.8 .....	98
Equation 4.2.9 .....	98
Equation 4.2.10 .....	102
Equation 4.3.1 .....	106
Equation 4.3.2 .....	107
Equation 4.3.3 .....	107
Equation 4.3.4 .....	108
Equation 4.3.5 .....	108
Equation 4.3.6 .....	108
Equation 4.3.7 .....	108
Equation 4.3.8 .....	109
Equation 4.4.1 .....	118
Equation 4.5.1 .....	125
Equation 4.5.2 .....	125
Equation 4.5.3 .....	125
Equation 4.5.4 .....	126
Equation 4.5.5 .....	126
Equation 4.5.6 .....	127
Equation 4.5.7 .....	127
Equation 4.5.8 .....	128
Equation 4.5.9 .....	131

Equation 4.5.10 .....	131
Equation 4.5.11 .....	131
Equation 4.5.12 .....	132
Equation 4.5.13 .....	132
Equation 4.5.14 .....	132
Equation 4.5.15 .....	132
Equation 4.5.16 .....	132
Equation 4.5.17 .....	132
Equation 4.5.18 .....	133
Equation 4.5.19 .....	133
Equation 4.5.20 .....	133
Equation 4.5.21 .....	133
Equation 4.5.22 .....	134
Equation 4.5.23 .....	134
Equation 4.5.24 .....	134
Equation 4.5.25 .....	134
Equation 4.5.26 .....	135
Equation 4.5.27 .....	135
Equation 4.5.28 .....	135
Equation 4.12.1 .....	180
Equation 4.12.2 .....	180
Equation 4.12.3 .....	182
Equation 4.12.4 .....	182
Equation 5.3.1 .....	201
Equation 5.3.2 .....	202
Equation 5.3.3 .....	202
Equation 5.3.4 .....	202
Equation 5.3.5 .....	202
Equation 5.3.6 .....	202

## LIST OF ABBREVIATIONS AND SYMBOLS

Amperometric gas sensor.....	AGS
Analog to digital converter .....	ADC
Anodic peak current.....	$i_{pa}$
Anodic peak potential .....	$E_{pa}$
Anodic stripping voltammetry .....	ASV
Approximately .....	<i>ca.</i>
Cathodic peak current .....	$i_{pc}$
Cathodic peak potential.....	$E_{pc}$
Cathodic stripping voltammetry .....	CSV
Chronoamperometry .....	CA
Cyclic voltammetry.....	CV
Deionized .....	D.I.
Digital to analog converter.....	DAC
Double pulse chronoamperometry.....	DPCA
Gas-phase electrochemical arsine sensor.....	GEAS
Hydride Generation Gas diffusion Flow Injection Analysis.....	HG-GD-FIA
In other words .....	<i>i.e.</i>
Inductively coupled plasma .....	ICP
Input and output .....	I/O
International Union of Pure and Applied Chemistry .....	IUPAC
KiloOhm .....	$k \Omega$
Linear scan voltammetry.....	LSV
Liter .....	L
MegaOhm .....	$M \Omega$
MicroAmpere .....	$\mu A$
Microampere .....	$\mu A$
MicroCoulomb .....	$\mu C$
Millifarad .....	mF
Milliliter .....	mL
Millimeter .....	mm
Molar or mole/L.....	M
Multiple pulse chronoamperometry .....	MPCA
Nanoampere .....	nA
Ohm .....	$\Omega$
Open circuit potential.....	OCP
Personal computer .....	PC

Propylene carbonate when referring electrolyte .....	PC
Pulse chronoamperometry .....	PCA
Silver silver chloride reference electrode .....	SCC
Single step chronoamperometry, interchangeably used with CA .....	SSCA
Standard calomel electrode .....	SCE
Versus .....	vs.
Volts .....	V

## ABSTRACT

### GAS-PHASE ELECTROCHEMICAL DETECTION OF TRACE ARSENIC IN DRINKING WATER

Jinsoo Hong, Ph.D.

George Mason University, 2012

Dissertation Director: Dr. Abul Hussam

The presence of toxic levels of inorganic arsenic in drinking water is a worldwide problem. Measurement of millions of field samples for arsenic is an analytical challenge and the first step to solve the problem. This work is an attempt to develop new sensor chemistry for electrochemical detection of arsine produced from arsenic in water. The sensor based on reaction between  $\text{AsH}_3$  and  $\text{Ag(s)}/\text{AgNO}_3 // \text{Ag}^+/\text{Ag(s)}$  redox couple on a filter paper substrate has shown high sensitivity with potentiometry and conductometry as analytical techniques. Amperometry sensor is based on chemical reaction of  $\text{AsH}_3$  and iodine, followed by electrochemical reaction of iodide generated from the first chemical reaction. In potentiometry, the signal response ranged from 4.3 to 200 mV for 10  $\mu\text{g/L}$  to 400  $\mu\text{g/L}$   $\text{As(III)}$ , respectively with limitation of detection of 11  $\mu\text{g/L}$   $\text{As(III)}$ . The conductometric detection based on alternating bipolar square potential pulses exhibited linear calibration curve and a minimum detection limit of 88  $\mu\text{g/L}$   $\text{As(III)}$ . A novel electrochemical cell:  $\text{C(s)}/\text{I}^-/\text{I}_2, \text{AsH}_3(\text{g}) // \text{I}^-, \text{AgI}/\text{Ag(s)}$  where  $\text{I}^-/\text{I}_2$  mediated  $\text{AsH}_3$

oxidation occurred was developed for chronoamperometric detection with limit of detection of 47  $\mu\text{g/L}$  As(III). Here, Au, Pt, and C exhibited similar anodic current responses but the porous thin carbon fiber electrode yielded highly efficient arsine mass transport. A mathematical model of mass transfer of  $\text{AsH}_3(\text{g})$  and following electrochemical reaction was developed and successfully applied to the simulate experimental data. The sensor developed requires 2.0 mL of water sample, 2.0 mL of  $\text{NaBH}_4$  as arsine generating agent, and 50  $\mu\text{L}$  of 10 mM iodine. The sensor is robust, compact, easy to fabricate, and field-deployable.

## 1. CHAPTER ONE

### 1.1. Introduction

Arsenic poisoning was called by the World Health Organization (WHO) the largest mass poisoning disaster in human history<sup>1</sup>. There might be up to 57 million people drinking water contaminated with arsenic in Bangladesh.<sup>2</sup> Approximately 11 million wells in Bangladesh alone need immediate examination.<sup>3</sup> About 10,000 drinking water supplying utility needs treatment of arsenic in the Unites States of America.<sup>4</sup> A recent article in the consumer reports magazine in November, 2012 shows that uncooked rice produced in US and in other countries contains arsenic at alarming level of 231  $\mu\text{g}/\text{kg}$  on average.<sup>5</sup> It also reports that 15 batches out of 32 batches of rice contains more than 5  $\mu\text{g}$  inorganic arsenic per meal and the average is 4.7  $\mu\text{g}$  of inorganic arsenic per meal. Anderson<sup>4</sup> et al. note that Newly implemented laws by USEPA (Unites States Environmental Protection Agency) in 2002 demand that arsenic in drinking water be less

---

<sup>1</sup> Bagla, P. Arsenic-Laced Well Water Poisoning Bangladeshis, **2003**, *National Geographic News*, June 5.

<sup>2</sup> Feeney, R.; Kounaves, S.P., Voltammetric Measurement of Arsenic in Natural Waters. *Talanta*, **2002**, 58, 23.

<sup>3</sup> Kinniburgh D.G.; Kosmus W. Arsenic Contamination in Ground Water: some analytical considerations. *Talanta*, **2002**,58, 165-180

<sup>4</sup> Anderson R.D.; McNeil, L.S.; ASCE, A.M.; Edwards, M.; Morton S.C, Evaluation of a New Field Measurement Method for Arsenic in Drinking Water Samples, *Journal of environmental engineering*, **2008**, May, 382-388

<sup>5</sup> <http://consumerreports.org/cro/arsenicinfood.htm>

than 10 µg/L arsenic, which called for rigorous monitoring approximately 4,000 water utilities in U.S.

A metalloid occurs ubiquitously, being the 20<sup>th</sup> abundant element in the earth crust, and is a component of more than 245 minerals in the nature<sup>6</sup>. Geologically, arsenic is mobilized by weathering in the rocks and then transported by rain, river, and into ground water. The thermodynamically stable form of inorganic arsenic, arsenate adsorbed in the soil spread arsenic in the environments through some characteristics biogeochemical processes. Arsenic in the air, soils, food, and drinking water can enter human body.

Arsenic contamination of drinking water is geogenic in nature. However, some industrial and old agricultural land effluents containing high arsenic (EPA superfund sites) pose danger to the well being of human society.

Mechanism of arsenic contamination in ground water has been intensively studied and reported in the literature.<sup>6</sup> Due to weathering of arsenopyrite in the presence of oxygen and water, arsenic is released into groundwater:

**Equation 1.1.1**



Arsenic containing pyrite (FeS) is probably the most common mineral source of arsenic. As man-made source, mine tailings can be attributed to the source of arsenic release into water. In Bangladesh and India, the aquifer sediments are derived from weathered materials from Himalayas. Arsenic typically occurs at concentration of 2-100

---

<sup>6</sup> Ahuja, S. Mechanism of arsenic contamination of water, Chapter 2: Delineation of a major worldwide problem of arsenic-contaminated groundwater, Handbook of Water Purity and Quality, **2009**, 24-27

$\mu\text{g/L}$  in these sediments, much of which is sorbed onto hydrated ferric oxides, phyllosilicates, and sulfides. The mechanism of release of arsenic from sediments has been a topic of intense debate. Both microbial and chemical processes have been proposed. The oxidation of arsenic-rich pyrite has been invoked. Other studies proposed that reduction of arsenic-rich Fe(III) oxyhydroxide in the aquifer may lead to the release of arsenic into the groundwater.

In US, metal-reducing bacteria in arsenic mobilization has been proposed as a theory of mobilization of arsenic in groundwater.<sup>6</sup> Anoxic waters are areas of sea water or fresh water where dissolved oxygen is depleted. In anoxic water, reduction of As(V) instead of oxygen molecule proceeds via dissimilatory process where energy for microorganism is generated. To date, at least 19 species of organisms have been found to respire arsenate anaerobically. Arsenate/Arsenite, i.e. As(V)/As(III) redox potential is 135 mV. This can be coupled with oxidation of organic matter. These microbes are collectively referred to as dissimilatory arsenate-reducing prokaryotes (DARPs). In Unites States, *Sulfurospirillum barnessi*, in western Nevada, *Desulfotomaculum auripigmentum* in eastern Massachusetts, *Bacillus arsenicoselenatis* and *B. selenitireducens* in Mono Lake, California have been found to utilize As(V) as electron acceptor in their respiratory system.

Analogously, in sediments of Ganges delta in India, the role of indigenous metal reducing bacteria to reduce arsenate to arsenite has been examined.<sup>6</sup> The experiments showed that addition of acetate to anaerobic sediments, as a proxy for organic matter and electron donor for metal reduction, resulted in reduction of Fe(III), followed by As(V)

reduction, thereby releasing of As(III) ensued. PCR (polymerase chain reaction) technique and cultivation-dependent technique were used to identify the species involved in mobilization of arsenate. The study showed that *Geobacter* species were culprit. It is believed that *arrA* gene provides machinery for As(V)/As(III) respiration. Two species, i.e. *G. unraniumreducens* and *G. lovleyi* among *Geobacter* possess *arrA* and were found in Cambodian sediments. *G. unraniumreducens* is known to reduce soluble and sorbed As(V), mobilizing arsenite, As(III). Other arsenate, As(V) reducing bacteria including *Sulfurospirillum* species were found in West Bengal(India) and Cambodia, thus the validity of this theory is asserted.

The metabolic path of arsenic in human body is also well studied.<sup>7</sup> Generally, ingested arsenic species are metabolized in the human body in the liver where it becomes monomethylatedarsenate(MMA) via methylation of arsenate by arsenic methyltransferase enzymes and further methylation gives rise to dimethylarsinate (DMA). In the urinary excretion of human, 20 % inorganic arsenicals, 20 % MMA, and 60 % of DMA were found. Although 76 % of arsenic ingested were excreted in urine in 8 days, complete excretion of arsenic is not achieved in human metabolic system. Studies showed that accumulation of arsenic in human body occurs with aging. It is reported in England that mean levels of arsenic ( $\mu\text{g/L}$  dry weight) in liver, lung and spleen in infants vs. adults are 9.9 vs. 48, 7 vs. 44, and 4.9 vs. 15, respectively.

---

<sup>7</sup> Mandal, B. K.; Suzuki, K.T. Arsenic round the world: a review, *Talanta*, **2002**, 201-235.

Various adverse health effects due to arsenic intake could happen.<sup>7</sup> These are dermal changes (pigmentation, hyperkaratoses, and ulceration), respiratory, pulmonary, cardiovascular, gastrointestinal, hematological, hepatic, renal, neurological, developmental, reproductive, immunologic, genotoxic, mutagenic, and carcinogenic effects.



Keratosis on palm



Mucous melanosis



Diffuse melanosis

Figure 1.1.1 Diseases caused by chronic exposure to arsenic<sup>6</sup>

## 1.2. General aspects of arsenic detection methodology and challenges associated with current methods

For years, the Gutzeit kit method has been used in the field.<sup>8</sup> With such a simple design and at low cost, the method has provided the inhabitants of arsine-stricken countries with semi-quantitative measure as to determination of the level of the arsenic in drinking water.<sup>9</sup> The operational principle is the reaction between arsine and  $\text{HgBr}_2$ .

<sup>8</sup> Gutzeit, H., *Pharmaz. Zeitung*. **1879**, 24, 263. cited in Vangreen, A.; Cheng, Z.; Seddiquie, A.A.; Hoque, M.A.; Geman, A.; Graziano, J.H.; Ahsan, H.; Parvez, F.; Ahmed, K.H. Reliability of a commercial kit to test groundwater for Arsenic in Bangladesh, *Environmental Science and Technology*. **2005**, 39, 299-303.

<sup>9</sup> Feldmann, J., Salaun, P, Field test kits for arsenic: evaluation in terms of sensitivity, reliability, applicability, and cost. In *Arsenic contamination of Groundwater, Mechanism,*

Color developed by formation of complex between arsine gas and  $\text{HgBr}_2$  has been used widely in one of the most arsine stricken country, Bangladesh where *ca.* 57 million people suffer from drinking water contaminated with arsenic at harmful level.

Regardless of whether its oxidation state is 3 or 5, arsine gas is generated slowly from the reaction of arsenate or arsenite with Zn powder in the presence of concentrated hydrochloric acid. Color developed on mercury bromide strip is then compared with color scale provided by the manufacturer. However, comprehensive field studies on the accuracy of the colorimetric test kit (Merckoquant, NIPSOM, and GPL) showed that 68 % of false positive (labeled as unsafe) were in fact safe. Newer generation field test kit (Hach EZ arsenic kit) seemed to improve the accuracy of the test. About 88 % of the test results were turned out to be correct when 50  $\mu\text{g/L}$  is taken as the drinking water standard. Surely, the accuracy will dramatically drop if 10  $\mu\text{g/L}$  standard is applied. This method is prone to have interpersonal variance, which makes the kit unreliable.

Highly improved instrumentation built upon the principle of Gutzeit test is reported.<sup>10</sup> In the commercial instrument, colorimetric determination of arsine gas concentration was achieved by measurement of the intensity of reflected light. Paper tape that contains material similar to mercury bromide as in Gutzeit test kit gave the best results. Changes in colors upon exposure to arsine gas results in change of the intensity of the reflected light, which is an analytical signal. The reflected light from this paper strip

---

*Analysis, and remediation*; Ahuja, S. Ed.; John Wiley & Sons: New Jersey, U.S.A., **2008**, pp 183-188.

<sup>10</sup> Anderson R.D.; McNeil, L.S.; ASCE, A.M.; Edwards, M.; Morton S.C, Evaluation of a new field measurement method for arsenic in drinking water samples, *Journal of environmental engineering*, **2008**, May, 382-388.

was monitored for its absorbance. The instrument worth approximately 5,000 US \$ was a Scott Instrument Autostep Plus Portable Monitor (Model No. 2740-0045) and 175 ml to 50 ml of water sample was treated with a mixture of NaBH<sub>4</sub>, KI, and ascorbic acid. The novel feature of this method is its disposable probe that can sense arsine concentration. Although the aforementioned method reported sub µg/L sensitivity, authors stated that the validity of operation heavily relied on the degree of supervision provided to the operator. In India and Bangladesh where people are most severely stricken by arsenic loaded water and its population supersedes 1 billion. It is a daunting task and should not be expected that any institute or organization supervise carefully individual operators. This method involves collection of generated arsine gas in expensive Teflon bag. It requires special training in handling. We, therefore, used much robust and convenient system for monitoring the arsenic.

Other than Gutzeit test, there are several choices in selecting the accurate and reliable methods in this matter. Hydride generation atomic absorption<sup>11</sup> and fluorescence<sup>12</sup> techniques and inductively coupled plasma (ICP) spectroscopic technique have been employed. However, the costs and complexity of operation of these kinds of instruments prohibits its use in the field or even in places with inadequate laboratory

---

<sup>11</sup> Samanta, G.; Chowdhury, T. R. ; Mandal, B. K.; Biswas, B.K.; Chowdhury, U.K.; Basu, G.K.; Chanda, C.R.; Lodh, D.; Chakraborti, D. Flow injection hydride generation atomic absorption spectrometry for determination of arsenic in water and biological samples from arsenic-affected districts of west bengal, india, and Bangladesh, *Microchemical Journal* , **1999**, **62**, 174–191.

<sup>12</sup> Featherstone, A. M.; Butler, E.C.V; O’Grady, B. V.; Michel, P. Determination of arsenic species in sea-water by hydride generation atomic fluorescence spectroscopy. *Journal of Analytical Atomic Spectroscopy*, **1998**, **13**, 1355–1360.

infrastructures. More specifically, transportation of all samples to the central laboratory and book keeping of results are daunting tasks. For example, there are ten million tube wells in Bangladesh and measuring arsenic in these wells, even once, is becoming a challenge both in scientific and financial terms.

The detection of arsenic in drinking water *in the field* is the best solution and it has been a challenging task for years to analytical chemists. Among field deployable methodologies, we explored the most economic way of detecting arsenic. Portability of the detection system is an important requirement for field deployable instrumentation. Electrochemical sensor is the most compact and the most inexpensive instrument and this is the reason why we want to make electrochemical sensor for arsenic. In addition, it can be a highly sensitive method. Stripping voltammetric method and chronoamperometric method are excellent choices for implementing portable sensors for arsenic detection.

Other than electrochemical method, photoionization detector was proposed in the literature<sup>13</sup>. After arsenic is converted to arsine by various reducing agents, arsine gas can be detected by photoionization detector. Tanaka simultaneously detected arsine along with phosphine (PH<sub>3</sub>) and hydrogen sulfide by separating arsine from other species on Porapak QS column. His absolute detection limit ( $3\sigma$ ) was 2, 280, and 4 ng for phosphorus, sulfur, and arsenic. This method has implication that if aqueous sample concentration is 4 µg/L, one can determine arsenic using photoionization detector (PID) if there is no interference from hydrogen sulfide produced during the hydride generation.

---

<sup>13</sup>Tanaka, T; Nakamura, Y.; Mizuike, A.; Ono, A. Simultaneous Determination of phosphorous, Sulfur, and arsenic in steel by hydride generation and gas chromatography, *Analytical Sciences*, **1996**, 12, February 77-80

There are many commercially available hand-held PIDs which suggest research in this direction might bear fruitful results for arsenic detection in the field. A commercial company, Gray Wolf sensing solution, actually manufactures arsine gas sensors along with sensors for other volatile gas employing photoionization detector<sup>14</sup>. However, these methods are used for sensing pure arsine in absence of other interfering gases. In PID, UV light source that ionizes arsine will also ionize all other species with lower ionization potential. The lack of selectivity of PID inherent in its nature deters any attempt to implement field deployable instrumentation.

### **1.3. Review of electrochemical techniques for arsenic detection and measurement**

Thus far we have reviewed general methods of detection of trace arsenic in literature. Here we will go over electrochemical system which has been extensively used in this work. There are several electrochemical methods widely used to detect gas. For detecting species dissolved in aqueous phase, stripping voltammetry has been used. We review anodic and cathodic stripping methods first and then gas phase amperometry. Stripping method concentrates analyte on the electrode electrochemically first, which is called pre-concentration step, after which electrochemical process takes place to detect the analyte. However, gas phase amperometry generates the analytic hydride in gas phase and subsequently, electrochemical reactions detect the hydride on electrode. Generation of gas from solution serves two purposes, namely, pre-concentration and elimination of interference. First, pre-concentration or sample enrichment is achieved during gas

---

<sup>14</sup> [www.wolfsense.com](http://www.wolfsense.com)

generation. Second, gas generation eliminates interference from other species in solution during detection stage. We review here theoretical aspects of these methodologies and practices in laboratories, merits, demerits, and limitations of these methods. In all cases, the electron transfer from liquid phase electrolyte to a metal electrode is the signal and measurable quantity. Depending on the methods, mathematical theories have been established and various measurable quantities such as peak height of the current, integrated current, and limiting current are proportional to the concentration of the analyte.

### **1.3.1. Anodic stripping voltammetry**

Stripping voltammetric analysis is an analytical method that utilizes a bulk electrolysis step (*pre-electrolysis*) to pre-concentrate a substance from solution into a small volume of a mercury electrode or onto the surface of a planar electrode. After this electrodeposition step, the material is redissolved, more figuratively speaking, “stripped” from the electrode using a voltage ramp. As schematically shown in the figure, the species of interest is deposited in the cathode for fixed interval, and the sample is highly concentrated on the surface of electrode. Then the potential gradually increases to positive direction to oxidize the reduced species. There have been many successful examples of aforementioned anodic stripping voltammetry (ASV). In the real world problem where we mainly focus on, Rasul et. al. applied ASV to 960 samples collected from 18 districts of Bangladesh. Randomly chosen 238 samples from 960 samples were analyzed.

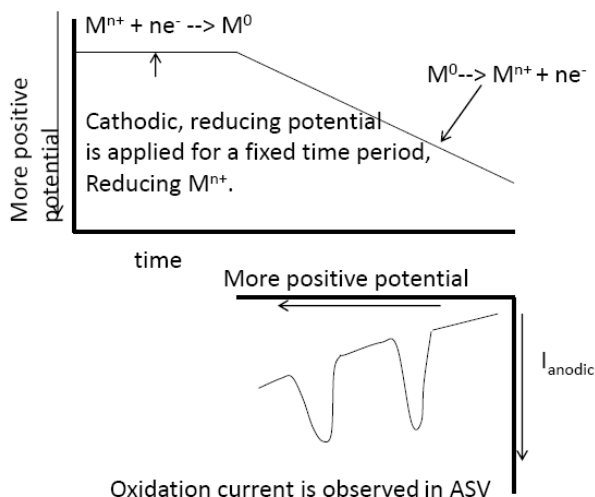


Figure 1.3.1 Schematic representation of LSASV ( linear scan anodic stripping voltammetry).

Pre-concentration of analyte on a working electrode was achieved in ASV and subsequent anodic current of reduced species is recorded while potential moves toward more positive direction. Rasul et al. reported that ASV could be used to detect arsenic with Au film on glassy carbon electrode. The validity of the ASV was cross-checked with four distinct instrumental techniques<sup>15</sup>. The agreement between ASV and other techniques were within experimental error at concentration below  $100 \mu\text{g L}^{-1}$ . The working electrode was constructed by depositing  $\text{Au}^{3+}$  on the glassy carbon electrode and the reference electrode was Ag/AgCl in saturated KCl isolated from the test solution by Vycor. Deposition potential of  $-150 \text{ mV}$  was applied for  $100 \text{ s}$  to ensure complete reduction of  $\text{Au}^{3+}$  on glassy carbon, after which  $500 \text{ mV}$  potential was applied to remove all impurities that might be co-deposited on the gold electrode. Repeated operation of this

<sup>15</sup> Rasul, S.B.; Munir, A.K.M.; Hossain, Z.A.; Khan A.H.; Alauddin, M; Hussam, A. Electrochemical measurement and speciation of inorganic arsenic in ground water of Bangladesh, *Talanta*, **2002**, 58, 33-43

procedure gave shiny gold film which was visually verified by the mirror placed under the cell. In a typical experiment, the following values for parameters were used: initial potential -150 mV, final potential 500 mV, step potential 5 mV, scan rate 50 mV s<sup>-1</sup>, initial delay 60 s (deposition time), quiet time delay 30 s, and stirring rate 600 rpm. When the sample gave the signal within the dynamic range, two more additional measurement were performed using standard solution to determine the final concentration of As(III). The reduction of As(V) to As(III) was done with SO<sub>2</sub> (g), which was generated from acid decomposition of Na<sub>2</sub>SO<sub>3</sub>. The analytical merit of this method is capability of speciation between As(III) and As(V). No interference from Fe<sup>3+</sup>/Fe<sup>2+</sup> at the level of 1-10 mg L<sup>-1</sup> was observed from samples. The disadvantage is that the working electrode could be used only about 20 times and throughput was only 20-30 samples per day. The lengthy operation of preparing new working electrode and the necessity of purging gold solution with water-saturated nitrogen gas to remove impurities such as Cl<sub>2</sub> and NO<sub>2</sub> raise the barrier when one wants to deploy this method in the field.

Yamada et al. reported a gold modified BDD (boron-doped diamond) as working electrode whose advantages is a wide potential window in aqueous media, low background currents, and weak adsorption of polar molecules<sup>16</sup>. Gold was electrodeposited to the BDD at -0.4 V. Supporting electrolyte was 0.1 M phosphate buffer (pH 5). Reference and counter electrode were Ag/AgCl (saturated KCl) and Pt respectively. The authors deposited As(V) as well as As(III) at a very negative potential

---

<sup>16</sup> Yamada D.; Ivandini, T.A.; Komatsu, M; Fujishima, A.; Einaga, Y. Anodic stripping voltammetry of inorganic species of As(III) and As(V) at gold modified boron doped diamond electrodes, *J. Electroanal. Chem.*, **2008**, 615, 2, 145-153.

at -1.5 V, at which hydronium ion also was reduced to hydrogen molecule. During stripping step starting at -0.4 V, hydrogen molecule during co-deposition along with As(III) and As(V) also was oxidized and contributed to the anodic currents. Notably, the authors eliminated the hydrogen molecules on the Au surface by applying -0.4 V for 10 s to remove all hydrogen molecule before stripping scan started. The merits of this method come from discriminating ability of electrochemical cell against oxidation state of inorganic arsenic. Deposition potential of working electrode dictates which species among As(III) and As(V) should be deposited on the working electrode. Depending on whether the potential was -1.5 V or -0.4 V vs. reference electrode, both As(V) and As(III) or As(III) alone were deposited on Au electrode. When -0.4 V vs. Ag/AgCl(KCl) was applied for deposition, only As(III) was deposited on Au surface. When -1.5 V was applied, both As(V) and As(III) were reduced, therefore quantitation of individual species was realized. No doubt that analytical merit was clearly demonstrated. This method calls for double experiments if determination of both As(V) and As(III) are required. Furthermore, as in other typical cases of ASV, the preparation of working electrode before measurement was rather cumbersome. The author stated that BDD was pretreated by ultrasonication on 2-propanol for 10 minutes followed by rinsing with high purity water to remove organic impurities.

Andrew O. Simm and others reported that silver electrode as working electrode in 0.1 M nitric acid system superseded the performance of gold(Au) electrode in 0.1 M HCl system.<sup>17</sup> They compared three metals, Ag, Au, and Pt as working electrode. The

---

<sup>17</sup> Simm, A.O.; Banks, C.E.; Compton, R.G. The Electrochemical detection of arsenic(III)

counter electrode was coiled bright large platinum wire and a saturated calomel electrode was the reference electrode. Deposition of As(III) was optimized at -0.6 V vs. SCE reference electrode. Interestingly, the authors found that in the absence of Cl<sup>-</sup> ion, Ag oxidation was suppressed and in the linear scan voltammogram, the potential could go up to 0.3 V vs SCE without making AgCl salt. The limitation of Ag electrode due to oxidation of Ag at 0 V was overcome. His cyclic voltammogram using gold, platinum, and silver clearly demonstrated that the Ag had biggest oxidation current at 0.15 V. Scan rate was 100 mV/s and the potential was swept from 0.5 V ( 0.3 V only for Ag due to oxidation) to -0.5 V vs SCE in 0.1 M nitric acid. Using square wave ASV (pulse amplitude 90 mV, step potential 9 mV, frequency 75 Hz), the detection limit was 1.05 µg/L with sensitivity of 11.2 ±1 ampere per mole . These values were very close to the values of cell made of gold working electrode. The outstanding merit of this method is cost saving results from replacing gold with silver for any portable detector. Hitherto, gold has been the most popular electrode for ASV, but this publication suggests that silver as well as gold should be considered when one constructs electrochemical cells.

In another method, arsine gas was dissolved in acidic aqueous media, and anodic stripping voltammetry was performed with the dissolved arsine<sup>18</sup>. The authors mentioned American Conference of Governmental Industrial Hygienists (ACGIH) has changed TLV( Threshold Limit Value) to 5 µg/L (Time Weighted Average (TWA)) from 50 µg/L

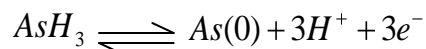
---

at a silver electrode, *Electroanalysis*, **2005**, 19, 1727-1733.

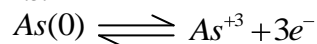
<sup>18</sup> Iyandini, T.A.; Daisuke Yamada, D.; Watanabe, T.; Matsuura, H.; Nakano N.; Fujishima, A.; Einaga, Y. Development of amperometric arsine gas sensor using gold-modified diamond electrodes, *J. Electroanal. Chem.*, **2010**, 645, 58–63.

(TWA), and their sensor barely met the requirement by achieving detection limit of 4.43  $\mu\text{g/L}$ . Arsine was bubbled into the 0.1 M sulfuric acid, based on the equation below, then  $\text{AsH}_3$  was first deposited on Au electrode at a negative potential after which a linear scan was performed to get the signal.

**Equation 1.3.1**



**Equation 1.3.2**



A high level of arsine concentration was studied by ASV, i.e., 100  $\mu\text{g/L}$  level of arsine was deposited at -0.4 V for 60 sec as pre-concentration step on the surface of electrode and linear scan was performed at the rate of 100 mV/sec from -0.1 to 0.1 V.

This paper gave the clue to the design of arsine sensor. Gold salt,  $\text{HAuCl}_4$  was electrodeposited on the specially fabricated boron doped diamond electrode at -0.4 V. The paper ambiguously stated that bubbling 1  $\mu\text{g/L}$  arsine for 10 minutes was achieved without reporting the flow rate of the gas. It must be noted that the work was done with dissolved  $\text{AsH}_3$  in strongly acidic media and not as a gas phase sensor.

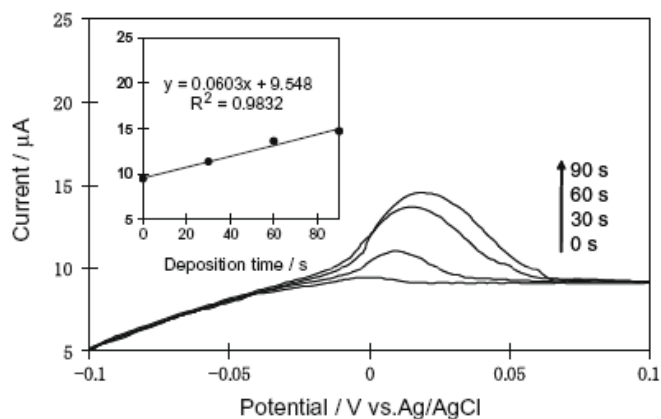


Figure 1.3.2 Overlay of LSV (linear sweep voltammograms) of cells containing different amount of arsine.<sup>18</sup> Anodic peak current depends on deposition time in ASV. A stream of 1  $\mu\text{g/L}$   $\text{AsH}_3$  gas was bubbled into an electrolyte solution of 10 M  $\text{H}_2\text{SO}_4$ . Au-BDD electrode was used as working electrode. Stripping voltammetry parameters were  $E_{\text{dep}} = -0.4$  V (vs. Ag/AgCl) and scan rate = 100 mV/s. Inset shows the dependence of peak currents vs. the deposition time.<sup>18</sup>

The moles of arsine dissolved in aqueous media for the measurement is not clearly indicated. Their final configuration for arsine detection is amperometric method where  $\mu\text{g/L}$  level of arsine gas along with inert nitrogen carrier gas was blown at 500 ml/min. In this laboratory, we have pursued getting signal from arsine generated from  $\mu\text{g/L}$  level of arsenic in 2 ml of sample solution.

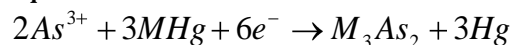
### 1.3.2. Cathodic stripping voltammetry (CSV)

In CSV, pre-concentration step is achieved by reduction of analyte first. Then cathodic current is recorded while the potential moves toward more negative direction.

The two steps in CSV stripping is shown as:

Deposition:

Equation 1.3.3



Stripping:

**Equation 1.3.4**



where M is Cu or Se .

Generally, CSV with hanging dropping mercury electrode (HDME) for arsenic exhibits advantage and disadvantage due to use of Hg.<sup>19</sup> The advantage is that fresh formation of Hg always guarantees the electrode is always working; the disadvantage is that Hg is environmentally not friendly. It poses problems with its waste disposal.

In the cited review<sup>16</sup>, the name of the game is how to deposit arsenic species on the Hg electrode efficiently before obtaining reduction current. All complex operation is centered around making “intermetallic species” or “adsorption complex” on Hg electrode. In addition, complicated pretreatment of sample was necessary to reduce As(V) to As(III) for speciation. HDME obviates the need for cleaning electrode in contrast to ASV. However, toxicity of Hg is a concern to operators and poison to environment. Moreover, excessive use of chemical reagents for efficient deposition of arsenic species on cathode discourages one to develop As sensor in this way. To overcome these difficulties and disadvantages of solution phase electrochemical sensors, direct measurement of arsine produced from soluble arsenic species appears to be promising. A review of such sensors is presented in the following section.

---

<sup>19</sup> Mays, D.E.; Hussam, A. Voltammetric methods for determination and speciation of inorganic arsenic in the environment-A review, *Anal. Chim. Acta*, 2009, 646, 6-16.

#### 1.4. Electrochemical gas sensors: general overview

We review a simple structure of electrochemical sensors for clear understanding of gas sensor.<sup>20</sup> There are two categories of sensor depending on whether the electrolyte is renewed or not. Namely we call them stationary and dynamic configuration. Dynamic configuration has been used in hydride generation gas diffusion flow injection analysis (HG-GD-FIA) system. We first introduce a stationary configuration. Structurally, the working electrode is sometimes placed right behind the hydrophobic membrane where only gas can diffuse through. The hydrophobic membrane holds the electrolyte and prevents it from leaking out from the cell. The counter electrode and reference electrode

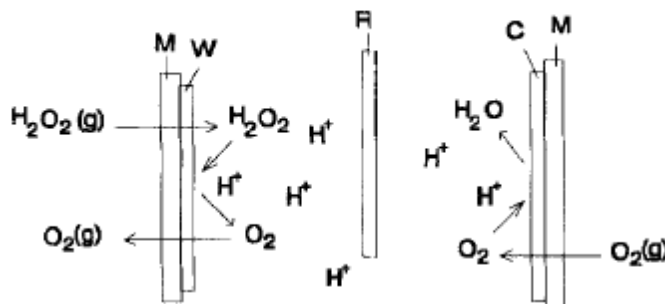


Figure 1.4.1 Schematic of typical electrochemical oxygen gas sensor. Figure 1. 1 Abbreviations indicate: M: a membrane; W: porous working electrode; C: a porous counter electrode; R: a reference electrode.<sup>20</sup>

are separated from the working electrode. In general, electrochemical sensing of gases is based on liquid collection interface. First, gas of interest moved into electrolyte through a diffusion barrier, a hydrophobic membrane and is accumulated in the electrolyte. Second, concomitantly, the electrochemical reaction takes place at the working electrode and at

<sup>20</sup> Huang, H.; Dasgupta, P. K. Electrochemical Sensing of Gases Based on Liquid Collection Interfaces, *Electroanalysis*, **1997**, 9 (8), 585-591

the counter electrode, simultaneously. Third, the products move away from the electrode by diffusion or escape the cell if they are gaseous. The disadvantage of this configuration stems from the alteration of internal electrolyte if the products are accumulated in the electrolyte. The porosity of electrodes in gas sensor poses technical challenging task of designing sensors. Making porous noble metals porous to use as a working electrode is not a simple task. However, to increase sensitivity of sensor, this requirement should be fulfilled. In this dissertation, we circumvent this requirement by employing a bundle of thin fiber electrode as a working electrode.

To overcome this problem of adulteration of electrolytes, the internal electrolyte is renewed either continuously or on stop-and-go basis in several examples. A dynamic configuration is illustrated in Figure 1.4.2. Either stop-and-go or continuous renewal of electrolyte has been extensively adopted in gas sensor world.

Most of gas sensors use chronoamperometry (CA) as the technique where diffusion current is measured at a constant potential. In amperometry, steady state kinetics of electron transfer at the electrode is recorded whereas in potentiometry, chemical and diffusion process must be at thermodynamic equilibrium to obtain accurate open circuit potential between the two electrodes<sup>21</sup>. In amperometry, signal is current which is directly proportional to the concentration of

---

<sup>21</sup> Stetter, J.; Li, J. Amperometric gas sensors-a review, *Chemical Reviews*, **2008**, 108, 352-366.

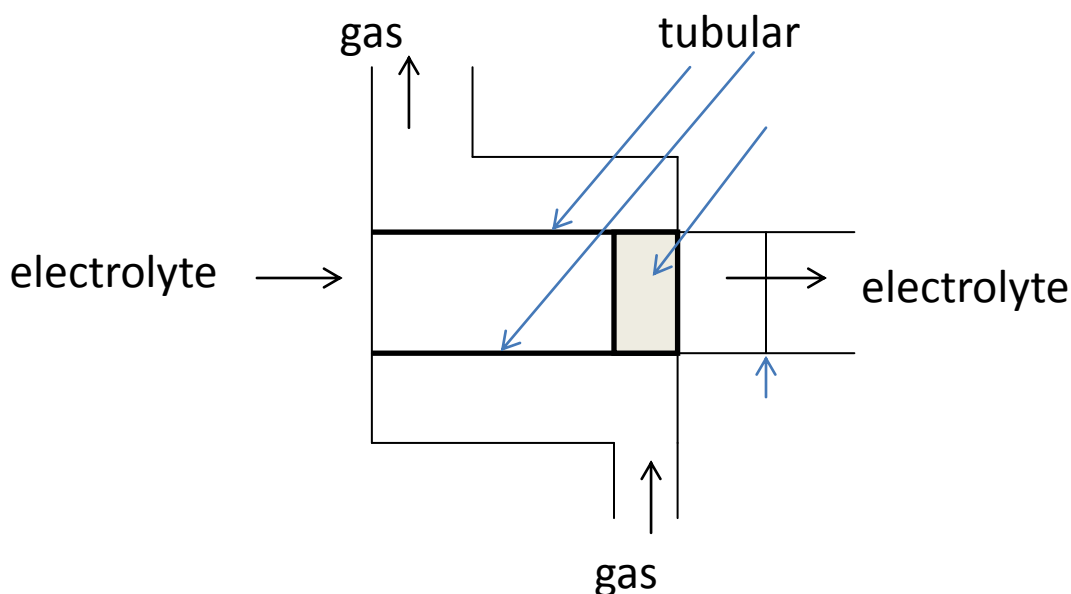


Figure 1.4.2 Schematic of a stop-and-go electrolyte renewal system for a gas sensor.<sup>20</sup> Analyte gas diffuses through the tubular membrane while the valve is closed during enrichment step. After measurement, valve is opened to renew the electrolyte and measurement of blank is conducted to subtract background signal.

analyte, whereas in potentiometry, signal is voltage and is proportional to logarithm of the concentration of analyte. The advantage of amperometry is the linearity of the signal which is proportional to the concentration of analyte whereas in potentiometry, the signal increases nonlinearly and slowly as logarithmic function does. In other words, signal, i.e. voltage increases only 0.0591 V per 10 fold increase in the concentration of the analyte. We have focused on the amperometric method in this work. In the following, we examined electrochemical kinetics and diffusion for amperometric sensors.

#### 1.4.1. Kinetically controlled vs. diffusion controlled system

The current in AGS is dictated by the two disparate processes. One is the rate of transfer of electron at the surface of electrode ( $r_r$ ) and the other is the rate of species

arriving at the surface of electrode ( $r_d$ ). When  $r_r$  is much greater than  $r_d$ , the process is called “diffusion controlled.” Since as soon as the electroactive species arrives at the surface of electrode, the species disappears, a concentration gradient is developed. The concentration in the region which is far away from the surface called “bulk solution’ is much higher than that at the surface of electrode. When  $r_d$  is much greater than  $r_r$ , we always have abundance of electroactive species on the surface of the electrode and now it is described as ‘kinetically controlled.’ Kinetically controlled process is not very analytically useful in that the current generated, which is signal, depends heavily on the catalytic activity of the electrode which varies widely during the life time of the electrode. In order to have invariably stable signal that only depends on the concentration of the analyte of interest, we want to have diffusion-controlled system.

Mathematically, the kinetically controlled system is described by the Butler-Volmer equation as follow.<sup>22</sup>

**Equation 1.4.1**

$$i = F A k^0 (C_0(0,t) e^{-\alpha f (E - E^{0'})} - C_R(0,t) e^{(1-\alpha) f (E - E^{0'})})$$

, where F is faraday constant, A is the area of the electrode surface,  $k^0$  is standard rate constant,  $C_0(0,t)$  is concentration of oxidized species,  $\alpha$  is the transfer coefficient, E is the applied potential,  $E^{0'}$  is the formal potential, and f is F/RT. In the diffusion controlled limit, we have a much simpler expression for disk ultramicroelectrode (UME):

---

<sup>22</sup> Bard, A.J.; Faulkner, L.R. *Electrochemical Methods, fundamentals and applications*, 2nd ed.; John Wiley & Sons: New Jersey, **1994**, pp 92-107.

Equation 1.4.2

$$i = \frac{4nFAD_oC_o^*}{\pi r_0} = 4nFD_oC_o^*r_0$$

, where  $D_o$  is diffusion coefficient for oxidized species,  $C_o^*$  is concentration of oxidized species in the bulk and  $r_0$  is the radius of disk electrode. As this equation indicates, the current is proportional to the concentration present in the electrolyte. Therefore, there is no dependence on the catalytic activity of the electrode surface which can vary significantly.

Although kinetic parameters are not friendly for analytical purpose, there have been efforts in developing gas sensors based on the kinetic behavior of the electroactive species.<sup>23</sup> We consider here an illustrative example of kinetically controlled electrochemical process where useful signal is obtained from combination of adsorption of analyte and redox reaction. Development of CO sensor also has the same problem as we face with arsine sensor. Standard reduction potential of CO is -0.1038 V which is very close to zero where hydrogen redox reaction takes place. The same problem of co-oxidation of hydrogen and arsine is encountered as equilibrium potential of arsenous acid/arsine is 0.01 V. In measuring CO in the excessive amount of hydrogen gas, the electrode was operated in two different modes. In one mode at 1.000 V vs. counter electrode for 200 ms, both H<sub>2</sub> and CO were oxidized and in the next mode at 0.350 V for 800 ms, only the H<sub>2</sub> was oxidized. In this journal article, people successfully recovered the full catalytic activity of the Pt electrode by applying substantially high potential at 1.0

---

<sup>23</sup> Planje, W.G.; Jassen, G.J.M.; de Heer, M.P. A two-electrode sensor cell for CO detection in a H<sub>2</sub>-rich gas, *Sensors and Actuators B*, **2004**, 99, 544-555

V to oxidize both species adsorbed on the surface of electrode (clean-up mode). During measurement mode, mathematical modeling of surface adsorption and desorption and electrochemical reaction at equilibrium using Nernst equation, the current density was fully spelled out in an explicit equation. The current density equation showed faster current decay when the electrode was covered more with CO gas. Due to its complex nature of surface adsorption and desorption, the equation ended up with messy system of differential equation. However, simplified equation was quite telling. Approximate current density on the anode reads,

**Equation 1.4.3**

$$j_{approx} \cong F\rho q_1(1 - 2r_1t)$$

, where, F is faraday constant,  $\rho$  is the amount of total Pt sites per unit electrode area.

The  $q_1$  and  $r_1$  are defined as follows:

**Equation 1.4.4**

$$q_1 = k_{a,H_2} P_{H_2} \rho$$

**Equation 1.4.5**

$$r_1 = k_{a,CO} p_{CO}$$

, where  $k_{a,H_2}$  is adsorption rate constant of hydrogen gas on the anode,  $P_{H_2}$  is the partial pressure of hydrogen gas,  $k_{a,CO}$  is the adsorption rate constant of CO and  $p_{CO}$  is the partial pressure of CO. Equation 1.4.3 shows that the current density is proportional to density of Pt catalytic site and partial pressure of  $H_2(g)$ . It also indicates that the current density decreases linearly depending on the partial pressure of carbon monoxide. As it is clearly shown, the current density depends on all the rate constants which can vary much.

However, the author surprisingly employed this equation to predict the decay of current in the presence of varying amount of CO in the excess amount of hydrogen.

This is introduced here because the gas under investigation in this work involves generation of arsine gas using  $\text{NaBH}_4$  which inevitably accompanies large excess of hydrogen gas evolution. This work hints on how to describe current solely generated from hydrogen oxidation in the presence of analyte gas that partially covers the surface of electrode, decreasing the available catalytic site.<sup>23</sup> However, it is unknown whether arsine will be adsorbed in a manner similar to CO adsorbed on the Pd catalytic surface to block the site to prevent hydrogen from accessing gold surface. Also, after arsine is oxidized and deposited as  $\text{As}^0$  on the surface of gold electrode, it is not clear whether that arsenic will not be conducting as CO is on the Pd metal surface. This is due to the fact  $\text{As}(0)$  is a metalloid and still might have good conductivity to catalyze hydrogen oxidation. So we dropped this idea of doing kinetically controlled experiments. In short, kinetically controlled current as signal is mathematically complicated, but diffusion controlled current is not. Limiting current measured is simply proportional to concentration of the analyte. Additionally, diffusion controlled current also does not depend on the catalytic activity of electrode, which renders the sensor more reliable.

#### **1.4.2. Electrochemical arsine gas sensor**

Literature survey was performed to find suitable configuration of arsine gas sensor that can be used in the field. In 1996, Farrel reported that portable, field deployable, instrument for contaminated soil was developed for arsenic.<sup>24</sup> The so called, HG-GD-FIA (Hydride Generation Gas diffusion Flow Injection Analysis) has been

repeatedly used in gas sensor design. The conductometric method is based on the electrochemical reaction that occurred when reaction between arsine and aqueous bromine produced ions such as proton and bromide. In the amperometric detection the electrochemical reaction was described in Equation 1.4.6. The working electrode (gold) was immersed in aqueous electrolyte consisted of 0.01 M sulfuric acid and 1.2 V vs. Ag/AgCl reference electrode was applied.

Anode (oxidation):

Equation 1.4.6



Cathode (reduction):

Equation 1.4.7



This work has been cited by other scientists and recently in 2008, Lolic et al. stated that LOD ( $3\sigma$ ) was 5  $\mu\text{g/L}$  and on the platinum electrode at the 0.1 V vs. Ag/AgCl reference electrode gave 10  $\mu\text{A}$  signal when 0.2 ml of 1  $\mu\text{g/L}$  As(III) ( total of 0.2 ng) was injected.<sup>25</sup> Instead of using bromine, iodine ( 1 mg/L) and 0.05 M KI was used as acceptor solution and cathode reaction is as follows:

Equation 1.4.8



Table 1.4.1 summarizes electrochemical sensors for arsine and references are given in the footnote. When the cathode reaction is not mentioned in literature, we assume the reduction of oxygen in electrolyte in the counter electrode reaction as follows:

Equation 1.4.9



Almost identical configuration of electrochemical system surprisingly worked well. The possible interfering species such as of Sb(II), Sn(II), Se(IV), and As(V)

**Table 1.4.1 Electrochemical arsine gas sensor**

References	Potential	Working Electrode material	Electrolyt -e	Anode reaction; working	Cathode reaction; counter	Analytical method	Limit of detection
<sup>24</sup>	1.2 V vs Ag/AgCl	Au	0.01 M H <sub>2</sub> SO <sub>4</sub>	Arsine oxidation	Reduction of oxygen	HG-GD-FIA	10 µg/LV
<sup>25</sup>	0.1 V vs Ag/AgCl	Pt	0.1 M HCl	Reduction of iodine	Oxidation of iodide	HG-GD-FIA	5 µg/LV
<sup>26,27</sup>	1.35 V vs. saturated KCl/HgCl <sub>2</sub> /Hg	Hg doped Au-PTFE Electrode	1.0 M H <sub>2</sub> SO <sub>4</sub>	Arsine oxidation	Reduction of oxygen	Separation over Porapak Q	0.2 µg/L(As(III) in solution)
<sup>28</sup>	0.05 V between working and counter electrode	Pt, Pd, Au(best selectivity) coated PTFE membrane	12 M H <sub>2</sub> SO <sub>4</sub>	Arsine oxidation	Reduction of oxygen	HG-GD-FIA	Linear from 10 µg/LV to 300 µg/LV, LOD = 10 µg/LV

with concentration of a few µg/L did not affect the signal generated from anode.

<sup>24</sup> Farrel, J.R.; Iles, P.J.; Yuan, Y.J., Determination of arsenic by hydride generation gas diffusion flow injection analysis with electrochemical detection, *Ana. Chim. Acta*, **1996**, 334, 193-197

<sup>25</sup> Lolic, A.; Nikolic, S.; Mutic, J. Optimization of a Flow Injection System with Amperometric Detection for Arsenic Determination, *Analytical Sciences*, **2008**, 24, July, 877-880

<sup>26</sup> Gifford, P.R.; Brukenstein, S. Pneumatoamperometric Determination of parts per billion dissolved gas by Gas evolving reactions. *Analytical Chemistry*, **1980**, 52, 1024-1028

<sup>27</sup> Gifford, P.R.; Brukenstein, S. Separation and Determination of Volatile Hydrides by Gas Chromatography with Gold Gas-Porous Electrode detector. *Analytical chemistry*, **1980**, 52, 1028-1031

<sup>28</sup> Kumar, M. B.; Suzuki, K. T. Arsenic round the world: a review. *Talanta*, **2002**, 58, 201-235

In the arsine sensors described by Brukenstein, positive potential of +1.35 V versus SSC was applied between gold working electrode and counter electrode, which is rather large potential considering the electrochemical windows of usual aqueous electrochemical cells. Water can be electrolyzed at such high potential. The standard reduction potential of  $\text{Au}^{+1}/\text{Au}$  and  $\text{Au}^{+3}/\text{Au}^{+1}$  is 1.69 V and 1.41 respectively, which suggests that high potential used here endanger the integrity of gold electrode.

When mixed with other hydride species, these hydrides interfere with the signal from arsine alone, therefore, people attempted to separate these species and indeed arsine was separated from other hydride gases.<sup>29</sup> Funazaki reported a selective  $\text{AsH}_3$  sensor<sup>30</sup>. The selectivity coefficients for gases relative to arsine gas were  $10^{-6}$  for hydrogen,  $10^{-6}$  for acetone, toluene,  $10^{-5}$  for carbon monoxide,  $10^{-4}$  for ethanol, 0.27 for sulfur dioxide, and 0.25 for nitrogen dioxide. The test gas was delivered by an air pump at the flow rate of 300 ml/min to the sensor where gold with particle size from 0.25 to 1.0  $\mu\text{m}$  in diameter sintered on PTFE was used as working electrode and Au as counter electrode. Low potential of 50 mV was applied between Au working and counter electrode. The selectivity of this sensor is nearly suitable if we consider the case where 1  $\mu\text{g/L}$ (ng/ml) arsenic is dissolved for analysis. If we add 0.3 ml of 0.7 % (w/w) sodium borohydride to this solution, we generate  $5.55 \times 10^{-5}$  moles of hydrogen. Arsine will be around  $6.5 \times 10^{-11}$  moles when 5 ml of 1  $\mu\text{g/L}$  (ng/ml) arsine sample is analyzed. About selectivity of

---

<sup>29</sup> Tanaka, T.; Nakamura, Y.; Mizuike, A.; Ono, A.. Simutaneous Determination of phosphorous, Sulfur, and arsenic in steel by hydride generation and gas chromatography, *Analytical Sciences*, **1996**, 12, February, 77~80

<sup>30</sup> Funazaki, N.; Satoshi, K.; Hemme, A.; Ito, S.; Asano, Y. Development of catalytic electrochemical gas sensor for arsine. *Sensors and Actuators B*, **1993**, 13-14, 466-469

$8.5 \times 10^{-5}$  is required and the reported selectivity of this sensor warns that one needs to develop gold electrode with high selectivity for arsine sensor.

### 1.4.3. Thermodynamic of direct oxidation of arsine in electrochemical cells

Amperometric arsine gas sensors described above involves electrochemical reactions, i.e. direct oxidation of arsine on the working electrode. The thermodynamic of direct oxidation of arsine is treated in this section. The following Table 1.4.2 below lists half cell reactions in arsine sensor and standard reduction potential for each half reaction. We assume the sensor being used in the ambient air, which is an open system. Therefore, we include  $O_2(g)$  in following discussion. Unless special treatment is conducted, we generally have dissolved oxygen molecules in the electrolyte.

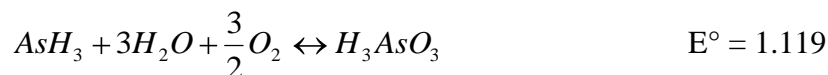
**Table 1.4.2 Standard reduction potential of half reactions involving direct oxidation of arsine.**

Half cell reaction	Standard reduction potential, V
<b>Equation 1.4.10</b> $As(s) + 3H^+(aq) + 3e^- \leftrightarrow AsH_3(g)$	-0.238
<b>Equation 1.4.11</b> $H_3AsO_3(aq) + 3H^+(aq) + 3e^- \leftrightarrow As(s) + 3H_2O$	0.2475
<b>Equation 1.4.12</b> $H_3AsO_3(aq) + 6H^+(aq) + 6e^- \leftrightarrow AsH_3(g) + 3H_2O$	0.0095
<b>Equation 1.4.13</b> $2H^+(aq) + 2e^- \leftrightarrow H_2(g)$	0.000
<b>Equation 1.4.14</b> $\frac{1}{2}O_2(g) + 2H^+ + 2e^- \leftrightarrow H_2O$	1.2291

An electrochemist removes dissolved  $O_2$  from the electrolyte by bubbling argon and nitrogen gas in laboratory. However, we assume user of the sensor will not perform

such complicated operation in the field. The thermodynamics of electrochemical reaction is dictated by standard reduction potential of half cell. Equation 1.4.12 is obtained by adding Equation 1.4.10 and Equation 1.4.11. By subtracting Equation 1.4.14 from Equation 1.4.12, we obtain the overall reaction as follows:

**Equation 1.4.15**



As Equation 1.4.12 and Equation 1.4.13 indicate, these redox potential of the two different species lies very closely to zero V vs. NHE. From this thermodynamic ground, chemists anticipate interference from hydrogen will inevitably jeopardize the measurements of arsine signal. To see if any dramatic shifting of redox potential of arsine is feasible, we calculate the theoretical redox potential of arsine. At constant pressure and temperature, the maximum energy we can harness from this galvanic cell is

= - 6 x 96,485.4 (C/mol) x 1.1196(J/C) = - 648.15 kJ/mol. The actual free energy has dependence on the activities of species involved. Therefore, it will be lower than that in standard condition where pressure is 1 atm and concentration is 1 M as the following equation indicates.

**Equation 1.4.16**

$$E = E^\circ - \frac{0.0591}{6} \log \frac{[\text{H}_3\text{AsO}_3]}{P_{\text{AsH}_3} P_{\text{O}_2}^{3/2}}$$

Even if oxygen pressure on the counter electrode is only  $10^{-5}$  atm, the contribution to the potential is only -0.0738 V to the system compared to the condition when oxygen is 1 atm. Likewise, the arsine pressure and amount of arsenous acid in the electrolyte does not contribute much to the overall Gibbs free energy. Even if we minimize the

introduction of oxygen into counter electrode to lower the concentration of dissolved  $O_2$ , the decreased pressure of oxygen cannot contribute significantly in terms of thermodynamics. At given potential of the counter electrode, standard electrochemical reduction of oxygen molecules remains virtually the same as before. Coupling of oxidation of  $H_2(g)$  and reduction of dissolved  $O_2(g)$  is a readily available process in the air with Gibbs free energy change of  $-237.2$  kJ/mol. Although the reaction is thermodynamically favorable, it is possible that the reaction is kinetically extremely slow compared to oxidation of arsine. It is merely stated by many authors in the literature that gold is kinetically very inert to hydrogen gas and the reason is not very well explained.

As long as one produces arsine from arsenate or arsenite, there is always accompanying hydrogen gas generated from the solution regardless of chemicals used. Thus produced hydrogen interferes with signal, i.e. oxidation current which is greatly increased by the oxidation of hydrogen. Therefore much consideration was given in this work as to how to deal with excessive presence of hydrogen gas. Several possibilities could be explored to solve this problem. The easiest option is to subtract background signal. The electrochemical behavior of arsine in aqueous media is not well understood as very little information is available in the literature. The standard reduction half cell reaction of arsenous acid is based on measurement when partial pressure of arsine is 1 atm.

Equation 1.4.15 shows that arsine oxidation is a thermodynamically feasible process and both arsenous acid,  $H_3AsO_3$  and arsenic acid,  $H_3AsO_4$  could form at potentials generally near the positive limit of effective electrochemical window of

electrolytes and electrode. At these extremely positive potentials, gold electrode could be oxidized into  $\text{Au}^{3+}$  (aq) and be dissolved into acidic solution unless a robust oxide layer on its surface prevents this dissolution. Although in literature on arsine sensors, bias potential of 1.2 V vs. SSC is applied, it is not clear how these affect the overall electrochemistry in acidic solution. We used these in solution using Au wire with 100  $\mu\text{m}$  in diameter as the working electrode. Low potential between working and counter electrode was applied.

## **1.5. Redox reactions of halide in determination of As(III) and arsine**

As discussed in the previous section, direct oxidation of arsine in the presence of  $\text{H}_2$  (g) is inevitably problematic due to co-oxidation of  $\text{H}_2$ (g). We found in literature that oxidation of As( III) and  $\text{AsH}_3$  did not occur electrochemically and only chemical redox reaction took place in measurement of As(III) and  $\text{AsH}_3$ . Halides have been used to oxidize As(III) and  $\text{AsH}_3$  to measure change of concentration of these species. Colorimetry, potentiometry and amperometry have been conducted to reflect the concentration of As(III) and  $\text{AsH}_3$ .

### **1.5.1. Analytical methods for As(III) and arsine using iodine as oxidant: Early work**

The introduction of halides in determining arsenic(III) dates back to year 1908. The work describes volumetric determination of arsenious acid using iodine as titrant. The so called iodometric determination of arsenious acid was reviewed by Edward W. Washburn.<sup>31</sup> The first halogen that had been utilized to oxidize arsenious acid,  $\text{H}_3\text{AsO}_3$  to

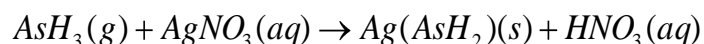
---

<sup>31</sup> Washburn, E.W. The Theory and Practice of the Iodometric Determination of

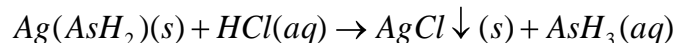
arsenic acid,  $H_4AsO_4$  was chlorine in 19<sup>th</sup> century. Gay Lussac employed redox titration of arsenious acid with chlorine in 19<sup>th</sup> century. Iodine was used as a replacement for more toxic chlorine for determination of arsenious acid appeared subsequently. Friedrich Mohr was quoted in this review to introduce this method of iodometry by using solution of iodine to titrate arsenious acid and starch was added to titrand as indicator. For more permanent end point detection, Mohr recommended addition of base to arsenious solution such as sodium carbonate or ammonium carbonate.

A more sophisticated volumetric method of determination of arsine with iodine was introduced in 1932 in literature. Gutzeit method is a colorimetric method of determining arsine generated from the water sample. Literature showed that generated arsine was trapped in  $AgNO_3$  solution as in Gutzeit method and the addition of HCl liberated arsine from the precipitation,  $AsH_3(aq)$ , which was titrated by 2 mM iodine<sup>32</sup>. The following chemical reactions are assumed in this method.

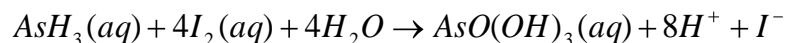
**Equation 1.5.1**



**Equation 1.5.2**



**Equation 1.5.3**




---

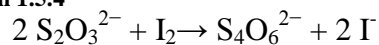
Arsenious Acid. *J. Amer. Chem. Soc.*, **1908**, 31~46.

<sup>32</sup> Wiley R.C. et al. Determination of Arsenic: Iodometric Acidimetric Method, *Industrial and Engineering Chemistry*, **1932**, 4(4), 396~397.

To extract more arsine from the aqueous solution, the author boiled the solution in the generator where reduction of arsenious acid was achieved by Zn metal. This type of procedure suggested the feasibility of generating iodide by reacting arsine with iodine as shown in Equation 1.5.6. Also, given the fast rate of reaction, quantitation of the generated iodide from arsine directly leads to the quantitation of arsine.

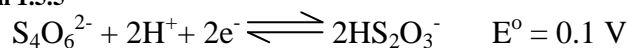
As previously described, titrating residual iodine after reacting arsine with iodine was performed. Instead of trapping arsine with silver nitrate solution and subsequent liberation of arsine from silver-arsine complex, the authors reduced the known amount of iodine with arsine. As the initial amount of iodine was known and the remaining iodine can be determined by titration with thiosulfate, therefore, an indirect determination of arsine was achieved. The redox reaction below is used for determination of excess iodine that was left after reaction with arsine.

**Equation 1.5.4**



The residual iodine was titrated with sodium thiosulfate using starch as indicator. There is a large difference of standard reduction potential between tetrathionate and iodine, which was employed in this method. The reduction potential of tetrathionate to thiosulfate is 0.1 V and the reduction potential of iodine to iodide is 0.620 V.

**Equation 1.5.5**

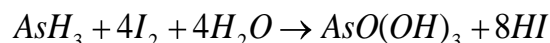


**Equation 1.5.6**



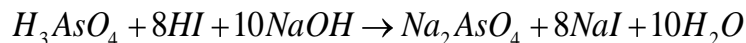
From this paper, the chemical reaction between and iodine and arsine was described as follow:

**Equation 1.5.7**



For a large amount of sample (greater than 50 mg of arsenious oxide in 20 mL), the solution was neutralized by sodium bicarbonate and then arsenic acid was titrated back with standard iodine. For a small amount of sample (less than 50 mg of arsenious oxide in 20 mL), authors were able to determine the amount of arsenic by titrating the hydrogen iodide (hydroiodic acid) with NaOH using phenolphthalein as indicator in the following equation.

**Equation 1.5.8**



The advantage of titration in this case is that one mole of arsenic requires 10 moles of NaOH, which increases the accuracy of measurement. Although the procedures are very lengthy and inconvenient to employ even in chemistry laboratory, these authors in 1932, successfully determined arsenic down to 20 µg in 20 to 30 mL, which is around 1 mg/L (1 mg/L). We extended this method to amperometric method, let's say, potentiostatic coulometry with increased sensitivity.

### **1.5.2. Measurement of AsH<sub>3</sub> by chronoamperometry with iodine/iodide redox couple**

Measurements of arsenic were often achieved by arsine generation from arsenic containing sample which minimizes the interference of measurement process from other ion species. A so called, hydride generation-flow injection methodology has similarity to our measurement system and motivated us to invent this sensor, so a brief review on this kind of methodology is given here. Typically, arsine is generated by mixing two streams

of sodium borohydride solution and sample carrying solution and arsine gas enters into a detection system where acceptor stream is flowing in the detector. When arsine enters into the acceptor stream, physical properties of the acceptor stream are changed. Monitored physical properties in the detection cells are conductance, anodic or cathodic current, and UV absorbance in literature. The reason why we need to use flow system, i.e. three streams of different reagents in flow injection system is as follow. One must ensure that all chemical reagents are freshly renewed. As a result, all components in the detection cell are constant. Renewed, i.e. fresh solution is flowing through the detection system constantly, thus constant properties of the acceptor stream guarantees invariance of detector system. Only when analyte of interest is introduced, measureable quantity changes accordingly.

Arsine is a reducing gas and reduces halide and one occurrence of utilization of bromine reduction by arsine was reported by Farrell.<sup>24</sup> In conductometric method where arsine entered the electrochemical cell after which reaction with bromine ensued. The reaction of bromine is similar to that with iodine and number of ionic species increased. This was detected with a commercial conductometric cell, Bio-Rad flow-through conductometric detector. In addition, amperometrically, the arsine was detected by direct oxidation of arsine in the presence of 10 mM sulfuric acid.

An amperometric method of detection of arsine mediated by iodine to iodide reduction was introduced by Lolic et. al.<sup>25</sup> The opposite aspect of electrochemical reaction of iodine/iodide couple was used by the authors. Instead of measuring oxidation current, they measured the reduction current. Electrochemical reaction used for

measurement of arsine is the reduction of iodine to iodide whereas our measurements are based on the oxidation of iodide to iodine. The following diagram shows the system. The chemicals for reagent stream R was 0.2% NaBH<sub>4</sub> in 0.1% NaOH; carrier stream C, 0.1 M HCl; and acceptor stream A, 1 mg/L I<sub>2</sub> in 0.05 M KI. The flow rate for A was 0.9, B for 1.1, and C for 1.1 mL/min. The electrochemical system consisted of three electrodes; working electrode: rotating platinum disk (RDE); reference electrode, Ag/AgCl in potassium chloride (3 M); and auxiliary platinum electrode. For observation of reduction current of iodine to iodide, CV was performed and the following graph clearly showed that there was decrease of reduction current when arsenic sample (200 μL of 1 mg/L in 0.1 M HCl) was introduced from the injection valve V. The claimed limit of detection of arsenic was 5 μg/L. An advantage of flow injection system comes from the invariance of the baseline signal. Constancy of concentration gradient of iodine and iodide is provided by constant flow of the acceptor stream. Regardless of whether reduction current or oxidation current is monitored, there is always constant gradient of concentration on the surface of the Pt electrode. As a result, baseline current is flat. In literature and also experiments in this laboratory, the reduction current of iodine on Pt electrode revealed interesting properties of iodine. The iodine chemisorbed on the surface of Pt electrode and reduction current observed in double step potential amperometry exhibited flat line. This was done in static solution in the absence of renewal of electrolyte. Even then a horizontal line with time axis persisted for a long period of time, which was ascribed to the chemisorbed iodine on the Pt surface.

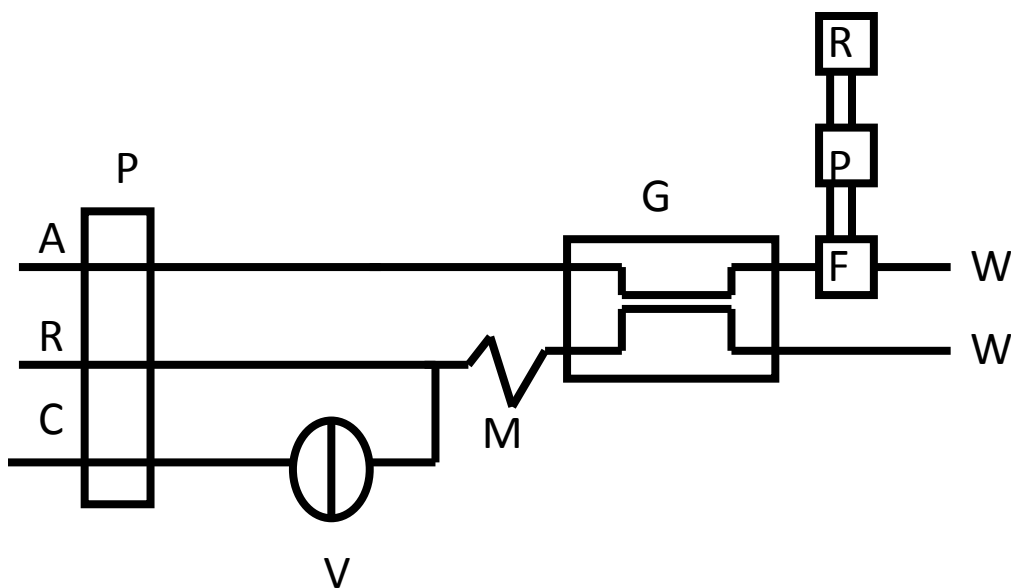


**Figure 1.5.1** Flow injection system used by Lolic<sup>25</sup> in flow injection system. Abbreviations indicates: Carrier (C), reagent(R), acceptor flow stream (A), peristaltic pump (P), injection valve (V), mixing coil (MC), gas diffusion unit (GDU), electrochemical flow through cell (FC), potentiostat(PO), recorder(RE), waste (W).

The authors measured the reduction current of the iodine at 0.1 V. The electrochemical system consisted of Pt electrode and iodine/iodide electrolyte on top of PTFE membrane. The arsine generated from arsenic and NaBH<sub>4</sub> reaction crossed the PTFE membrane and the arsine reduced iodine to iodide which resulted in decrease of reduction current of iodine to iodide on Pt electrode. The optimized condition for the potential was 0.1 V versus Ag/AgCl and the peak height of the reduction current was 10  $\mu$ A. Their cyclic voltamogram appeared in their paper for iodine to iodide reduction. Experimentally, at 0.1 V, the signal was maximized and it was adopted for amperometric measurement accordingly.

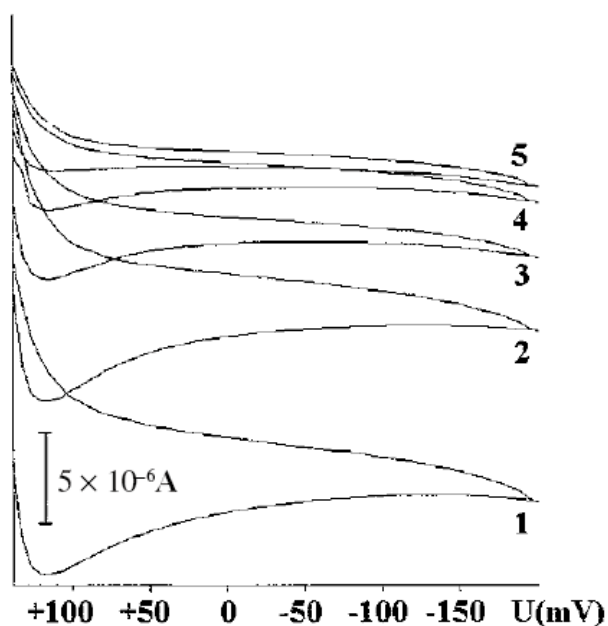


**Figure 1.5.2 CV of the flow injection system.<sup>25</sup> The curve 1 represents the CV of blank sample and curves, 2,3,4, and 5 represent CV when 1 mg/L arsenic was introduced to the system. Gradual decrease of reduction current was observed in curves 2,3,4, and 5. The scan rate was 100 mV/s and 0.1 V was applied in amperometry.**

Although instrumentation for flow injection system employed in this work is different, the method of detection of arsine shares the commonality, i.e. iodine/iodide redox reaction. The hydride generation reaction was performed and arsine diffused into an electrochemical cell where reduction of iodine to iodide occurred and decreased iodine concentration resulted in lowering the reduction current in their system. A disadvantage of this system lies in the complexity of instrumentation requirements. Different flow rates of reagents were employed, being independently controlled from each other. Also rotating disk electrode is not a simple electrochemical system. The PTFE membrane integrity for gas diffusion should be preserved. The author mentioned that the Pt

electrode was washed periodically, suggesting maintenance of the working electrode was necessary.

The same principle of measurement based on redox reaction of arsine with reducing agents and almost identical instrumentation using pervaporation-flow injection-hydride generation system was reported by Rupasinghe<sup>33</sup>. The basic principle of measurement is to monitor change of absorbance of 0.1 mM KMnO<sub>4</sub> solution due to reaction between arsine and KMnO<sub>4</sub>. The detection limit was reported to be 0.18 µg/L. We will not delve into the details of this measurement method here as the measurement was based on spectrophotometric measurement, UV absorbance at 528 nm rather than electrochemical one. Still, it is important to note here that arsine is a reducing gas which reacts with a variety of oxidizing agents in acceptor systems, resulting in change of measureable properties of the acceptor systems such as reduction current, oxidation current, conductance, and optical absorbance. Again, generation of excessive toxic chemical waste, KMnO<sub>4</sub> solution is the single most disadvantage of this methodology. If one wants to use this method, one can look at the reflectance change due to disappearance of permanganate color in a static system. The standard reduction potential of KMnO<sub>4</sub> is 1.5 V and it is readily reducible. Monitoring of reduction current of this species when arsine is introduced on the sensor will be a feasible approach for field deployable instrumentation.

---

<sup>33</sup> Rupasinghe, T.W.; Cardwell T. J.; Cattrall. R.W.; Kolevb. S. D. Determination of Arsenic by pervaporation-flow injection hydride generation and permanganate spectrophotometric detection, *Anal. Chim. Acta*, **2004**, 510, 225-230.

## 1.6. Amperometry using iodine and iodide redox couple

Tomcik et. al. reported interdigitated array electrodes where, electrogenerated iodine could be used to detect As(III) in solution.<sup>34</sup> Anodically generated iodine from 10 mM KI diffuses into the cathode where iodine is reduced to iodide. When the incoming flux of arsenite, As(III) is greater than the flux of outgoing iodine, there was no current at the cathode. Therefore, this quantitative relationship between arsenite concentration and collector current was employed in their diffusion layer titration method shed light on the design of our sensor.

Gerald Hignett et. al. developed system where one can detect As(III) in water with electrogenerated iodine.<sup>35</sup> These experiments resemble experiments that had been performed in this laboratory in that added arsenite to electrolyte in the cell increased the concentration of iodide through the reaction of arsenite, probably arsenious acid, with iodine. The difference is that we add arsine instead of arsenious acid and held potential at a constant value instead of linearly increasing the potential. The commonality with their experiments is that iodine was generated electrochemically and it reacted with the analyte, i.e. As(III) in their experiment and AsH<sub>3</sub> in our experiment. The most important foundation in these experiments is that arsenic can increase the amount of iodide and nothing else could do. Hignett was concerned that the oxidation current signal arose not

---

<sup>34</sup>Tomcik, P.; Jursa, S.; Mesaros, S.; Bustin, D. Titration of As(III) with electrogenerated iodine in the diffusion layer of an interdigitated microelectroarray, *J. Electroanal. Chem.*, **1997**, 423, 115~118.

<sup>35</sup> Hignett, G.; Wadhawan, J.D.; Lawrence, N.S.; Hung, D. Q.; Prado C.; Marken, F.; Compton, R.G. Electrochemical Detection of As(III) via Iodine Electrogenerated at Pt, Gold, Diamond or Carbon-Based Electrodes. *Electroanalysis*, **2004**, 16, No. 11, 897~903.

only from iodide to iodine oxidation but also from oxidation of arsenite. Direct oxidation of As(III) on Pt was observed, but there was no linear relationship between As(III) concentration and peak current. Specifically, LSV revealed an oxidation peak at 0.78 V vs. SCE for a solution containing 40  $\mu\text{M}$  As(III) in 0.1M  $\text{H}_3\text{PO}_4$  (pH 1.9).

On Pt electrode, a proposed mechanism of oxidation involves platinum oxide layer on Pt electrode. Direct oxidation of As(III) on Au electrodes were observed at 1.1 V which was well separated from oxidation current of iodide in LSV. For a solution containing 100  $\mu\text{M}$  KI in 0.1M  $\text{H}_3\text{PO}_4$  (pH 1.9) revealed an oxidation current at 0.54 V (vs. SCE). However, no oxidation peaks of As(III) were observed on boron-doped diamond electrode and glassy carbon electrode. Despite direct oxidation of arsenic could have compromised measurement, LSV data demonstrated that limiting current obtained with all these different electrodes furnished quantitative results. As increasingly higher As(III) were added, proportionally increased limiting currents were always observed in all cases including Au and Pt electrodes. In their experiments, LSVs showed that limiting current increased as the As(III) increased from 10 to 20, 30, 40 and 50  $\mu\text{M}$ . Pt and Au electrode were used and 100  $\mu\text{M}$  KI was electrolyte as gradually increased amount of As(III) was added. With boron doped diamond electrode, the detection limit of 0.11  $\mu\text{M}$  was achieved. This was attributed to the lower background current at this particular electrode. Response current increased over pH range 0.9 to 5.5. However, at higher pH solvent break down current overlaid iodide oxidation current, preventing the resolution of voltammetric peak. We think that as soon as iodine was electrochemically generated, it reacted with As(III), thus increasing the limiting current. As long as this reaction occurs

fast enough compared to the direct oxidation of As(III), all current will be generated from iodide to iodine oxidation.

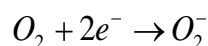
### **1.7. The use of nonaqueous electrolytes for gas sensor**

Almost all of the experiments carried out thus far have employed aqueous electrolyte in the electrochemical cells. Originally, nonaqueous solvent system was developed because of various reasons. The main reason lies in the fact that due to high vapor pressure of water, the water evaporates and drying out of electrolyte disables the sensors completely. Problem of replacing liquid electrolyte with solid polymer electrolyte (S.P.E.) has been attempted. The degree of wetness of solid polymer electrolyte dramatically affects conductivity of S.P.E., thus rendering it very unreliable. Despite the name suggesting invariable stability of solid, drying out of solid polymer electrolyte poses the same problem that one encounters in aqueous electrolyte. Electrochemists always find that drying out of solvent due to high volatility of water disables the electrochemical sensor completely.

In this perspective, it is well justified that we need to use something that can not be dried out over time. The motivation of using room temperature ionic liquid ( R.T.I.L. ) comes from this past experience. The advantages of using R.T.I.L. are enumerated as follows; 1)R.T.I.L.s have high ionic conductivity. 2)Ionic conductivity is high at room temperature and it does not require very high temperature as molten salts does. 3)A negligible vapor pressure of R.I.T.L. does not cause drying out of the liquid electrolytes. 3)The longevity of electrolyte ensures the reliability of the sensors.

R.I.T.L.s have much wider electrochemical windows than water-based electrolyte. This enables electrochemical cells to detect gas in unfavorable situation where bias voltage lies outside of electrochemical windows of aqueous media.

**Equation 1.7.1**



**Equation 1.7.2**



**Equation 1.7.3**



**Equation 1.7.4**

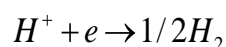


Table 1.7.1 Electrochemical cells employing nonaqueous electrolytes show occurrences of nonaqueous electrolytes discussed in this section. Compton first found that ammonia can be oxidized in the electrochemical cells with very wide potential window due to high anodic limit when non aqueous electrolyte system is used. Although we were not able to find arsine gas sensor using non-aqueous media in any publication, we found the ammonia gas sensors that measure the current from oxidation of ammonia. Ji et. al. reported that as a result of reduction of proton present in his system, H<sub>2</sub> gas oxidation current ( anodic current) occurs in their cyclic voltammetric response.<sup>36</sup> However, if the proton is wiped out by preconditioning electrochemical cell at reduction voltage, one can remove all proton before ammonia gas pass by the electrochemical cell, but the paper did not show whether any such attempts was made. In their electrolytes, 0.1

---

<sup>36</sup>Ji, X.; Banks, C.E.; Compton, R.G. The direct electrochemical oxidation of ammonia in Propylene Carbonate: A Generic Approach to Amperometric Gas Sensors, *Electroanalysis*, **2006**, 18, No. 5, 449 – 455

M TBAP (tetrabutyl ammonium perchlorate) in polypropylene carbonate or imidazolium salt of organic counter ions were used. The imidazolium salt was

**Table 1.7.1 Electrochemical cells employing nonaqueous electrolytes**

ref		Electrodes	Electrolytes	Reactions on w	Reactions on c	Method
37	Step potential -0.2 V to -0.8 V	w-Disk glassy carbon; c-Pt; ref-Ag;	1-ethyl-3-methylimidazolium tetrafluoroborate(EMIBF <sub>4</sub> )	Reduction of oxygen to oxygen anion radical	Reduction of oxygen to oxygen anion radical	DSCA
38	Scan rate from 50 to 1000 mV/s in -1.2 to 1.6	w-Glassy; Carbon c-Pt wire; ref-Ag wire	0.1 M TBAP in PC(Polypropylene carbonate)	Oxidation of ammonia	Oxidation of ammonia	CV
39	100 mV At constant Potential	w-Pt-bonded; Teflon or Pt-Ir; c-Pt; ref- black Pt	0.5 M tetrabutylammonium hexafluorophosphate in PC	Oxidation of ammonia	Oxidation of ammonia	CA

Abbreviations indicate: chronoamperometry (CA), double step chronoamperometry (DSCA), cyclic voltammetry (CV), working electrode (w), counter electrode (c), reference electrode.

<sup>37</sup> Wang, R.; Okajima, T.; Kitamura, F.; Ohsaka, T. A novel Amperometric O<sub>2</sub> sensor based on Supported room temperature Ionic Liquid Polyethylene membrane-Coated Electrodes. *Electroanalysis*, **2004**, *16*, 66- 72

<sup>38</sup> Ji, X.; Banks C.E.; Silvester D.S.; Aldous L; Hardacre, C.; Compton, R.G.. Electrochemical Ammonia Gas Sensing in Nonaqueous Systems: A Comparison of Propylene Carbonate with Room Temperature Ionic Liquids. *Electroanalysis*, **2007**, *19*(21), 2194-2201

<sup>39</sup> Mishima, B.A.; Mishima H.T. Ammonia sensor based on propylene carbonate, *Sens. Actuators, B*, **2008**, *131*, 236-240.

1-ethyl-3-methylimidazolium bis(trifluoromethylsulfonyl)imide. There was no porous hydrophobic membrane for this cell. Working electrode directly made contact with electrolyte solution which was only 20  $\mu\text{L}$  in volume in a very small cell which is in equilibrium with the exposed gas. Oxidation current from hydroquinone (0.5 mM) which was deprotonated by ammonia was detected as signal and 0.129  $\mu\text{A}/(\mu\text{g/L})$  was the slope of the calibration curve. Unfortunately, special equipment and instrumentation such as laser patterning are required to fabricate electrodes reported in the literature in these days. In typical university laboratory, these kinds of special fabrication process can hardly be realized.

Various type of non conventional electrodes were used by Compton, i.e. glassy carbon electrode (GC), boron-doped diamond electrode (BDD), edge plane pyrolytic graphite electrode (EPPG), and basal plane pyrolytic graphite electrode (BPPG) along with PC. the vapor pressure of propylene carbonate is negligible compared to that of water, i.e., for PC<sup>33</sup>, 0.03mm Hg at 20 °C but for water 17.5 mmHg at 20 °C. The benefit of low volatility was emphasized and clearly stated. The sensor lifetime may be greatly extended as a result of using PC. Compton found that GC and BDD electrode has wider electrochemical windows than others and highest anodic limits ( 2.7 V for GC and 3.0 V for BDD vs. Ag wire). At 1.6 V, ammonia oxidation current was observed and analytically useful signal was found for GC electrode. Such high oxidation potential cannot be used in conventional aqueous electrochemical cell where hydrolysis of water will occur. From this ground, we are motivated to use organic electrolyte as our conducting medium for amperometric arsine sensor. Compton did not use any membrane

for this work, which encouraged us to make the sensor without membrane. Small volume of electrolyte, i.e. only 20  $\mu\text{L}$  was used in this work, which was innovative.

## 2. CHAPTER TWO

### 2.1. Motivation and purpose

Literature review lead to the design of gas sensors with new distinctive features. We disclose here the motivations and purposes that have driven us to conduct unique experiments. We understand the reason behind the generation of arsine gas from arsenic in aqueous phase, used thin layer filter paper cells, and used iodine/iodide couple.

### 2.2. Purpose of generating arsine gas from aqueous sample

Sensing arsine generated from drinking water involves generation of arsine from inorganic arsenic ions dissolved in water. Due to high toxicity of arsine gas, this is neither pleasant nor safe method. We asked the question of why we generated arsine. To answer the question, we performed simple calculation using ideal gas law. It convinced us fully that gas sensor approach could be a practical way of inventing highly sensitive arsenic sensor for drinking water.

Suppose we analyze 5 ml of arsenic solution with concentration of 5  $\mu\text{g/L}$  (ng/ml). We know the total mass of As in this sample is 25 ng. By definition, 1 ppmV means that 1ml of gas in 1000 liter of air. The number of moles of arsine in this gas is  $3.34 \times 10^{-10}$ . Therefore, 0.025  $\mu\text{g}$  of arsenic in original sample will occupy  $8.177 \times 10^{-9}$  liters of the volume at 1 atm as shown below:

$$V = nRT/p = \frac{3.34 \times 10^{-10} \times 0.0821 \times 298.5}{1} = 8.2 \times 10^{-9} \text{ L}$$

Let's say the internal volume of the gas sensor including hydride generation chamber is 30 ml. If instantaneously complete conversion from inorganic arsenic species to arsine gas occurs, the corresponding concentration of the analyte gas is

$$\frac{8.17767 \times 10^{-9}}{0.030} = 2.7 \times 10^{-7}, \text{ which is } 0.27 \text{ } \mu\text{g/LV. In short, } 5 \text{ } \mu\text{g/L of arsine in } 5 \text{ ml of}$$

sample can generate gas concentration of 0.27  $\mu\text{g/LV}$ . Generation of arsine gas in a small chamber performs sample enrichment step without using any trapping media. Despite its high toxicity, it is this argument that motivated greatly us to develop arsine gas sensor with limit of detection with sub  $\mu\text{g/LV}$  level. In short, pre-concentration of analyte is achieved by generation of arsine from dissolved arsenic.

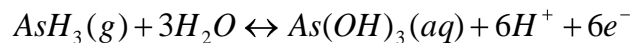
However, the advantage of pre-concentration of analyte is balanced out by a disadvantage. The disadvantage comes from the process of the pre-concentration step itself, which involves generation of excess  $\text{H}_2$  gas. Sensitive arsine detection in the presence of excessively high concentration of  $\text{H}_2$  in electrochemical sensor is a challenge. Here we illustrate the challenge with simple numerical calculation. Typically, 0.3 ml of 0.7 % w/v sodium borohydride in 0.5 M NaOH is added to the highly acidic sample. If the 30 ml vial is closed, the partial pressure of hydrogen is 0.1823 atm and the total pressure is 1.1823 atm. At 1 atm, the hydrogen gas will occupy 5.4 mL. As the internal volume of the generator vial is 30 ml, this corresponds to  $1.54 \times 10^5$  ppmV. For gas sensor designed to detect a few ppbV level of concentration, this amount is huge. Even if the response factor of arsine gas sensor is  $1.54 \times 10^5$  times higher than that of hydrogen, the

sensor read 2 ppmV when 1 ppmV arsine gas comes in. This is due to the fact that arsine is oxidized at the potential where hydrogen gas is also oxidized as shown in Equation 1.4.13. As long as one produces arsine from arsenate or arsenite, there is always accompanying hydrogen gas generated from the solution regardless of what chemical is used. Thus produced hydrogen interferes with signal, i.e. oxidation current which is greatly increased by the oxidation of hydrogen. Therefore much consideration was given as to how to deal with excessive presence of hydrogen gas. This would be done by generating secondary redox couple as described in the following section.

### 2.3. Arsine sensor based on I<sup>-</sup>/I<sub>2</sub> redox couple

Amperometric experiment involves direct oxidation of arsine on the surface of noble metal electrodes producing H<sub>3</sub>AsO<sub>3</sub> (aq) as follows.

Equation 2.3.1



The electrolyte is acidic and this causes high current from oxidation of hydrogen gas to hydronium ion, which is a major drawback of this methodology. The H<sub>2</sub> evolution signal masks the arsine signal completely. Encouraged by the works using iodine/iodide redox couple, we embarked on looking into the measurement of oxidation current of iodide in this laboratory. We initially speculated that non-acidic electrolytes in iodine/iodide system eliminate oxidation of H<sub>2</sub>(g). We have interrogated whether interference from H<sub>2</sub>(g) oxidation was the predominant process in non-acidic environment.

Greatly influenced by the paper from Hignett et al., we tested the hypothesis that the amount of oxidation current of iodide formed from redox reaction of arsine with

iodine was proportional to the amount of arsine. We initially generated iodine electrochemically *in situ* as in the paper and thus looked into the reaction of arsine and electrochemically generated iodine. The oxidation current response was observed. No oxidation current was observed when blank samples were used. In later stages of works, we used iodine from the beginning without having to generate it from iodide *in situ* in the cell. The method of direct use of iodine also yielded oxidation current signal which was proportional to the concentration of arsine, which was in turn proportional to that of arsenic in the analyte.

This method is an indirect method whereas oxidation of arsine in acidic media is a direct method. The shortcoming of direct method stems from the media that must be used to oxidize arsine. To avoid the side reaction of hydrogen gas oxidation to hydronium ion, we were looking into a different type of reaction of arsine. Instead of oxidizing arsine directly on the working electrode, we let arsine reduce other oxidizing reagent that can be easily oxidized back to the oxidizing reagent. The measurable is now arsine-mediated oxidation current of iodide. Here arsine has never been directly oxidized on the surface of the working electrode and only acts as a mediator. The real current is from iodide.

Arsine participates in a chemical reaction and iodide takes part in an electrochemical reaction to give rise to the measurable signal, oxidation current here. Arsine immediately reduces iodine and iodide can be easily oxidized on different electrodes. Iodine can be easily generated from  $I^-$  oxidation which chemically reacts with arsine to generate iodide ion. This chemically generated iodide reacts electrochemically on the surface of electrode and generates amperometric signal which was used in the

experiments. In these works, amperometric determination of arsine-generated iodide was performed to detect arsenic in drinking water. Before we describe the amperometric method, it is useful to illustrate how this idea of measuring iodide was conceived. An idea of using iodine as oxidizing agent for determination of arsine has the commonality in amperometric and potentiometric methods. In potentiometry, one measures change in potential due to chemical reaction of arsine with iodine. In amperometric method, one measures either the oxidation current due to oxidation of iodide to iodine. Alternatively, one measures the reduction current due to iodine to iodide as chemical reaction of arsine with iodine changes the concentration of iodine. Regardless of whether one employs potentiometric method or amperometric method, one obtains the measureable signal from the same chemical reaction. In this regard, we review examples of titration of arsine with iodine as quantitation purpose.

#### **2.4. Filter paper matrix-electrolyte based sensor**

One of the motivations of this work is to develop inexpensive materials for arsenic measurement in the field. In this regard, making a thin layer cell with filter paper is conceived by the combination of the Gutzeit test kit and the commercial sensor made by Nemoto Inc. This approach is new and different from any other previous attempts. Examples of filter paper based arsine kits abound in literature. Gutzeit test kits are commercially available and widely used in the field. As filter paper is inexpensive and readily available, we have used filter paper to develop arsine sensor in this work. In this laboratory, color change of the silver nitrate on a filter paper due to formation of silver-arsine complex formation strategically observed with reflectance detector by Joan

Rozario in this laboratory. We review here how filter paper based sensors have been used for arsine detection.

In the experiment performed in this laboratory, we employed hydride generation method using  $\text{NaBH}_4$ , which is known to reduce  $\text{As(V)}$  as well as  $\text{As(III)}$ . However, we suspect that vigorous and excessive generation of hydrogen gas also contributed to the oxidation current that should have been solely from oxidation of arsine. In the most popular and widely used Gutzeit method, arsine is generated from 6 M HCl or sulfuric acid and zinc granule. To help reduction of  $\text{As(V)}$ , concentrated potassium iodide and stannous chloride was added. For safety reason, solid acid, sulfamic acid instead of 6 M HCl was used in the commercial kits, Arsenator and Hach arsenic kit. The detection is colorimetric. The color is developed by the reaction between arsine and mercuric bromide on a piece of paper. Originally, silver nitrate was used, but this was replaced by mercuric chloride and subsequently mercuric bromide. The kit contains color scale that is visually compared with the color developed on the disposable paper slip. To improve the sensitivity, the light with narrow range of wavelength passes through the yellow spot on paper and intensity of transmitted light is measured as analytical signal. Alternatively, the intensity of incident light that is reflected from the paper is measured as analytical signal. Detection limits of  $0.5 \mu\text{g/L}$  to  $2 \mu\text{g/L}$  were reported for absorbance and reflectance techniques, respectively. The disadvantage is sensitivity to hydrogen sulfide which is either already present or generated from reduction of sulfur containing compounds from the sample. Hydrogen sulfide forms black mercury sulfide that cannot be stained by arsine and produces grey color, obscuring arsenic coloration. Fortunately, hydrogen

sulfide is removed by glass wool impregnated by lead acetate before it reaches mercury bromide paper. In standard Hach kit, potassium peroxy monopersulfate ( $\text{KHSO}_5$ ) is used to oxidize sulfide to sulfate, which cannot be reduced to hydrogen sulfide by zinc. Caution has to be exercised in usage of zinc as arsenic is always associated with zinc ores, and very high purity zinc free of arsenic should be used to increase the sensitivity of this method.

Although the slower process of production of  $\text{H}_2$  to generate  $\text{AsH}_3$  with Zn in sulfuric acid is a disadvantage compared with  $\text{NaBH}_4$  solution, we suspect that less amount and low rate of hydrogen gas produced in this process might cut down the oxidation current coming from  $\text{H}^+/\text{H}_2$  redox pair. Introduction of nonaqueous media as electrolyte such as ionic liquid is expected to further cut down the oxidation signal from hydrogen gas.

Another important consideration for disposable filter is given here. If measurement of arsenic is performed for 1 hour with flow injection system with the flow rate of 1 mL/min, we will generate 60 mL of solution of 1 mg/L of iodine and 50 mM KI. The throughput is reported to be 7 runs per hour, which is comparable to that of our system where we can measure arsenic every 6 min.

## **2.5. Insights gained from a commercial sensor**

Clues to how to design an electrochemical sensor in a compact form was obtained mainly from structure of a commercial sensor (NEMOTO NAP 505). We disassembled and studied the internal structure of the commercial cell. We were hoping to get critical motifs in this sensor by detailed study of the geometric configuration. The commercial

sensor specifically designed for CO detection contains all the necessary hardware for development of ideas. All three electrodes are available in one unit, which we purchased from Nemoto company in Japan. Schematic of internal structure of the commercial gas sensor is shown in Figure 2.5.1. The sensor has porous Teflon onto which a porous carbon disk electrode was bound. The counter electrode and reference electrode are all carbon and printed on a filter paper. The filter paper was soaked with sulfuric acid. The essential feature of this sensor is that there exist diffusion barriers for gas shown as 1, 2, 3, and 4. After the barriers, the gas permeates through porous Teflon membrane to make contact with porous carbon working electrode. The carbon electrode is on the one face of the filter paper which holds electrolyte. On the opposite face of the filter paper, counter and reference electrode is bound to the surface of the filter paper. The structural motif of the sensor is the filter paper, matrix holding electrolyte, and three electrodes on each side of the filter paper. The sensor is operated at atmospheric pressure. Since the gas permeable electrodes and diffusion barrier are all porous, the pressures of the inside and the outside of the sensor are identical. However, in our developments that deals with arsine generated from a 30 mL vial, the pressure difference between the outside and the inside of the sensor was high and it had to be dealt with. This was because  $\text{AsH}_3$  generator and the sensor were connected in a sealed system. The commercial sensor was just exposed to the air and there was no transfer line for the analyte gas.

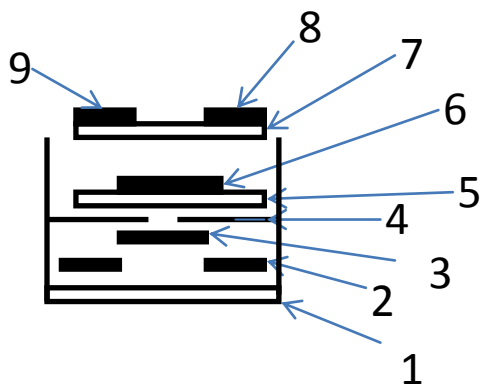


**Figure 2.5.1 Schematic of a commercial sensor. Numbers indicates: wool (1), holder with a pinhole (2), carbon filter (3) , plastic case with holes (4); Teflon membrane (5), carbon electrode (6), filter paper with electrolyte (7), carbon electrode as counter electrode (8), carbon electrode as reference electrode (9)**

The sensor contains acidic electrolyte which is not known due to proprietary rights claimed by Nemoto. In many published journal articles, if not all, each working electrodes was fabricated in special ways, which hardly can be duplicated in academic institutes. However, Nemoto kindly provides about two dozens of electrochemical cells to us which could be reconstructed for our research purposes. We figured out that even after removing the existing electrolyte with different electrolyte from our own laboratory, the electrochemical cell was functioning well as expected. The CV and CA demonstrated usual behavior of functioning electrochemical cell. Therefore, we always could replace the original electrolyte with one with desired property, hopefully, organic and ionic liquid type in an hope that we turned this into a arsine sensor. However, we never succeeded in adapting this cell as arsine sensor because of various reasons explained in Chapter 4.

We performed cyclic voltammetry and chronoamperometry experiments to see if we can reconstitute electrolyte at our own will, and the results were encouraging. Figure 2.5.2 Schematic of typical gas sensor experiments for arsine. The arsine was generated by

reducing agents. Numbers indicate: diffusion barrier (1), working electrode (2), filter paper (3), counter electrode (4), reference electrode (5) acidic media containing arsenic (6), syringe containing  $\text{NaBH}_4$  (7), Teflon tubing (8). schematically shows the general construction of the tried sensor. In all experiments, we produced arsine with  $\text{NaBH}_4$  or Zinc. For Zn, we put powder form of Zn inside the sample whereas for  $\text{NaBH}_4$ , we added the solution of it to generate arsine. Zn is known to produce hydrogen gas more slowly than  $\text{NaBH}_4$ , and less amount at given time compared to sodium borohydride. We suspected whether the less interference from hydrogen gas increases the sensitivity of arsine sensor. The commercial cell has carbon fiber as working electrode and very highly sensitive to hydrogen as described in manufacturer's manual. Although originally developed for CO sensor, this sensor has roughly 50 % sensitivity to hydrogen compared to carbon monoxide. We used different type of hydrophobic gas permeable membrane to see if the effect of pore size of the membrane could play crucial role in changing the shape and magnitude of current signal coming from amperometric sensor. However, using the Teflon membrane did harm rather than good. Because of the membrane, the arsine could not transfer to the cell efficiently.

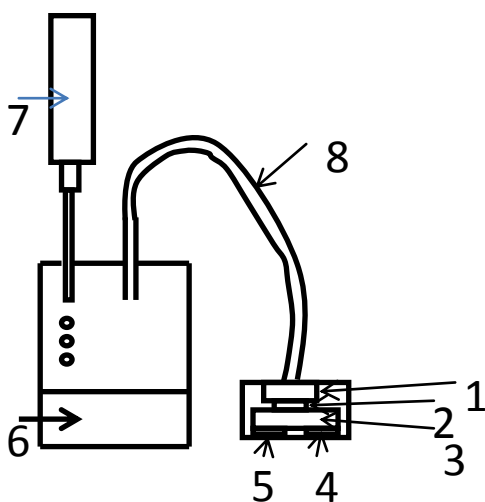


Figure 2.5.2 Schematic of typical gas sensor experiments for arsine. The arsine was generated by reducing agents. Numbers indicate: diffusion barrier (1),working electrode (2),filter paper (3),counter electrode(4),reference electrode (5)acidic media containing arsenic (6),syringe containing NaBH<sub>4</sub> (7),Teflon tubing(8).

## 2.6. The use of Zn as reducing agent

The motivation of using zinc as reducing agent comes from the complicated process of storing and preparing chemicals including NaBH<sub>4</sub> reagent. The preparation of NaBH<sub>4</sub> solution in 0.5 M NaOH requires analytical balance and accurate weighing of solid material. Even in the most developed countries, for example, in the states, such special instruments are not available in regular household and normal residential area. Considering the fact that stability of these reagents in aqueous solution is only 2 weeks, it is unlikely that the measurement from old chemical reagents will fall within the acceptable errors. There will be no one who is available to record the date of preparation and no one who follows the expiration date religiously. We have used Zn in place of NaBH<sub>4</sub> earlier stage of development process. Although we did not observe meaningful signal with Zn, it is impossible to say that Zn could not be used. Merely we indicate here

slow process of generating arsine from As(III) discouraged the use of Zn. If this would have been successful, paper strip with known amount of zinc powder could be provided and this is a good alternative to expensive NaBH<sub>4</sub>. Disposable paper strip with minimal amount of Zn reagents has definite advantage. This approach drastically reduced the amount of chemicals required for measurement. However, use of NaBH<sub>4</sub> has been satisfactory overall as the amount needed was only 2 mL of 2 % (v/v) in water. It is known to reduce As(III) and As(V) indiscriminately. Use of NaBH<sub>4</sub> obviates the need of complex operation involving KI and ascorbic acid for arsenate reduction.

## **2.7. Motivation for use of organic salts as electrolytes**

We used organic electrolyte as conducting medium such as propylene carbonate and various organic salts such as tetrabutyl ammonium perchlorate. A successful application of organic electrolyte is demonstrated by the Sensoric cell manufactured by City Technology. The Sensoric cell claims zero sensitivity up to 3000 ppmV of hydrogen. The manual merely states that they used propylene carbonate and inorganic salt.

The aqueous electrolyte has been extensively used but has been posing the problem of drying out the electrolyte, therefore as stated in section 1.7, we used nonaqueous electrolyte that resists evaporation. In ionic liquid, the water content can be much lower than 1 % and available hydronium ion can be dramatically small. In such case, hydrogen oxidation to hydronium ion will be negligible due to high overpotential needed to drive oxidation reaction in the absence of proton.

Thus, in organic media, the effective potential needed to be applied to oxidize hydrogen can be substantially higher than 0 V vs. NHE. This will lead to wider separation of oxidation potential between the arsine and hydrogen molecule. Change of activity coefficient also can dramatically shift the redox potential, which is expected when arsine and hydrogen is in contact with organic medium. From this view, it is very highly likely that anodic signal of hydrogen gas can be suppressed or effectively removed in organic electrolyte where negligible amount of water and hydronium ion is present.

### 3. CHAPTER THREE

#### 3.1. General Instrumentation

Electrochemical experiments require a good potentiostat which is ideally immune from noise. In order to digitalize the obtained data for storage and plotting in PC, one needs a data acquisition card. We purchased and used a generic data acquisition card from Measurement Computing Corporation (model number USB-1208FS). The data acquisition card has two DAC channels and 8 single ended ADC channels. For digital I/O, 5 VDC TTL logic signal, two 1 byte (8 bit) ports were provided. The commercial data acquisition card was powered by USB port of PC and this power was also used to supply power to the potentiostat analog circuit.

#### 3.2. Fabrication of Potentiostat

An electrochemical cell is excited by applying suitable wave forms. Excitation of the electrochemical system and recording of the cell response is performed with a potentiostat. We designed printed circuit board with extensive ground plane, i.e. copper pouring for amperometric gas sensing and it is illustrative to look at the generic potentiostat circuit in Figure 3.2.1 , which has been implemented in our first printed circuit board. For clarity, power supply lines are omitted. Operational amplifier such as OP97 draws negligible current on input pins and negative terminal and positive terminal maintain the same potential. In the first operational amplifier U1, positive terminal is

grounded and the negative terminal is virtual ground. Currents from  $e1/R1$ ,  $e2/R2$ ,  $e3/R3$ , and  $e4/R4$  are all added at S, summing point. The sum of these current should be almost zero as long as the operational amplifier has extremely high input impedance. The following relationship is established when all four resistors, R1, R2, R3, and R4 have the same resistance.

**Equation 3.2.1**

$$e1 + e2 + e3 + e4 = 0$$

Here we provide a schematic of the potentiostat circuit.

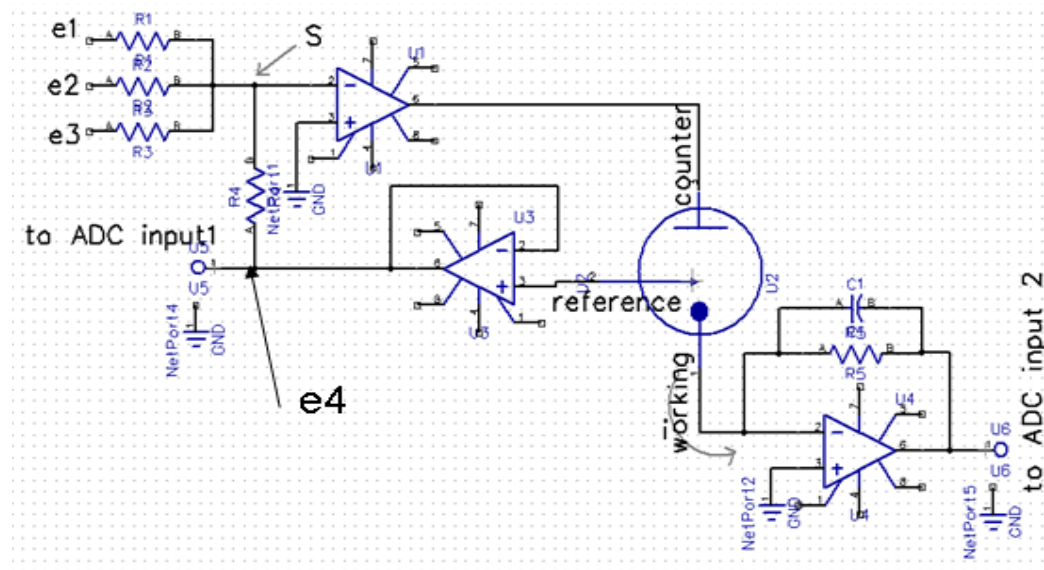


**Figure 3.2.1** Schematics of potentiostat circuit. The basic unit of modern potentiostat where all four currents from  $e1/R1$ ,  $e2/R2$ ,  $e3/R3$ , and  $e4/R4$  are added at the summing point, S. There is a potential follower, U3, with infinite impedance. U4 is current to voltage converter OpAmp where working electrode is virtual ground due to general requirement of OpAmp.

At summing point S, the potential is zero. The counter electrode is connected through electrolyte of cell to the reference electrode and exactly the same potential of reference electrode is the output of voltage follower U3. Therefore, the output of the U1

goes back to the input terminal of U1 itself via reference electrode and this forms a feedback circuit of U1. U1 is doing its best to make the potential at S zero. The voltage follower U3 draws negligible amount of current from the cell. If any one of e1, e2, and e3 varies, the U1 will adjust U1.6 so that via U3, Equation 3.2.1 holds true. If we look at U5 (ADC input 1), we observe the potential changes of reference electrode that makes electrical contact with the counter electrode through conducting electrolyte. The working electrode is grounded, so the potential of working electrode vs. reference electrode is  $-V_{ref}$  when  $V_{ref}$  is potential of reference electrode vs. ground. The electrochemical reaction generates movement of electrons on the surface of working electrode, amplified on U4 as this is the current-voltage converter.

The picture of actual potentiostat circuit is shown in Figure 3.2.2.

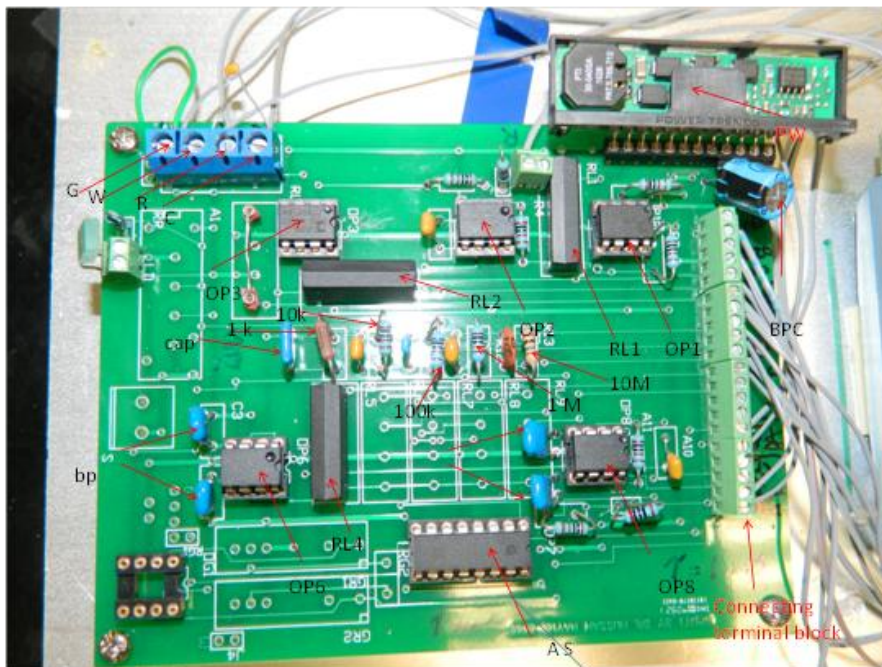


Figure 3.2.2 Potentiostat circuit board used in this work. Legends are described in Table 3.2.1.

The components of the printed circuit board are described in Table 3.2.1.

**Table 3.2.1 Table of electronic components used for the potentiostat circuit**

Component	Function	Description
OP1	Operational amplifier	OP90,
OP2	Operational amplifier	OPA604AP
OP3	Operational amplifier	OP90
OP6	Operational amplifier	OPA604AP
OP8	Operational amplifier	OP90
AS	Analog switch	ADG441BN,
RL1	Single pole single throw-normally open	HE3621A0500, Hamlin, 1 ms
RL2	Single pole single throw-normally open	HE3621A0500, Hamlin, 1 ms
RL4	Single pole single throw-normally open	HE3621A0500, Hamlin, 1 ms
PW	Power supply	PT5061N
1k	Resistor	1 k $\Omega$ in parallel with 1 $\mu$ F, 1 ms
10k	Resistor	10 k $\Omega$ in parallel with 0.1 $\mu$ F, 1 ms
100k	Resistor	100 k $\Omega$ in parallel with 0.01 $\mu$ F, 1 ms
1M	Resistor	1M $\Omega$ in parallel with 1 nF, 1 ms
10 M	Resistor	10 M $\Omega$ in parallel with 0.1 nF, 1 ms
G	Ground	grounded to the case
W	Working electrode terminal	
R	Reference electrode terminal	
C	Counter electrode terminal	
BPC	Bypass capacitor	10 $\mu$ F

In order to vary the gain of current to voltage (i/v) converter, we used an analog switch (AS) in the board. In Figure 3.2.1, we use only one resistor (R5) and capacitor (C1) for converting current to voltage. However, we want to use different resistor as well for different gain. Therefore, four different resistors can be connected through analog switch and one can select one resistor among four to get different level of gain. The picture shows the four digital I/O input terminals, i.e. IN1, IN2, IN3 and IN4 for this

device. We send out different bits to these input terminals and had the current to voltage converter to amplify the current to a different range of voltage.

ADG441 chip reads the value in each terminal and D and S is either close or open circuit. When the input voltage at IN1 is 0, the S1 and D1 becomes short circuit and when IN1 is at 5 VDC, S1 and D1 is open circuit. This is counter intuitive, but the chip is designed in this manner. The reverse of this logic is used in ADG 442 where when input is at 5 VDC, the source (S) and drain (D) is short circuit. The screw terminal 11 is connected to IN1, terminal 12 to IN4, terminal 13 to IN3, and terminal 14 to IN2. Digital logic 1 ( 5 VDC in this case) on each input terminal, makes Dx and Sx open circuit. Digital logic signal 0 makes Dx and Sx short circuit where x is 1,2,3, or 4.

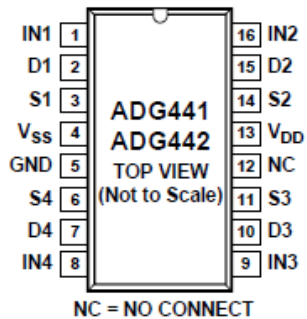


**Figure 3.2.3 Analog Switch(AS), ADG441, used on our board. When IN1 is high ( 5 VDC) for digital logic. S1 and D1 is open circuit, i.e. broken. When IN1 is low ( 0VDC), S1 and D1 is short circuit, i.e. closed. ADG442 follows the reverse logic.**

For the gain control, we used an analog switch, ADG 441 from analog device which is connected to PORT A of the data acquisition card. Not all bits of digital I/O PORTA were used and only 5 bits of the card was used to get different gain from

operational amplifier with inverting configuration. The following table shows the PORT A bit in decimal numbers and binary number for different gains.

**Table 3.2.2 Bit of PORTA to select different gain of i/v converter**

PORT A in decimal/binary	Feedback resistor, $\Omega$	Gain
31/11111	10 k	1
30/11110	100 k	10
26/11011	1 M	100
22/10111	10 M	1000

More elaborate design was implemented and detailed discussion is included in Appendix 5.2. To remove noise from the signal, we connected capacitor to each resistor which gave *c.a.* 10 ms time constant. For example, for 10 k $\Omega$  resistor, we had 1  $\mu$ F capacitor, i.e.  $10 \times 10^3 \times 1 \times 10^{-6} = 0.01$  s. The counter and reference electrode were connected to the system by turning on normally open relay and the digital logic was controlled from PORT B of the card. The lowest digit in PORT B,  $2^0=1$  was used to connect the counter electrode. When this bit was off, there was no counter electrode connected to the electrochemical cell and the potential is measured from ADC input 1. ADC input 0 was used to measure the voltage amplified from the feedback resistor. DAC 0 was used to send out input voltage for cyclic voltammetry and chronoamperometry. The data acquisition card came with voltage reference of 2.4 V and this was used to synthesize the necessary voltage in the adder operational amplifier. The fourth bit of PORT B,  $2^3=8$  was used to turn on the relay connected to the peristaltic pump that adds reductant to arsine generator vial. Digital to analog converter in this instrumentation was

a 12 bit DAC. The DAC had 0 to 5 VDC range and therefore, 1.2 mV is the bit resolution. Ideally, if there was no noise from the board, 0.0244 % of the full scale is the noise due to limitation in the number of bits in 12 bit ADC. However, this cannot be realized in the real world. We measured the noise by running voltage ramp at 100 mV/s in Figure 3.2.4. We fabricated another potentiostat with extensive copper pouring or ground plane and a multiplexer was used for different gain control. Detailed depiction of circuit design is provided in section 5.2 in appendices.

Our i-V ( current to voltage) converter,  $\pm 10 \mu\text{A}$  current was amplified to  $\pm 10 \text{ V}$  by 1 M $\Omega$  resistor which was read by 12 bit ADC. The bit resolution of 12 bit ADC for  $\pm 100 \mu\text{A}$  full scale was 48.8 nA, which was sufficiently precise for our work. Normally much higher noise from the potentiostat circuit board was observed. In order to estimate the noise level solely from the potentiostat circuit excluding the electrochemical cell, we connected 10 k $\Omega$  resistor between working electrode and counter electrode with reference electrode shorted to counter electrode. The voltage was scanned from +500 mV to -500 mV at the scan rate of 100 mV/s to record a straight line. The graph in the following shows the noise level of this potentiostat circuit by running voltage ramp on 10 k resistor in this work. Here voltage ramp means that voltage was increased from -500 mV to 500 mV at 100 mV/s, and then decreased back to -500 mV. In this dissertation, negative current is shown with positive potential, following non-IUPAC convention which is used in the textbook, *Electrochemical methods: fundamentals and applications*, 2<sup>nd</sup> edition by A. J. Bard and L. R. Faulkner. IUPAC convention is opposite to our convention. At positive potential, the current is supposed to be positive too. However, in this work, we

take negative sign for oxidation ( anodic) current and positive sign for reduction (cathodic) current.

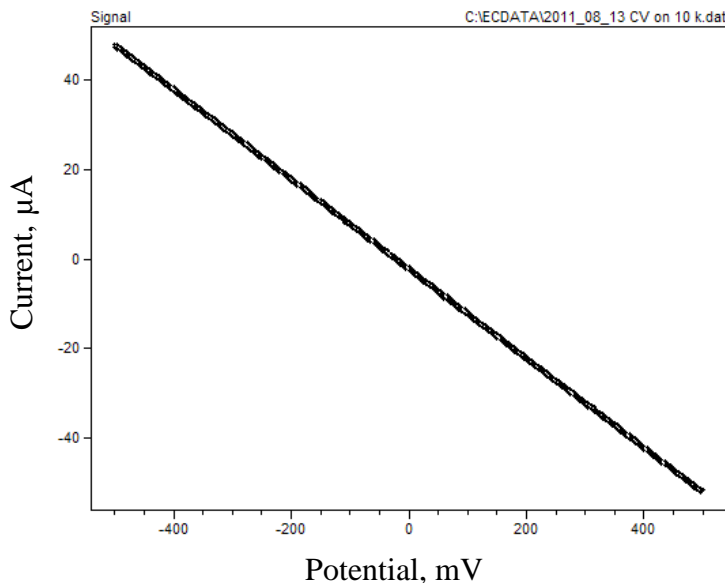


**Figure 3.2.4** Voltage scan on 10 k $\Omega$  resistor with the potentiostat. Voltage was scanned from -500 mV to 500 mV at the scan rate of 100 mV/s. The current linearly moved from -50  $\mu$ A to 50  $\mu$ A.

The straight line shows the slope of 9.9688 with standard error of  $\pm 0.09156$  and intercept of -26.0985 with standard error of  $\pm 0.133$   $\mu$ A. Therefore, when the measurement was made in the full scale range of  $\pm 100$   $\mu$ A, we had error of  $\pm 0.133$   $\mu$ A. Therefore, 0.133 % of the full scale range is the error of measurement. Uncertainties in DAC such as bit resolution and electrical noises propagate into the ADC through the adder logic in the summing point. This is the estimation of error associated with instrument itself. The electrochemical cell is not a resistor and there is noise from the electrochemical cell. Thus, the error reported in here is the minimum and the errors in the actual measurement are greater than 0.133 %.

To deliver  $\text{NaBH}_4$  at a constant rate, we used a peristaltic pump. The peristaltic pump ( Instech, model no.: P720/66) should be operated during a specific time period. Typically, we wanted to turn on the pump between 120 s and 240 s, so we counted time with our software until the time reached 120 s and turned on the pump. We counted time until time reached 240 s, and turned off the pump. This was achieved by using a single pole single throw relay. More specifically, a solid state relay (Sharp, S202 TY202 TY2, S) was controlled by a bit of PORB B in MCC data acquisition card. The 5 VDC digital output from the MCC data acquisition card was connected to  $1\text{k}\Omega$  resistor to supply 1 mA for opto relay activation. The peristaltic pump was operated at the flow rate of 1 mL/min.

### **3.3. General experimental procedure**

This section describes general chemicals and materials. Each experiment has its own additional material and method section to clarify how these chemicals and materials were used to conduct each experiment. These are described in respective sections. When no specific description is provided, the chemicals and material listed here were used.

In this work, the sign of current follows non-IUPAC standard as mentioned in the general instrumentation section. Unless specifically mentioned, non-IUPAC convention was followed.

#### **3.3.1. Chemicals**

All chemicals used in this experiment are guaranteed reagents (GR) suitable for use in the chemistry laboratory which meet or exceed American Chemical Society (ACS) requirements where required. Standard stock solutions of As(III) were prepared at concentrations of  $1000\ \mu\text{g/L}$  using sodium arsenite ( $\text{NaAsO}_2$ , Baker & Adams). In most

cases 2.5 M H<sub>2</sub>SO<sub>4</sub> was used for dilution of stock solution immediately before use. The 2.5 M H<sub>2</sub>SO<sub>4</sub> solution was prepared from concentrated H<sub>2</sub>SO<sub>4</sub> (95–98% ACS Reagent, Sigma Aldrich). Assuming that H<sub>2</sub>SO<sub>4</sub> is 18 M, 69.4 mL of the concentrated sulfuric acid was dissolved in 500 mL of DI water. The reducing agent, 2% NaBH<sub>4</sub> solution for hydride generation, was prepared from sodium borohydride (sodium tetrahydroborate, NaBH<sub>4</sub>, 99% reagent plus, Sigma Aldrich) dissolved in 0.5 M NaOH prepared from solid sodium hydroxide pellets (NaOH, Amresco). Typically, 20.0 g of NaOH was dissolved in 1.0 L of DI water. NaOH was used to stabilize the borohydride.

Silver nitrate (AgNO<sub>3</sub>) was dissolved in 0.5 liter of 18 MΩ DI water using a 0.5 liter volumetric flask to prepare 10 mM silver nitrate solution. The silver nitrate container was wrapped with black electrical tape to shield light to keep it under complete darkness.

Prior to use, quality of laboratory DI water was monitored with TDS meter (model no.: TDS-4M, HM Digital, Inc.) and the meter always showed 0 ppm for D.I. water obtained from water purifier (Hydro Service and Supplies, Inc., 513 United Drive, Durham, NC 27713). Deionized water from room 402 in Science and Tech 1 building displayed 95 ppm which was not suitable for electrochemistry. The reducing agent, 2% NaBH<sub>4</sub> solution for hydride generation, was prepared from sodium borohydride (sodium tetrahydroborate, NaBH<sub>4</sub>, 99% reagent plus, Sigma Aldrich) dissolved in 0.5 M NaOH prepared from solid sodium hydroxide pellets (NaOH, Amresco). Stock solution of 10 mM silver nitrate (certified A.C.S. grade, Fisher, cat. No. S181-100) was prepared in laboratory deionized water. Solutions of 100 mM tetraethylammonium perchlorate (Sigma Aldrich, cat. no.: 86646, electrochemical grade), and tetrabutyl ammonium

hexafluorophosphate (Sigma Aldrich, 86879-25G, electrochemical grade) in propylene carbonate (Sigma Aldrich, 414220-1L) were prepared as electrolyte. Solution of 10 mM potassium iodide (Sigma Aldrich, cat. no. 221945-500G, ACS grade) in DI water was prepared and appropriate concentration (typically 20 mM) of iodine (Sigma Aldrich, cat. no. 207772-5G) in DMSO (Fisher, D-128, ACS) was prepared.

### **3.3.2. Materials**

A commercial CO sensor, NAP-505 from Nemoto (1610-2 Higashi-Ohashi, Ishioka-shi, Ibaraki-ken 315-0031, Japan) was purchased and its detailed internal geometrical structure was studied in introduction section of this dissertation. In section 4.1, for amperometry experiments, we modified a commercial cell purchased from Nemoto, i.e. cell A, B, and C in section 4.1. A 6-way gas-sampling valve (Upchurch Scientific, cat. no. V-450) was used to inject gas to the cell. In the loop experiments, Each end of Teflon transfer line (1/16" od, 0.03" id) was connected to the generator vial to a 6-way gas-sampling valve. In the inject position, the content of the loop with 680  $\mu$ L internal volume was delivered to the cell. The injector in the load position allows a slow stream of air to flow through the cell. For modified commercial cell C, to generate hydrogen gas, 312 mg of Zn granule (Aldrich, cat/no. 243469-500G, ACS reagent) was added to a solution of 5.0 mL of 5.0 M sulfuric acid in 20.0 mL vial, while the mixture was stirred by a magnetic stirrer. CV was performed to observe electrochemical signal response of the cell when hydrogen was generated by reacting 430 mg of Zn with 2 mL of 5 M sulfuric acid (see Figure 4.1.3).

In section 4.2.1, Plexiglas material from compact disk (CD) case was used for the cell body and a filter paper was inserted between two coiled silver wires. A square shaped filter paper from Schleicher and Schuell (5.08 x 5.08 x 0.69 mm) was soaked with 1 mL of 10 mM AgNO<sub>3</sub>. Also circular disk filter papers ( Whatman no 4) were used (0.17 mm in thickness, 27.40 mm in diameter). Silver wire had diameter of 0.41 mm and length of 10 cm and was coiled three times.

Gold wire was purchased from Alfa Aesar ( cat. no.: 10968, lot no. L16W035, 0.1 mm diameter, 99.998 % pure) and cut to be placed on syringe filter. The gold wire with 100 µm in diameter and 20 cm in length was used as a working electrode. Platinum foil was purchased from Strem Chem( cat. no. 78-0005, 0.025 mm thick, 25 mm x 25 mm) and cut as needed described in the individual experimental section. Ag/AgCl reference electrode was purchased from Chi instruments ( cat. no. CHI111P). The reference electrode was immersed in 3 M KI solution when not in use. Carbon fiber was made from unidirectional fiber cloth ( cat. no. RPA-TC09U12 12) purchased from James Town distributor.<sup>40</sup> Silver fabric electrode was purchased from less EMF Inc. ( high performance silver mesh fabric, cat. no. A1222) and was cut to a square (1.5 cm x 1.5 cm).<sup>41</sup> The material was made to shield electromagnetic interference and examined with open circuit potential experiments. For amperometry on syringe filter, filter papers ( Whatman no 4) were cut to disks by a pair of scissors ( 0.17 mm in thickness, 27.40 mm in diameter). After the filter paper was soaked with 50 µL of 30 mM KI in DMSO, it was inserted between counter and working electrode. The syringe filter was made from

---

<sup>40</sup> <http://www.jamestowndistributors.com>,

<sup>41</sup> <http://lessemf.com>

commercial syringe filter (Cole-Parmer, part no. F2602-1, NYLON + GL, 30 mm diameter, 0.2  $\mu\text{m}$ ). The syringe filter was cut in the middle and the membrane was removed. The thickness of the cell body was 2.5 mm and diameter was 32.18 mm. The female Luer port in the middle was connected to the arsine gas transfer line.

### **3.3.3. Electrochemical characterization of silver fabric electrode with Ag/AgI system**

We needed to characterize the silver fabric electrode to see if it could be used as a silver electrode. This was important as the silver fabric purchased from less EMF Inc. was not rated for electrochemical experiments and there could be other electroactive metal impurities in the silver coated fabric. We examined the silver fabric with two different electrolytes, first with KI and  $\text{AgNO}_3$ . In the first examination, when the silver fabric electrode is immersed in 100 mM KI solution, the equilibrium Nernst potential is given by the following equations:

**Equation 3.3.1**

$$E = E_{\text{Ag} / \text{AgI}} - E_{\text{Ag} / \text{AgCl}}$$

**Equation 3.3.2**

$$E = E_{\text{Ag} / \text{AgI}}^{\circ} - 0.0591 \log[I^{-}] - 0.222$$

**Equation 3.3.3**

$$E = -0.152 - 0.0592 * (-1) - 0.222 = -0.315$$

In this experiment, working electrode was silver fiber and reference electrode was Ag/AgCl. And also Pt counter electrode was used as we apply small potential such as 0 V initially to observe the signal. This 0 volt signal was applied for 2.5 seconds between the counter and reference electrode and when the counter electrode was disconnected from the circuit, we measure the potential of difference between reference electrode and the

working electrode ( silver fabric in this case) and plot the potential,  $E = E(\text{working}) - E(\text{reference})$ . The equilibrium potential was observed to see how the equilibrium potential was reached. The volume of electrolyte used was 10 mL. The three different concentrations of potassium iodide solution was made; 1 mM and 10 mM , and 100 mM. The graphical overlay of three measurements is plotted in the picture below.

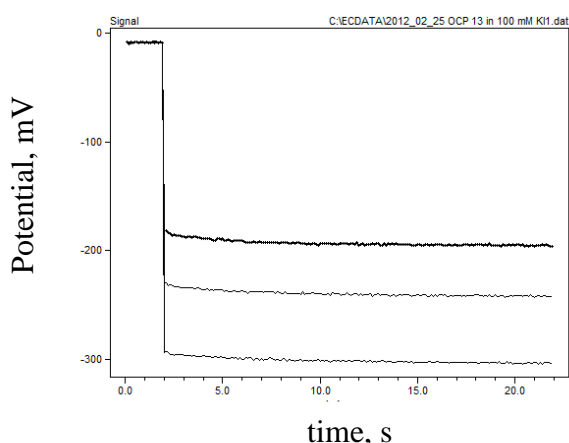


**Figure 3.3.1 Open circuit potential between silver fabric vs. SSC. Open circuit potential is logarithmic function of  $[I^-]$ . The  $[KI]$  used were as follows: Top line: 1 mM , Middle: 10 mM , Bottom: 100 mM Initial potential of 0 mV was applied.**

In 20 s, the potential reached the equilibrium potential. This quickly convinced us that the silver fabric electrode was indeed silver. And the silver fabric material shows very fast response to the iodide concentration. A table of numerical results of the open circuit potential measurement is provided along with error from the theoretical potential. This kind of error could be easily introduced while one prepared the electrolyte solution.

Log(KI), M	Measured, mV	Calculated, mV	Errors, mV
-1	-194	-196.7	2.7
-2	-240	-255.8	15.8
-3	-301.2	-314.9	13.7

Also, theoretical nernstian potential was plotted along with measured potential for clarity. The line marked with square is the theoretical line and the line marked with diamond is the measured potential.

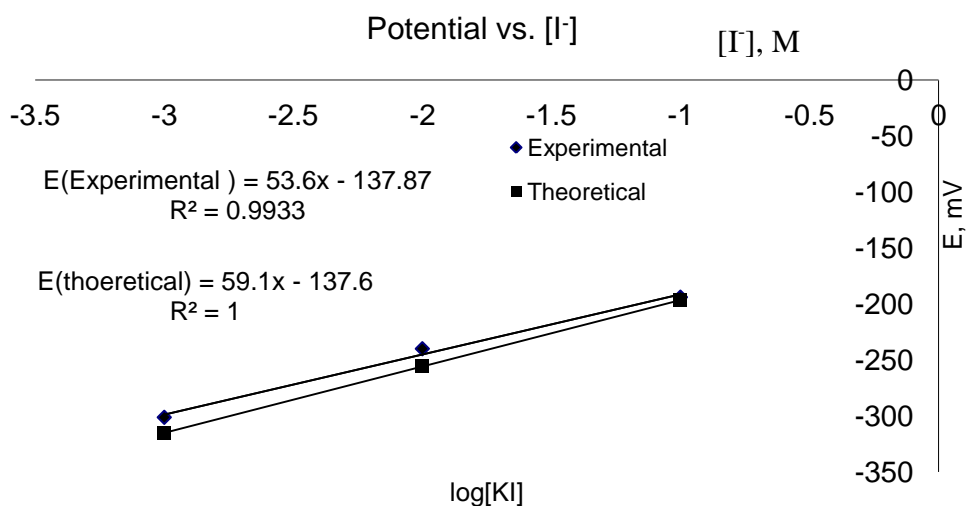


Figure 3.3.2 Plot of potential vs. log[KI]. Nernst potential measured and calculated are overlaid.

In the second test, the silver fabric was also examined in 10 mM AgNO<sub>3</sub>. The measured equilibrium potential of Ag/Ag<sup>+</sup> in the three electrode system cell was 434 mV,

which was in good agreement with theoretical potential of 457 mV using Nernst equation. The following equations show the calculation.

**Equation 3.3.4**

$$E = E_{Ag/Ag^+} - E_{Ag/AgCl}$$

**Equation 3.3.5**

$$E = E_{Ag/Ag^+}^o + 0.0591 \log[Ag^+] - 0.222$$

**Equation 3.3.6**

$$E = 0.7992 + 0.0592 * (-2) - 0.222 = 0.459$$

The graph of open circuit potential is shown below.

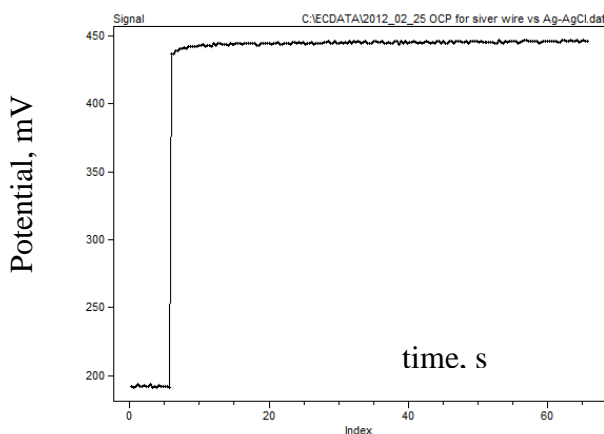


**Figure 3.3.3 Measurement of open circuit potential of silver fabric vs. SSC. Initial potential of 200 mV was applied for 10 sec and the counter electrode was disconnected to measure the equilibrium potential of silver fabric.**

These two short experiments proved that the silver fabric could be used as silver electrode and therefore, we continued to use it as silver electrode in development of this sensor and it was safe to assume that the electroactive redox couple in the system is Ag/AgI.

### 3.3.4. General amperometric experimental procedure with thin layer cell.

Suitable materials such as gold, Pt, and carbon electrode were used as working electrode from section 4.6 to section 4.12 . A disk of filter paper with suitable electrolyte was inserted between the working electrode and the counter electrode and the cell was tightened by various mechanism specified in individual section. Typically, filter papers ( Whatman no 4) were cut to disks by a pair of scissors (0.17 mm in thickness, 27.40 mm in diameter). After the filter paper was soaked with suitable electrolyte, it was inserted between counter and working electrode. When the syringe filter was used as a cell body to hold the electrodes and filter paper, a commercial syringe filter ( NYLON + GL 0.2  $\mu\text{m}$ ) was cut in the middle and the membrane inside was removed. The thickness of the cell body was 2.5 mm and diameter was 32.18 mm. The female Luer port in the middle was connected to the arsine gas transfer line. When all components were assembled, the cell was secured by paper clips or bolts. The dimension of the generator glass vial was 70.24 mm in height and 20. 69 mm in outer diameter and the internal volume of the generator was 15 ml. Typically, a solution of 1 or 2 %  $\text{NaBH}_4(\text{w/v})$  was added between 120 s and 240 s. Specific times of addition of  $\text{NaBH}_4$  and stop time are mentioned in individual sections. Potential was usually held at 1.1 V vs. reference electrode. Otherwise, the potential applied is mentioned. Amperometric signal was recorded with the software written in this laboratory. An aliquot of 2 ml of a certain concentration of As(III) in 2.5 M sulfuric acid was used to generate arsine gas and the arsine gas was deposited on the filter paper. For blank experiments, 2 ml of 2.5 M sulfuric acid in water

was used. For integration of the anodic current response, depending on the time of  $\text{NaBH}_4$  addition and stop, integration during this time period was performed.

## 4. CHAPTER FOUR

### RESULTS AND DISCUSSION

In this section we present the results on the measurement of arsenic in aqueous media by electrochemical cells developed and described earlier. A flow chart of the development process is provided here with detailed discussion as follows.

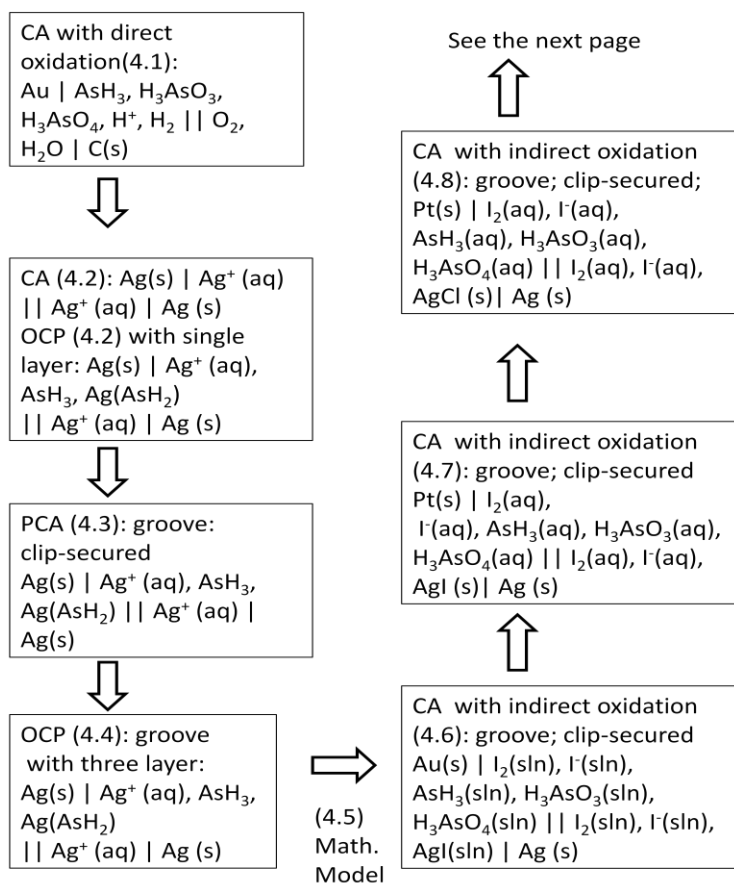


**Figure 4.0.1** Flow chart part 1 for development process. In this flow chart, the numbers in parenthesis are section numbers.

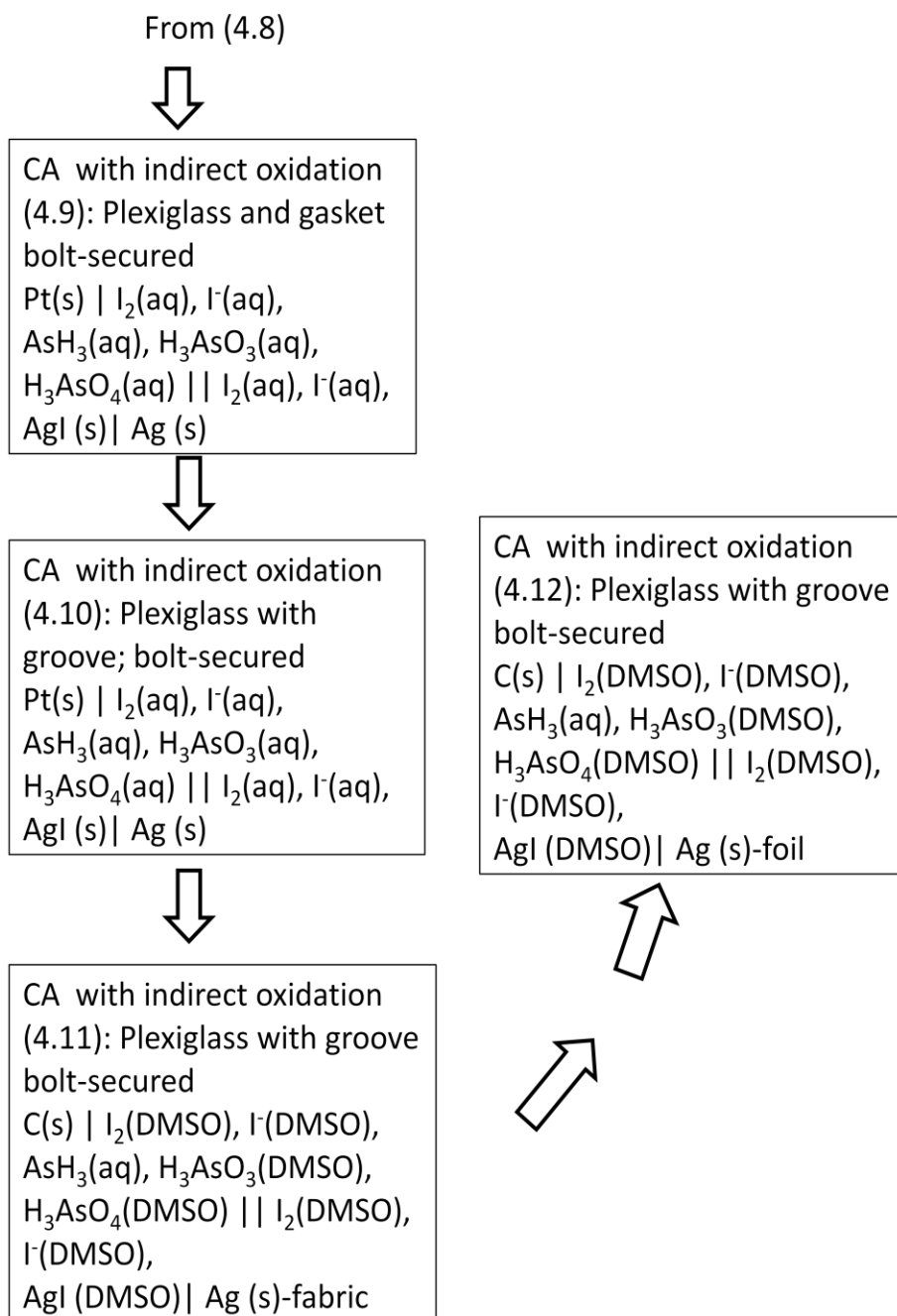


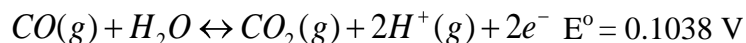
Figure 4.0.1 Flow chart part 2 for development process

#### 4.1. Direct oxidation of arsine to arsenious acid on modified commercial cells

We experimented with three different kinds of modified cells. These cells can be described as: Au / AsH<sub>3</sub>, H<sub>3</sub>AsO<sub>3</sub>, H<sub>3</sub>AsO<sub>4</sub>, H<sup>+</sup>, H<sub>2</sub> // O<sub>2</sub>, H<sub>2</sub>O / C(s).

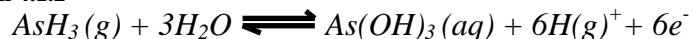
For the first one, cell A, we only replaced the carbon electrode with gold wire electrode. We still worked with aqueous acidic electrolyte in cell A. In cell B and C, we replaced the aqueous acidic electrolyte with organic salt in organic solvent as well as carbon electrode with gold. The idea came from the commercial CO sensor where the following electrochemical reaction occurs;

**Equation 4.1.1**



Arsine gas could also be detected in the same fashion. The commercial gas sensor is a new, low cost three electrode electrochemical cell designed for the detection and measurement of carbon monoxide in the range 0-1000 ppmV, in domestic carbon monoxide detectors, fire detectors and air quality monitors. Instead of this reaction, we wished to achieve the following redox reaction introduced in section at the working electrode by applying a suitable voltage.

**Equation 4.1.2**



The porous carbon-ink printed disk electrode originally used by the commercial sensor showed a huge oxidation signal saturating the detector for hydrogen gas as shown later. It also had very high capacitance background. We aimed to eliminate this saturation by using a different electrode, which had been used to detect arsine in literature. Literature survey showed that gold had been used for this purpose. We

explored this idea only to find out that interference of hydrogen gas co-produced in reduction process of As(III) overwhelmed the detection system.

We modified the commercial cell and its detailed configurations are given in Table 4.1.1.

**Table 4.1.1 Electrochemical cell configuration of modified commercial electrode.**

Cell	Working electrode	Counter electrode	Reference Electrode	Electrolyte
A <sup>a</sup>	Gold wire <sup>b</sup>	Printed carbon electrode on the filter paper	Printed carbon electrode on the filter paper	50 $\mu$ L of 5 M sulfuric acid
B	Gold wire	Printed carbon electrode on the filter paper	Printed carbon electrode on the filter paper	50 $\mu$ L of 100 mM tetraethyl ammonium perchlorate in propylene carbonate
C	Gold wire	Printed carbon electrode on the filter paper	Printed carbon electrode on the filter paper	50 $\mu$ L of 100 mM tetraethyl ammonium tetrabutyl ammonium hexafluorophosphate in propylene carbonate

<sup>a</sup>Gas sampling loop was used.; Legends indicate: <sup>b</sup>1 cm long, 100  $\mu$ m in diameter

We characterize the unmodified commercial cell with double pulse chronoamperometry first. Then we injected H<sub>2</sub>(g) into the cell using gas sampling loop. The original commercial cell exhibited extremely high capacitance current as shown in Figure 4.1.1 . Therefore it prohibited the use of the cell as arsine sensor. The left panel in Figure 4.1.1 shows that the capacitance current of original NAP505. Double pulse chronoamperometry with 10 mV and -100 mV was conducted to observe the signal

response from the original commercial cell. The clipped region indicated by horizontal line in the beginning stage of each step shows that the signal went beyond  $\pm 1$  mA which are the limits of current to voltage converting amplifier. We replaced the original printed carbon ink electrode with gold wire electrode to observe signal response. The right panel in Figure 4.1.1 shows the current response with the same experimental parameters (10 mV and -100 mV). The following section describes the signal response of gold working electrode in acid and in organic electrolyte for the detection of arsine.

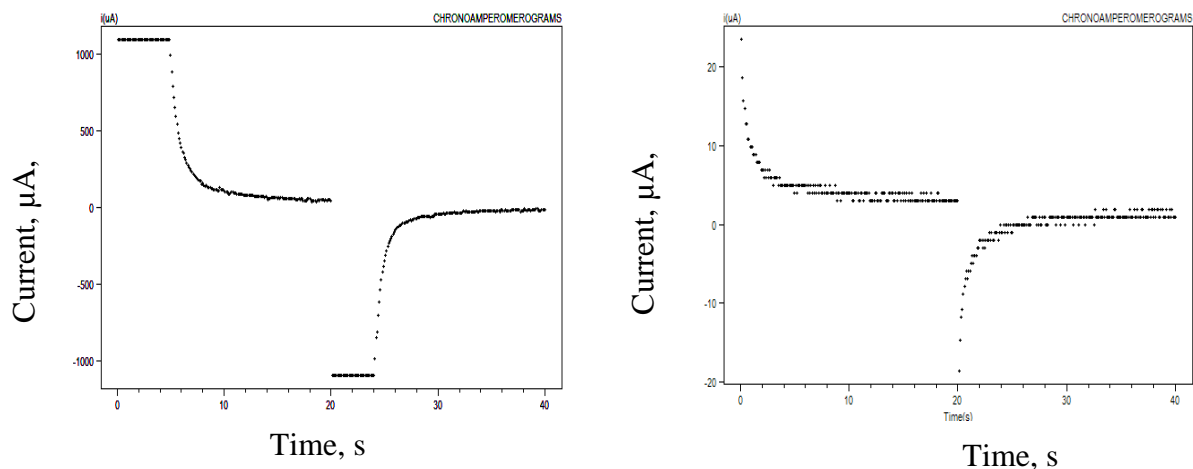


**Figure 4.1.1 DPCA of the unmodified commercial sensor and modified sensor. The left panel shows DPCA of the unmodified cell with high capacitance current. The right pane shows DPCA of modified cell with reduced capacitance current.**

Three different electrolytes were applied on a filter paper. The opposite side of the filter paper made contact with working electrode (Au). Either an aliquot of 1.0 mL of 0.7 %  $\text{NaBH}_4$  were injected to the vial from the standard solution or 200.0 mg of Zn granule were added to it for the generation of arsine and hydrogen gas.

The CV was performed in the presence of hydrogen gas and in the absence of hydrogen gas. Also double potential chronoamperometry experiment was performed in the presence of hydrogen gas to observe amperometric signal from the electrochemical cells. We had hoped to achieve low level of oxidation current of hydrogen by using neutral electrolyte.

#### **4.1.1. Chronoamperometry response from cell A**

In cell A in Table 4.1.1, hydrogen gas co-produced from the arsine generator produced signal that saturated the detector. In order to know how much interference occurred by this configuration, we injected known volume of hydrogen gas into the system. The 6-way gas sampling valve was switched from load to inject position at 90, 180, 340, and 500 s to inject hydrogen gas to the cell. A fairly constant signal was observed in a series of injections. The experiment had to be performed because the detector was saturated when the cell was exposed to hydrogen continuously. The integrated current, i.e. charge that flowed on the cell is  $2440.5 \pm 0.133 \mu\text{C}$ . We know from the error analysis of instruments, the error in measuring current is  $0.133 \mu\text{A}$ . Therefore, uncertainty in charge is  $0.133 \mu\text{A}$ . Modern PC measures time in millisecond precision, thus there is no appreciable error associated with time measurement. A powder of 312 mg of zinc can produce 4.77 mmols of hydrogen, which corresponds to 58.0 mL of hydrogen gas when ideal gas law is used to calculate the volume of the hydrogen gas at room temperature and at atmospheric pressure.

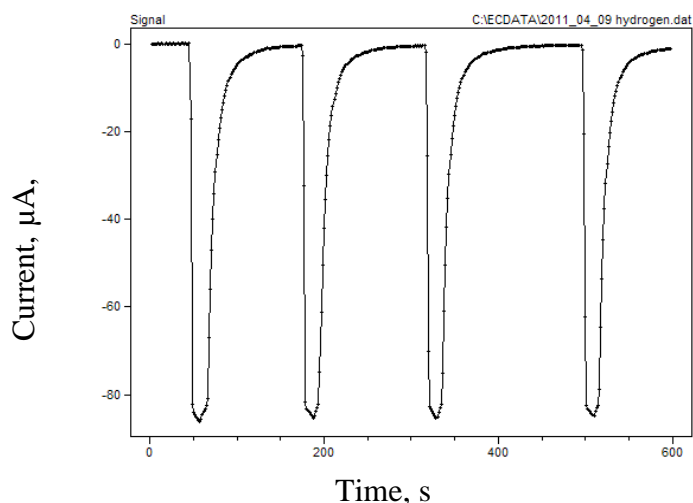


**Figure 4.1.2** Signal response of 680  $\mu\text{L}$  of hydrogen gas into the cell A. Reproducible anodic current indicates reproducible sample delivery by the sampling valve.

If we assume 100 % efficiency of the cell, 4.77 mmol of hydrogen gas can produce 920734 mC. We used only 1.16 % of the total hydrogen gas in this experiment and it already produced such a huge current. When 5 mL of 100  $\mu\text{g/L}$  of As(III) was present in the generator vial, the charge that will flow at 100 % efficiency is 3.863 mC. As the 1.16 % of the total hydrogen gas already produced 2.44 mC, 210 mC will be produced by hydrogen oxidation. The efficiency of the hydrogen gas oxidation is 0.0228 % and if the same efficiency of arsine oxidation occurs, the charge expected to flow on the gold electrode will be 0.882  $\mu\text{C}$ . Considering the uncertainties of  $\pm 0.133 \mu\text{A}$  with data acquisition system, observation of 0.882  $\mu\text{C}$  in the presence of 210 mC background charge is extremely challenging task. The hydrogen production process of zinc is very slow and took about 30 min to completely dissolve all zinc in the system. Therefore, the number will be further drastically reduced when we take it into account that the charge should be divided by a big number, 1800 sec to get current which is the observable.

#### 4.1.2. Chronoamperometry response from cell B

The cell B in Table 4.1.1 was characterized by cyclic voltammetry (CV). From

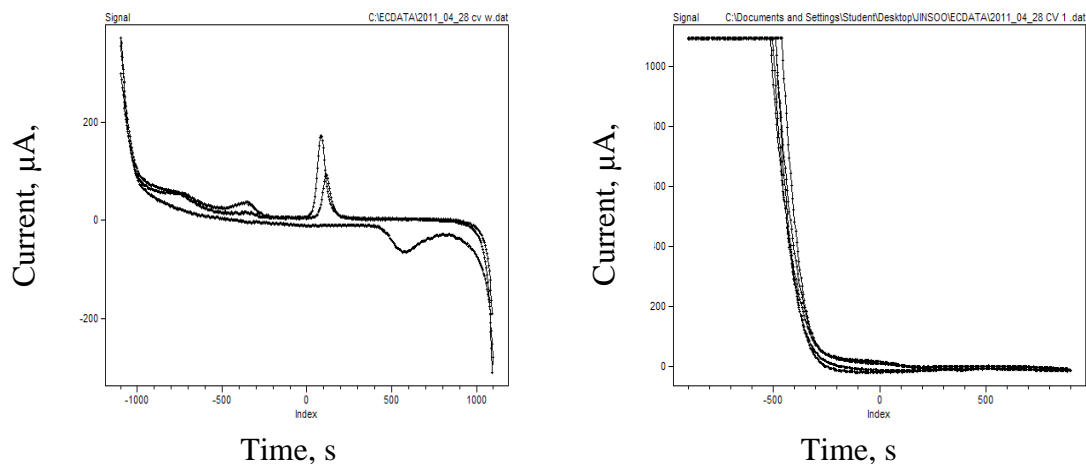


**Figure 4.1.3 CV of cell B in the presence of  $H_2(g)$  and in the absence of  $H_2(g)$ . (Left) CV of the cell B in the absence of  $H_2(g)$ : The cell was scanned with initial potential at 1100 mV to final potential at -1100 at the scan rate of 100 mV/s. The peak at 200 mV corresponds to the reduction peak of gold oxide in cathodic scan and a peak at 450 mV oxidation peak in anodic scan. At 1.1 V, oxidation of gold electrode was observed. (Right) CV of the cell B in the presence of  $H_2(g)$ : Reduction peak of gold oxide disappeared and the flat plateau was seen in the positive potential region.**

the observation made with the cell A in Table 4.1.1, it was necessary to monitor CV in the presence and absence of  $H_2(g)$ . The goal was to find the  $H_2$  oxidation current would disappear as predicted by the theoretical consideration. We discovered that the anodic current diminished in the presence of  $H_2$  as expected and the reduction current increased in the presence of  $H_2$ . The current responses are shown in Figure 4.1.3. Cyclic voltammogram of the same system in the presence of hydrogen gas was completely different from the one in the absence of hydrogen gas. The left panel in Figure 4.1.3 shows CV of cell B without any  $H_2$  and the right panel in Figure 4.1.3 shows CV when

H<sub>2</sub> is present in the cell. Around 500 mV, the reduction current was completely saturated with reduction of proton which was not seen in the absence of hydrogen molecules. In order to observe oxidation of arsine gas, we expected that current due to oxidation of arsine would be observed, which could be analytical signal of this system.

We were interested in observing oxidation current of AsH<sub>3</sub>(g) in the presence of H<sub>2</sub>, therefore, a sequence of potential step was applied to investigate the cell.

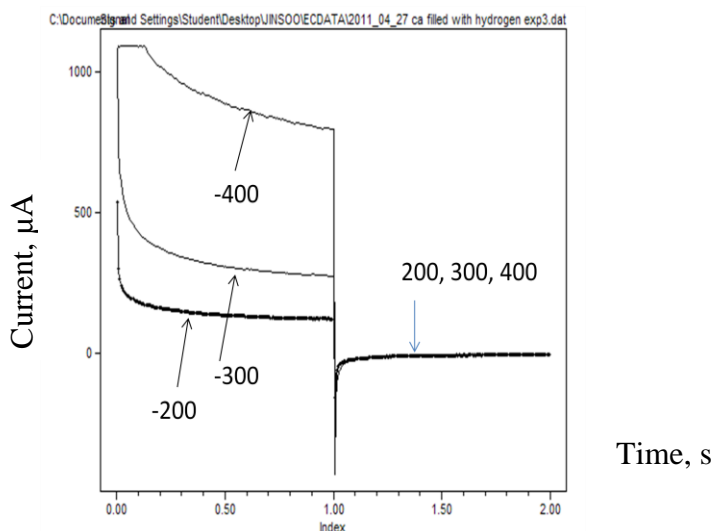


**Figure 4.1.4** Overlay of double potential step chronoamperometry with cell B of three different experiments with increasing potential steps. Double potential CA with +200/-200, +300/-300, and +400/-400 mV pulses were applied to observe increasing reduction current while hydrogen gas was generated. Numbers indicate potential applied to the cell. Negative potential was applied from 0 to 1 s and positive potential was applied from 1 to 2 s.

First, from time zero to 1 s, we applied negative potential, -200 mV and the resulting reduction current was observed. Then the positive potential, 200 mV was applied to see the current response in the presence of H<sub>2</sub>. The anodic current was negligibly small in all three experiments, where 200, 300, and 400 mV were applied. In the presence of hydrogen, magnitude of current was increased as the applied potential

increased as theory predicted. However, this did not match with increase in oxidation current. All anodic current overlapped with each other. This behavior was not observed with this cell in the absence of H<sub>2</sub>. The cathodic capacitance current and anodic capacitance current were the mirror image of each other in the absence of H<sub>2</sub> as shown in Figure 4.1.5.

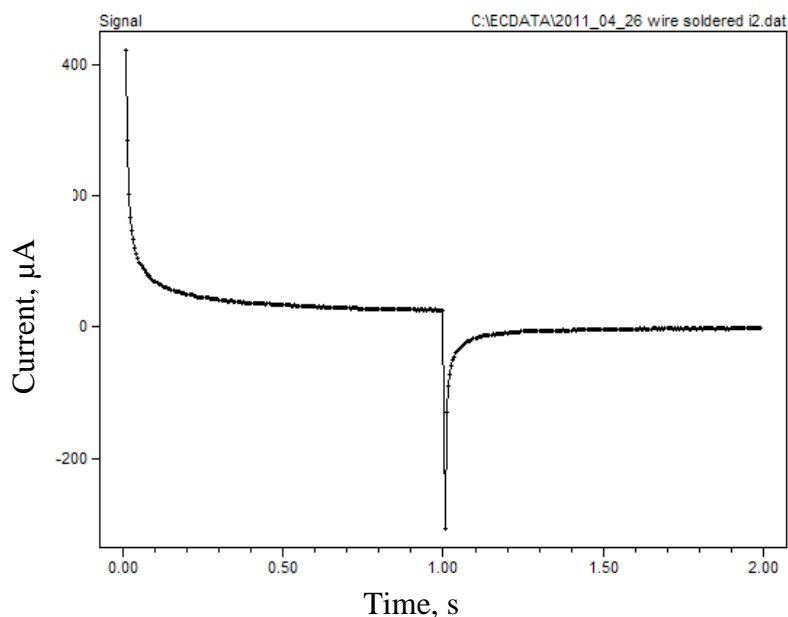
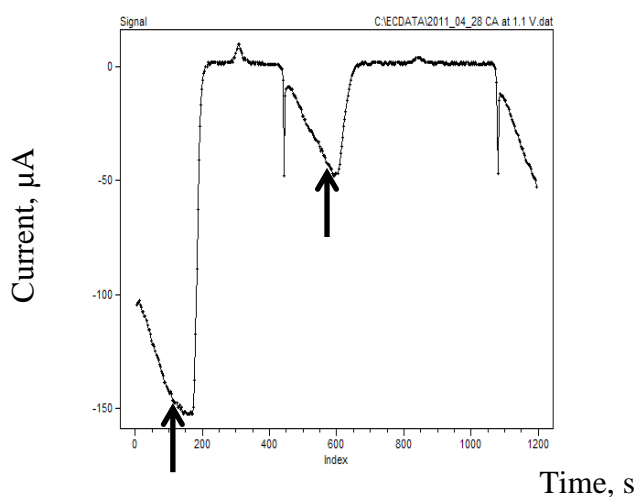


Figure 4.1.5 Double potential step chronoamperometry in the absence of H<sub>2</sub>.

There was dependence of cathodic current on potential applied. However, there was no dependence of anodic current on increase of potential. Although we did not see any interesting anodic wave on CV, we still explored amperometric signal response of the cell B in the following experiment. As the CA showed in Figure 4.1.6, at 1.1 V, oxidation current was observed. This motivated us to run CA at 1.1 V to see if there could be any

sign of detecting arsine gas at that potential. An aliquot of 2 mL of 5 M sulfuric acid and 200 mg of Zn granule was used to generate hydrogen gas in this experiment. The gold electrode was potentiostated at 1.1 V. At about 180 sec, H<sub>2</sub> was introduced to the cell, the signal went back to zero level when hydrogen was filling the cell compartment. After the cell was purged with air at 500 mL/min, the signal started to go down to the negative direction. At 600 sec, the air was stopped and hydrogen gas was



**Figure 4.1.6** CA of cell B at 1.1 V in the presence of H<sub>2</sub>(g). Arrows indicated the time point when H<sub>2</sub> was introduced. Immediately, the current response went to zero level. Spurious spikes were observed at ca. 450 s and 1150 s.

admitted to the cell. Then the cell went back to zero level. The zero current was observed in CV and the signal response matched the profile of CV. The cell did not exhibit oxidation signal at all, until the cell was purged with air again at 1100 seconds

### 4.1.3. Chronoamperometry response from cell C

In this section, we explored further the possibility of using organic electrolyte in organic solvent. We used 50 µL of 0.1 M tetrabutyl ammonium hexafluorophosphate in

propylene carbonate on the filter paper. A similar signal response of the cell resulted. The CV below showed similar electrochemical signal response of the cell C in Figure 4.1.7.

The current signal responded similar to the previous cell, cell B in Table 4.1.1

#### Electrochemical cell configuration

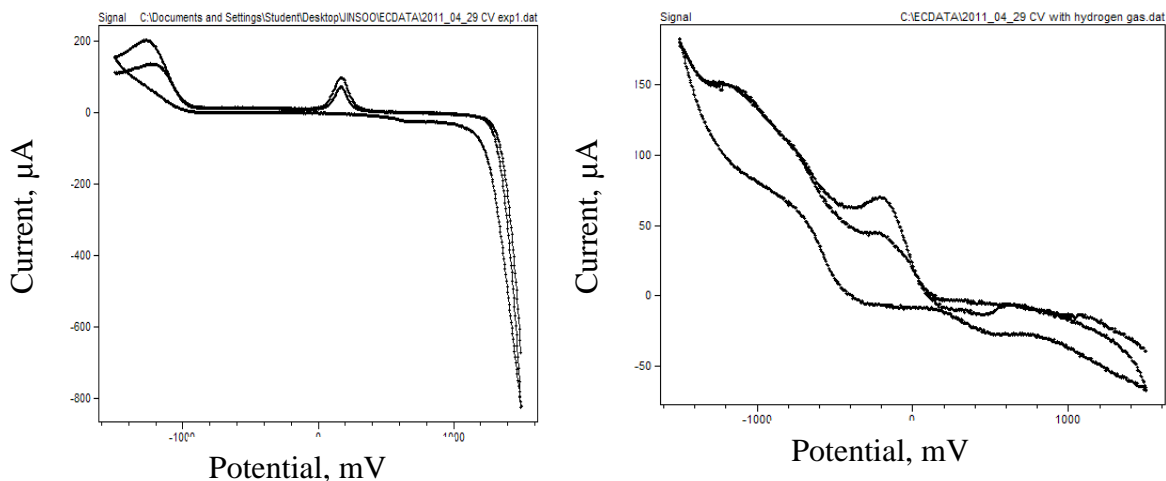


**Figure 4.1.7** CVs of the cell C in the presence and absence of  $H_2(g)$ . Potential initially moved from 1500 mV to -1500 mV at the scan rate of 100 mV/s. (Left) CV of cell C in the absence of  $H_2(g)$ . The gold oxide peak moved to more negative direction around 100 mV and large oxidation current due to gold to gold oxide above 100 mV was observed. (Right) Panel B: CV of cell C in the presence of  $H_2(g)$ . Diminished anodic current was observed when potential moved to positive direction.

At 200 sec and 600 sec , 1 mL of  $NaBH_4$  solution(0.7 % in 0.5 M NaOH) was added to the solution of 4 mL of 100  $\mu\text{g/L}$  As(III) in 2.5 M sulfuric acid. We observed that anodic current decreased. If arsine had been oxidized to arsenous acid and this would have been the dominant process, anodic current should have been observed. However, it did not move to more negative direction. In the absence of the  $H_2(g)$ , the gold electrode was oxidized at high positive potential as shown in Figure 4.1.7 . However, in the presence of  $H_2(g)$ , the gold oxidation was suppressed. To interpret these experiments, we refer to the

standard reduction potential of half reactions of gold in Table 4.1.2. Equation 4.1.9 indicated that gold can be oxidized at 1.3 V in the presence of water.

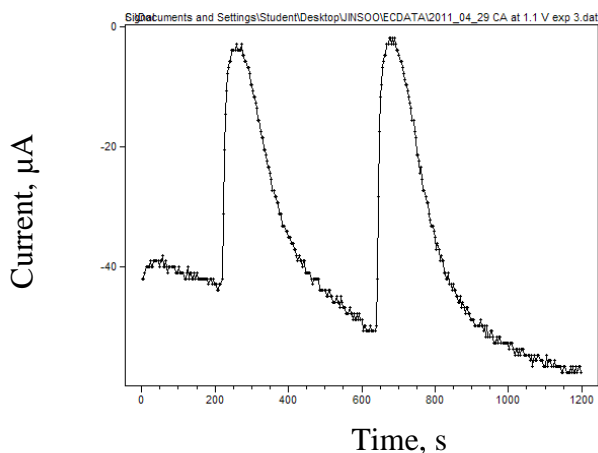
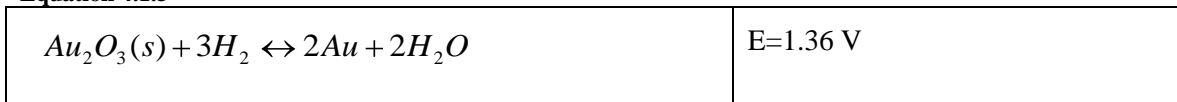


**Figure 4.1.8** Amperometric response of the cell C. Two times, the anodic current was decreased as a result of injection of  $\text{NaBH}_4$  solution.

The electrochemical cell was exposed to the ambient air and we assumed that we had water in organic solvents. Therefore, in this case, gold oxide formation was feasible process. However, when we had  $\text{H}_2(\text{g})$  in the system, we postulate that the following reduction process of gold took place.

**Equation 4.1.3**



This equation was derived from Equation 4.1.7 and Equation 4.1.9. The Gibbs free energy of this reaction is calculated,  $\Delta G = -nFE = -6 \times 96\,485 \text{ C mol}^{-1} \times 1.36 \text{ V} = -787.3 \text{ kJ/mol}$ . This large Gibbs free energy favors the reduction of gold oxide on the surface of the electrode. Hence, the removal of  $\text{Au}_2\text{O}_3$  from the surface of the gold electrode by  $\text{H}_2(\text{g})$  disfavors the oxidation of Au to  $\text{Au}_2\text{O}_3$ . This is the same logic behind

this experiment. We anticipated that removal of proton from the electrolyte would disfavor the oxidation of  $\text{H}_2(\text{g})$  to  $\text{H}^+$ . This explanation matches well with the annihilation of anodic current by the presence of  $\text{H}_2(\text{g})$  in Figure 4.1.8. The nice bell shaped diminishment curve on Figure 4.1.8 resembles the bi-exponential signal response function in chapter 4. The bell-shaped curve appeared twice as  $\text{H}_2(\text{g})$  entered the cell when reductant was injected into the 2.5 M  $\text{H}_2\text{SO}_4$  solution two times.

We performed chronoamperometry experiments to record oxidation current as we generated  $\text{AsH}_3$  using Zn without observing any perceptible signal response (data not shown here). Even if we did not get desired results, i.e. increase in anodic current in the presence of  $\text{AsH}_3$ , we sought to understand what electrochemical reaction took place. We speculated whether the oxidation of Au electrode was predominating process. Immediately after the chronoamperometry experiment, we verified the existence of gold oxide on the surface of working electrode with CV. As expected, a largest reduction signal of gold oxide was seen in the first scan in the range of -100 mV to -400 mV in Figure 4.1.9 and in the subsequent scans, the huge peak was gradually decreased and peak was shifted to 100 mV. The gold oxide formation was extensive after CA experiment with 1.1 V where we attempted to observe anodic current from 4 mL of 100  $\mu\text{g/L}$  As(III) standard. The anodic and cathodic peaks were well documented by Burke et al.<sup>42</sup>

---

<sup>42</sup> Burke, L.D.; Moran, J. M.; Nugent, P. F. Cyclic voltammetry responses of metastable gold electrodes in aqueous media. *Journal of Solid State electrochemistry*, **2003**, *7*, 529-538.

**Table 4.1.2 Standard reduction potential of half reactions of gold species.**

half reaction	$E^{\circ}$ , V vs. NHE
<b>Equation 4.1.4</b> $Au^{3+} + 3e^{-} \rightleftharpoons Au(s)$	1.498 <sup>a</sup>
<b>Equation 4.1.5</b> $AuOH^{2+} + H^{+} + 2e^{-} \rightleftharpoons Au^{+} + H_2O$	1.32 <sup>a</sup>
<b>Equation 4.1.6</b> $Au^{+} + e^{-} \rightleftharpoons Au(s)$	1.69 <sup>a</sup>
<b>Equation 4.1.7</b> $2H^{+} + 2e^{-} \rightleftharpoons H_2$	0.000 <sup>a</sup>
<b>Equation 4.1.8</b> $AuOH^{2+} + H^{+} + 3e^{-} \rightleftharpoons Au(s) + H_2O$	3.01 <sup>a</sup>
<b>Equation 4.1.9</b> $Au_2O_3(s) + 6e^{-} + 6H^{+} \rightleftharpoons 2Au + 3H_2O$	1.362 <sup>b</sup> , 1.51(calcd) <sup>b</sup>
<b>Equation 4.1.10</b> $AuO(s) + 2H^{+} + 2e^{-} \rightleftharpoons Au(s) + H_2O$	1.37 <sup>b</sup>
<b>Legends indicates:</b> <sup>a</sup> CRC Handbook of chemistry and physics. <sup>43</sup> , <sup>b</sup> Encyclopedia of electrochemistry of the elements <sup>44</sup>	

These behaviors were attributed to the metastable surface which could have been created during the manufacturing process of the gold wire electrode. The mechanical energy to deform the Au material can remain trapped in Au in the form of defects. The

<sup>43</sup> CRC Handbook of chemistry and physics, 93 edition, Hayes, W.M. table of electrochemical series, **2012-2013**, 5-80

<sup>44</sup> Schmid, G.M.; Curley-Fiorino, M.E., Chapter IV: Gold  
 In *Encyclopedia of electrochemistry of the elements*; Bard, A. J. Ed.; M. Dekker: New York, U.S.A., **1973**, p 94.

metastable metal surface explains well why the undesired oxidation and reduction peaks were observed in our work. Then screening Au electrode suited for arsine sensor is also a challenging task and maintaining the integrity of Au surface cannot be easily achieved.

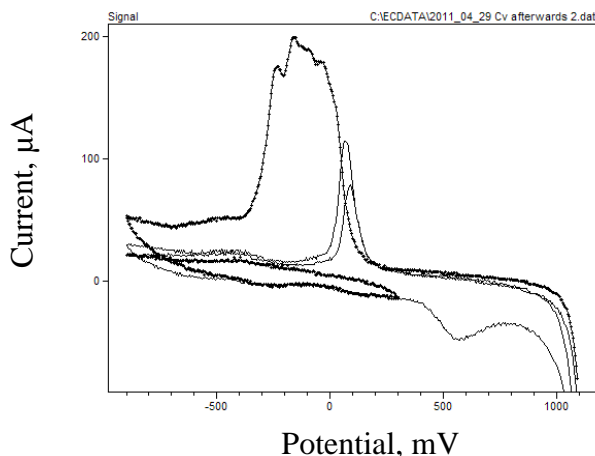


**Figure 4.1.9** CV of cell C immediately after CA with 1.1 V A largest cathodic wave was seen at the first scan and its size was reduced drastically in subsequent scans. The potential moved from 1100 mV to -900 mV at the scan rate of 100 mV in the first scan.

The original aim of this work was to decrease the oxidation current of hydrogen by using non-acidic, i.e. neutral organic electrolyte and observe the anodic wave from arsine gas. In the loop experiments, the ratio of charge of arsine to hydrogen is  $4.2 \times 10^{-6}$  if the same efficiency of oxidation process is assumed for the both species. This high number poses challenging hurdle for developing arsine sensor in this approach. Ideally there should be a system where oxidation of arsine is at least  $4.2 \times 10^6$  times more efficient than oxidation of hydrogen. This kind of enormous barrier dissuaded us from further pursuing sensor based on oxidation of arsine on gold working electrode on aqueous acidic media. Thus, we embarked on employing non-acidic media to avoid

hydrogen gas oxidation. However, in non-acidic media, decrease in anodic current even at 1.1 V was observed in the presence of H<sub>2</sub>. There might be arsine oxidation current at 1.1 V in organic electrolyte. However, the cancellation of anodic current due to reduction of gold oxide by H<sub>2</sub> was detrimental. Therefore, we abandoned the idea of seeking neutral electrolyte which removes hydrogen oxidation current. Oxidation of working electrode was clearly observed and this could compromise the proposed method of detecting arsine by electrochemical reaction. Oxidation of electrode and annihilation of anodic current during measurement was unexpected outcome in these cases. Still, we wondered whether it was feasible to exploit this type of signal response in electrochemistry for analytical detection. Diminishment of anodic current due to H<sub>2</sub> was seen in these experiments, which motivated us to exploit this idea in the next section.

#### **4.2. CA and OCP on silver-arsine complex formation.**

In the previous section, we described the system where we attempted to observe arsine oxidation current. Contrary to our expectation, annihilation of anodic signal was observed and this led to a new approach where one can observe change of current signal, namely, decrease of current. The cell notation is given below:

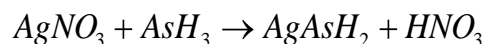


The second approach in this section is about measurement of potential change in Ag/Ag<sup>+</sup> redox couple. More specifically, open circuit potential experiment is described. Silver forms Ag(AsH<sub>2</sub>) complex and precipitates from the aqueous solution as with other halides. Therefore, decrease in concentration of Ag<sup>+</sup> should be reflected in the measured potential. In Gutzeit test, the method is based on color development due to silver-arsine

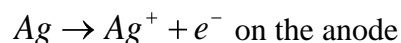
complex formation of arsine on the silver nitrate filter paper. However, in this section, we were experimenting with the idea of observing change in potential caused by the silver-arsine complex.

We used two identical silver wire electrodes making contacts with silver nitrate on a filter paper and hoped to observe current change due to silver arsine complex formation. The number of  $Ag^+$  is generated in the anode must be equal to the number of  $Ag^+$  reduced at the cathode, there must be a decrease in current when  $AH_3$  forms complex with  $Ag^+$ . The equation governing amperometry is as follows:

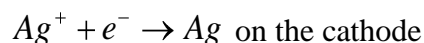
**Equation 4.2.1**



**Equation 4.2.2**



**Equation 4.2.3**



The current on the cathode is governed by Cottrell equation:

**Equation 4.2.4**

$$i = \frac{nFA[Ag^+]}{(\pi D_{Ag^+} t)^{1/2}}$$

, where F is Faraday constant, A is the area of the electrode in  $cm^2$ ,  $D_{Ag^+}$  is diffusion coefficient of  $Ag^+$  in  $cm^2s^{-1}$ , and t is time in second.

As the Cottrell equation suggests the current should decrease whenever there is decrease of concentration of silver ion on the surface of cathode. This is clear in the following diagram:

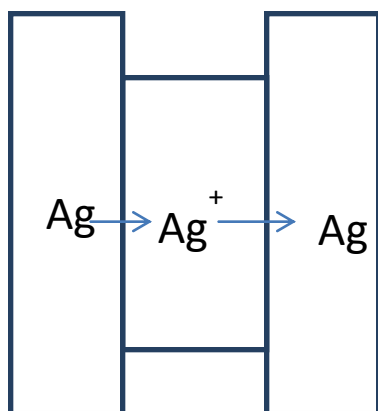


**Figure 4.2.1** Diagram of mass transfer of silver ion in the cell. Oxidation of silver occurs on anode and reduction occurs at cathode.

As the diagram shows the charge carrier silver ion is responsible for the current; therefore, when there is decrease in  $[Ag^+]$ , the current from  $Ag^+$  will decrease and this will be reflected in the chronoamperometry. Alternatively, change in concentration of  $Ag^+$  is reflected in change of potential. In open circuit experiment, we measure the difference of electrochemical potential between indicator and reference electrode.

**Equation 4.2.5**

$$E_1 = E_1^o - 0.0591 \log \frac{1}{[Ag^+]_c}$$

**Equation 4.2.6**

$$E_2 = E_2^o - 0.0591 \log \frac{1}{[Ag^+]_a}$$

**Equation 4.2.7**

$$\Delta E = E_2 - E_1.$$

#### **4.2.1. CA with cell D with silver wire**

Silver wire with diameter of 0.41 mm was coiled three times as shown in the Figure 4.2.2. The two identical wires were used as a working and a counter electrode,

respectively. Alligator clips were used to connect them to a homemade potentiostat. The cell D was characterized by CV and CA. For CV, the voltage was scanned from 0 V to 500 mV, to -500 mV and then to 500 mV at 100 mV/s. For CA, symmetric multiples steps of pulses with 200/-200 mV or 50/-50 mV were applied.

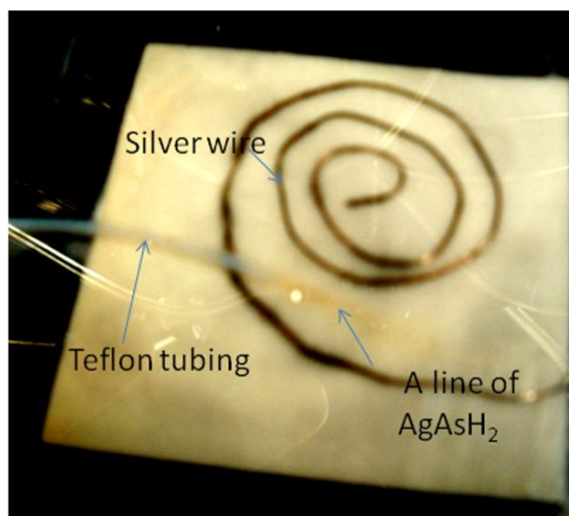


**Figure 4.2.2** Silver wire on a filter paper. Teflon tubing was used to deliver arsine on the filter paper. Right after the Teflon tubing, a line of reddish colored silver arsine was observed and this complex did not cause measurable change of current

The overall experimental setup is shown in Figure 4.2.3. As(III) in a suitable reference standard ( 2 mL of 100  $\mu\text{g/L}$  As(III) ) was reduced by manual injection of  $\text{NaBH}_4$  to generate arsine, which was transferred through Teflon tubing to the cell D. The arsine generated from the generator vial formed complex with silver ion on the filter paper and the rest of the gas passed through a cylinder and trapped in charcoal connected to the cylinder.

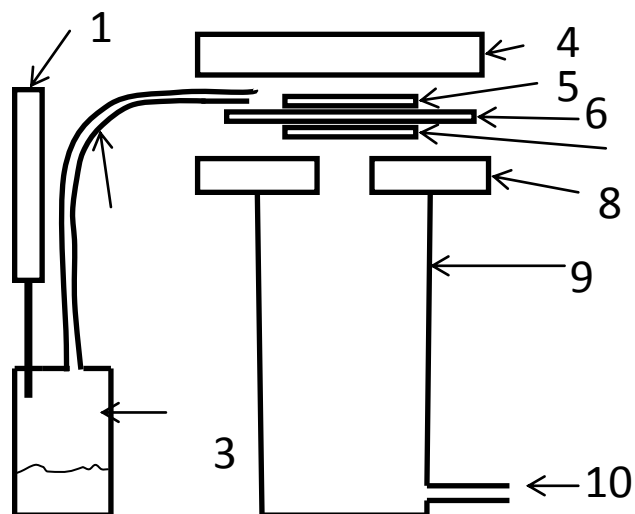


Figure 4.2.3 Schematic of system with the cell D. Overall setup of a thin layer cell D. Legends indicate: 1:  $\text{NaBH}_4$  syringe, 2: Teflon tubing, 3: arsine generator, 4: top Plexiglass, 5: silver wire as working electrode, 6: filter paper with electrolyte, 7: silver wire as counter electrode, 8: bottom Plexiglass, 9: cylinder, 10: vent to charcoal

The cell D was characterized with CV and CA. CV in Figure 4.2.4 showed symmetric oxidation and reduction peaks at  $\pm 150$  mV as expected since two identical silver wires were the electrodes. The two identical silver electrodes matched the theoretical half potential.

Equation 4.2.8

$$E_{1/2} = \frac{E_{pc} + E_{pa}}{2} = 0$$

Equation 4.2.9

$$\frac{i_{pc}}{i_{pa}} = -1$$

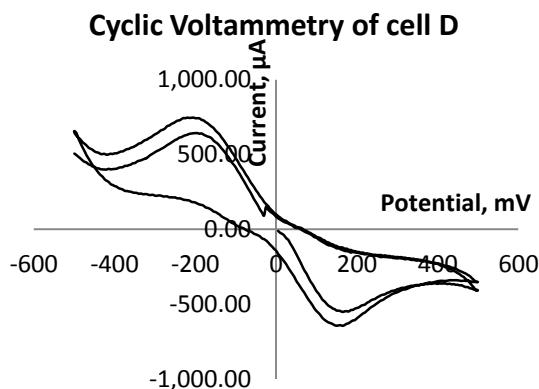


**Figure 4.2.4** CV of cell D. Two symmetric peaks were observed at  $\pm 150$  mV.

Multiple pulse chronoamperometry (MPCA) in the left panel of Figure 4.2.5 demonstrated that there existed a reversible redox couple and the currents were crippled due to saturation of the potentiostat. Therefore, the magnitude of applied pulses were reduced from  $\pm 200$  mV to  $\pm 50$  mV to get CA in the right panel of Figure 4.2.5. After the signal response of this electrochemical cell was characterized, CA experiments were performed to observe any current change due to arsine generation. More specifically, to a 3 mL of 100  $\mu\text{g/L}$  As(III) in 2.5 M  $\text{H}_2\text{SO}_4$  without stirring, 1 mL of  $\text{NaBH}_4$  (0.7 %) was added to see the response. CA was performed where the working electrode was held at 500 mV for 600 sec. At 30 sec,  $\text{NaBH}_4$  was added instantaneously from a syringe manually.

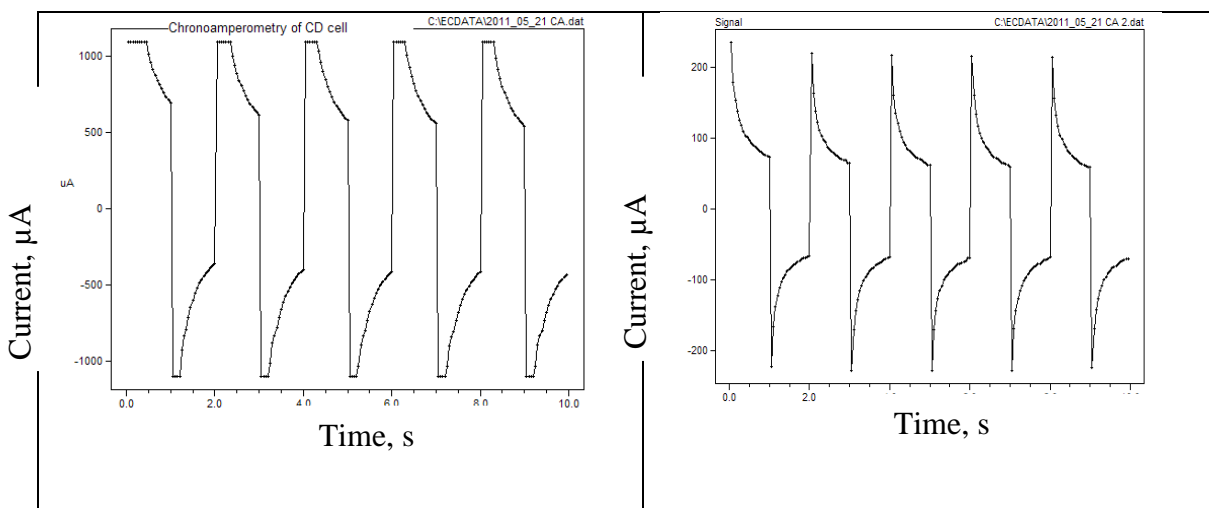


**Figure 4.2.5** MPCA of cell D. Left panel shows CA with  $\pm 200$  mV and the right one with  $\pm 50$  mV. (Left)MPCA with  $\pm 200$  mV with 1 s pulse width. (Right) MPCA with  $\pm 50$  mV with 1 s pulse width

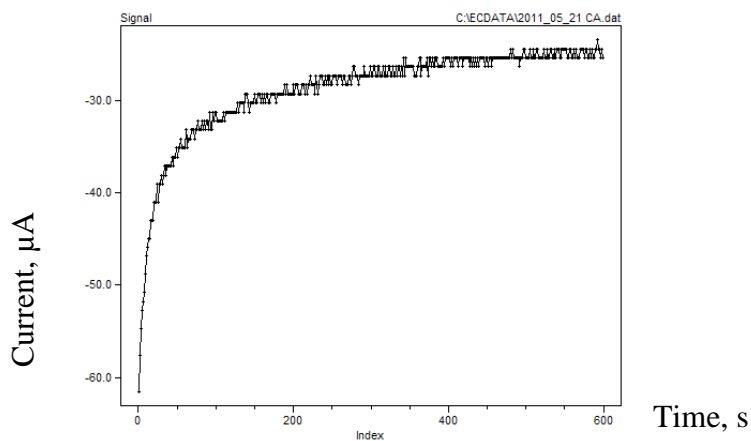


**Figure 4.2.6** Single pulse CA of cell D: No perceptible signal was observed. Potential was held at 500 mV and at 30 s, arsine was introduced Change of anodic current was expected to appear due to silver-arsine complex formation.

There was no perceptible signal response in the following Figure after  $\text{NaBH}_4$  was added at 30 s. The idea behind this experiment is the diffusion current should change due

to the Cottrell equation. When concentration gradient is changed, the diffusion current should reflect the concentration gradient on the surface of silver electrode. However, the observed signal response did not show perceptible change of current.

Open circuit potential was also measured before and after arsine generation to see if there was any potential change due to silver-arsine complex formation. A small potential of 50 mV was initially applied for a couple of seconds and counter electrode was disconnected to see the potential change for 1 min. OCP (open circuit potential experiment) did not yield useful information. Equation 4.2.5, Equation 4.2.6, and Equation 4.2.7 predict that potential difference should be developed due to change of  $[Ag^+]$ . Identically, the potential always approached 0 mV before and after arsine arrival. There was a line with reddish brown color formed right after the Teflon tubing in Figure 4.2.2 and this did not cause any substantial change of concentration of  $Ag^+$  ion on the filter paper. The right panel in Figure 4.2.7 shows that there was no measureable change in potential due to silver-arsine complex formation in the electrolyte. The reason was that although silver ion reacted with  $AH_3$  in a very small region where there was no silver electrode was available for sensing the decrease of  $[Ag^+]$ . We here estimate the time for  $Ag^+$  to travel a few cm. We use the equation of random walk. The diffusion coefficient of silver ion reported in literature is  $1.416 \times 10^{-5} \text{ cm}^2/\text{s}$ .<sup>45</sup> Therefore, It would take 35310 s ( 9.8 hours) for silver ion to move 1 cm. The root mean square of displacement,  $\bar{\Delta}$  by random walk at time t is

---

<sup>45</sup> Kraichman, M, B.; Hogge, E. A. The limiting current on a rotating-disk electrode in silver nitrate-potassium nitrate solutions. The diffusion coefficient of silver ion. *Journal of Physical Chemistry*, **1955**, 59, 986-987.

Equation 4.2.10

$$\bar{\Delta} = \sqrt{2Dt} \quad \text{where } D \text{ is diffusion coefficient of } \text{Ag}^+ \text{ and } t \text{ is time.}^{46}$$

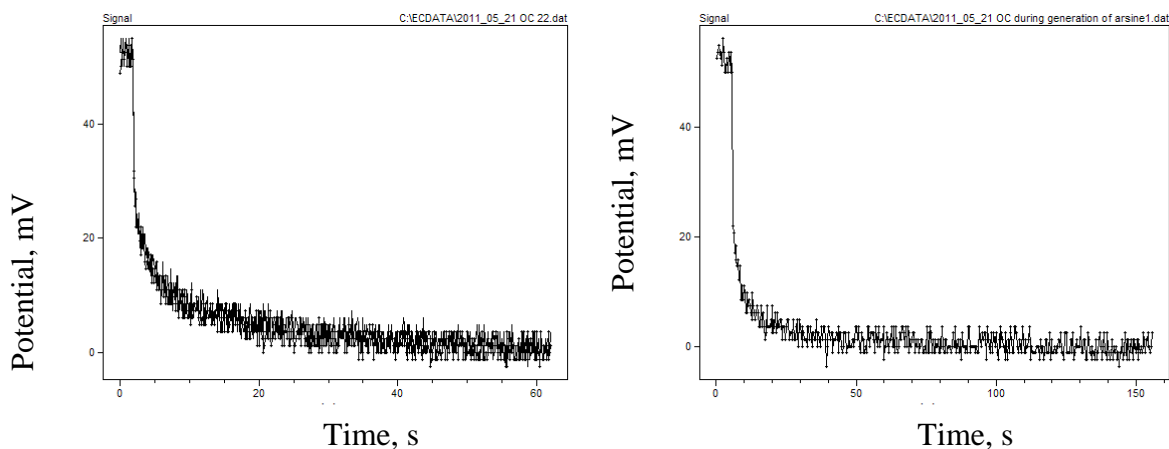


Figure 4.2.7 Potential measurements of the cell D before and after arsine exposure. No change of OCP was observed after arsine was delivered to the cell D. (Left) OCP was measured before arsine arrived on the filter paper. (Right) OCP was measured after arsine generated from 3 mL of 100  $\mu\text{g/L}$  As(III) arrived on the filter paper.

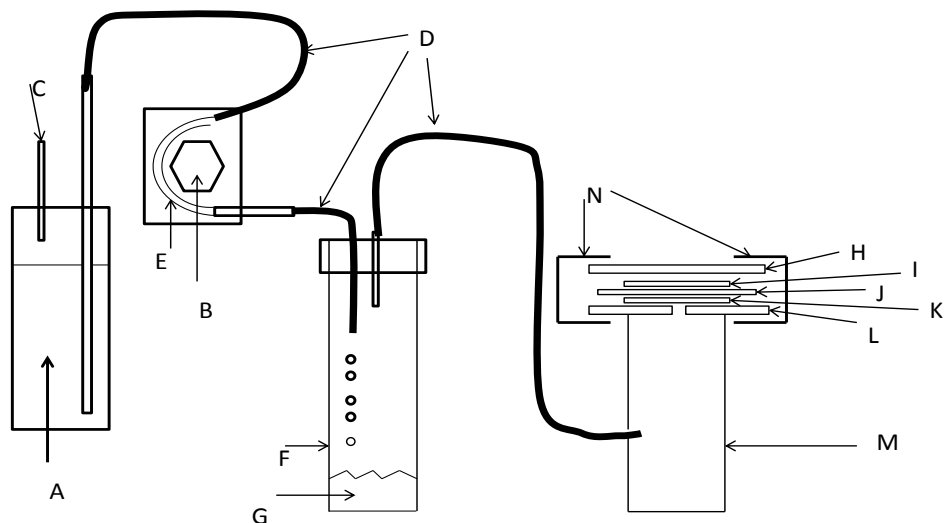
Even in a hypothetical experiments where one can measure extremely small change in potential, this will be the amount of time for one to wait to observe any change in potential. Consideration was given to this situation, and we partially overcame this problem later by aligning the pathway of  $\text{AH}_3(\text{g})$  on a small piece of silver fabric. The following Figure 4.2.7 shows plots of actual measurements.

---

<sup>46</sup> Bard, A.J.; Faulkner, L.R. *Electrochemical Methods, fundamentals and applications*, 2nd ed.; John Wiley & Sons: New Jersey, **1994**, pp 146-147.

#### 4.2.2. Cell E: Plexiglass with silver fabric

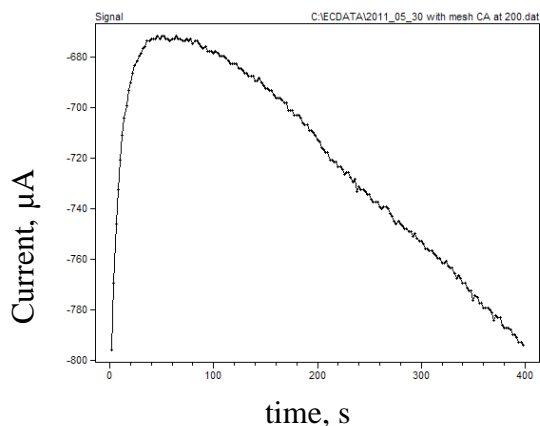
A different geometry of Plexiglass cell was made where the arsine gas came from the bottom of the cylinder. Arsine was diffused and transported from the bottom of the cylindrical chamber. The top Plexiglass has holes through which arsine was passed through a filter paper. The bottom electrode was the working electrode and the top electrode was the counter. This geometry was chosen to see if we could remove pressure pulse from the generator vial. Circular disk filter paper was also used with small amount of electrolyte, i.e. an aliquot of 100  $\mu\text{L}$  of 10 mM  $\text{AgNO}_3$ . An aliquot of 1 mL of 0.7 %  $\text{NaBH}_4$  was added to a 3 mL of 100  $\mu\text{g/L}$  arsenic solution to generate  $\text{AsH}_3$ . The cell E was potentiostated at 200 mV, and arsine was introduced at suitable points, at 80 sec. A mesh of silver fiber was used for this experiment to capture the concentration of change of silver ion better. The cell E had silver fabric electrode which covered the area where the silver arsine complex is formed. When the cell E was used, response signal indicated that silver fiber was being oxidized at 200 mV. The initial decay curve is attributed to the non-faradaic capacitance current. The current response was dramatically different from one to the other. This was attributed the change of geometry of the cell whenever replacement of the filter paper was made. Anodic current at maximum registered *ca.* 600  $\mu\text{A}$  in the left panel, but in right panel, the maximum was *ca.* 200  $\mu\text{A}$ . Inconsistency of signal response discouraged any further works with this type of cell.



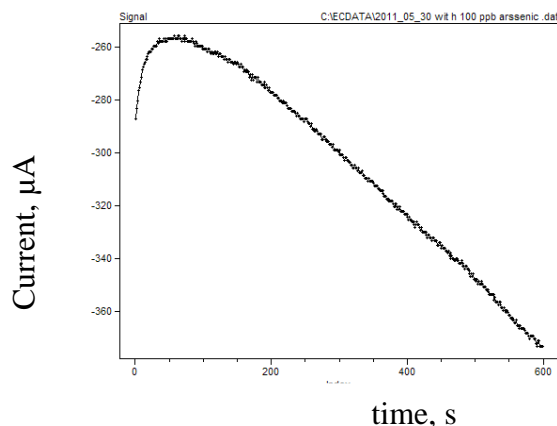
**A: NaBH<sub>4</sub> reservoir, B: peristaltic pump, E:silicon tubing, D: Teflon tubing, G: generator vial, H and L: plexiglass, I and K: silver fabric, J: filter paper, N: paper clamp**

**Figure 4.2.8 Setup of cell E. Arsine was injected into the bottom of the cylinder, after which diffusion of the arsine gas into the thin layer cell was monitored. Also NaBH<sub>4</sub> was slowly added at 1 mL/min.**

The amperometry signal response is shown in Figure 4.2.9. In conclusion, the cell E showed undesired signal response. For example, even if the same cell was used with the same experimental parameters, current responded significantly differently, as shown in above Figure 4.2.9. The Cell D showed a nearly horizontal baseline. However, this suggests that the silver electrode had been being oxidized. The typical base line should be exponentially decaying function of time. When this decaying curve is not shown, the faradaic process makes the line horizontal. The cell E showed increasing oxidation current as time elapsed. This is obviously oxidation current of silver electrode at 200 mV. Now the area of electrode touching the electrolyte was more extensive, the oxidation current was larger. In cell D, arsine-silver complex was formed



Response from blank, 3 mL of 2.5 M sulfuric acid



Response from 3 mL of 100 μg/L As(III) in 2.5 M H<sub>2</sub>SO<sub>4</sub>.

Figure 4.2.9 CA from blank (left panel) and CA from 3 mL of 100 μg/L As(III) (right panel). No perceptible signal response was obtained from As(III) standard.

immediately on the filter paper and they did not travel to the region where the silver electrode was making contact with silver nitrate solution. Therefore, the silver electrode resided in the same environment. The environment of silver electrode was just the identical electrolyte regardless of whether the arsine had arrived or not. This accounted for insensitivity of the cell D. In cell E, the predominant process was oxidation of silver electrode at anode. In two electrode system with identical material, one electrode is oxidized while the other electrode is reduced even with application of small potential difference of 200 mV here.

### 4.3. Development of pulse chronoamperometric technique for arsine detection

We attempted to measure faradaic current of redox couple in the preceding sections, which did not yield desired results. In this section, we measured nonfaradaic

current due to mobilization of the  $\text{Ag}^+$  ions under the electrical field. The cell notation used in this section is given below:



Thus far, all experiments were conducted to monitor faradaic current due to electrochemical reactions and  $\text{AsH}_3$  sensor had been always developed in this approach. We had been attempting measure the faradaic current due to  $\text{AsH}_3$  oxidation only to find that these electrodes were being oxidized. We turned to conductance measurement experiments here. In this regard, we review the definition of conductance and methodology of measuring conductance.<sup>47</sup> Electrolyte of the cell obeys Ohm's Law like any other conductor of electricity;

**Equation 4.3.1**

—

Here,  $R$  is resistance and  $E$  is potential of electrolyte. The conductance is defined as reciprocal of resistance. Therefore, when one measures the change in resistance by measuring current at given potential  $E$ , one measures the change in conductance of the electrolyte. The key concept of measurement in this section is the resistance change in the cell as a result of change of chemical composition of electrolyte due to silver-arsine complex formation. This could lead to a development of arsine sensor.

It is well known that arsine forms complex with silver ion, which has been still practiced in the field with Gutzeit test kit. Here we use conductometry as synonym of pulse chronoamperometry. The reason is that to measure conductance, one applies square

---

<sup>47</sup> Sime, R.J. *Physical Chemistry*, **1990**, Saunders College Publishing, a division of Holt, Rinehart and Winston, Inc. p 558-566.

wave pulse with equal magnitude of opposite signs in alternating manner. When we applied a small voltage such as  $\pm 100$  mV, we assumed that predominantly nonfaradaic current was flowing. Therefore, the name conductometry comes here. Speaking of methodology of conductometry, we measured the current difference between the two pulses of equal duration. This method originally comes from bipolar pulse conductometry.<sup>48</sup> Electrochemical cell is a complex entity which cannot be modeled easily by mathematics. We merely mention here that there are two different types of capacitance in electrochemical cell, parallel capacitance and series capacitance. Bipolar pulse conductance method removes these two capacitance components of electrochemical cell so that we can measure resistance only. Mobilization of dissolved ions in electrical field is the source of conductance of electrolyte. The method allows measurement of resistance, which is simply the reciprocal of conductance. When we use silver nitrate as electrolyte on the filter paper, arsine forms silver-arsine complex and proton as shown in the following chemical reaction:

**Equation 4.3.2**



, where the equilibrium constant is defines as

**Equation 4.3.3**

$$K = \frac{[H^+]}{[Ag^+][AsH_3]}$$

---

<sup>48</sup> Johnson, D.E.; Enke, C. G. *Analytical Chemistry*, **1970**, 42(3), 329

In dilute solution, the molar conductivities of strong electrolytes obey Kohlrausch's law.<sup>49</sup>

$\lambda_m = \lambda_m^0 - Kc^{1/2}$  where  $\lambda_m^0$  is the limiting molar conductivity,  $K$  is proportional coefficient, and  $c$  is concentration. As we are dealing with dilute concentration and the change of concentration of the  $Ag^+$  is negligibly small, we treat the molar conductivity as the limiting molar conductivity. Then the measured conductivity,  $\kappa$  is the sum of individual molar conductivity of ions.

**Equation 4.3.4**

$$\kappa = \sum_i \nu_i \lambda_i C_i$$

where  $\nu_i$  is the number of cations and anions appeared in the chemical formula,  $C_i$  is the concentration of ion  $i$ , and  $\lambda_i$  is the molar conductivity of  $i$  in  $S\ cm^{-1}$ .

When we apply this equation to our system, the following equation results:

**Equation 4.3.5**

$$\kappa = \lambda_{H^+} [H^+] + \lambda_{NO_3^-} [NO_3^-] + \lambda_{Ag^+} [Ag^+]$$

Using the equilibrium constant  $K$ , defined for silver-arsine complex formation;

**Equation 4.3.6**

$$[H^+] = K[Ag^+][AsH_3]$$

We use concentration notation instead of activity notation for  $AsH_3$ , usually represented by  $a_{AsH_3}$ . As  $[AsH_3]$  is dilute, we know that the activity approaches closely  $[AsH_3]$ .

Then the conductivity is expressed as,

**Equation 4.3.7**

$$\kappa = \lambda_{H^+} K[Ag^+][AsH_3] + \lambda_{NO_3^-} [NO_3^-] + \lambda_{Ag^+} [Ag^+]$$

---

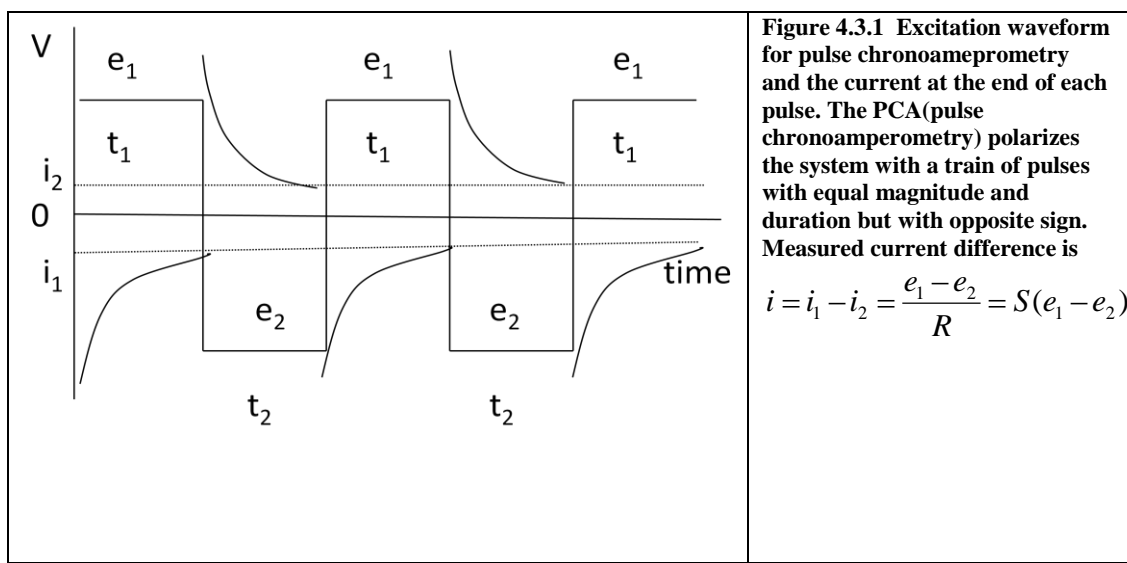
<sup>49</sup> Atkins, P.W. *Physical Chemistry*; Oxford University Press: Oxford, **1990**; P 752.

The conductivity  $\kappa$  is related to resistance,  $R$  as  $\kappa = \frac{A}{R} = AS$  where  $A$  is the cell constant depending on geometry of the cell and  $S$  is conductance. If the concentration of silver ion is in large excess to that of proton, we can safely state that  $[Ag^+]$  is constant after silver-arsine complex formation. The change in conductance,  $\Delta S$  due to  $Ag(AsH_2)$  formation is as follow;

**Equation 4.3.8**

$\Delta S = \kappa / A = k_1 / A + k_2 [AsH_3] / A$  where  $k_1$  is  $\lambda_{NO_3^-} [NO_3^-] + \lambda_{Ag^+} [Ag^+]$  and  $k_2$  is  $\lambda_{H^+} K [Ag^+]$ . The equation shows that the conductance is proportional to arsine dissolved on the filter paper. The specificity of signal came from the fact that only arsine gas can form complex and generate hydronium ion in electrolyte. This will increase conductance of the electrochemical cell, which is the analytical signal.

We measured the conductance by polarizing the cell with a square wave voltage pulse as shown in Figure 4.3.1. After voltage pulse  $e_1$  is applied and time  $t_1$  is elapsed, current  $i_1$  is recorded. The same is followed for pulse  $e_2$ . However this  $t_2$  is equal to  $t_1$ . We measure  $i_2$  at this point. The manner of applying voltage pulse removes undesirable capacitance current and pure resistance can be made with this method. We take the difference of  $i_1 (= e_1/R)$  and  $i_2 (= e_2/R)$  as the analytical signal. The conductance  $\Delta S$  reflects the change in arsine concentration in the cell as per Equation 4.3.8.



#### 4.3.1. Conductometry with silver fabric electrodes with cylindrical chamber (Cell 4.3.1)

The overall setup for conductance measurement is similar to that of Figure 4.2.8. Here, we deliver reductant using a peristaltic pump at slow rate. This is introduced here because that fast addition of reducing agent generated arsine too fast and the trapping efficiency of arsine on the filter paper was not adequate, which might account for no perceptible change in current in amperometric experiment or change in potential in potentiometric experiments. Two circular pieces of silver fabric with diameter of 22.3 mm were attached to two Plexiglass planes. The bottom plate was connected to a bottle cap that has hole with diameter of 12.6 mm through which gas can pass. The height of cylinder was 100 mm and the diameter of the cylindrical chamber was 27.3 mm. The 30 cm long Teflon inlet tubing (1/16 in. OD and 0.03 in. ID) from the generator vial was connected to the lower part of the cylinder which was 30 cm away from the bottom of the cylinder. Usual circular disk of filter paper with diameter of 27 mm was soaked with 50

$\mu\text{L}$  of  $\text{AgNO}_3$ . The counter electrode was silver fabric with the same size of the working electrode. The two planes of rectangular plastic planes were secured by four paper clips. The diagram shown below describes the cell used to detect arsine gas. The reservoir bottle was 50 mL size plastic bottle with vent. The peristaltic pump delivered 1 %  $\text{NaBH}_4$  in 0.5 M  $\text{NaOH}$  at the rate of 1 mL/min between 40 s and 100 s. In all conductance measurements, the height of the positive and negative pulse was + 100 and - 100 mV respectively and the delay between the two pulses was 200 ms. The data was obtained for 300 s at the frequency of 5 Hz. However, this total sampling frequency is 2.5 Hz as every single measurement was completed in 400 ms.

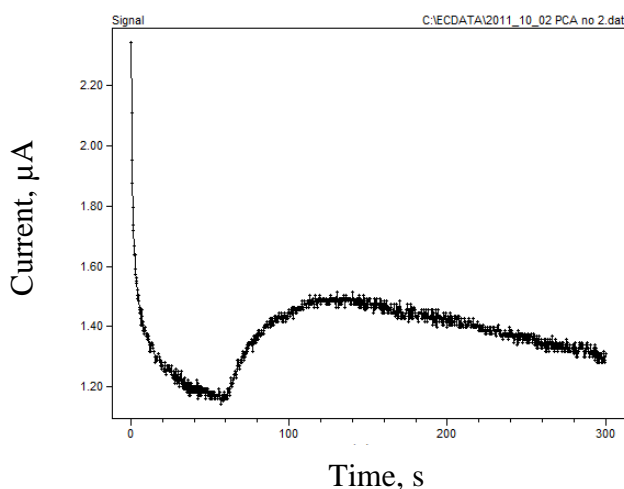


**Figure 4.3.2** Signal response of the cell with 4.3.1. Increase of conductance reflected in a rise of current response of 0.4  $\mu\text{A}$  was observed from 2 mL of 1 mg/L of arsenic.

The conductance of the cell sharply decreased initially due to decay of capacitance current, and then a rise of conductance was observed shortly after addition of  $\text{NaBH}_4$  started at 60 s. We wanted to remove capacitance current as the theory predicted;

however, the capacitance current was not removed completely. There was about 20 s response time after the addition and this was the time needed for the cell to sense the silver-arsine complex formation. The signal from 2 mL of blank and 2 mL of 1 mg/L of As(III) is shown below. The cell showed increase of conductance albeit the signal was only 0.4  $\mu$ A.

#### 4.3.2. Conductometry with silver foil on a syringe filter

Here, the overall setup is the same except a different detector was used. The detector was an electrochemical cell with silver foil electrode on a syringe filter. A rectangular piece of silver foil, 2.62 mm x 0.12 mm x 7.38 mm in size was used as working electrode and counter electrode. The electrodes were attached to a syringe filter with tape. The electrolyte was 50  $\mu$ L of 10 mM AgNO<sub>3</sub> on the filter paper (0.20 mm in thickness and 27 mm in diameter). An aliquot of 1.0 mL of NaBH<sub>4</sub> ( 1 % in 0.5 NaOH) was added to the cell, manually, 20 second post acquisition of PCA to generate arsine and hydrogen.



**Figure 4.3.3** Cell with silver foil electrode for conductance measurement.

Improved current response of Cell 4.3.2 was obtained as shown in Figure 4.3.4. Although the improvement was not great, as silver foils were used, the handling of the cell was easier than before. The signal from 2 mL of blank and 2 mL of 1 mg/L of As(III)

is shown below. The blank did not showed increase of conductance of the cell whereas the 1 mg/L arsenite sample showed increase in conductance of the cell. The signal was 0.8  $\mu\text{A}$  for 2 mL of 1 mg/L standard and the blank showed a monotonous decrease in conductance of the cell. Basically, any movement of the cell components (geometry) could cause a change in cell constant and thus the currents as shown in Figure 4.3.4(left). We have overcome this problem by securing the cell to prevent any movement.

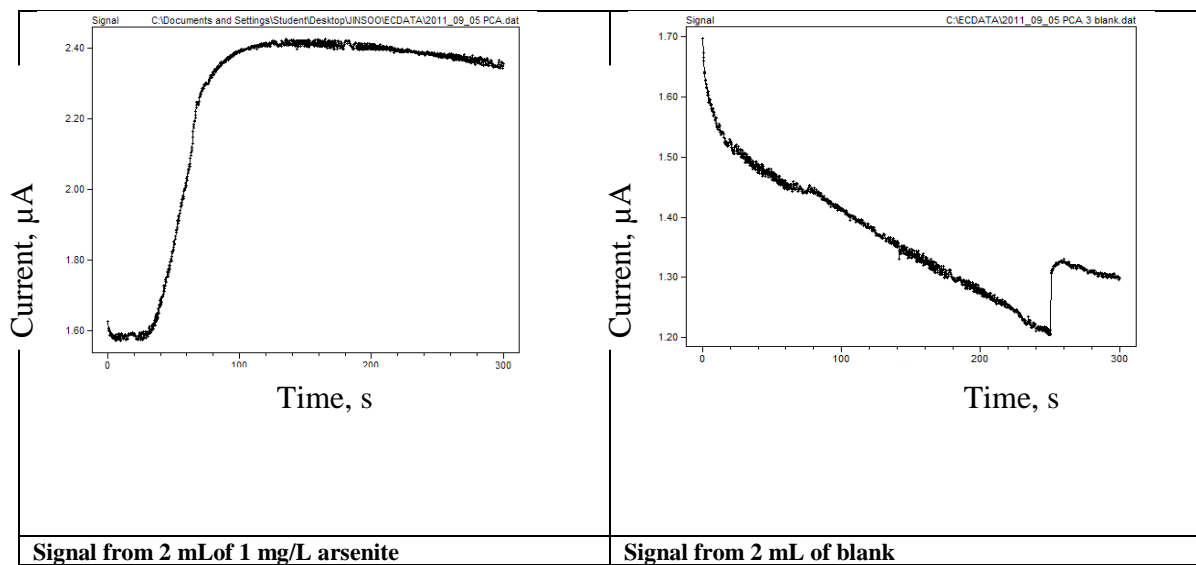
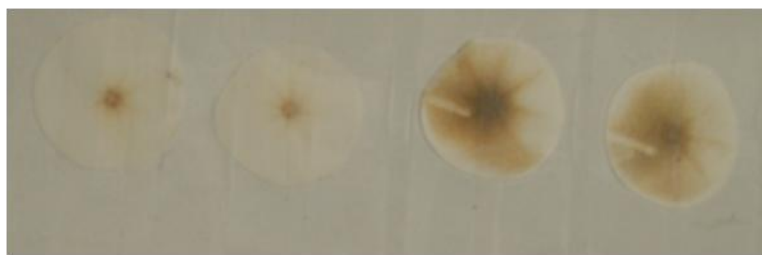


Figure 4.3.4 Comparison of arsenic standard (left panel) and blank (right panel). The spurious rise in the right panel was often seen with this type of sensor.

We examined the used filter to see what happened on the filter paper. We clearly observed the color developed on the filter paper due to silver-arsine complex formation. In figure 4.3.5 (third and fourth samples) we see a rectangular shaped region where silver foil was situated. As the filter paper was screened by the foil, there was no transfer of arsine underneath the silver foil.



**Figure 4.3.5** Filter paper stained with blank and arsenic standard. The left two filter papers were from blank experiment and right two filter papers were from 1 mg/L arsenite. The white rectangular regions on the left two filter papers were area where the silver foil made contact with the filter paper.

#### **4.3.3. Conductometry with silver fabric on a syringe filter**

We further tested this methodology with two pieces of silver fabric. To 2.0 mL sample in a generator vial with stirrer,  $\text{NaBH}_4$  was added slowly over 2 min at the flow rate of 1.0 mL/min while the cell conductance was measured by PCA technique. The signal is taken as the difference between the maximum value and minimum value.

The working electrode is a small piece of silver coated fabric and the counter electrode is the identical silver coated fabric. Between the two silver fabric electrodes, a disk of filter paper was inserted. The cell body is a syringe filter divided into two pieces. The inner side of the two syringe filter had the two silver fabrics and the female Luer port of the syringe filter was connected to Teflon tubing through which arsine traveled. The cell is secured by two paper clips. Signal response from cell 4.3.3 demonstrated highest sensitivity among sensors thus far tested. Initially the conductance decreased as electrolyte was being dried out. When  $\text{AsH}_3$  was delivered, the conductance



Figure 4.3.6 Inside of cell 4.3.3 with two pieces of silver fabric.

increased. The conductance slowly increased as arsine came in and reacted on the filter paper. Typical PCA current transient is shown in Figure 4.3.7.

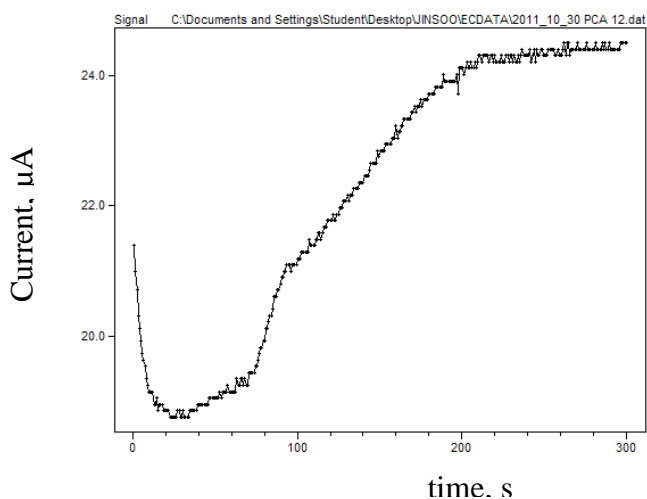


Figure 4.3.7 Typical current response profile of PCA from the cell 3.3.3. The signal is taken as maximum value subtracted from the minimum value in determining conductance.

Figure 4.3.8 shows a calibration curve for the measurement of As(III) in aqueous media by this technique. The analytical figures of merit for this technique are as follows: linear dynamic range of calibration: from 0 to 1000  $\mu\text{g/L}$  ( $r^2 = 0.9812$ ); sensitivity;

0.0486  $\mu\text{A}/(\mu\text{g}/\text{L})$ ; detection limit, 88  $\mu\text{g}/\text{L}$ .

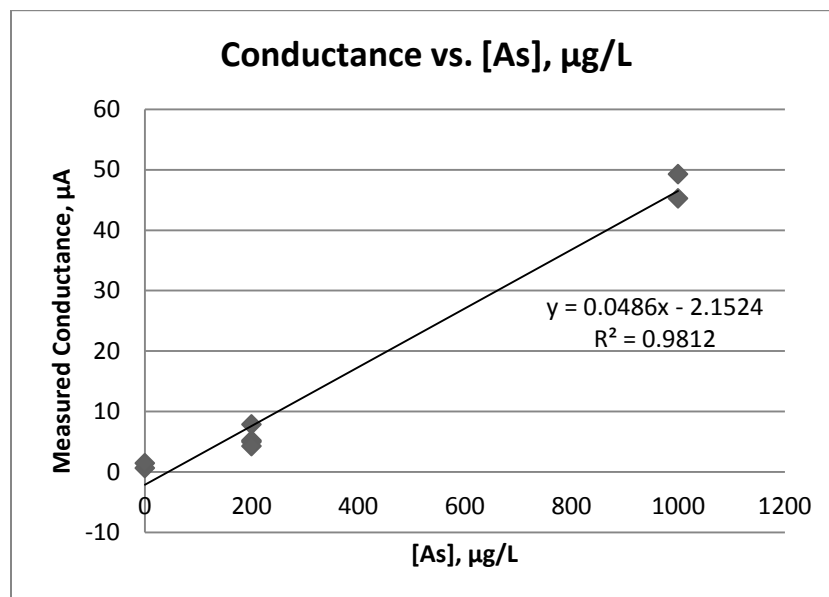
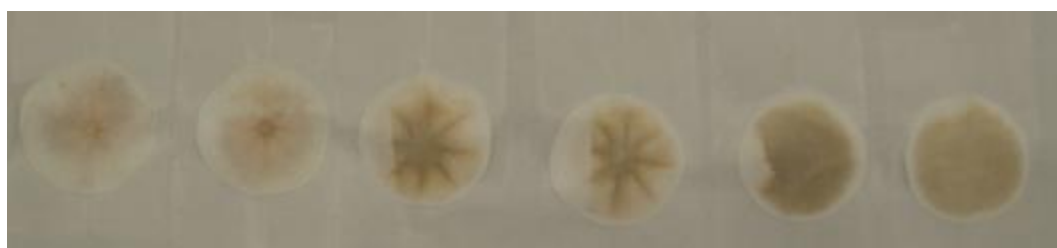


Figure 4.3.8 A calibration curve constructed from cell 4.3.3.

Here we show the filter papers with visible silver-arsine complex. It is clear to naked eyes that the higher the concentration, the more intense the spot. But no quantitative information can be obtained from these filter papers through visual inspection.



200      200      1,000      1,000      10,000      10,000

**Figure 4.3.9** A picture of filter paper from cell 3.3.3 after various amount of arsine from the generator vial. The number below each filter paper is concentration of As(III) in  $\mu\text{g/L}$ . Increasingly intense reddish yellow color was observed on the filter paper due to silver-arsine complex formation

In summary, all three cells were showing measurable signals. In cell 4.3.1, the rise of the signal was clearly seen albeit the signal obtained was very small ( $0.4 \pm 0.133 \mu\text{A}$  per 2 mL of 1 mg/L arsenite). Considering the amount of As(III) in 2 mL of 1 mg/L standard, this is a small signal. But it motivated us to use electrodes that could cover more area of the filter paper where silver-arsine complex formed. The silver strips clearly showed that the silver arsine complex could not be formed underneath the silver electrode because the silver strip was not porous to the gas. The silver strip could detect the conductance change of the electrolyte only from the periphery. This observation led us to use silver fabric which was porous to the gas and covered more extensively the area where the conductance change occurred. In the cell in section 4.3.2, as aqueous  $\text{AgNO}_3$  was used as electrolyte, the conductance changed slowly over time. We used the disk of filter paper once, and discarded it after each measurement. Whenever, a new filter paper was inserted to the next run of measurement, there arose change of resistance of the cell due to geometric change of the electrodes and electrolyte. The cell in section 4.3.3 gave the best results for conductance measurement and the linearity of the signal response was

shown in Figure 4.3.8. Encouraged by these results, we continued to use this cell for potentiometry with three layers of filter papers described in the next section.

#### 4.4. Development of arsine sensor based on potentiometry

We revisited the potentiometry more carefully and strategically used three layers of filter papers to obtain signals. The cell notation is given below:



##### 4.4.1. Potentiometry with Ag/AgNO<sub>3</sub> system for arsine detection

It is known that reaction between arsine and silver nitrate change transient [Ag<sup>+</sup>] in the reaction matrix. When we use two identical silver electrode, the potential difference between the electrodes,  $E = 0$ . The mass transfer of arsine generated from the sample vial could change the concentration of silver ion in the filter paper. In that case, the potential difference is given by  $E = E_1 - E_2$ , where  $E_1$  is the working electrode potential and  $E_2$  is that of the reference electrode:

**Equation 4.4.1**

$$E = E_1 - E_2 = 0.0591 * \log \frac{[\text{Ag}]_{\text{working}}}{[\text{Ag}]_{\text{reference}}}$$

The concentration drop on the surface of working electrode due to silver-arsine complex formation causes a change in the transient potential, which can be used as the analytically signal. We use 25  $\mu\text{L}$  of 10 mM AgNO<sub>3</sub> in the filter paper and expect to see a change of this concentration detected by a measurable potential change. This is the simplest As(III) sensor possible without the use of complicated instrumentation.

We had total number of  $1.51 \times 10^{17}$  of silver ion available for silver arsine complex formation reaction.

#### **4.4.1.1. Materials and methods**

The electrochemical cell was constructed on the syringe filter cell. A small piece of silver fabric was used as working electrode and the other larger piece of silver fabric was used as reference electrode. The reason for working electrode being small (2 mm x 10 mm strip of silver fabric) is that the entire electrode should be completely covered by the silver-arsine complex. The reference electrode was a donut shaped silver fabric whose diameter is 20 mm. The middle of the reference electrode was cut such that it did not sense the decreased  $[\text{Ag}^+]$ . The two electrodes were connected to a potentiostat for open circuit potential measurements. Initial potential difference between the working electrode and reference electrode was monitored for 1 min. Then arsine was generated from 60 sec to 120 sec slowly from the peristaltic pump. Initially one layer of filter paper containing 25  $\mu\text{L}$  of 10 mM  $\text{AgNO}_3$  was used, however, three layers of filter papers had to be used for reproducible measurement. The addition of reducing agents ( 0.2 %  $\text{NaBH}_4$  in 0.5 M  $\text{NaOH}$ ) was achieved in the same way and the volume of the standard in the generator vial was the same as in section 4.3.

After establishing that the silver fabric is indeed sensitive to  $\text{Ag}^+$  ion in section 3.3.3, we measured the potential change of silver electrode when it was exposed to arsine gas generated from 2 mL of 10  $\mu\text{g/L}$  to 400  $\mu\text{g/L}$   $\text{As(III)}$  in aqueous solution.

#### 4.4.1.2. Results and discussion

When the two silver fabric electrodes were connected to working and reference electrode prior to generation of arsine, the initial potential recorded was not zero, but had a small potential difference. This was due to the junction potential developed across the filter paper. However, we are interested in the change in potential drop from the initial potential due to a decrease in  $\text{Ag}^+$  ion on the surface of the working electrode. The first couple of experiments showed arsine broke through the filter paper and the colored spot was clearly seen on the opposite side of the filter paper. In other words, silver-arsine was formed on the top side of the filter paper as well as on the bottom side of the filter paper. As a result, the reference silver fabric electrode sensed the decreased  $[\text{Ag}^+]$ , therefore, the signal was cancelled out by this effect. It was desired that the reference electrode did not see any silver-arsine complex, so the middle of the reference electrode was cut out to minimize the contact with the spot. Not only this caution was taken, but also, three layers of filter paper containing the same amount of silver nitrate was placed to ensure that no breakthrough of arsine gas occurred to the reference electrode. The figure shows the absolute magnitude of the potential drop vs.  $[\text{As(III)}]$ .

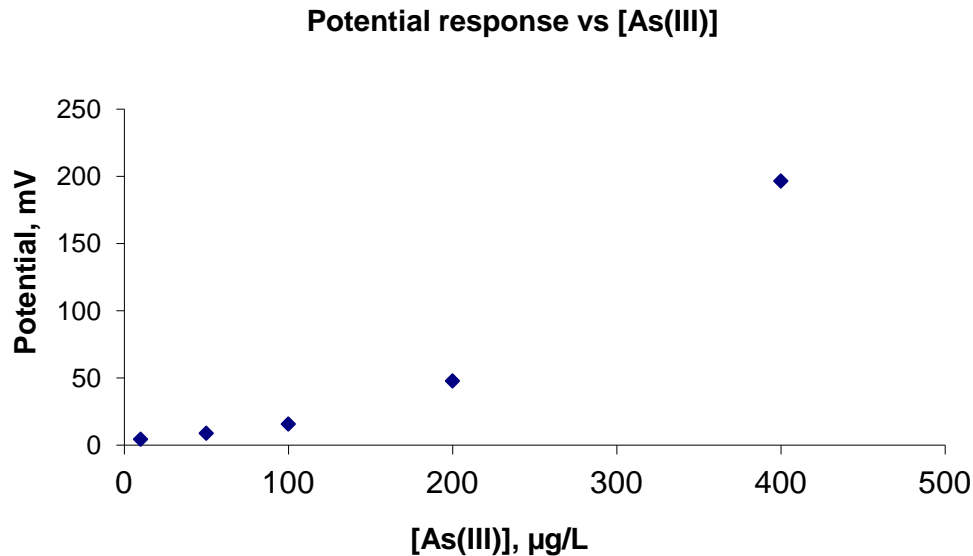


**Figure 4.4.1** Plot of the magnitude of potential drop vs. [As(III)]. Albeit signal response was nonlinear, the silver fabric sensor with three filter paper was sensitive to [As(III)].

The above graph demonstrated that the potential drop occurred and it was a strong function of the concentration of As(III) in the generator vial. However, it did not follow the Nernst equation. Let's hypothesize that  $\text{AsH}_3$  forms complex on the filter paper uniformly and the  $[\text{Ag}^+]$  is uniform on the first layer of the filter paper. Then we can calculate the ratio of  $[\text{Ag}^+]$  in the first filter paper and the third filter paper. The ratios in the second column in Table 4.4.1 Measured potential vs. calculated potential change represent these numbers.

**Table 4.4.1 Measured potential vs. calculated potential change.**

[As(III)], µg/L	Ratio of $[\text{Ag}^+]_{\text{working}}/[\text{Ag}^+]_{\text{ref}}$	Measured potential drop, mV	Predicted potential drop, µV
--------------------	---	-----------------------------------	------------------------------------

10	$1.07 \times 10^{-3}$	4.31	0.0274
50	$5.34 \times 10^{-3}$	8.76	0.137
100	$1.07 \times 10^{-2}$	15.6	0.276
200	$2.14 \times 10^{-2}$	47.6	0.554
400	$4.27 \times 10^{-2}$	196	1.12

In the last row of Table 4.4.1 there was 196 mV drop of potential. To have this much potential drop, we need to decrease the  $\text{Ag}^+$  by  $4.83 \times 10^{-4}$  fold. The ratio calculated in the table indicates that the concentration of arsine is only 4.27% that of  $\text{Ag}^+$ . If so, the potential drop would have been dropped by 1.12 mV. The only explanation for this phenomenon is that the local concentration of  $\text{Ag}^+$  was decreased drastically on the surface of the indicator electrode. This is nearly 200 times bigger than the value obtained if solution phase electrolyte had been used to trap arsine. Generally, the basis of potentiometric sensor obeys Nernst equation, i.e. potential vs. logarithmic of concentration of analyte is linear. However, the plot of potential vs.  $[\text{As(III)}]$  gave non-linear line. The non-linearity could be due to local non-equilibrium concentrations of  $\text{Ag}^+$ . Better cell design and efficient mass transport (better geometric configuration of the silver fabric and filter) could solve this problem, which is yet to be explored.

This is the powerful indication that the filter paper can amplify the electrochemical signal by concentrating the analyte in a small region of electrolyte. With solution phase electrolyte, where vortexing of solution and diffusion of ions occurs, this cannot be possible. It is important to note that, the silver-arsine spot is appreciably bigger when higher concentration of As samples were used. Therefore, the working electrode is covered by different area of silver-arsine spot. We do not know how to model this type

of phenomena, in which the indicator electrode is immersed in region where concentration gradient was developed. Conventionally, the indicator electrode is immersed in the homogeneous region of the analyte in terms of concentration. However, the  $[Ag^+]$  on the surface of Ag electrode differs drastically from the bulk  $[Ag^+]$  in this case.

Although this method opens up a new area of electrochemical method development, pursuit of potentiometry had been discontinued in our endeavors. Much effort had been made to make the indicator electrode small such that it could be covered entirely by silver-arsine spot. This is one of the limitations. It is this experience that motivated us to move into amperometric approach for detection of arsine on the filter paper. We assume that in amperometry, as long as arsine was delivered to the proximity of working electrode, the electroactive species would undergo redox reaction. The current would be proportional to the concentration of delivered arsine on the filter paper, which would be the analytical signal. In the next section, we discuss the discoveries of new amperometric gas sensors.

#### **4.5. Amperometric arsine sensor**

This section -describes amperometric gas sensors based on  $I_2/I^-$  couple. From experience gained from the previous experiments, we designed and fabricated amperometric gas sensors. Before we discuss the results of experiments, we provide theoretical background for the sensors in this work.

### 4.5.1. Origins and characteristics of signals

In electrochemistry the signal originates from redox reactions and chemical reactions. The signal baseline is not a flat horizontal line and the shape of the signals is not a bell-shaped Gaussian peak. A clear understanding of the system requires an understanding of the model used in electrochemistry. An electrochemical system, in its simplistic form, is an equivalent circuit connected by a resistor and a capacitor in series as shown in the following figure.

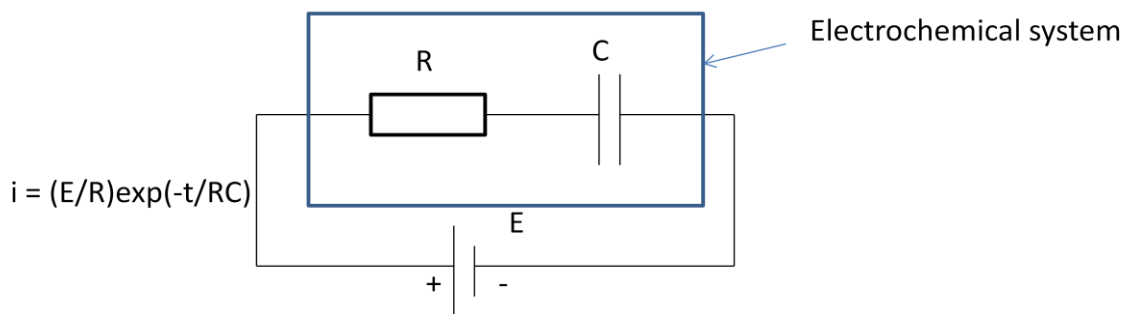
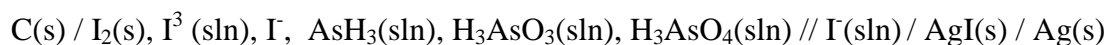


**Figure 4.5.1** An equivalent circuit of electrochemical cell. A schematic shows that a resistor and a capacitor are connected in series in an electrochemical cell and the equation on the left is the resultant current due to a voltage pulse, E.

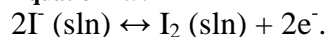
The baseline current (nonfaradaic),  $i$ , is an exponentially decaying current when the system is subject to a step potential. On top of this current  $i$ , we observe an oxidation wave which is a bi-exponential function, which we will formulate later in this section. The signal, a current from oxidizable species in the system, is not a symmetric Gaussian bell typically observed in liquid and gas chromatography because the oxidation current reflects the concentration of arsine arriving on the surface of the working electrode. The time-varying function of arsine is a bi-exponential function, i.e. a linear combination of

two exponential functions due to chemical kinetics. This will be explained in the theory section. In addition, the signal is also superimposed on a baseline which is decaying exponentially. Therefore, one needs to subtract the exponentially decaying baseline from the bi-exponential function to obtain the quantity of arsine delivered to the sensor. First let's consider the chemical reactions and electrochemical reactions in the sensors in detail. Here, we describe the system with cell notation. The notation "sln" means the species in solution phase. Also, when DMSO was used as solvent, AgI was in solution phase as AgI is soluble in DMSO. When aqueous system is used, AgI is predominantly in solid phase.



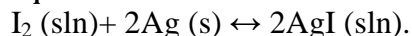
The electrochemical reaction on the surface of working electrode is

**Equation 4.5.1**



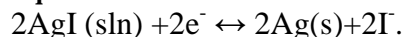
The chemical reaction on the surface of counter electrode is

**Equation 4.5.2**



The electrochemical reaction on the counter electrode is

**Equation 4.5.3**



Equation 4.5.3 clearly shows that  $\text{I}^-$  is generated from the counter electrode. The iodide generated from the cathode will travel to the working electrode (anode) where it will be oxidized. Therefore, we have to subtract this current,  $i_{\text{cathode}}$  from the total measured current at the anode. The concentration gradient by diffusion will be a straight

line across the thin filter paper eventually at equilibrium. The following diagram shows the concentration gradient at equilibrium.

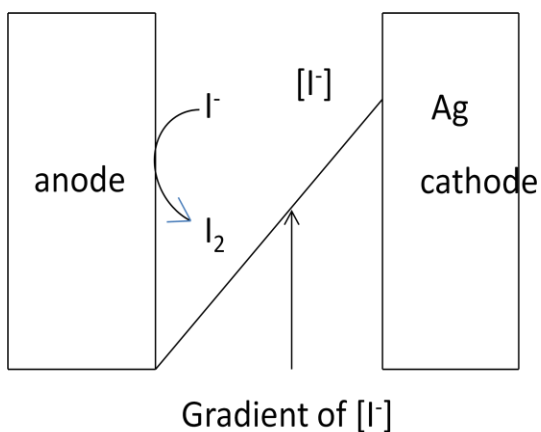


**Figure 4.5.2** Gradient generated from  $I^-$  from AgI reduction on the surface of Ag electrode. At steady state, the constant gradient is established, represented by a straight line.

Ficks first law of diffusion states that the flux of substance is proportional to the concentration gradient<sup>50</sup>,

**Equation 4.5.4**

$$-J = D_{I^-} \frac{\partial C_{I^-}}{\partial x}.$$

where,  $D_{I^-}$  is the diffusion constant of  $I^-$ , and the current is,

**Equation 4.5.5**

$$\frac{i}{nFA} = D_{I^-} \frac{\partial C_{I^-}}{\partial x}$$

<sup>50</sup> Bard, A.J.; Faulkner, L.R. *Electrochemical Methods, fundamentals and applications*, 2nd ed.; John Wiley & Sons: New Jersey, **1994**, pp 148-151.

, where,  $n$  is the number of electron in the half equation,  $F$  is Faraday constant and  $A$  is the area of the electrode. If we have a constant slope of  $[I^-]$ , we will have a constant current from this phenomena. Because of this current, we have two sources for anodic current, one from Ag electrode and the other one is from the reaction of arsine with iodine. The measured current is the sum of four components:

**Equation 4.5.6**

$$i = i_{nonFaradaic} + i_{Faradaic} + i_{impurity} + i_{cathode}$$

Here, we assume oxidation current from any residual impurities (not the analyte),  $i_{impurities}$  and  $i_{cathode}$  are negligible. The symbol  $i_{cathode}$  is current due to iodide generated from the reduction of AgI generated from the cathode. This  $I^-$  is also contributing faradaic current to the measured current. However, we represent it as  $i_{cathode}$  to focus on the current generated by  $I^-$  from the reaction between arsine and iodine. The current,  $i_{cathode}$  is always there regardless of the presence of arsine, a reducing gas. Let's consider nonfaradaic current,  $i_{nonfaradaic}$  and faradaic current,  $i_{faradaic}$ . Here,  $i_{nonfaradaic}$  is the current due to the cell capacitance, and  $i_{faradaic}$  current is the current due to the oxidation of iodide generated from the reaction of arsine with iodine. The non-Faradaic, capacitance current is decaying exponentially with time as follows:

**Equation 4.5.7**

$$i_{nonfaradaic} = \frac{E}{R} \exp(-t / \tau)$$

, where  $\tau = RC$ , the cell time constant. In addition, we define here nonspecific current,  $i_{nonspecific}$ . The nonspecific current is the sum of nonfaradaic current and  $i_{cathodic}$  described in Equation 4.5.5 and Equation 4.5.3.

**Equation 4.5.8**

$$i_{nonspecific} = \frac{E}{R} \exp(-t / \tau) + i_{cathode}$$

The equation predicts that the base line current will decay exponentially approaching a constant value as time elapses. The faradaic component of the nonspecific current,  $i_{cathode}$  is constant at equilibrium. This approach was taken in real experiments and a certain period of time was awaited before arsine arrives on the cell. Only the  $i_{specific}$  current causes increase of current in magnitude. The total measured current always has the nonfaradaic component.<sup>51</sup>

In a simplified model, we subtract the non-specific current from the total current to obtain the specific current as following manner. In all cases of experiments, the baseline signal decays exponentially and there is no peak between A and B when no arsine is generated. Here we use IUPAC convention for the sign of current. The positive direction here means oxidation current is generated. In the plots of chronoamperometry, the opposite sign was used.

---

<sup>51</sup> Bard, A.J.; Faulkner, L.R. *Electrochemical Methods, fundamentals and applications*, 2nd ed.; John Wiley & Sons: New Jersey, **1994**, p 9.

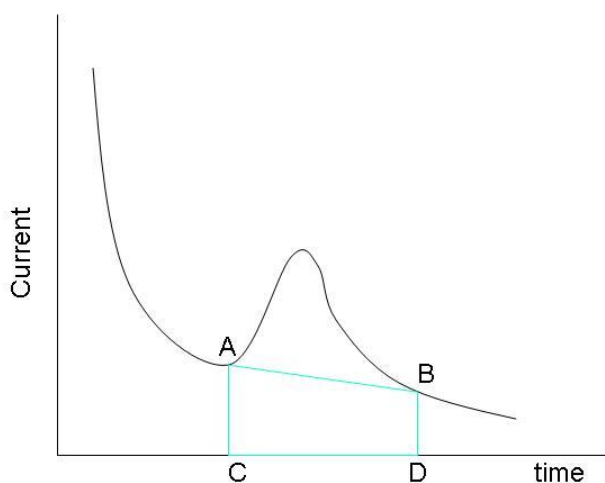


**Figure 4.5.3** A sketch of a typical amperometric signal. The non specific signal due to capacitive current is approximated by a straight line from A to B for clarity. A trapezoid ABCD represents the charge due to capacitance current. This non specific current should be subtracted from the specific current. From the area under the curve between time points C and D, the area of the trapezoid ABCD should be subtracted to get the current solely due to the reaction of arsine with iodine.

It is only when reducing gas arsine generated from the vial is transported on the filter paper that the signal shows a peak above the baseline AB. The actual baseline from A to B is an exponentially decaying curve that can be obtained by fitting the exponential function from time zero to the time immediately before reducing agent is added. We can draw a straight line from A to B to get the baseline in real measurement when the error associated with it is small. Actual data fitting and results of measurement is discussed in section 4.12.1. This simplification worked well for the type of measurement we performed as the successful construction of calibration curves demonstrated. In more precise treatment of data requires fitting an exponential curve. However, it is deemed unnecessarily complicated. A practical reason is that each baseline of all measurement follows a slightly different curve. The baseline from one to the next run varies to a certain degree due to changes in resistance and capacitance. The variation comes from the

manner the cell was used. We used a new filter paper in each measurement and the placement of the filter paper in the cell was always slightly changed every time we placed the filter paper. In addition, the filter paper was not truly identical as all filter paper was cut by hand and application of an aliquot of electrolyte had variance. As a consequence, the cell capacitance and cell resistance always changed substantially. We attempted to fit the curve to an exponential baseline in a hope that we get a better, correlation coefficient,  $R^2$  value as described in section 4.12.1. However, we found that a straight line connecting a point A and a point B approximated the base line very well as the goodness of  $R^2$  showed.

#### **4.5.2. A model for signal response**

We will derive a mathematical expression of this current here. We focus on specific current, a current due to oxidation of iodide generated from reducing gas arsine. We measure signal while arsine is generated and also afterwards until the current decays back to baseline. For clarity we divide the process into two stages. The amperometric response occurs when  $\text{NaBH}_4$  generates  $\text{AsH}_3$  for a couple of minutes. The current is dictated by mass transport equation of arsine. A measurable quantity in experiments is the total current the sum of  $i_{\text{nonspecific}}$  and  $i_{\text{specific}}$ . Here we will derive an equation for  $i_{\text{specific}}$ . In treatment of the data, we subtracted the baseline current according to Equation 4.5.8.

#### **4.5.3. Mass transfer of arsine during continuous addition of $\text{NaBH}_4$**

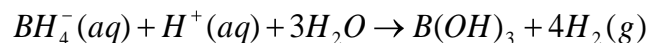
Wagenen et al depicted the peak shape of the atomic absorption spectroscopy with kinetic model.<sup>52</sup> The mass transfer of arsine generated from the generator vial was

---

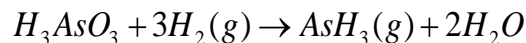
<sup>52</sup> Van Wagenen. S.; Carter. D.E. Kinetic control of peak shapes in atomic absorption

dictated by the kinetics of chemical reaction of arsenious acid with NaBH<sub>4</sub>. The chemical reactions for generating arsine are as follows:

**Equation 4.5.9**



**Equation 4.5.10**



We assume that nascent hydrogen species that can reduce H<sub>3</sub>AsO<sub>3</sub>(aq) in water is at constant concentration.<sup>53</sup> The stoichiometry of Equation 4.5.9 reveals that the one mol of sodium borohydride consumes one mol of hydronium ions. Therefore, after 2 mL of 2 % (w/v) of NaBH<sub>4</sub> in 0.5 M NaOH is added to 4 ml of 2.5 M sulfuric acid, the solution becomes 1.5 M in sulfuric acid. However, nascent hydrogen capable of reducing arsenite species in aqueous phase is very limited and short-lived. Also, the reactive hydrogen has very limited solubility in water. As soon as it is formed, it should react with arsenious acid or escape the aqueous phase as H<sub>2</sub>(g). The rate of generation of arsine is as follows:

**Equation 4.5.11**

$$\frac{d[AsH_3]}{dt} = k' [H_3AsO_3][H^*]$$

Here we denote nascent hydrogen as [H\*] which is reactive hydrogen that can reduce arsenious acid. When concentration of reactive hydrogen is at a constant level, the rate of generation of AsH<sub>3</sub> is first order as the following equation:

---

arsenic determinations by arsine generation, *Analytical Chemistry*, **1987**, 57, 891-896  
<sup>53</sup> Kumar, R.; Ryazuddin, P. Mechanism of volatile hydride formation and their atomization in hydride generation atomic absorption spectroscopy, *Analytical Sciences*, **2005**, 21, 1401-1410.

**Equation 4.5.12**

$$-\frac{d[H_3AsO_3]}{dt} = \frac{d[AsH_3]_{aq}}{dt} = k_1[H_3AsO_3]$$

The solution of this first order differential equation is as follows:

**Equation 4.5.13**

$$[As(OH)_3] = [As(OH)_3]_0 \exp(-k_1 t)$$

We assume that the rate of escaping of AsH<sub>3</sub> gas is proportional to the initial pressure of arsine in the reaction vial. Then the disappearance of arsine in solution phase is expressed as follows:

**Equation 4.5.14**

$$\frac{d[AsH_3]_{aq}}{dt} = k_1[H_3AsO_3] - k_2[AsH_3]_{aq}$$

The solution of the coupled first order differential equations, Equation 4.5.12 and

Equation 4.5.14 is as follows:

**Equation 4.5.15**

$$[AsH_3]_{aq} = \left(\frac{k_1}{k_2 - k_1}\right)\alpha\{\exp(-k_1 t) - \exp(-k_2 t)\}$$

where,  $\alpha$  is the initial concentration of arsenious acid,  $[As(OH)_3]_0$ . Let's define a constant  $K_{arsine}$  for arsine in aqueous phase and arsine in gas phase equilibrium constant:

**Equation 4.5.16**

$$K_{arsine} = \frac{[AsH_3]_{gas}}{[AsH_3]_{aq}}$$

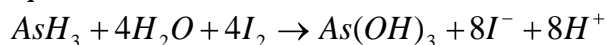
Then,  $[AsH_3]_{gas}$  is simply  $[AsH_3]_{aq}$  multiplied by  $K_{arsine}$ . Hence, the concentration of arsine in gas phase is given as:

**Equation 4.5.17**

$$[AsH_3]_{gas} = K_{arsine}[AsH_3]_{aq} = K_{arsine}\left(\frac{k_1}{k_2 - k_1}\right)\alpha\{\exp(-k_1 t) - \exp(-k_2 t)\}$$

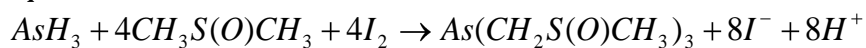
It is known that, DMSO (dimethyl sulfoxide) is known to absorb moisture from the ambient environment (air and moisture from reaction vial). Therefore, water becomes one of the reactants as follows:

**Equation 4.5.18**



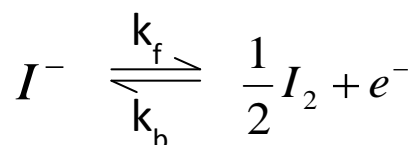
Alternatively, in absence of moisture, which is very rare in the field, one can consider the following reaction also.

**Equation 4.5.19**



Either way the production of  $I^-$  is quantitative. The chemical reaction is coupled with an electrochemical reaction, which is written as follows.

**Equation 4.5.20**



Here,  $k_f$  is the rate constant for forward reaction and  $k_b$  is the rate constant for backward reaction. We safely assume that there is no backward reaction when the working electrode is held at a high potential, 1.1 V. Regardless of chemical reaction is used, the same mathematical expression is obtained. The concentration of solvent is constant and will be factored into a constant. If we use DMSO as reactant,

**Equation 4.5.21**

$$\frac{1}{8} \frac{d[I^-]}{dt} = \lambda [AsH_3]_{cell} [DMSO] [I_2]^4 - k_f [I^-]$$

Here  $\lambda$  is the rate constant of the chemical reaction which does not include solvent. One can incorporate solvent concentration into the rate constant  $\lambda$ . The rate of change in the concentration of iodide is now:

**Equation 4.5.22**

$$\frac{1}{8} \frac{d[I^-]}{dt} = k[AsH_3]_{cell}[I_2]^4 - k_f[I^-]$$

Typically, 50  $\mu$ l of 20 mM iodine in DMSO was used on the filter paper. This corresponds to 1  $\mu$ mol of iodine on the filter paper. Let's assume that arsine is generated from 4 ml of 100  $\mu$ g L<sup>-1</sup> standard solution. The number of moles of arsenic (atomic weight, 74.92160) in this case is 5.339 nmol. Therefore, it is valid that iodine is present in large excess to arsine. We further simplify the expression by incorporating the  $[I^-]$  term to the rate constant.

**Equation 4.5.23**

$$\frac{1}{8} \frac{d[I^-]}{dt} = k_{pseudo}[AsH_3]_{cell} - k_f[I^-]$$

Now we apply the steady state condition. The rate of change of iodide is constant. The rate of production of iodide by chemical reaction is balanced out by consumption of iodide by electrochemical reaction. Consequently, there is no net change of  $[I^-]$ . Then one obtains,

**Equation 4.5.24**

$$k_{pseudo}[AsH_3]_{cell} = k_f[I^-].$$

The left hand side is the rate of generation of iodide from chemical reaction between arsine and iodine, and the right hand side is the rate of disappearance of iodide due to electrochemical reaction. The right hand side is immediately related with anodic current.

**Equation 4.5.25**

$$\frac{i}{nFA} = k_f[I^-]$$

Now we define a equilibrium constant, K between gas phase arsine and solution phase arsine.

**Equation 4.5.26**

$$K = \frac{[AsH_3]_{cell}}{[AsH_3]_{gas}}$$

We know time dependence of  $[AsH_3]_{cell}$ , which is expressed as follows:

**Equation 4.5.27**

$$[AsH_3]_{cell} = K[AsH_3]_{gas} = K(K_{arsine})\alpha\left(\frac{k_1}{k_2 - k_1}\right)A\{\exp(-k_1t) - \exp(-k_2t)\}$$

The current is given as:

**Equation 4.5.28**

$$i = nFAk_{pseudo}[AsH_3]_{cell} = nFAk_{pseudo}K(K_{arsine})\alpha\left(\frac{k_1}{k_2 - k_1}\right)A\{\exp(-k_1t) - \exp(-k_2t)\}$$

Here,  $\alpha$  is the initial concentration of arsenious acid, which is separated from the time dependent part. The term in the bracket { } does not depend on original concentration of arsenite. The amperometric signal response is given by the equation.

As demonstrated in the experiments we performed, integral of this current gives a linear relationship between the original concentration of arsenite and integrated signal. The reason is clear as mentioned before; in the integration,  $\alpha$  is constant and is factored out from the rest of the expression. The integration corresponds to the charge flowed during oxidation of iodide to iodine and this is why this method can be called coulometry. The charge passed due to iodide oxidation is proportional to the number of arsenious acid in the original solution. Arsine in gas phase does not know where the carbon electrode and filter paper is located, so it arrives on the surface of carbon electrode and filter paper indiscriminatingly. Part of the  $AsH_3$  lands on region where  $AsH_3$  reacts with  $I_2$ , after which, the formed  $I^-$  travels by diffusion to the surface of the electrode yielding diffusion

current. Not all  $\text{AsH}_3$  will be able to move to the close proximity of the electrode. When the working electrode covers sparsely the region where  $\text{AsH}_3$  is deposited, we will get tiny signal. Larger current will be obtained by covering the region more extensively.

#### **4.6. A thin layer cell with Au electrode on a syringe filter**

The cell notation below is the electrochemical system for this section:

$\text{Au(s)} / \text{I}_2(\text{sln}), \text{I}^-(\text{sln}), \text{AsH}_3(\text{sln}), \text{H}_3\text{AsO}_3(\text{sln}), \text{H}_3\text{AsO}_4(\text{sln}) // \text{I}_2(\text{sln}), \text{I}^-(\text{sln}), \text{AgI}(\text{sln}) / \text{Ag (s)}$

The goal is to get the quantitative signal proportional to the number of moles of iodide generated by arsine. To achieve the goal, we explored several different electrochemical systems. The generated iodide, if it can be detected more conveniently, would be potentially an excellent analytical method. We believed that the oxidation current should be proportional to iodide generated by arsine. And we indeed succeeded in measuring oxidation current proportional to iodide generated by arsine. In terms of experimental works, realization of this excellent idea took numerous trials of making cells with different materials than we initially thought. These cells with different electrode materials, cell bodies, and geometric arrangements are discussed.

Here the notation sln means either DMSO or water. See Table 4.6.1 the results of comparison studies using different electrolytes and addition time of  $\text{NaBH}_4$  for individual experiment. The first system tried with this idea was a gold electrode on a syringe filter. More specifically, a gold wire electrode on a syringe filter was used as working electrode and a strip of silver fabric was used as a reference and a counter electrode. The generator vial generated arsine as usual and the arsine was transferred into the filter paper where

arsine reacts with iodine which had been electrochemically generated for a certain period of time. In this very simple configuration, a signal from very dilute sample whose concentration was as low as 50  $\mu\text{g/L}$  was clearly observed to our excitement. However, pressure developed in the arsine generator vial imposed devastating effects on a flimsy system where electrodes and filter paper with electrolyte were secured by just paper clips. The pressure increased the surface area of the electrode by pressing hard the gold wire against the filter paper. This in turn increased the current measured on the system. In spite of these technical difficulties that had to be overcome later, the experimental results from these experiments greatly motivated us to further develop sensors based on indirect measurement of arsine gas. The solutions to uncontrollable factors were not known for long time. The change in signal due to the pressure pulse generated from excess hydrogen was identified as one of the sources. Although, solution with regard to the pressure pulse had not been solved, the indirect measurement of arsine worked fine. It is fruitful to discuss them as a development process. In a more stable system, there is no doubt that this type of system can be a practical system of measurement of arsine gas. Experiment timing was varied to get the optimal condition for measurements. Changes in concentrations and volume of electrolytes were made to observe to find good conditions for the electrochemical system.

#### **4.6.1. Materials and Methods**

A gold electrode wire with 100  $\mu\text{m}$  in diameter and 20 cm in length was placed as a working electrode. A counter with function of reference electrode was a strip of silver fabric ( a 1.5 cm x 1.5 cm square, high performance silver mesh fabric, cat. no. Filter

papers (Whatman no 4) were cut to disks by a pair of scissors (0.17 mm in thickness, 27.40 mm in diameter). After the filter paper was soaked with 50  $\mu\text{L}$  of 30 mM KI in DMSO, it was inserted between counter and working electrode. The syringe filter was made from commercial syringe filter ( NYLON + GL 0.2  $\mu\text{m}$ ). The syringe filter was cut in the middle and the membrane was removed. The thickness of the cell body was 2.5 mm and diameter was 32.18 mm. The female Luer port in the middle was connected to the arsine gas transfer line. When all components were assembled, the cell was secured by a paper clip shown in the picture. Generator vial was 70.24 mm in height and 20.69 mm in outer diameter and the internal volume of the generator was 15 ml. A solution of 1 %  $\text{NaBH}_4(\text{w/v})$  was added between 60 and 120 sec. The addition stopped at 180 sec for comparison studies.

Potential was held at 1.1 V and amperometric signal was recorded. An aliquot of 2 ml of 1 mg/L As(III) in 2.5 M sulfuric acid was used to generate arsine gas and the arsine gas was deposited on the filter paper. For blank experiments, 2 ml of 2.5 M sulfuric acid in water was used. For integration of the anodic current, integration from 60 s to 200 s was performed in all cases except one case where integration parameters were specified.

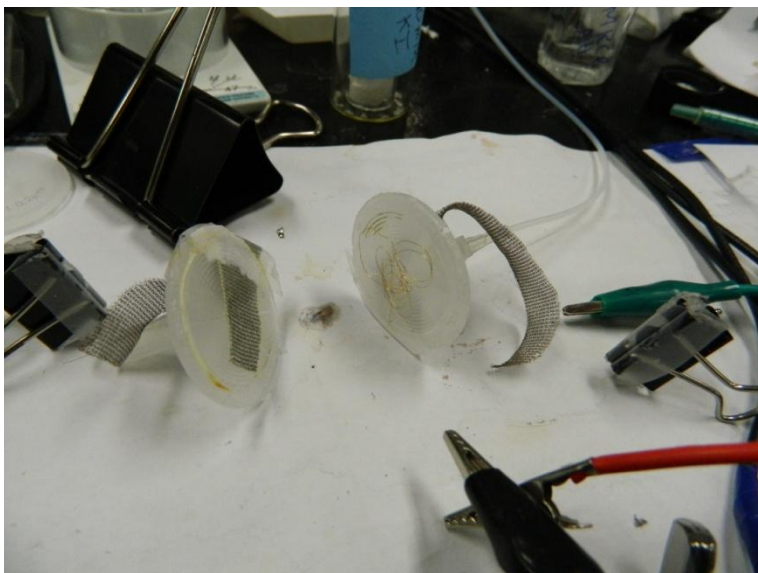
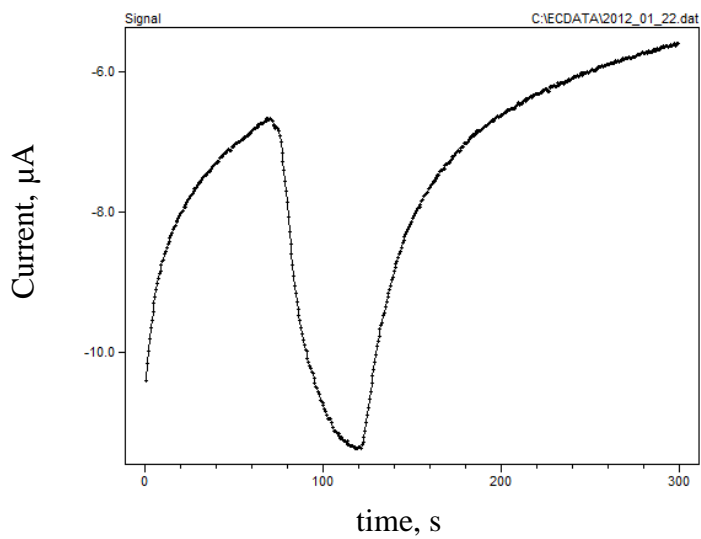


Figure 4.2. 1 A picture shows a thin layer cell with gold wire electrode. Two pieces of syringe filter were used to install the electrodes. A disk of filter paper was inserted, the cell was secured by a paper clip.

#### 4.6.2. Results and discussion

A typical signal obtained from highly concentrated As(III) standard is shown in Figure 4.6.1.



**Figure 4.6.1** A typical amperometric signal response. Arsine gas was generated and deposited on the filter paper as soon as sodium borohydride addition started at 60 s and the current decayed at 120 sec when addition of borohydride stopped. The signal was obtained from 2 mL of 1 mg/L As(III).

The charge that flowed between 60 s and 120 s was -262.0  $\mu\text{C}$  and the background charge was -943.4  $\mu\text{C}$ . As explained in the general instrumentation section, the error of the measurement is  $\pm 0.13 \mu\text{C}$ . The height of the signal was about  $4.7 \pm 0.13 \mu\text{A}$ . Hereafter we will omit the error terms. To see if increased signal could be obtained at the expense of more chemical reagent,  $\text{NaBH}_4$ , the addition was performed for extended time, i.e. from 60 sec to 180 sec. The amperometric signal was increased in entry 2. We changed electrolytes, time of addition of reducing agent, and concentration of As(III) to investigate the system. Here we provide a table for discussion.

**Table 4.6.1** the results of comparison studies using different electrolytes and addition time of  $\text{NaBH}_4$

Exp. no.	Sample concentration	Height of signal, $\mu\text{A}$	Integrated current, Charge, $\mu\text{C}$	Background	$\text{NaBH}_4$ addition start/stop	Electrolyte
1	1 mg/L	4.7	-262	-934	60/120	25 $\mu\text{L}$ of 30 mM KI in DMSO
2	1 mg/L	4.9	-313.4	-909	60/200	25 $\mu\text{L}$ of 30 mM KI in DMSO
3	1 mg/L	13	-767.9	-4210.9	60/120	12 $\mu\text{L}$ of 10 mM KI in water plus 12 $\mu\text{L}$ of 60 mM KI in DMSO
4	1 mg/L	20	-1137.6	-9201.2	60/120	25 $\mu\text{L}$ of 100 mM KI in water
5	50 $\mu\text{g/L}$	n/a	104.1*	-19140.6	60/120	25 $\mu\text{L}$ of 100 mM KI in water
6	50 $\mu\text{g/L}$	n/a	21.5*	-2761.7	60/120	25 $\mu\text{L}$ of 10 mM KI in water
7	50 $\mu\text{g/L}$	0.5	-33.0	-1195.3	120/180	25 $\mu\text{L}$ 30 mM KI in DMSO + 5 $\mu\text{L}$ of DI water.
8	50 $\mu\text{g/L}$	0.66	-43.4	-652.1	300/360; Integration:	25 $\mu\text{L}$ of 45 mM iodine in DMSO

					300/420	
9	50 µg/L	0.1	-11.6	-539.4	60/120	5 µL of water plus 25 µL of 45 mM iodine in DMSO

\*: The signal could not be integrated properly as the base line went down to fast.

In entry 2, the NaBH<sub>4</sub> was added from 60 sec to 180 sec. In all other cases, the reducing agent was added from 60 sec to 120 sec.

In entry 7, the signal was integrated from 120 sec to 200 sec. In all other cases, the signal was integrated from 60 to 200 sec in all cases.

One important observation is that iodide in the electrolyte caused a much larger background signal than iodine as demonstrated by experiment 5 and experiment 6. The signal could not be integrated to show negative number when higher [I<sup>-</sup>] was used in entry 5 and entry 6. Secondly, aqueous electrolyte gave rise much higher baseline current, jeopardizing accuracy of the sensor as demonstrated by experiment 2 and 3. In experiment 3, we have about the same concentration of potassium iodide as in experiment 2; however, the baseline current is more than 4 times higher in experiment 3.

Comparison of experiment 6 and experiment 7 demonstrated that the delayed addition of NaBH<sub>4</sub> enhanced the signal. In experiment 6, iodine was generated for 1 min whereas in entry 7, iodine was generated for 2 min. Longer generation of iodine increased response, current signal generated from iodide to iodine oxidation. A special consideration was given in experiment 8. The cell was potentiostated at 1.1 V for 300 s before addition of NaBH<sub>4</sub>. This ensured that any capacitance current decayed to very small value. At the expense of increasing measurement time, we get cleaner baseline for measurement. That experiment showed that 45 mM iodine gave the best results among studies performed with this particular sensor. Entry 9 showed that effect of added water

to the electrolyte is detrimental rather than beneficial. This is attributed to increased capacitance current which unfavorably affected the baseline.

The experiment with gold electrode taught three important lessons. First of all, iodine did not have to be generated electrochemically *in situ*, as iodine as reagent, when present initially, could be used. Secondly, aqueous media shows higher capacitance current than organic media. For favorable baseline, we could use organic solvent. Third, delay in addition of NaBH<sub>4</sub> favored sensitivity of the system. This is also related to baseline issue which is a consequence of the capacitance current in all electrochemical cells.

#### **4.6.3. Cyclic voltammetry (CV) of iodide to iodine**

This experiment was based on oxidation of iodide to iodine to characterize the cell system using CV as a diagnostic technique. The iodide oxidation to iodine is known to be a two step processes.<sup>54</sup> It was of our interest to observe this behavior with syringe filter cells, which were far different from conventional solution phase cell with standard reference electrode. Two different cells were made for observing iodide to iodine oxidation on the syringe filter cell. A schematic of these cells are provided below.

---

<sup>54</sup> Rogers, E.I.; Silvester, D. S.; Aldous, L.; Hardacre, C.; Compton, R. G. Electrooxidation of the iodides [C4mim]I, LiI, NaI, KI, RbI, and CsI in the room temperature ionic liquid [C4mim][NTf2]. J. Phys. Chem. C 2008, 112, 6551-6557.

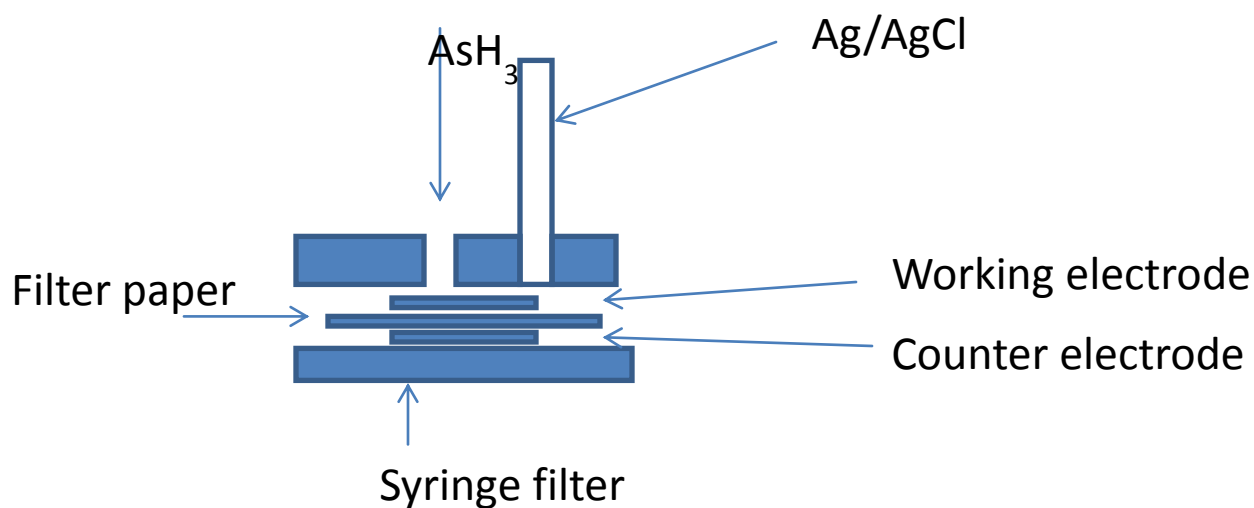


Figure 4.6.2 A schematic diagram of the syringe filter cell (cell B). A standard Ag/AgCl reference electrode was used.

The configuration of the cells is shown below. The cell A is identical to the one used in the pulse chronoamperometry experiments.

Table 4.6.2 Configuration of electrochemical cells.

Type	Working electrode	Reference	Counter	Cell body	Electrolyte
Cell A	Gold wire	Silver fabric	Silver fabric	Syringe filter secured by paper clip	25 $\mu$ L of 100 mM KI
Cell B	Gold wire	Ag/AgCl	Pt foil	Syringe filter secured by paper clip	50 $\mu$ L of 10 mM KI

#### 4.6.4. Results and discussion

##### 4.6.4.1. Characterization of cell A:

Here we give a cell notation for cell A in this section, which was characterized by cyclic voltammetry. The abbreviation, sln, indicates solution phase and other abbreviations mean usual meanings. This is because DMSO dissolves iodine and AgI.

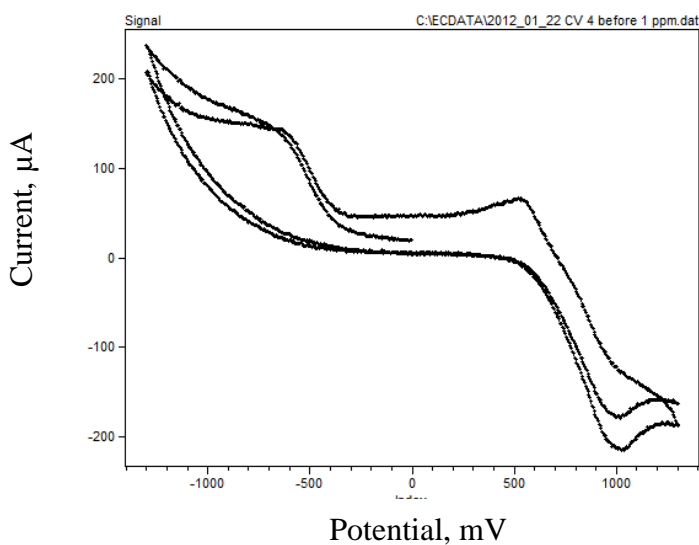
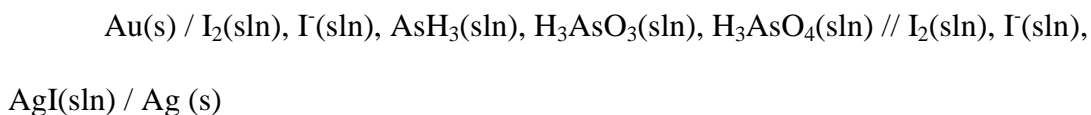


**Figure 4.6.3** Cyclic voltammetry of the cell A. CV was conducted from initial potential 0 V to the final potential of 1.3 V with vertex potential of -1.3 V at the scan rate of 100 mV/s.

At 1100 V, there was indeed an anodic wave, which was used for amperometry experiments. This wave confirms that iodide to iodine oxidation occurred and we are measuring it for arsine detection. The syringe filter cell was not very stable system and

the amperometric signal was subject to pressure increase. When the cell body was grabbed by hand and pressed hard, the amperometric signal increases. Therefore, more robust system was designed and built for the next experiments. Also, the flimsy 100  $\mu\text{m}$  gold wire was easy to be snapped off and caused many problems whenever one wants to open and close the cell.

#### 4.6.4.2. Characterization of cell B:

In this section, the cell notation is given as follows:

$\text{Au(s)} / \text{I}_2(\text{sln}), \text{I}^-(\text{sln}), \text{AsH}_3(\text{sln}), \text{H}_3\text{AsO}_3(\text{sln}), \text{H}_3\text{AsO}_4(\text{sln}) // \text{I}_2(\text{sln}), \text{I}^-(\text{sln}), / \text{Pt(s)}$

It was not entirely clear where the oxidation of iodide and reduction of iodine occurs. More pronounced peak of iodide to iodine oxidation current was observed with slight modification of the syringe filter cell. The Table 4.6.2 shows configuration of the cell B. Interestingly, two anodic peaks at 450 mV and 900 mV appeared. A weak cathodic peak at 510 mV and at 400 mV appeared. Starting from 0 V, potential was swept at the scan rate of 100 mV/s to 1300 mV and went back to -1300 mV.

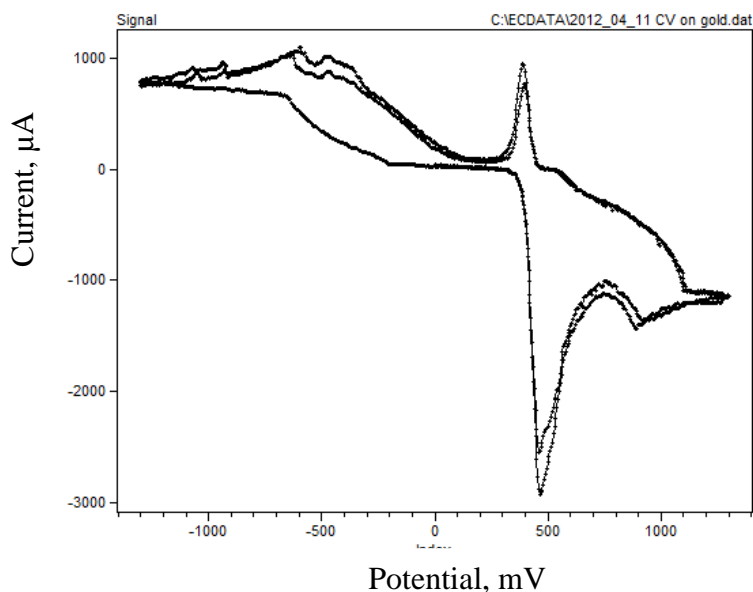


**Figure 4.6.4** Cyclic voltammetry of gold wire electrode. Anodic wave of iodide to iodine oxidation was observed at 450 mV and 900 mV. The scan started from initial potential of 0 V to final potential of -1.3 V with vertex potential of 1.3 V at the scan rate of 100 mV/s.

The two anodic peaks at 450 mV and 900 mV unambiguously indicated that two stage oxidation of occurred. A huge oxidation peak at 450 mV was followed by another oxidation peak at 900 mV. The peak was not seen when silver fabric was used as counter electrode. This is attributed to the change in the counter electrode reaction where iodine was reduced to iodide when oxidation of iodide occurred on Au working electrode.

#### **4.7. Amperometry using Pt as working electrode on Plexiglass cell body.**

With experience gained up to this point, a new cell was constructed. We replaced the syringe filter with more rigid body, Plexiglass to see if the erroneous signal response from pressure pulse could be removed entirely. To preserve the potential of the reference electrode at constant value, Ag/AgI reference electrode used. Cell notation for this cell is as follows:

Pt(s) / I<sub>2</sub>(aq), I<sup>-</sup>(aq), AsH<sub>3</sub>(aq), H<sub>3</sub>AsO<sub>3</sub>(aq), H<sub>3</sub>AsO<sub>4</sub>(aq) // I<sub>2</sub>(aq), I<sup>-</sup>(aq), AgCl(aq) / Ag(s)

#### 4.7.1. Material and method

The Ag/AgI reference electrode was made by emptying the AgCl electrolyte from the commercial Ag/AgCl reference electrode (CHI Inc.) and refilling with aqueous 100 mM AgI. The syringe filter was replaced between two Plexiglass support. Table 4.7.1 is the cell configuration.

**Table 4.7.1 Cell components in the Plexiglass cell.**

Counter	Reference	Working	Body	Electrolyte	Sample	Reductant
Pt, the same size as the working electrode	Ag/AgI, 100 mM KI	Pt, 4 mm x 3 mm square; perforated foil	Plexiglass	50 μL of 10 mM KI(aq)	400 μg/L	0.5 % NaBH <sub>4</sub>

For clear understanding, we provide a schematic of the cell in Figure 4.7.1 An aliquot of 50 μL of 10 mM KI in DMSO was applied to the filter paper described in the global list of materials. As KI was used, iodide was to be oxidized to iodine for 300 s during which electrogenerated iodine was chemisorbed to the Pt electrode. The Pt electrode punctured with a needle manually. It had several perforated holes with 1 mm diameter for passage of arsine gas though the filter paper and an outlet hole was provided on the bottom panel of the cell body. The cell was secured by two large paper clips as shown in Figure 4.8.2.

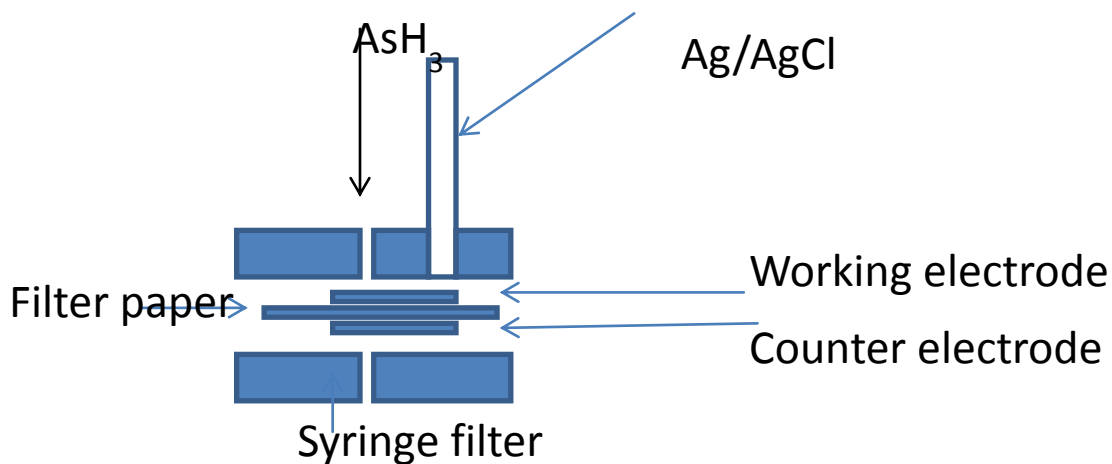
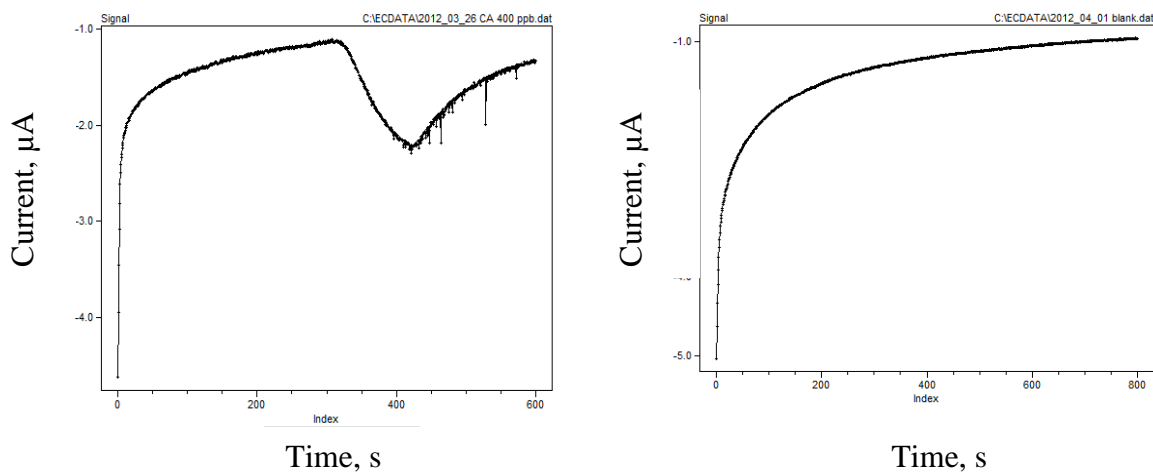


Figure 4.7.1 Schematic diagram of Pt electrode on syringe filter. The working electrode was Pt foil and a standard reference electrode was used.

#### 4.7.2. Results and Discussion

Figure 4.7.2 shows typical response for arsenic detection in this cell. A clean signal was obtained. The integrated value was obtained from 2 mL of 400  $\mu\text{g/L}$  As(III) standard. Integration of the current signal between 300 s and 600 s was -328.1 with the background charge of -169.9  $\mu\text{C}$ . A replicate experiment was run, which yielded the integrated value of -385.7 with background charge of -197.8. However, the system was not robust enough for measurement. Clogging of the frit on the reference electrode was frequently occurred. The clogging was subsequently cleaned by immersing in aqua regia, a mixture of nitric acid and hydrochloric acid in a volume ratio of 1:3. Even if

analytically useful signal could not be observed, here we show the signal response in Figure 4.7.2. The signals from 2 mL of 400 µg/L of As(III) and the blank were definitely different and we were convinced that we had been on the right track. The left panel in Figure 4.7.2 shows spikes, which were attributed to noise in the system.



**Figure 4.7.2** An amperometric signal from Pt foil electrode on a syringe filter. The signal was obtained from 2 mL of 400 µg/L is shown on the left panel and one from blank.

#### **4.8. Pt electrode on flat surface of Plexiglass with Ag/AgCl reference electrode.**

In the previous section we explored a cell with Ag/AgI system on Plexiglass. A disadvantage is that 100 mM KI in the reference electrode could come out to make the filter paper more concentrated in iodide ion. The replacement of Ag/AgI electrode with Ag/AgCl was made to see if this could ameliorate the problem. Here we provide the cell notation for this cell:



#### 4.8.1. Materials and method

More robust cell body was pursued in this configuration and two plates of Plexiglass were used for the cell body. The thickness of the plate was 9.3 mm and the both sides of the squared shaped plates were 67 mm. To insure the constancy of potential of the reference electrode, Ag/AgCl reference electrode was used. The purpose was to verify that the constancy of the potential of the reference electrode would yield more accurate amperometric signal.

Three electrode system was used and both of the working and counter electrode were pieces of Pt foil ( 4 mm x 3 mm), which were taped on the top of the Plexiglass plate. The table below summarizes the configuration of this cell. The thick cell body made of Plexiglass was used to hold the filter paper and the system was secured by paper clips which partially served the purpose of having the fixed geometry of the system.

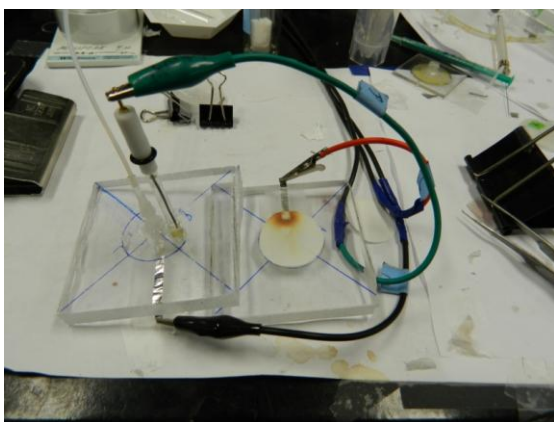


**Figure 4.8.1 Internal structure of the cell. A round circle iodine around Pt electrode was formed as a result of redox reaction.**

After complete assembly, the picture of the electrochemical cell is shown in Figure 4.8.2

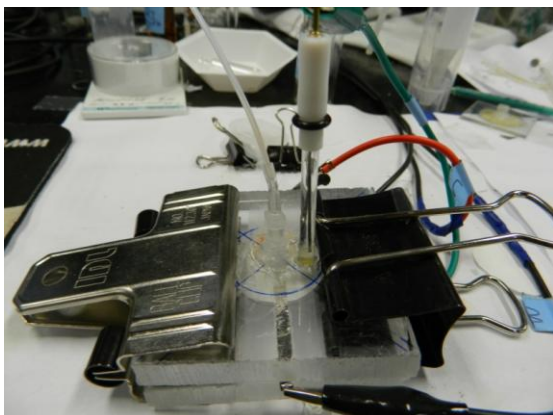
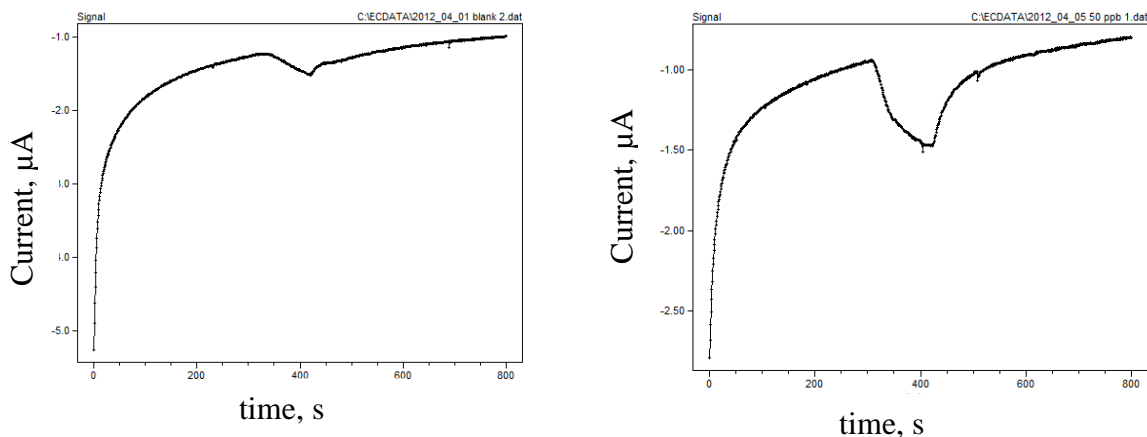


Figure 4.8.2 A completely assembled cell. The cell was secured by two paper clips. Reference electrode, Ag/AgCl electrode is shown.

#### 4.8.2. Results and Discussion

The figure below shows a response from 2 ml of blank, 2 mL of 2.5 M sulfuric acid. A signal response from 2 mL of 50  $\mu\text{g/mL}$  As(III) is shown in Figure 4.8.3.

Integration of the current started from 300 s to 480 s to give 29.1  $\mu\text{C}$  with a sensitivity of 0.582  $\mu\text{C}/(\mu\text{g/L})$ . However, the sensor did not yield reproducible results. The relative standard deviation of three injections of 10  $\mu\text{g/L}$  standards was 18 % from the data of entry 2, 3, and 4 in Table 4.8.1. One of the reasons might be the metastable surface atoms of noble metal electrode. It could be that the surface property of Pt was changed over time. Another reason is again the geometric limitation in our cell design. Although the Plexiglass material is very rigid, and the two blocks of Plexiglass cell body was secured by paper clips. This did not fix the geometry of the cell completely. We still observed irregular current responses.



**Figure 4.8.3** Comparison experiments with blank and 50 µg/L standard. (Left) Signal response from a blank sample. (Right) Amperometric signal response curve from 2 ml of 50 µg/L As(III).

We experienced many difficulties with this type of cell. To illustrate one of major limitation of this sensor, we show a signal response from 100 µg/L As(III) standard in Figure 4.8.4. There was supposed to be a larger current response than that from 50 µg/L As(III) standard. However, irregular signal response yielded only -6.5 µC.

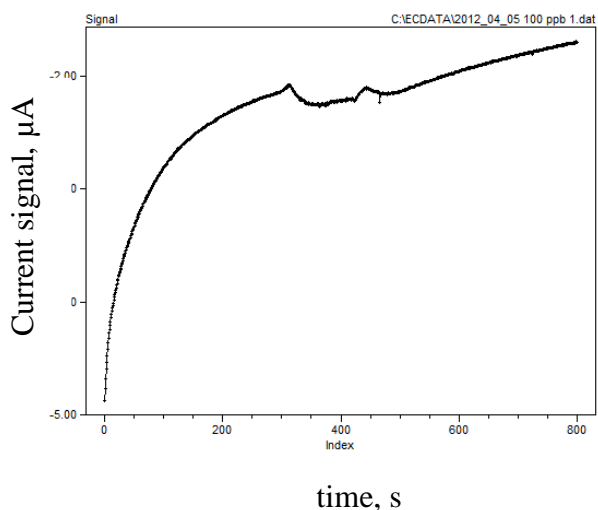


**Figure 4.8.4** A current signal with 2 mL of 100 µg/L As(III). Signal response was recorded from highly concentration sample, revealing that the response was neither reproducible nor proportional to [As(III)] . A

current signal with 2 mL of 100 µg/L. The signal was not quantitatively correlated with arsenic present in the sample. Also a dip was observed due to pressure pulse.

For discussion of amperometric responses from this cell, we provide Table 4.8.1 Amperometric responses obtained from this sensor where parameters were changed to find the analytical usefulness.

**Table 4.8.1 Amperometric responses obtained from this sensor**

	[As], µg/L	Background subtracted signal, µC	Background, µC
1	0	-11.0	-232.9
2	10	-41.1	-290.9
3	10	-28.8	-230.3
4	10	-35.2	-272.0
5	50	-29.1	-234.7
6	50	-45.8	-182.8
7	100	-6.5	-259.3

These data showed that the amperometric signal is not very stable between replicate runs. Entry 2 is a signal response from 10 µg/L As (III) and entry 5 from 50 µg/L, respectively. Therefore, further experiments were not performed with this cell. To demonstrate the limitation of this cell, we show a signal response from this cell when the cell was subjected to pressure pulses. All spikes were generated by squeezing the cell and the irregular shaped curve was observed.

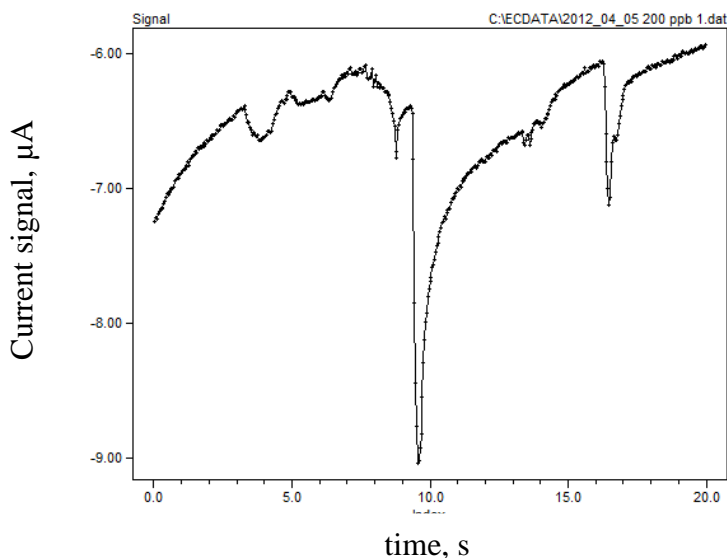


**Figure 4.8.5 Amperometry data while the sensor was held by hand and pressure was applied by squeezing the cell. The potential was held at 1.1 V while no gas was produced from the generator vial.**

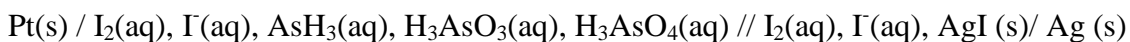
The data above suggested that one needs to construct more robust system where pressure cannot change amperometric signal response. When pressure can change the contact between the electrode and the filter paper, erroneous spikes are generated.

We had been able to reach the point where the cell responded to dilute solution of As(III). The rigid body of Plexiglass cell clamped by paper clips was not the best material for this type of work. The spikes appeared in the previous figure explicitly explained why we could not obtain reproducible results from the same samples. Up to this point, we had been partly aware of the problems. However, from this observation, we had dealt with the pressure pulse issues more adroitly. In a couple of new trials of design of the cell, we became successful in removing the pressure pulse issues. In the next section, the introduction of bolts and nuts for securing the contacts between filter paper and electrode is discussed.

#### 4.9. Design and fabrication of pressure insensitive gas sensor

In this section, we described a thin layer cell that was secured mechanically.

The cell notation is as follows:



In terms of keeping constancy of the geometry of the cell, a thin layer cell with one-piece configuration was reported in literature. Wonsawat et al. reported a one-piece thin layer flow cell where no gasket was used.<sup>55</sup> All components were assembled into one body of Plexiglass such that no gasket was needed. In this geometric arrangement, one-piece Plexiglass was cut and carved such that all three electrodes could be screwed into the three holes, making contact with single thin layer conduit for the analyte. This arrangement suggested that carbon paste could be used as working and counter electrode for a thin layer cell and a SSC reference electrode could be screwed into the cell body of the system. We did not have sophisticated tool and access to machine shop to make this type of cell and thus we did not pursue this approach. Furthermore, there is no doubt that one-piece configuration will not permit fixation of filter paper in the system.

The advent of bolts and nuts configuration for the cell is described in this section. The idea for the geometry of the cell and securing mechanism of the cell came from electrochemical HPLC flow cell. The pressure on the eluent after the HPLC column is regulated and the post column pressure stays usually at 100 to 200 psi. The reason is that degassing of eluent causes impaired the measurement of UV absorbance in UV flow cell.

---

<sup>55</sup> Wonsawat, W. et al. Highly Sensitive Determination of Cadmium and Lead Using a Low-cost Electrochemical Flow-through Cell Based on a Carbon Paste Electrode.

Moreover, without constantly and rigidly fixing cell geometry of the working electrode and counter electrodes, measurement of amperometric signal of eluent is not possible. We indeed found critically important information from the cell geometry of the HPLC amperometric sensor. Lucie Maixnerova et al. described arrangement of an amperometric HPLC cell in a published article<sup>56</sup>. In their thin-layer cell, a screw clamp was used to press a working electrode ( a thin film of boron-doped diamond on a disk of silica support) against a Kel-F body via a Viton gasket. We did not take the same geometry of the cell, but we took the idea that we need a screw to tighten a working electrode against the cell body. The cell has a Viton gasket with groove whose volume is about 10  $\mu\text{L}$  right where the working electrode makes intimate contact with the gasket. We adopted this idea and immediately construct a cell with Mylar gasket. We also made four holes for four bolts on the periphery of the Plexiglass body.

#### **4.9.1. Fabrication of the cell.**

The new cell was constructed with four bolts and nuts to secure Plexiglass cell. In this case, the cells are squeezed by the bolts and filter paper and electrodes were pressed against hard. This thinking bears fruits as demonstrated by the following sections. An attempt was made to make use of completely flat surface of the plastic plane separated by a gasket. Inside the cavity created by the gasket, we placed the electrodes and filter paper. The drawing below shows the schematics of the cell fabricated for this experiment. The dimension in the drawings is cm. The Pt electrodes were 0.3 cm x 1.0 cm x 0.003 cm

---

<sup>56</sup> Maixnerova, L. et al. Thin-Layer and Wall-Jet Arrangement of Amperometric Dectector with Boron-Doped Diamond Electrode, *Electroanalysis*, **2012**, 24, No. 3, 649-658

foils that were placed as the shape of gamma character. The gasket has 0.22 mm thickness and the filter paper has about 0.18 mm thickness ( a rectangle of 1.3 cm x 1.8 cm). Thickness of silver fabric was 0.25 mm. Two pieces of peek tubing ( 1/16 inches OD and 0.03 inches ID) were attached for inlet and outlet line for gas introduction. The body of the two Plexiglass plate was secured by four bolts.

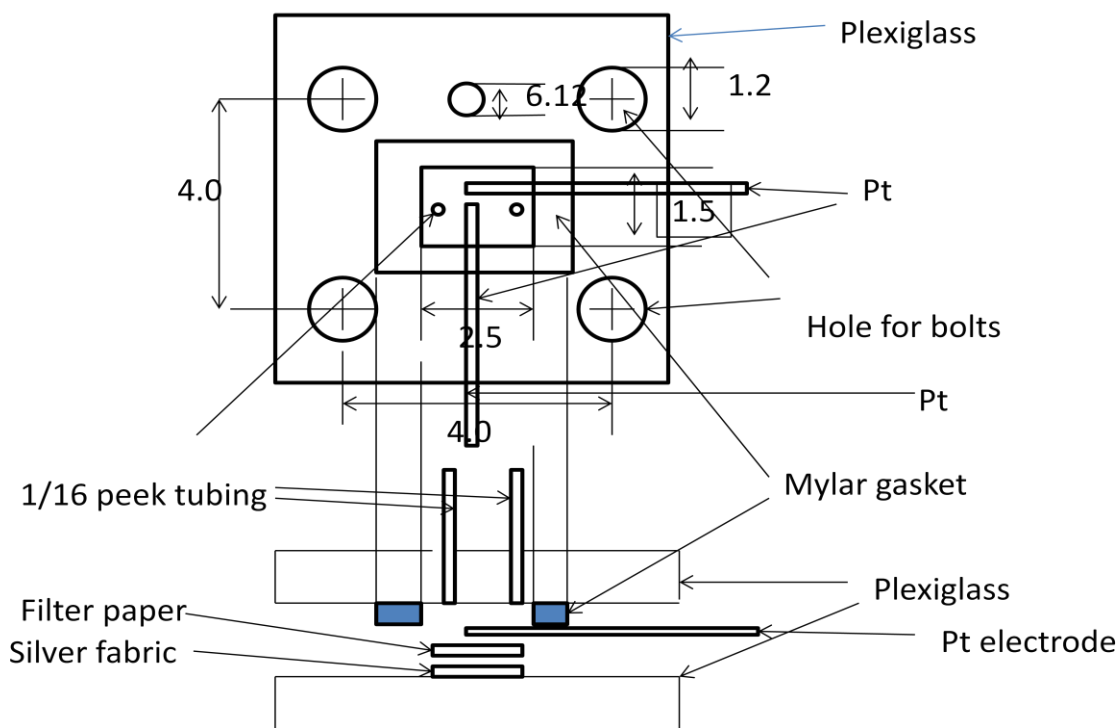


**Figure 4.9.1** Cell fabricated with four bolts and nuts to remove the pressure pulse. The numbers indicate length in cm. Four holes were made for four bolts.

The components of the cell are summarized in Table 4.9.1. We used Mylar gasket to seal the cell such that only way of gas to travel is though the 1/16 inches peek tubing which was sealed with polypropylene hot glue.

**Table 4.9.1 Components of the cell**

Counter	Ref	Working	Cell Body	Electrolyte	Sample	Reductant
Pt foil	Silver fabric, Ag/AgI	Pt foil	Mylar gasket between Plexiglass planes	20 $\mu$ L of 10 mM KI (aq)	400 $\mu$ g/L or blank	2 % NaBH <sub>4</sub>

Iodine was electrochemically generated from 20  $\mu$ L of 10 mM KI in DMSO.

Alternatively, in later experiment, 20  $\mu$ L of 20 mM iodine in DMSO was used.

#### 4.9.2. Results and discussion

The cell notation is given here for clarification:

Pt(s) / I<sub>2</sub>(aq), I<sup>-</sup>(aq), AsH<sub>3</sub>(aq), H<sub>3</sub>AsO<sub>3</sub>(aq), H<sub>3</sub>AsO<sub>4</sub>(aq) // I<sub>2</sub>(aq), I<sup>-</sup>(aq), AgI (s)/ Ag (s)

A typical signal from the blank and sample with significant amount of arsenic were not very different. Signal from blank and 400  $\mu$ g/L As(III) in the presence of the gasket is shown below and the integrated current was only -49.5  $\mu$ A and background was -780.5  $\mu$ C. Encouraged by this results, we replaced the electrolyte from 10 mM KI to 20 mM iodine to improve sensitivity of the sensor. But the signal definitely showed pressure pulse and slow transfer of arsine from generator vial. The problem was apparent during the experiments. When the screw cap of the generator vial was opened, gas popped out. It was suspected that arsine was redissolved into the solution of generator. We attribute the cause to inefficiency in mass transfer.

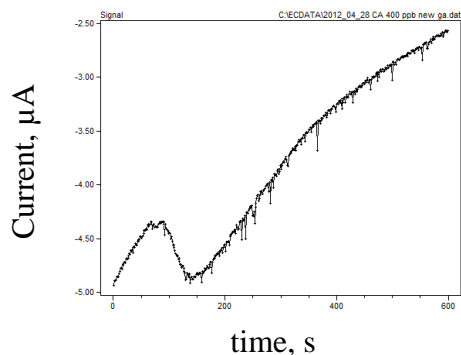


Figure 4.9.2 A signal from 2 mL of 400 µg/L arsenite in 2.5 sulfuric acid. The reductant was added between 60 and 240 s.

The transfer line has 0.03 inches inner diameter and we did not think that there would be a problem, but this was not the case. The tubing inner diameter was small enough to build up pressure on the sensor. The sensor had filter paper contacting metal electrodes and even small pressure made them move. The spurious signal response was attributed to the back pressure built up by the narrow bore peek tubing.

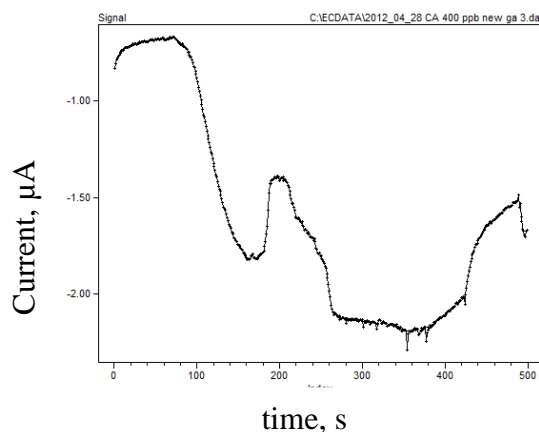
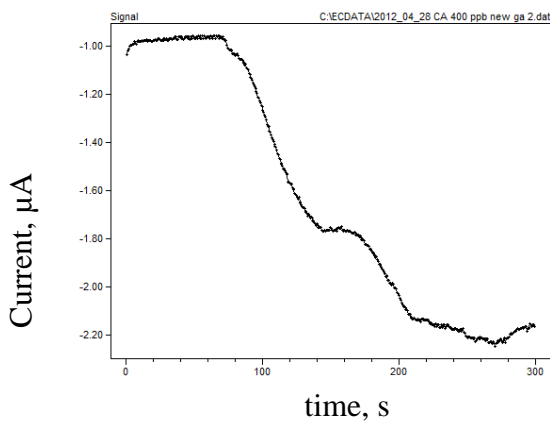
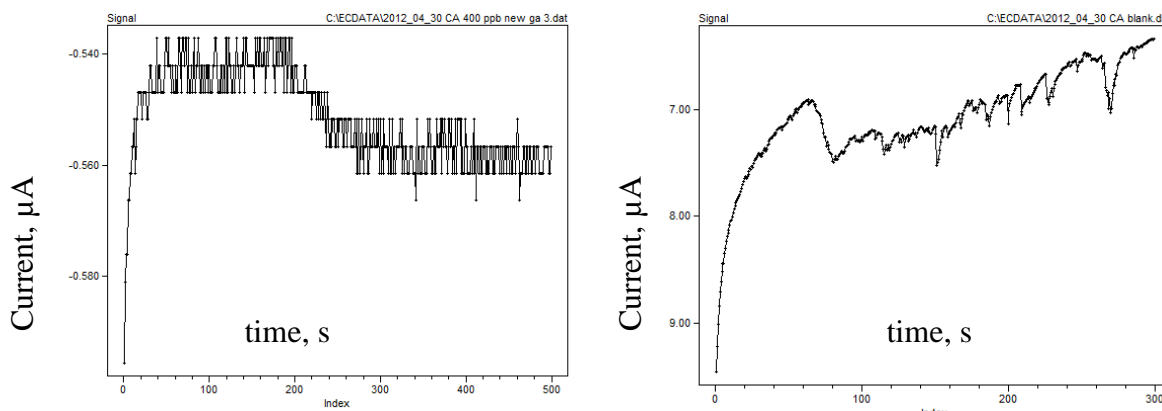


Figure 4.9.3 Signals from the two runs from 400 µg/L standard. Undesirable pressure pulses were recorded.

As the pressure was built up, only miniscule amount of the arsine was transferred. In addition, as the silver wire was thick, leakage could occur. Therefore, flattened silver wire was used to see if improvements could be made. More specifically, silver wire was flattened to have 0.22 mm thickness to become a 1 mm x 50 mm rectangle. However, as Figure 4.9.4 shows the signal was decreased dramatically. The problem was evident during the measurement. The H<sub>2</sub> gas built up pressure in the generator vial, and when the screw cap was opened, gas was popping out from the vial.



A signal from 2 mL of 400 µg/L

A signal from 2 mL of blank

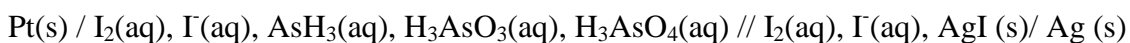
**Figure 4.9.4** Signal response from two different standards. For such a high concentration sample, 400 µg/L, on the left panel signal was unacceptably small. Furthermore, The signal from blank evidently showed that the cell was experiencing pressure pulse from the generator vial.

The signal from 2 mL of 400 µg/L As(III) was unacceptably small. Mass transfer of the analyte gas, arsine was not efficient. Ideally, arsine gas transfer should be complete within a couple of minutes. The magnitude of the signal response depends on the manner and efficiency of the mass transfer. Additionally, we did not have a sophisticated machine for fabricating this type of cell; fabrication of gasket from suitable

gasket material was also a challenging task. The unexpected and undesirable outcome of this results lead us to the use of syringe filter cell in which grooves on the surface of syringe filter provided efficient vent for mass transfer.

#### **4.10. Pt electrode on the surface of grooved surface of syringe filter**

The cell notation in this section is as follows:



In the previous experiments with the gasket, we concluded that the system suffered from impaired mass transfer. The conclusion leads us to use of the syringe filter material again, which obviated the need of fabricating gasket. The grooves were already provided for easy passing by the surface of the filter paper. Furthermore, the teeth of the grooves made the Pt electrode have firm contact with the filter paper. In order to secure the electrodes on the filter paper, the syringe filter had to be attached to the Plexiglass by polypropylene glue.

The syringe filter with grooved surface was attached to each plate of Plexiglass and four holes were made for bolts that secured the cell. This configuration eliminated the erroneous signal resulted from pressure pulse felt by the sensor. Figure 4.10.1 shows the working electrode on the syringe filter.

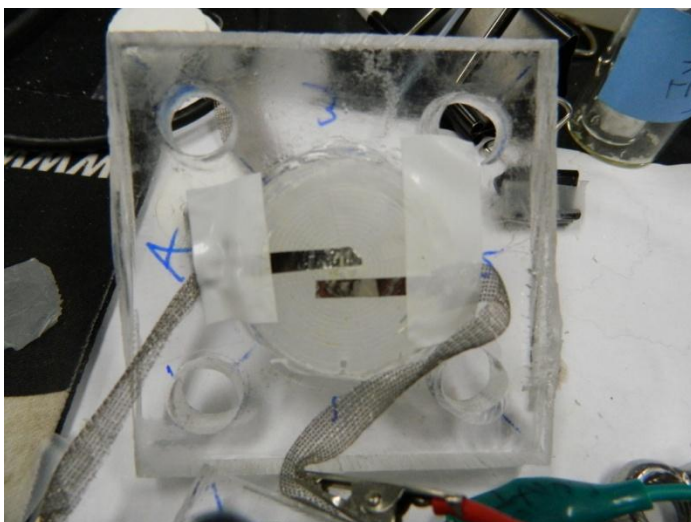


**Figure 4.10.1** Two parallel Pt electrodes as working electrode on the top unit.

On the bottom Plexiglass, we attached a silver fabric as a counter electrode shown in Figure 4.10.2.

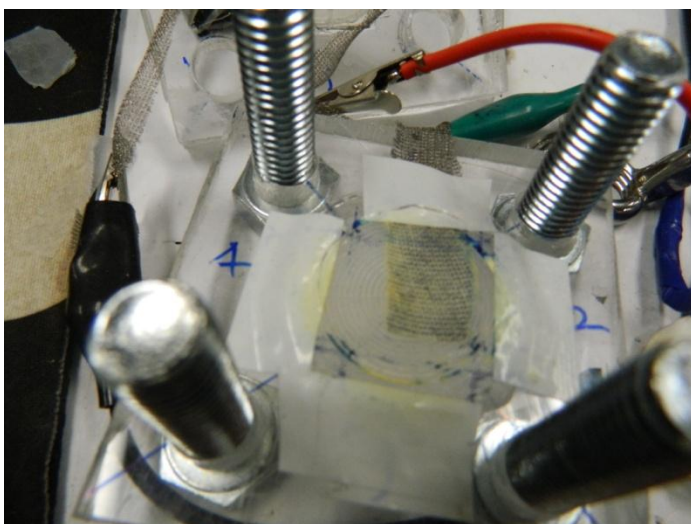


**Figure 4.10.2** Silver fabric electrode on the bottom unit.

As this cell configuration is so important for this work, we provide a schematic of this cell. The top view is provided. The cell has four holes for bolts and the syringe filter was attached to the Plexiglass plate which was described in detail in the previous section.

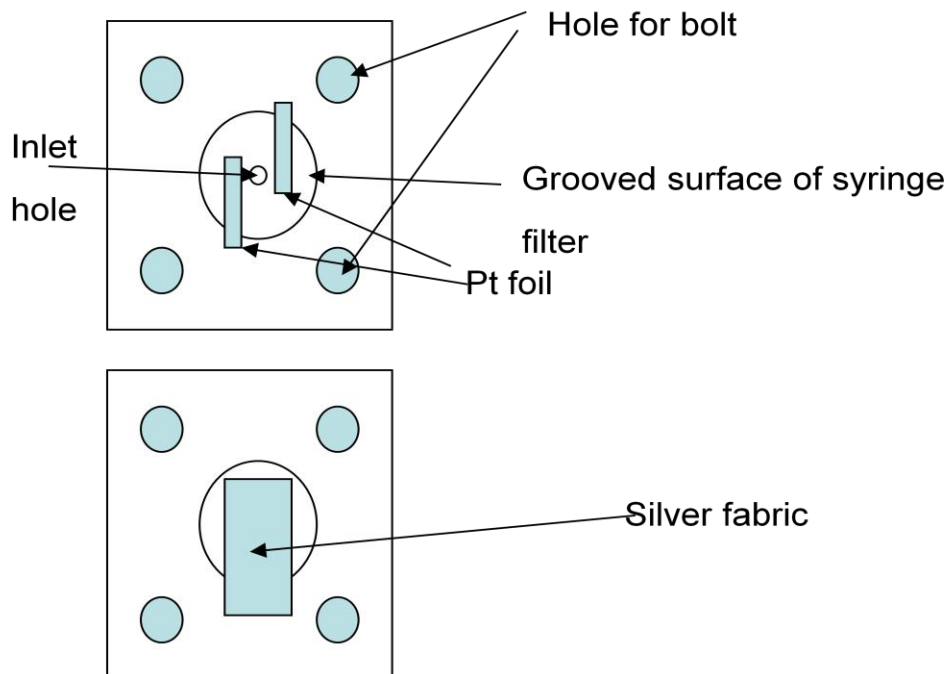


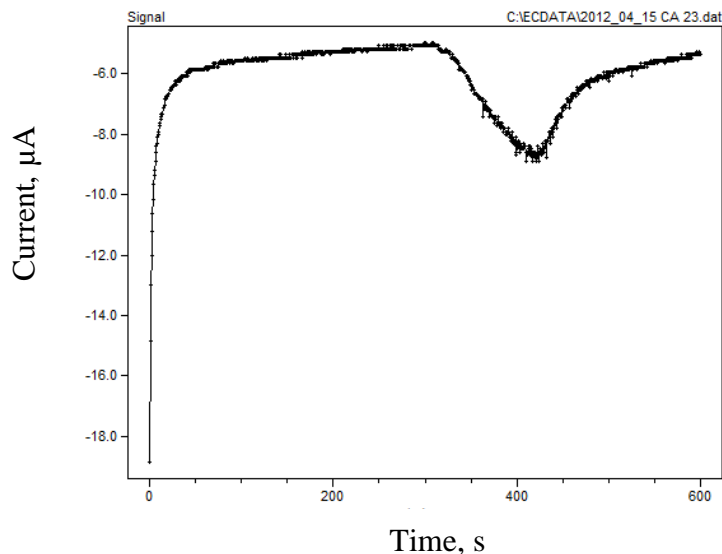
Figure 4.10.3 The internal structure of Pt foil cell. The Pt electrode was placed adjacent to the inlet hole where arsine is coming

Table 4.10.1 shows the actual components for constructing this cell.

Table 4.10.1 Cell configuration

Counter	Ref	Working	Body	Electrolyte	Sample	Reductant
Silver fabric	The same electrode as counter electrode	Two Pt foil	Syringe filter attached on Plexiglass	50 $\mu$ L of 10 mM KI in water	400 $\mu$ g/L	2 % NaBH <sub>4</sub>

The response from 2 mL of 400  $\mu\text{g/L}$  As(III) was obtained and charge that flowed as a result from reaction of arsine with iodine was  $-238.9 \mu\text{C}$ . The background charge was  $-1019.5 \mu\text{C}$ .



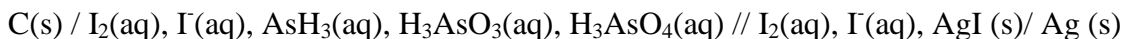
**Figure 4.10.4 Amperometric signal response from 2 mL of 400  $\mu\text{g/L}$ .  $V=1100 \text{ mV}$   $\text{NaBH}_4$  addition was performed from 300 to 420 sec.**

As the signal response in

Figure 4.10.4 shows, the cell was exhibiting interesting shape of curve. The baseline went to a very flat line quickly and on top of this flat base line, we have a skewed bell shaped amperometric signal. However, the current we were observing was disappointingly small, considering that we had been looking into developing sensor for 10 to 50  $\mu\text{g/L}$  of arsenic. Therefore, we came up with an idea of using a thin fiber electrode as working electrode that extensively cover the region where  $\text{AsH}_3(\text{g})$  was deposited on the filter paper. In the next section we will discuss thin carbon fiber electrode.

#### 4.11. Thin carbon fiber as working electrode

In this cell, the cell notation is as follows:



We have two different cells in this section, but the same cell notation can be used.

We will discuss thin fiber electrode which gave the best results amongst all the cells we experimented for this work. Here we describe two different cell configuration of Plexiglass cell. The Plexiglass cell was the best solution to deal with desensitizing the pressure pulse. All throughout the development process, the pressure pulses had been a headache which could not overcome easily. With four bolts that secure the electrodes against filter paper to prevent any movement of objects, this problem was solved cleanly. However how to collect the oxidation current from electrochemical reaction, i.e., iodide to iodine conversion were to be figured out. When Pt foil electrode was used, arsine could not be deposited on the region where the Pt foil resided. Arsine made iodide only on the periphery of the Pt electrode. This limited the area where the working electrode could collect the current. We could use very fine wires of Pt or other material. Fortunately a bundle of fine wires of carbon electrode was available commercially. As this fiber had very thin diameter, we could easily spread fibers on the top of the filter paper. This configuration most closely resembles the porous working electrodes described in the literature of arsine gas sensors. The ideal material will be a disk of very porous Pt or carbon which makes intimate contact with the filter paper, i.e. electrolyte. In this section, a bundle of fine wires of carbon electrode as working electrode is first

introduced and to our expectation, successful measurement of arsine oxidation current was achieved.

#### 4.11.1. Materials and Methods

The table and picture shows the geometric configuration of the cells. The potential was held constant at 1100 mV and the data was acquired for 300 s. An aliquot of 2 mL of 500  $\mu\text{g/L}$  As(III) was used and 2 %  $\text{NaBH}_4$  in 0.5 M NaOH was added between 60 s and 180 s at the flow rate of 1 mL/min. An aliquot of 50  $\mu\text{L}$  of 20 mM iodine was applied onto the filter paper. A reference electrode from CHI was used and when not in use, the electrode was stored in 1 M KCl as the manufacturer recommended.

**Table 4.11.1 Two different cells with carbon fiber electrode.**

Cell	working electrode	counter	reference
Cell A	carbon fiber	silver fabric	silver fabric
Cell B	carbon fiber	silver fabric	Ag/AgCl, KCl(1 M)

A picture of the actual cell is provided below for illustration.

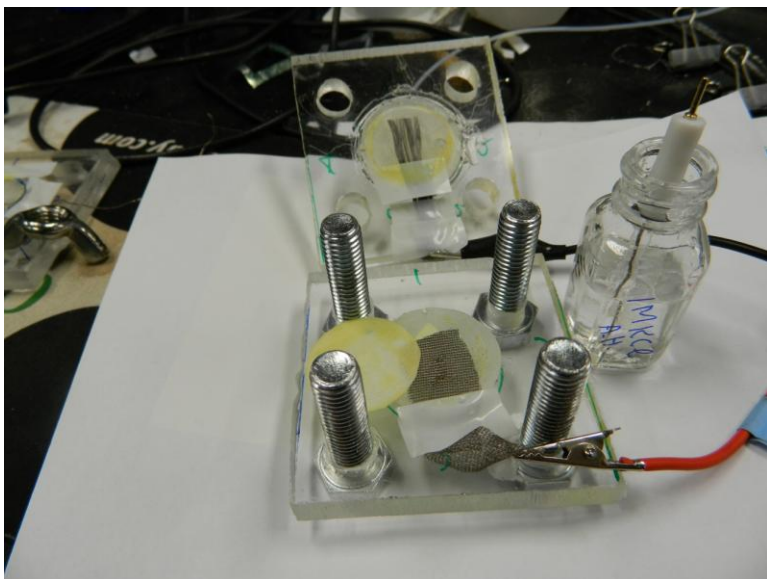


Figure 4.11.1 Carbon fiber electrode and silver fabric electrode

#### 4.11.2. Results and discussion

We used the standard reference electrode (SSC, CHI Inc.) in three electrode system in configuration B and pseudo reference electrode in two electrode system in configuration A. We compared the behavior of the two cells to see if there was any benefit of using the commercial reference electrode.

##### 4.11.2.1. Amperometric response from cell A

The signal depended on whether the outlet hole was closed or open. We performed the experiments with the same standard, 2 mL of 500  $\mu\text{g/L}$  As(III). When the hole was closed by a piece of tape, we obtained larger signal. This is because, the arsine was bound to spread in radial direction from the inlet port and there was more arsine reacting with iodine. When the outlet hole was open, the arsine gas flow passed through

the filter paper and less arsine was available for reaction with iodine. The charge, integrated current, was less with the same sample as shown in Figure 4.11.2.

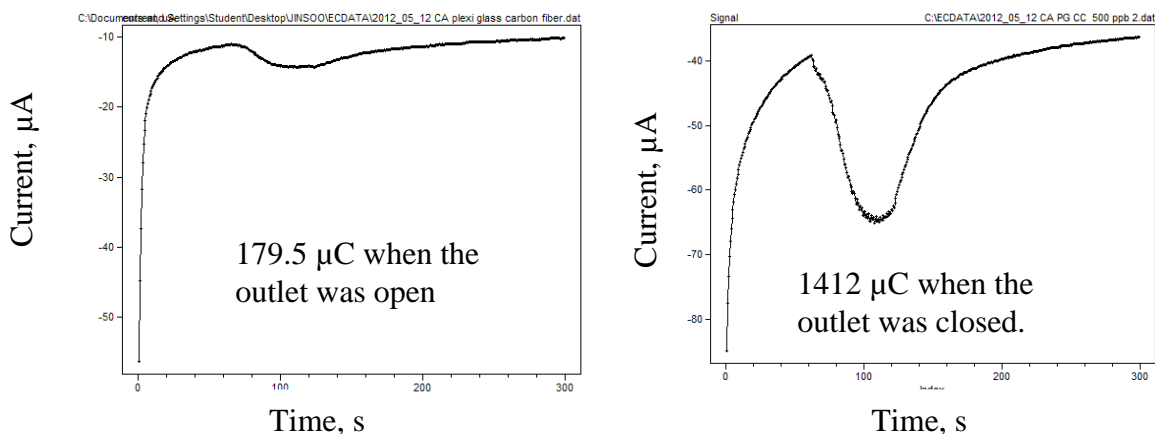


**Figure 4.11.2** Comparison experiments of the same cell. When the outlet hole is closed as shown in the right panel, the magnitude of the current signal is larger than that of the one with open outlet hole (left panel).

A repetition of this measurement gave 1124  $\mu\text{C}$  which was not very far off from the previous measurement. Blank experiment also was performed to see the signal disappeared completely. The blank gave a small signal; 106.2  $\mu\text{C}$  as expected. Even the blank sample could produce current as all materials contained trace level of As (III) or other impurities.

#### **4.11.2.2. Amperometric response from cell B.**

The same cell notation can be used in this system. Only difference is the reference electrode here. We tested the cell with a commercial reference electrode to see if we could get the comparable results. The cell gave smaller signal; 750.9  $\mu\text{C}$  and this

verified that the potential applied on working electrode, 1100 mV vs. Ag/AgI reference electrode was close to the potential applied vs. a standard Ag/AgCl electrode.

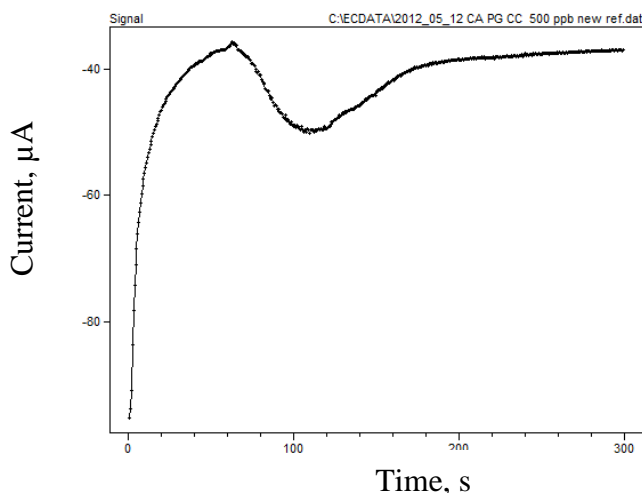


Figure 4.11.3 Signal from cell B. Charge Integrated charge, 750.9  $\mu\text{C}$  for signal and 4564.5  $\mu\text{C}$  for background charge were observed for 2 mL of 500  $\mu\text{g/L}$  of [As] sample.

In conclusion, carbon fiber electrode was the best material for our purpose and silver/silver iodide pseudo reference electrode can replace the expensive commercial reference electrode ( *ca.* 50 US \$). The outlet hole should be closed to enhance distribution of the analyte gas on the filter paper. The silver fiber electrode was not very robust as many runs of measurement gradually removed the silver from the silver fiber. After about ten runs, signal started to decreased dramatically. This prompted us to use silver foil which has infinite supply of silver metal and also played additional role. The additional role of this silver foil was to completely close the outlet hole, making the only direction for arsine to travel to be in parallel direction with the filter paper. The grooves on the filter paper also help even distribution of the arsine on the filter paper. The

grooves are conduit for arsine gas movement and also as gas moves freely through conduits without obstruction, it relieves surge of pressure pulse in the cell. Reference electrodes such as Ag/AgX where X is halide had been used for developmental processes. However as mentioned numerously before, the problems were clogging of the frits of the reference electrodes. The blockage of the frit made the reference electrode useless. We salvaged the broken reference electrode by cleaning the frit in aqua regia, a solution of concentrated nitric acid and hydrochloric acid in a volumetric ratio of 1 to 3. This cleaned up the blockage and refilling the electrolyte resurrected the dead reference electrodes. It was this observation that we abandoned idea of using standard reference electrode for the sensors.

#### **4.11.3. Effect of iodine concentration**

Having figured out the cell geometry and materials for electrodes, we embarked on the study of signal dependence on iodine concentration. The purpose of developing this sensor is to measure arsenic in drinking water in the field. The sensor and instrumentation should be affordably inexpensive, portable, safe to operate, robust in the field, and easy to fabricate. The total cost of the sensor is less than 2 US \$. The sensor is robust and has not shown any degradation of signal for long term. A 50  $\mu$ L of 20 mM iodine is not environmentally hazardous. The limitation lies in the necessity of 2 % NaBH<sub>4</sub> and sulfuric acid. By this method, one use 2 ml of NaBH<sub>4</sub> solution and 0.645 ml of sulfuric acid per measurement. Therefore, carrying too much chemicals is not required.

Iodine concentration was 20 mM in DMSO in all experiments in measuring arsine gas in real samples. However, the response can be larger when I<sub>2</sub> is more highly

concentrated in the electrolyte. Therefore, iodine concentration on the filter paper was varied to see whether we can observe increase in the response of the sensor. Iodine (MW 253.81) in DMSO solution was prepared as shown in A 2 % NaBH<sub>4</sub> was prepared freshly on the day when the measurement was performed. A powder of 800 mg of NaBH<sub>4</sub> was weighed out and dissolved in 40 ml of 0.5 M NaOH. An aliquot of 4 ml of 50 µg/L was used as samples in these experiments. Table 4.11.2 Iodine solution preparation. shows the preparation of iodine used in the experiments.

**Table 4.11.2 Iodine solution preparation.**

[I <sub>2</sub> ], mM	Calculated weight in 10 mL g	Weight measured, g
20	0.050762	0.051
40	0.101524	0.1014
80	0.203048	0.204
200	0.50762	0.508

#### 4.11.4. Description of sensor

The sensor is two electrode system where anode is carbon fiber and cathode is a strip of silver foil. The cell notation is as follows:



The sensor was made of two Plexiglas plane. On each of the Plexiglas, a syringe filter was attached with polypropylene glue. The carbon fiber electrode was taped on the edge of the syringe filter to fix the position of carbon fiber. The silver plate was also taped on the edge of syringe filter. Between these two syringe filter, a filter disk was placed and the top and bottom Plexiglass body of the cell was secured by four bolts.

Securing these bolts by hand was extremely important as pressure generated from the arsine generator changed the geometry of the sensing working electrode, which normally resulted in increase of current. The voltage bias between the working electrode and counter electrode was 1.1 V all throughout measurements. The table below summarizes the charge that was integrated.

**Table 4.11.3 Amperometric signal and background dependence on integration time and reductant addition timing**

Entry	[I <sub>2</sub> ], mM	Signal, $\mu\text{C}$	Background, $\mu\text{C}$	Integration starts, s	Integration ends, s	NaBH <sub>4</sub> start, s	NaBH <sub>4</sub> stops, s
1, A	20	-600.1	-6414.1	120	280	120	240
2, C	40	-694.6	-10800.8	400	600	400	520
3, D	80	-841.8	-10546.9	600	800	600	720
4	4	-308.6	-6007.8	120	280	120	240
5, B	40	-344.6	-7769.5	150	280	120	240

To get an idea we plot the charge vs. [I<sub>2</sub>] in Figure 4.11.4. The figure shows that there was tendency of increase in signal response as [I<sub>2</sub>] increased. However, the benefit is counterbalanced by the requirement of waiting longer time before one generates hydride to get the amperometric signal.

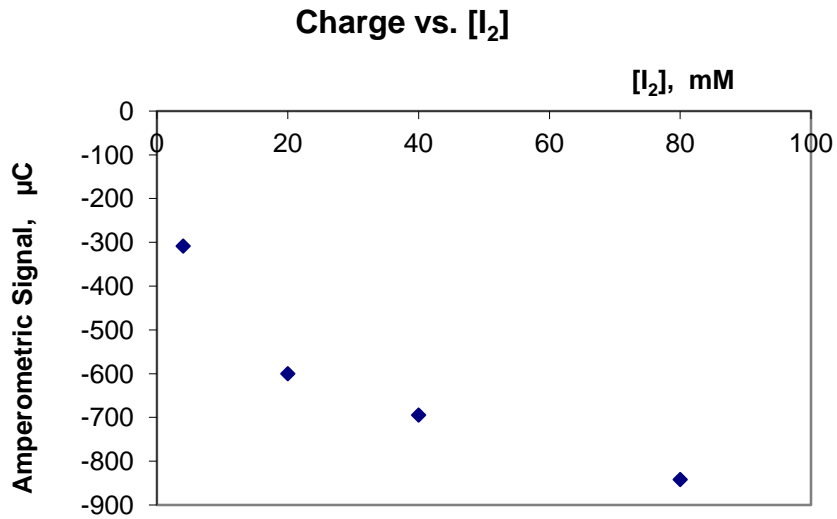


Figure 4.11.4 Amperometric signal dependence on  $[I_2]$  on the filter paper.

The background current also increases by about two fold as more concentrated  $[I_2]$  was used.

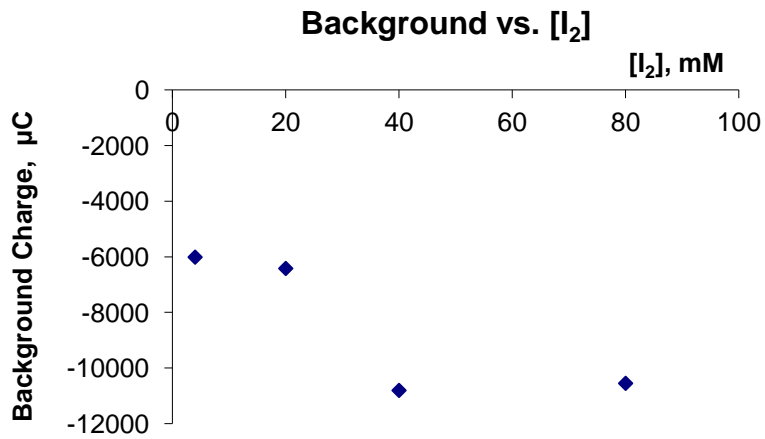
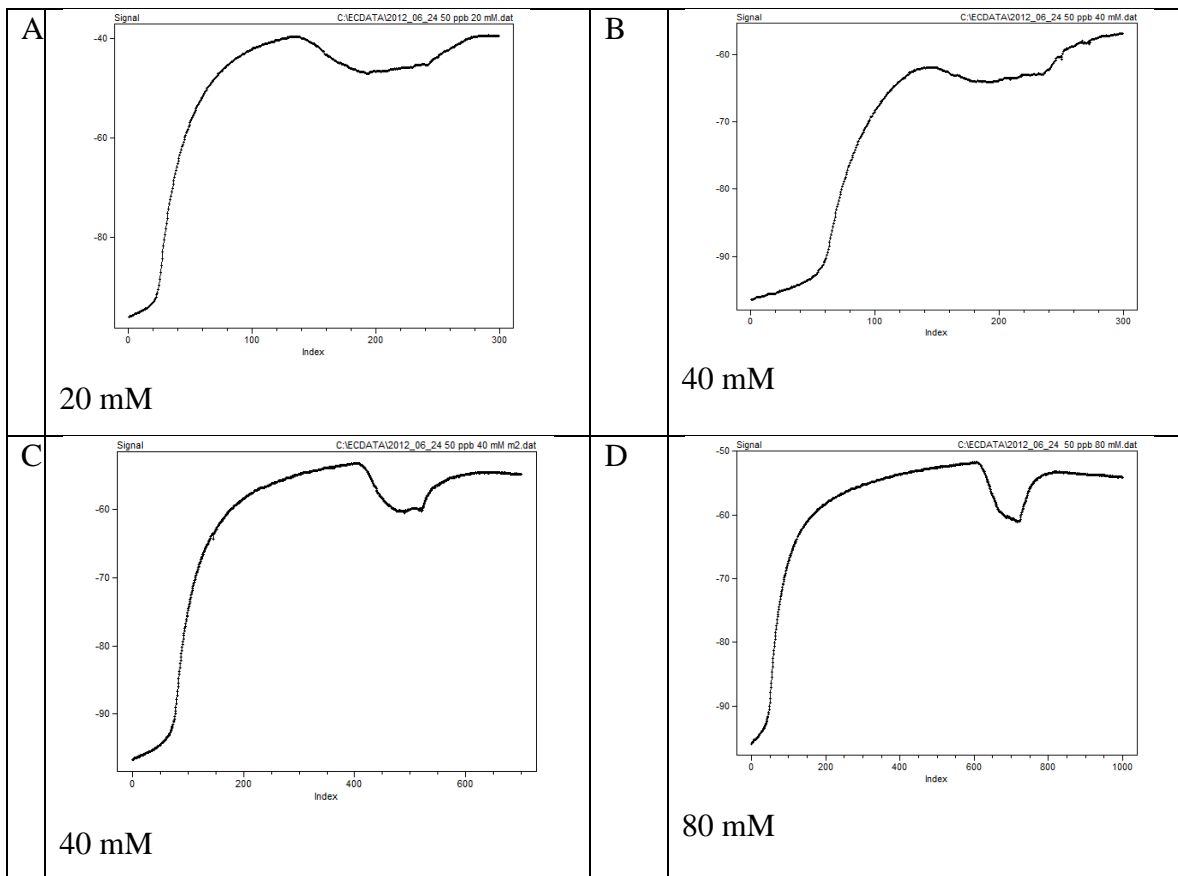


Figure 4.11.5 Background current vs.  $[I_2]$ . The more concentrated  $[I_2]$  more background current (nonfaradaic signal).

To provide visual illustration of shape of background current and faradaic currents, we plot four curves here. The alphabets in capital in each panel are the identifiers, entries in Table 4.11.3 and numbers are  $[I_2]$  in mM.



**Figure 4.11.6** Background charge dependence on  $[I_2]$  on the filter paper with various conditions. X axis represents time in s and y axis represents current in  $\mu\text{A}$ .

#### 4.11.5. Results and Discussion

Table 4.11.3 clearly demonstrated that the amperometric signal can be enhanced by using more iodine, but also it increases the measurement time. Chart A and B showed that due to increased capacitance of the cell at 40 mM  $[I_2]$  compared to that that with 20

mM [I<sub>2</sub>], we need to wait longer time to measure the arsine gas. When the capacitance current did not fully decay, the specific current could not be measured optimally since the specific current and decaying background current canceled each other, thus resulting in diminished overall signal. Being aware of this knowledge, signal was obtained at different time point in panel D. With 80 mM iodine solution, at 600 s, reducing agent was added and the charge obtained was significantly higher than that from 20 mM iodine. The magnitude was increased by 40 %. However, the measurement time increased substantially from 300 sec to 10000 sec.

Based on the results, it is not ideal to use highly concentrated iodine on the filter paper. It took longer time for the base line to go to low level and this high current observed is due to increased capacitance of the cell. Therefore, it is optimal to use 20 mM of [I<sub>2</sub>] in the rest of the experiments.

#### **4.12. Amperometric detection of arsine on carbon fiber electrode in filter paper cell.**

Carbon fiber electrode described in the previous section was used to make the calibration curve. This is because the signal response was greatest when carbon fiber was used. The cell notation is given as follows:

C(s) / I<sub>2</sub>(DMSO), I<sup>-</sup>(DMSO), AsH<sub>3</sub>(aq), H<sub>3</sub>AsO<sub>3</sub>(DMSO), H<sub>3</sub>AsO<sub>4</sub>(DMSO) // I<sub>2</sub>(DMSO), I<sup>-</sup>(DMSO), AgI (DMSO)/ Ag (s)

##### **4.12.1 Construction of calibration curve with Method A:**

In method A, 2 ml of standard in 2.5 M sulfuric acid was used to construct a calibration curve. For real sample, 2 ml of real sample and 2 ml of 5 M sulfuric acid was added to make the solution acidic. NaBH<sub>4</sub> was added between 120 s and 240 s at 1

ml/min. A calibration curve was constructed to see if the signal response is linear. The curve shows linearity in the figure. The first figure was obtained from the straight line base line, as we discussed in the introduction section. While arsine is being oxidized, we cannot measure the baseline exactly. Only the sum of the background and the specific current will be recorded in the data acquisition system. It is not easy to predict that what would have been the baseline. However, we anticipated that the baseline would be close to a straight line from the experimental observation of the signal. Hence, we draw a line from the point at 120 s to 280 s. This is done solely from experience on measuring amperometric signal. The signal went down to baseline level at 280 s even if the  $\text{NaBH}_4$  addition stopped at 240 s. Based on the integrated charge of each standard of As(III), we attempted to make a calibration curve and the following figure shows the calibration curve.

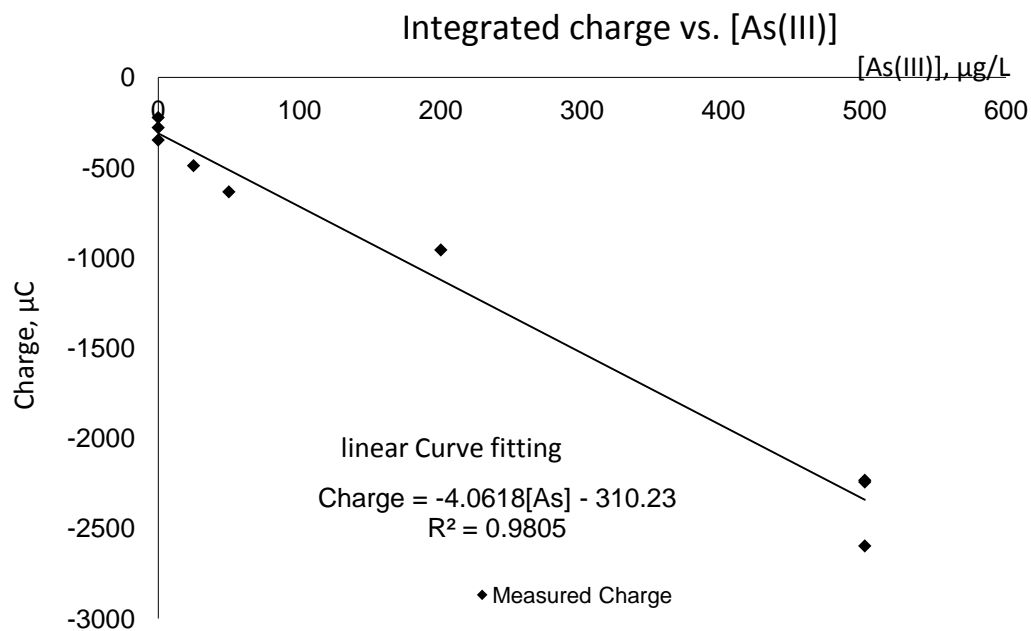


Figure 4.12.1 Calibration curve constructed from carbon fiber electrode

Here we provide the analytical figure of merits, sensitivity and limit of detection in Table 4.12.1.

Table 4.12.1 Sensitivity and limit of detection based on calibration curve

Sensitivity, $\mu\text{C}/(\mu\text{g/L})$	$-4.0618 \pm 0.2163$
Limit of detection, $\mu\text{g/L}$	47

In real samples, there are many dissolved ions which interferes the measurement of As(III). In order to know the specificity of the sensor, we used the following EPA standards containing many other species in Table 4.12.2 and Table 4.12.3 were used.

**Table 4.12.2 Table of 200 µg/L [As(III)] EPA standard containing interfering ions**

Ions	Concentration, µg/L
Al, As, Sb, Ba, Be, B, Cd, Ca, Cr, Co, Cu, Fe, Pb, Li, Mg, Mn, Mo, Ni, Se, Na, Sr, Tl, Sn, V, Zn	200
P, K, Si	1000
Ag	50

**Table 4.12.3 Table of 50 µg/L [As(III)] EPA standard containing interfering ions**

Ions	Concentration, µg/L
Al, As, Sb, Ba, Be, B, Cd, Ca, Cr, Co, Cu, Fe, Pb, Li, Mg, Mn, Mo, Ni, Se, Na, Sr, Tl, Sn, V, Zn	50
P, K, Si	250
Ag	12.5

An equal volume of 2.0 mL of EPA standard and 5.0 M H<sub>2</sub>SO<sub>4</sub> were mixed for interference study. Acidification procedure of the EPA standards with H<sub>2</sub>SO<sub>4</sub> halved the concentration of dissolved ions. The two 200 µg/L and 50 µg/L standard became 100 µg/L and 25 µg/L, respectively. In the following table, we show the results of measurement and method validation based EPA standard.

**Table 4.12.4 Results of measurement of EPA standards containing other competing species and method validation.**

EPA [As], µg/L	Measured As(III), µg/L
100	121 ± 24
25	bdl

**bdl – below the detection limit**

The 100  $\mu\text{g/L}$  EPA standard was recovered with an error of 24 %. The 25  $\mu\text{g/L}$  EPA standards were measured and the calculated signals were below the detection limit of this particular technique. Therefore, the method cannot determine such low level of concentration. Apparently, hydrides of P, Sn, Se, Sb could have reduced the efficiency of arsine generation and therefore its detection may be compromised. This may lead to higher detection limit as observed. However, the interference from a host of non hydride generating metal ions are absent in this technique. Even under such circumstance the interference studies showed moderately good results. Since the sensor demonstrated high specificity, more work with this type of sensor is warranted. Optimization of geometry could yield sensor with higher sensitivity and lower limit of detection.

#### **4.12.2 Error analysis**

To improve the background correction procedure we examined the following approach. As stated before in the introduction section, the baseline of the capacitance curve is exponentially decaying. Therefore, applying this nonlinear baseline, we constructed two calibration curves. The data with square markers was obtained from integration between 120 and 280 s and data with oval markers was calculated from integration between 120 and 240 s. Although the  $\text{NaBH}_4$  stopped at 240 s, residual arsine might have been still introduced into the system. Hence, we included 40 s more time to include the residual  $\text{AsH}_3$ . We obtained the following two straight line equations. For integration with interval between 120 and 240,

**Equation 4.12.1**

Charge =  $(-4.7 \pm 0.3) \times [\text{As}] - 224.4 \pm 83.7$ , where the charge is integrated signal in  $\mu\text{C}$  and  $[\text{As}]$  is concentration of arsenic in  $\mu\text{g/L}$  and the numbers after  $\pm$  signs are standard errors associated with the curve

Similarly, for integration with interval between 120 and 280,

**Equation 4.12.2**

Charge =  $(-5.5 \pm 0.4) \times [\text{As}] - 245.3 \pm 131.2$

A linear calibration curve in this way is shown below to compare the goodness of fits among three different numerical methods. Despite the added complexity of calculating the exponentially decaying baseline, it did not yield much improved linearity at all.

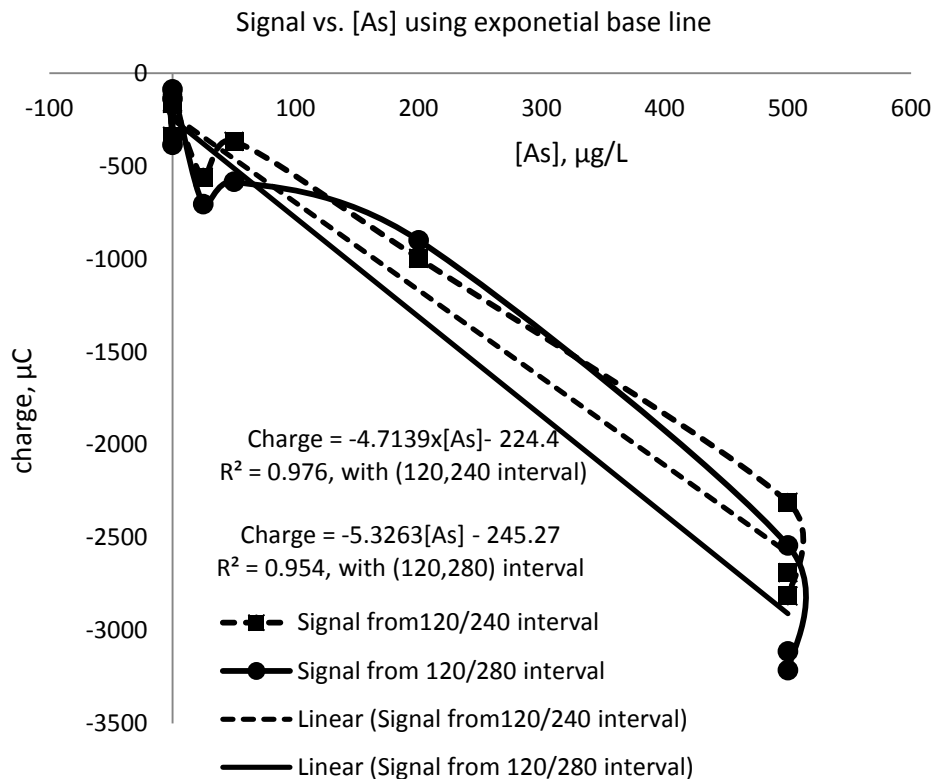


Figure 4.12.2 Linear curve fittings with exponential baselines. Dotted line was obtained from integration between 120 and 240 s for data represented by square maker and bold line was obtained from 120 and 280 s with data represented by oval marker.

Figure 4.12.2 shows that the exponential baseline fitting did not yield improved calibration curves. Nonetheless, the linearity parameter,  $R^2$  dropped instead.

#### 4.12.1. Data fitting with the theoretical model.

A typical data obtained for a construction of the calibration curve was shown below and data fitting to the mathematical model was achieved in this section. The equation we consider in this data is as follows:

**Equation 4.12.3**

$$i = f(t) + \text{baseline}$$

,where  $f(t)$  is the specific current from  $\text{AsH}_3$ . The function  $f(t)$  is the bi-exponential function we derived in the introduction section from chemical kinetics consideration.

The baseline is an exponentially decaying function we described in the introduction section. More specifically, the baseline current is the sum of two components:

**Equation 4.12.4**

$$\text{baseline} = \frac{E}{R} \exp(-t/RC) + K$$

,where here  $E$  is applied potential,  $R$  cell resistance,  $C$  cell capacitance,  $K$  a constant current. The  $K$  is a constant current arising from the iodide gradient generated by the cathode. The cathode is electrochemically active and thus generates iodide by  $\text{AgI}$ . We hypothesize that there was a constant gradient through the thin filter paper. The proposed baseline model fits well with the experimentally measured baseline curve as shown in Figure 4.12.3 Curve fitting to the proposed model. The baseline is fitted to the measured current during the first 2 min and we extrapolate the baseline from 120 to 280 or 240 s to obtain hypothetical baseline. From this hypothetical baseline, we were able to calculate the signal response from the specific current. The following figure shows the fitted curve.

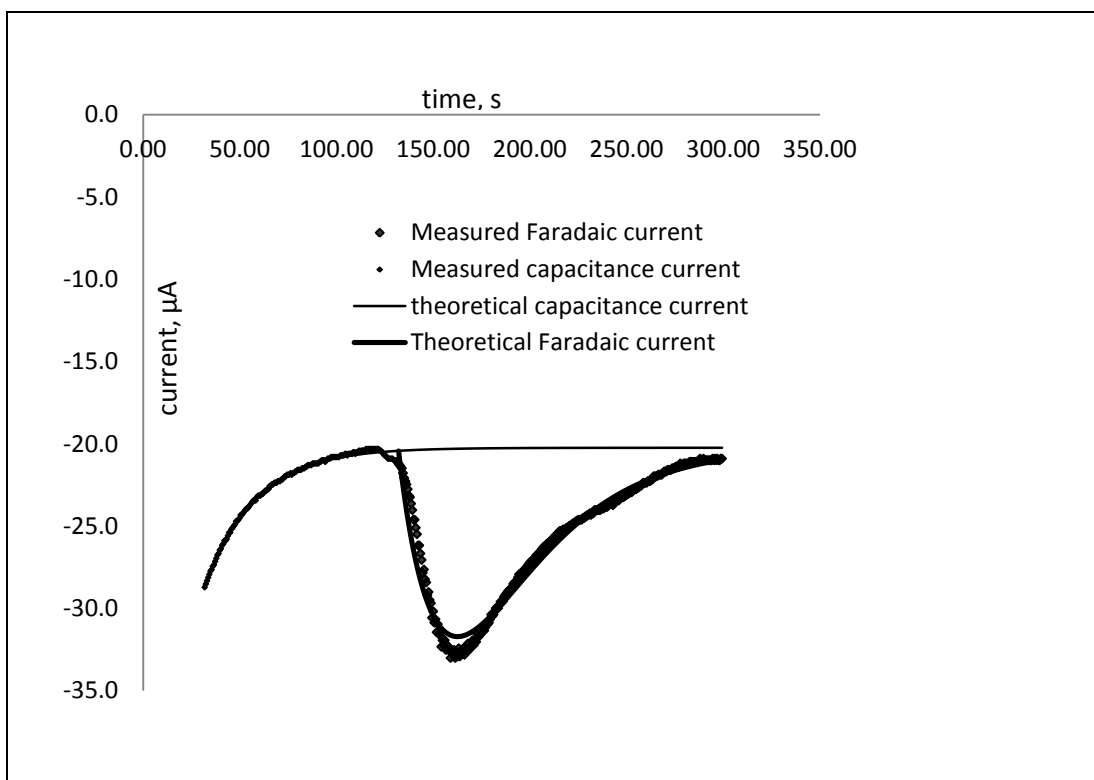


Figure 4.12.3 Curve fitting to the proposed model.

The exponential baseline was almost a straight line where faradaic process started, which motivated us to use the straight line as a baseline for constructing calibration curve. This obviated the need for curve fitting of the initial data to an exponential function and it did not cause any loss of goodness of fit as  $R^2$  showed. The curve fitting of the baseline yielded the resistance and capacitance of the cell in each measurement. Table 4.12.5 shows several values obtained from the data acquired for calibration curve. In ideal cell, all three parameters, R, C, and K should be constant. However, whenever we inserted a new filter paper, we have variation of geometry in the cell. This error propagated into the measurement errors though baseline variation.

**Table 4.12.5 Computed characteristics of the electrochemical cell obtained from curve fitting to the model**

Measurement	R, k $\Omega$	C, $\mu$ F	K, $\mu$ A	Time constant, RC, s
2012_06_03 CA 200 ppb i1	8.32	4.24	45.6	28.3
2012_06_03 CA 500 ppb i1	8.23	4.17	43.5	29.1
2012_06_03 CA 500 ppb i2	8.56	3.91	38.6	29.9
2012_06_03 CA 25 ppb i1	7.70	5.43	40.2	23.9
2012_06_03 CA 50 ppb i2	12.8	2.62	29.6	29.8
2012_06_03 CA 0 ppb i2	11.0	2.95	47.5	30.8

Abbreviations indicate, C: capacitance, R: resistance, K: constant current,  $\tau$ : RC time constant in equation.

Here we list the standard deviations of each parameter.

**Table 4.12.6 Error analysis of the characteristics of the carbon fiber cell**

	R, k $\Omega$	C, $\mu$ F	K, $\mu$ A	1/RC=1/ $\tau$ , s
Average	9.44	3.89	40.83	28.63
Standard deviation	2.01	1.01	6.42	2.47
Relative standard deviation, %	21	26	16	8.6

It shows that most significant variances came from change in capacitance of the cell. The amperometric signal is also governed by kinetic parameters. These kinetic rate constants were introduced in the introduction section to explain the shape of the signal response. Although we used the same chemicals during constructing a calibration curve, the rate of generation of arsine and transfer into the sensor varied to a certain extent. For

the kinetic parameters, we obtained the following values in Table 4.12.7. To discuss the variability of these parameters, we calculated the standard deviations.

**Table 4.12.7 Computed parameters for bi-exponential function**

Measurement	$k_1$	$k_2$	C
2012_06_03 CA 200 ppb i1	0.0335	0.0335	38.54
2012_06_03 CA 500 ppb i1	0.0407	0.0295	78.35
2012_06_03 CA 500 ppb i2	0.0483	0.0208	72.85
2012_06_03 CA 25 ppb i1	0.0143	0.0219	21.01
2012_06_03 CA 50 ppb i2	0.0360	0.0360	14.07
2012_06_03 CA 0 ppb i2	0.0327	0.0327	5.45

The relative standard deviation of the rate constant for the rate of generation of arsine was 33 % in the measurements. Here, the unit of rate constants,  $k_1$  and  $k_2$  is  $s^{-1}$ .

**Table 4.12.8 Average and standard deviation of rate constants,  $k_1$  and  $k_2$**

	$k_1, s^{-1}$	$k_2, s^{-1}$
Average	0.034	0.029
Standard deviation	0.011	0.006
Relative standard deviation, %	33.1	21.8

From this table, it is evident that the first parameter  $k_1$  representing the rate of generation of arsine from the sample has the largest variation. We therefore ensure that fresh chemicals for hydride generation should be used.

#### **4.12.2. Sensitivity study with increased volume of sample: Method B**

Using more sample one can get a calibration with higher sensitivity. For example, we doubled the volume of the standard (4.0 mL) to construct a calibration curve. In

method B, a 4.0 ml of standard in 2.5 M sulfuric acid was used to construct a calibration curve. For real sample, 0.65 ml of 18 M sulfuric acid was added to 4.0 ml of real samples to acidify the samples for NaBH<sub>4</sub> reduction of arsenic. NaBH<sub>4</sub> was added between 120 s and 240 s in usual manner. It produced a calibration line with R<sup>2</sup> of 0.9782 and sensitivity of -7.73 μC/(μg/L) and the limit of detection of 62 μg/L( 3 times standard deviation/sensitivity).

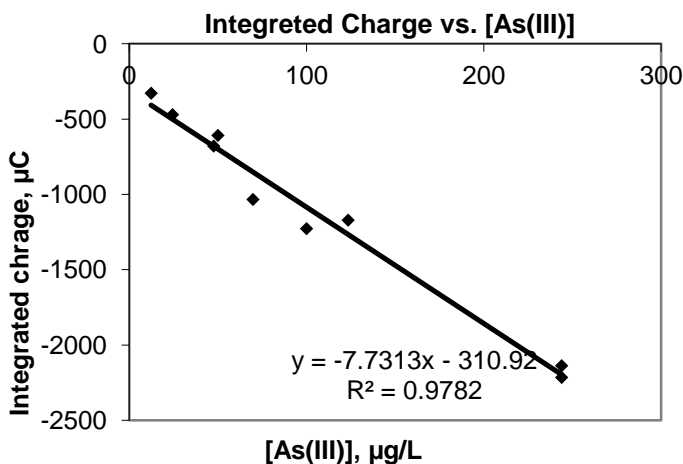


Figure 4.12.4 Calibration curve constructed from Method B

#### 4.12.3. Real sample analysis with Method B

Samples obtained from the field were analyzed with the cell as described. These were analyzed with 4.0 mL of sample and a new calibration was made with the same volume of standards. A control standard was also included to check the validity of the technique. To estimate the error, 100 μg/L of As(III) standard was injected 7 times and we found that the relative standard deviation was 23.7 % at 100 μg/L As(III).

**Table 4.12.9 Measurement results of As(III) of real samples.**

File	Description	Signal, $\mu\text{C}$	Measured As(III), $\mu\text{g/L}$
2012_06_13 L1	Seskyon mountain, Oregon	-1068.8	98.0
2012_06_13 I1	GW 100 m Natron Egypt	-271.8	bdl <sup>a</sup>
2012_06_13 J1	GW 60 m, Natron Egypt	-300.8	bdl
2012_06_13 100 $\mu\text{g/L}$ 4 ml	Control Standard	-1154.7	109.1
2012_06_13 G1	Aritima Giris, Turkey	-539.2	29.5, bdl
2012_06_13 K1	SONO filtered water, Kushtia, Bangladesh	-386.5	9.8, bdl
2012_06_15 N1	Nile Water, Egypt	-177.1	bdl
2012_06_13 O1	SONO filtered, Egypt	-441.6	16.9, bdl
2012_06_15 N2	Nile Water, Egypt	-392	10.5, bdl
2012_06_15 P1	Well water from Oakton, VA	-369.9	7.6, bdl
2012_06_15 Q1	Sudan, house water	-201.6	bdl
2012_06_15 R1	Nile Water	-412.4	13.1, bdl

<sup>a</sup>: bdl denotes below detection limit. GW- Groundwater

Thus far, we presented results from innovatively created sensors. The sensor demonstrated linear response quite well. However, measurement validation of field samples by other proven techniques such as atomic emission, atomic fluorescence, and gas phase chemiluminescence spectroscopic techniques remains to be done. In the next

section, we will provide the conclusion of these approaches and future directions of electrochemical arsine gas sensor development.

#### **4.12.4. Conclusion**

This work is an attempt to develop new sensor chemistry for electrochemical detection of arsine produced from arsenic in water. The sensor based on reaction between  $\text{AsH}_3$  and  $\text{Ag(s)}/\text{AgNO}_3 // \text{Ag}^+/\text{Ag(s)}$  redox couple on a filter paper substrate has shown high sensitivity with potentiometry and conductometry as analytical techniques. Amperometry sensor is based on chemical reaction of  $\text{AsH}_3$  and iodine, followed by electrochemical reaction of iodide generated from the first chemical reaction. In potentiometry, the signal response ranged from 4.3 to 200 mV for 10  $\mu\text{g/L}$  to 400  $\mu\text{g/L}$   $\text{As(III)}$ , respectively with limitation of detection of 11  $\mu\text{g/L}$   $\text{As(III)}$ . Non-equilibrium process taking place in potentiometry demands more theoretical studies in this area. However, experimentally measured change in potential demonstrated that the potentiometric measurement technique is a highly promising approach. Instrumentation requirement for potentiometry is simplest and thus merits further investigation.

The conductometric detection based on alternating bipolar square potential pulses exhibited linear calibration curve and a minimum detection limit of 88  $\mu\text{g/L}$   $\text{As(III)}$ . The conductometry cell must have constant geometry of cell components. This could be realized by construction of stop and go basis cell introduced in section 1.4. This will minimize the variances of the cell constant for the conductometry.

In amperometry, a novel electrochemical cell: C(s)/ I/I<sub>2</sub>, AsH<sub>3</sub>(sln), H<sub>3</sub>AsO<sub>3</sub>, H<sub>3</sub>AsO<sub>4</sub> // I<sup>-</sup>, AgI /Ag(s) where I/I<sub>2</sub> mediated AsH<sub>3</sub> oxidation was developed for chronoamperometric detection with limit of detection of 47 µg/L As(III). Here, Au, Pt, and C exhibited similar anodic current responses but the porous thin carbon fiber electrode yielded highly efficient arsine mass transport. Often metal electrode surface changes its physical properties, depending on the history of its use. A pristine surface of Au and Pt electrode cannot be easily realized in the field. However, solution phase chemical reaction does not require such highly active surface of metal electrode, therefore, its feasibility in field is promising. A mathematical model of mass transfer of AsH<sub>3</sub>(g) and following electrochemical reaction was developed and successfully applied to the simulate experimental data. The model predicts that consistency in the rate of generation of AsH<sub>3</sub> is critically important in accurate measurement. Therefore, freshness of the chemicals is required in this set up. Also the rate of escape of AsH<sub>3</sub> from the aqueous media is playing an important role. The model indicates that efficient transfer of AsH<sub>3</sub> yields sharper amperometric signal, which results in improved accuracy. Among Au, Pt and carbon fiber electrode, carbon fiber electrode was the best material. The merit comes from the dimension of fiber and geometric shape of the electrode rather than its electrochemical property. The most important requirement for sensing miniscule amount of gas is the porosity of the electrode. In literature, fine particles of Pt or Au in electrical continuity are bound to gas diffusion membrane, through which gas is permeating. Undoubtedly, the effective area where the analyte in gas phase makes triple junction is maximized when such porous electrodes is used. Here triple junction refers to electrode-

electrolyte-analyte gas interface. However, fabrication of such triple junction calls for sophisticated techniques. The thin carbon fiber material resembles porous electrode where gas permeate through easily and is inexpensive.

The sensor developed requires 2.0 mL of water sample, 2.0 mL of NaBH<sub>4</sub> as arsine generating agent, and 50 μL of 20 mM iodine. The sensor is robust, compact, easy to fabricate, and field-deployable. This is evident when we consider flow injection hydride generation method. To realize that method, we need delivery pumps for iodine solution and also excessive chemicals to achieve the renewal of electrolyte, which adds complexity of instrumentation. In this methodology, renewal of electrolyte is achieved by simple manual insertion of a new filter paper with minimum amount of electrolyte. We fabricate the sensor more than several times in a couple of hours, which always worked. Therefore, mass production is not a problem for those people who need to carry it in their pocket.

## 5. Appendices

### 5.1. Appendix A: Operation Instruction

As the sensor could be used in the field as arsenic sensor in drinking water, we supply operational instruction below.

#### A) Laboratory preparation:

- 1) Weigh out 50.7 mg of iodine (FW 253.81) and add 10 ml of DMSO. This is 20 mM iodine in DMSO
- 2) Cut and wet filter paper with 50  $\mu$ L of 20 mM iodine solution in DMSO. Place them in a tightly closed container.
- 3) Prepare 2.5 M sulfuric acid.
- 4) Prepare 2 % NaBH<sub>4</sub> in 0.5 M sulfuric acid freshly on the date when the measurement is performed.
- 5) Construct calibration curve by using 4 ml of standard ranging from 10  $\mu$ g/L to 500  $\mu$ g/L. Five different concentrations shall be used.

#### B) Field measurement instruction:

- 1) Clean the generator vial with DI water. Pipette 4 ml of drinking water to a 40 ml generator vial. Add 0.645 ml of sulfuric acid to the sample to be analyzed.
- 2) Place filter paper between the two block of cell. The filter paper should be loaded in the center of bottom silver electrode.
- 3) Connect the working electrode lead to the carbon fiber electrode and counter and reference electrode to the silver plate electrode.

- 4) Close the two blocks and tighten the cell with 4 screws. Turn the ear of the ring as far as one can do.
- 5) Fill the hydride chamber with 2 % NaBH<sub>4</sub> solution
- 6) Flush the transfer line for 1 min when this is the first run of the day by entering 8 in the bit value box in the TEST tap.
- 7) Stop the addition by entering 0 in the bit value box.
- 8) Enter 120 for the start time and 240 for the stop time.
- 9) Enter 120 for start integration time and 280 for stop integration time.
- 10) Run blank ( 4 ml of 2.5 M sulfuric acid).
- 11) Run 200 µg/L standard. Verify that the calibration curve is still valid.
- 12) Start acquisition by clicking run button.
- 13) The result will be displayed in the “Faradaic charge” edit box and “Background” edit box.
- 14) Enter the slope and intercept of the calibration curve in the edit box.
- 15) The measured concentration will be displayed on the software.

## 5.2. Appendix B: Potentiostat circuit

A potentiostat circuit was made for this work and the schematic is provided. The overall layout of schematic is presented below and for visibility, the schematic is divided into four quadrants for visualization and all quadrants, A, B, C and D are presented in the subsequent pages.

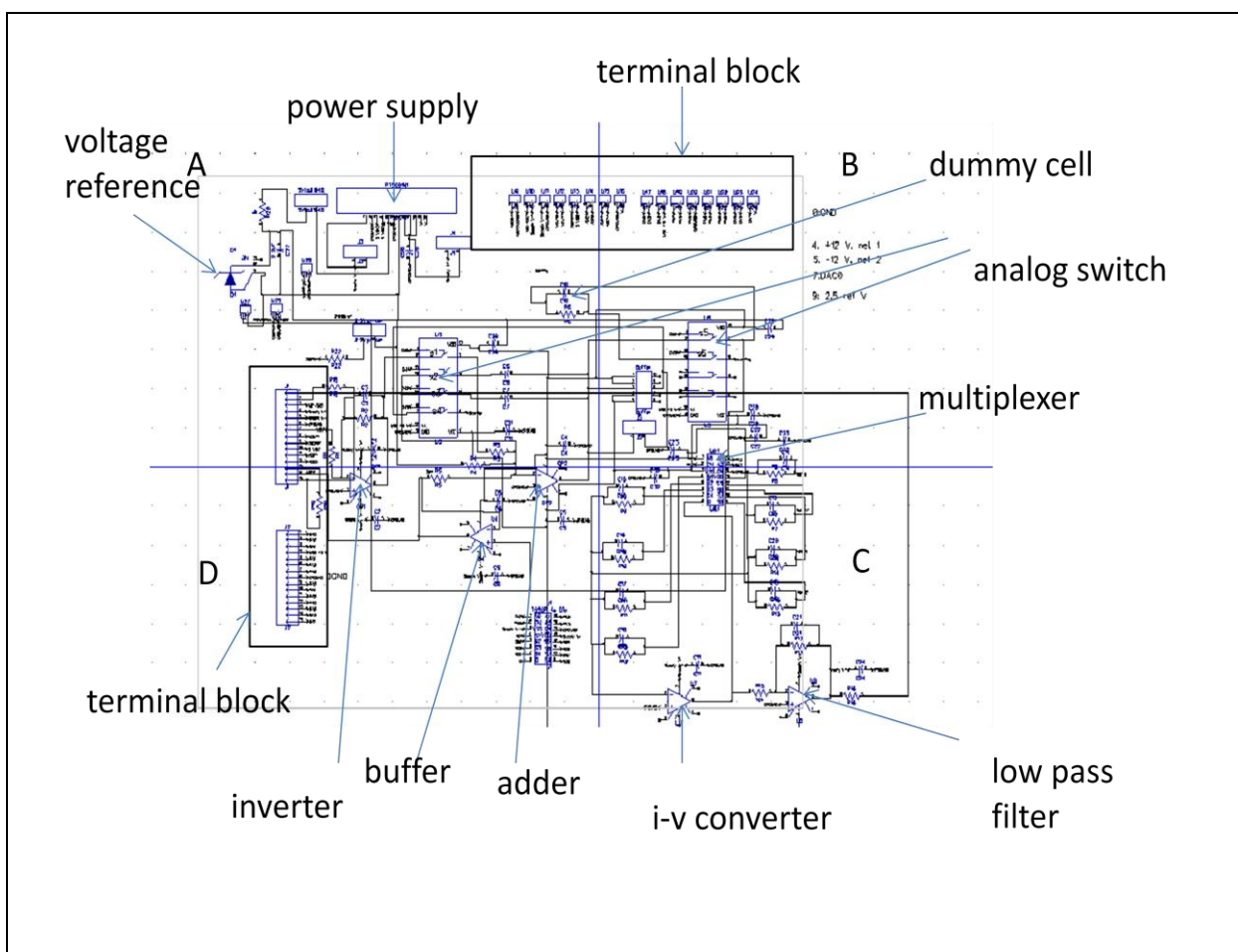


Figure 5.2.1 Schematic of the potentiostat fabricated. Quadrant A, B, C, and D are expanded and shown in following figures.

In Figure 5.2.2, D1 is reference voltage that is added through adder operational amplifier introduced in the general instrumentation section. We used PT5061 switching power supply whose voltage source is from the 5 VDC of the USB port.

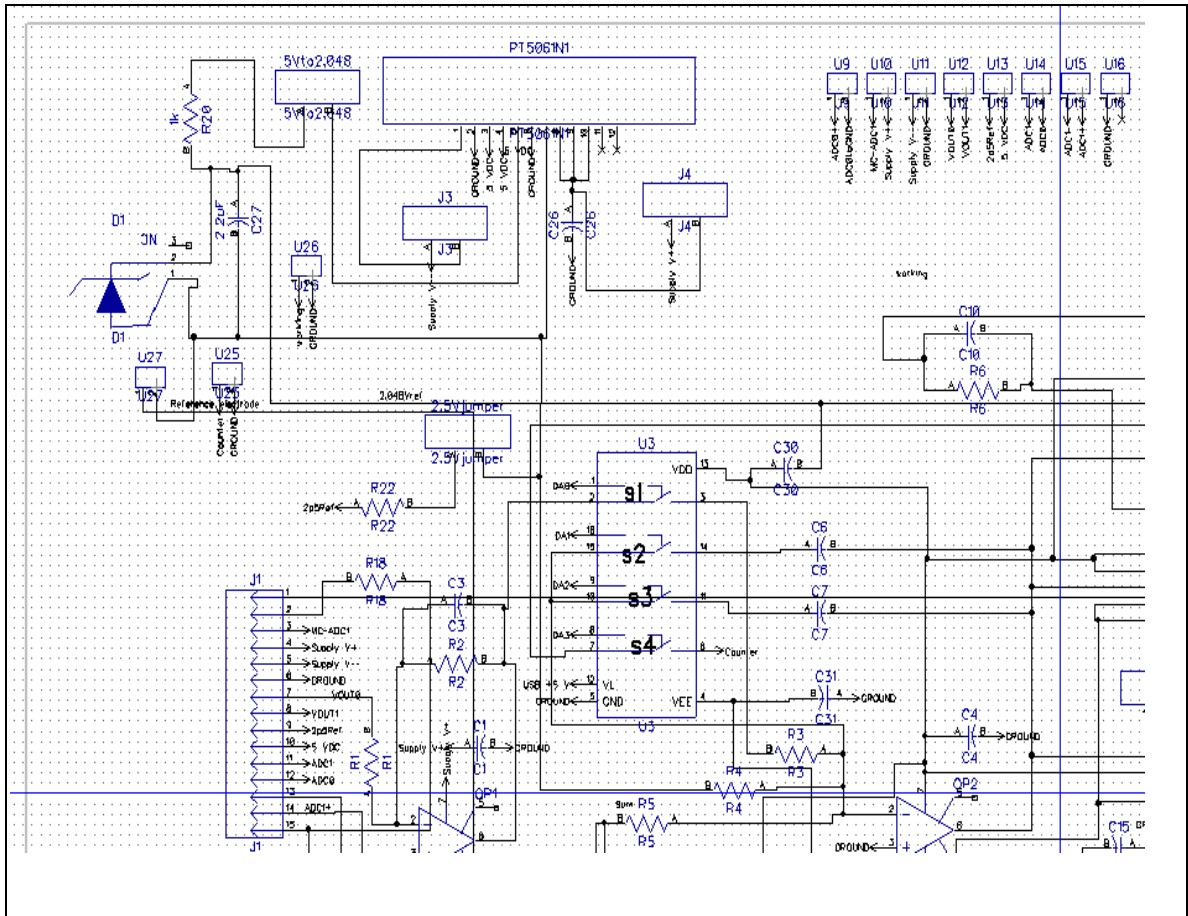


Figure 5.2.2 Quadrant A of potentiostat circuit. Analog switch 1, 2, 3, and 4 are operated by digital port of data acquisition card( USB 1208FS from measurement computing inc.)

The S1, S2, S3, S4, S5, and S6 switches are controlled by digital output of the data acquisition card and the truth table below shows the bits necessary for amperometry

experiments. We implemented on board, internal dummy cell for checking the potentiostat circuit and the bit configuration is shown for internal dummy cell.

**Table 5.2.1 Bits for amperometry experiment and for dummy cell**

SW6	SW5	SW4	SW3	SW2	SW1	Decimal
0	0	1	0	1	1	11
1	1	0	0	1	1	51

Here is the quadrant B.

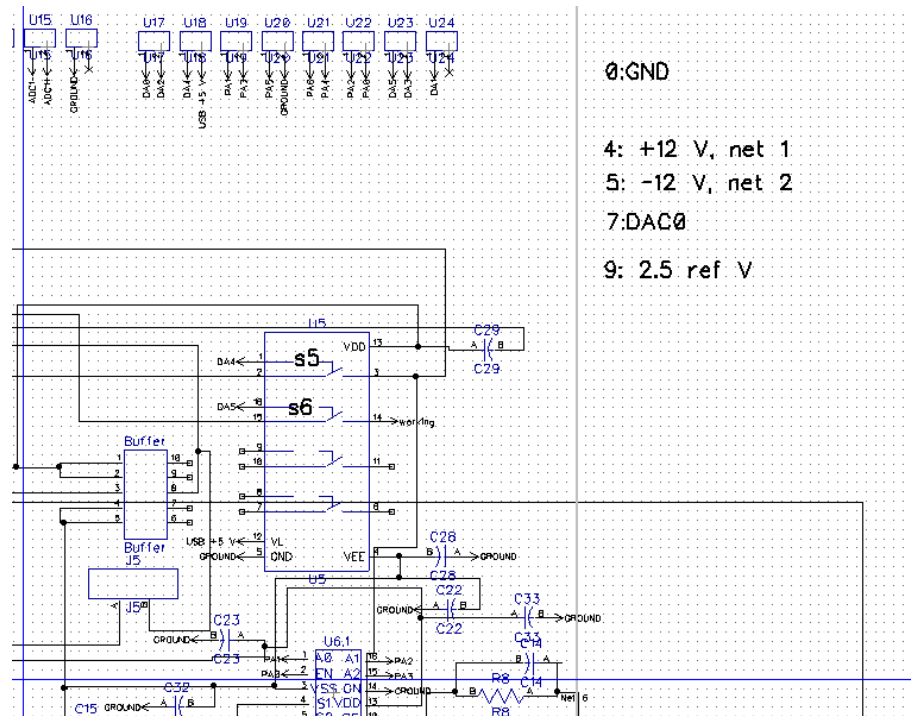


**Figure 5.2.3 Quadrant B**

The second, third, and fourth quadrants are listed in following three figures.

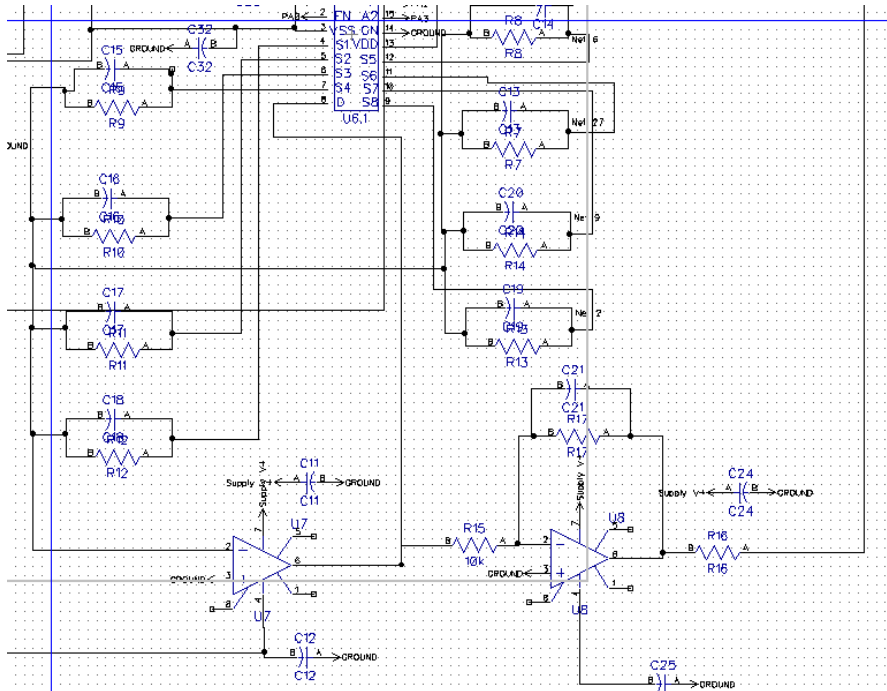


Figure 5.2.4 Quadrant C.

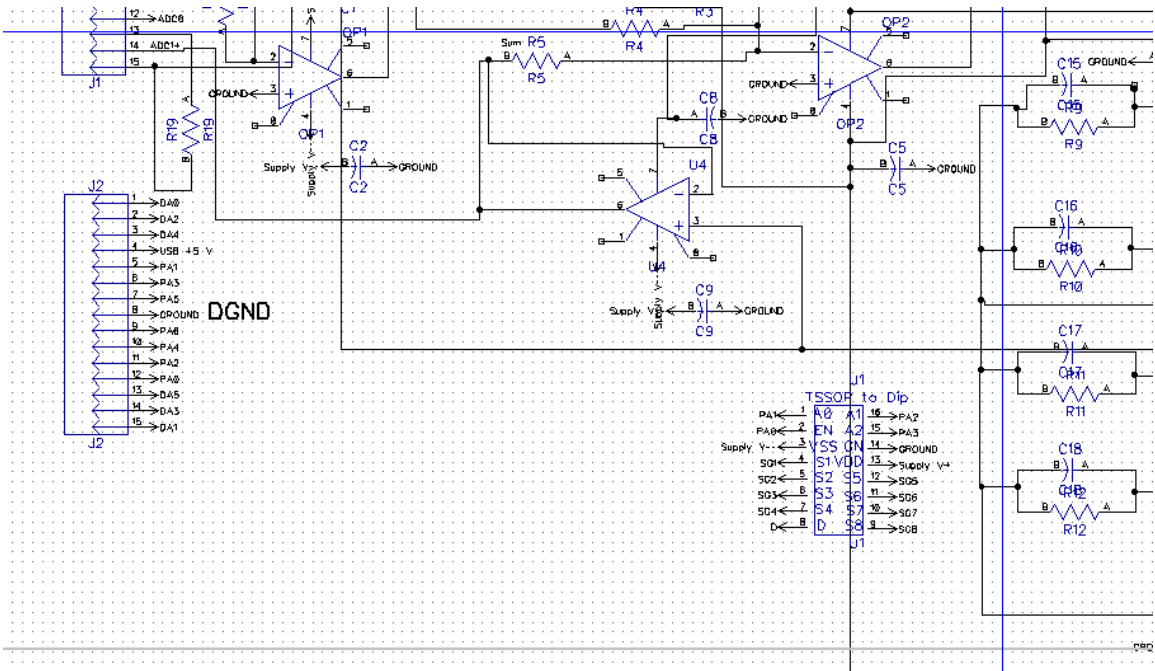


Figure 5.2.5 Quadrant D.

A multiplexer ( ADG 1208 from analog device) was used to select different gain of current to voltage amplifier. The ADG1208 had on resistance around  $120 \Omega$ ,<sup>57</sup> and therefore there was a slight voltage drop when two terminals of the source and drain were connected. However, we seldom used  $1 \text{ k}\Omega$  as a feedback resistor. The smallest resistor was  $10 \text{ k}\Omega$  on the transimpedance amplifier and therefore, the error associated with on resistance of multiplexer was 1.2 % of the total measure voltage. The schematic below shows the actual circuit. Here, U7 is a current to voltage converter in inverting configuration and U 8 is a low pass filter to remove noises from the signal. As the current to voltage amplifier inverts the sign of the voltage, another inverting amplifier is needed to restore the sign of the current signal. In this circuit diagram, 8 different sets of resistors and capacitor are connected to 8 different terminals represented by  $S_x$  where  $x$  ranges from 1 to 8. These 8 sources share on drain represented by D.

---

<sup>57</sup> Datasheet of ADG1208/ADG1209, Analog Devices, Rev. B, p3.

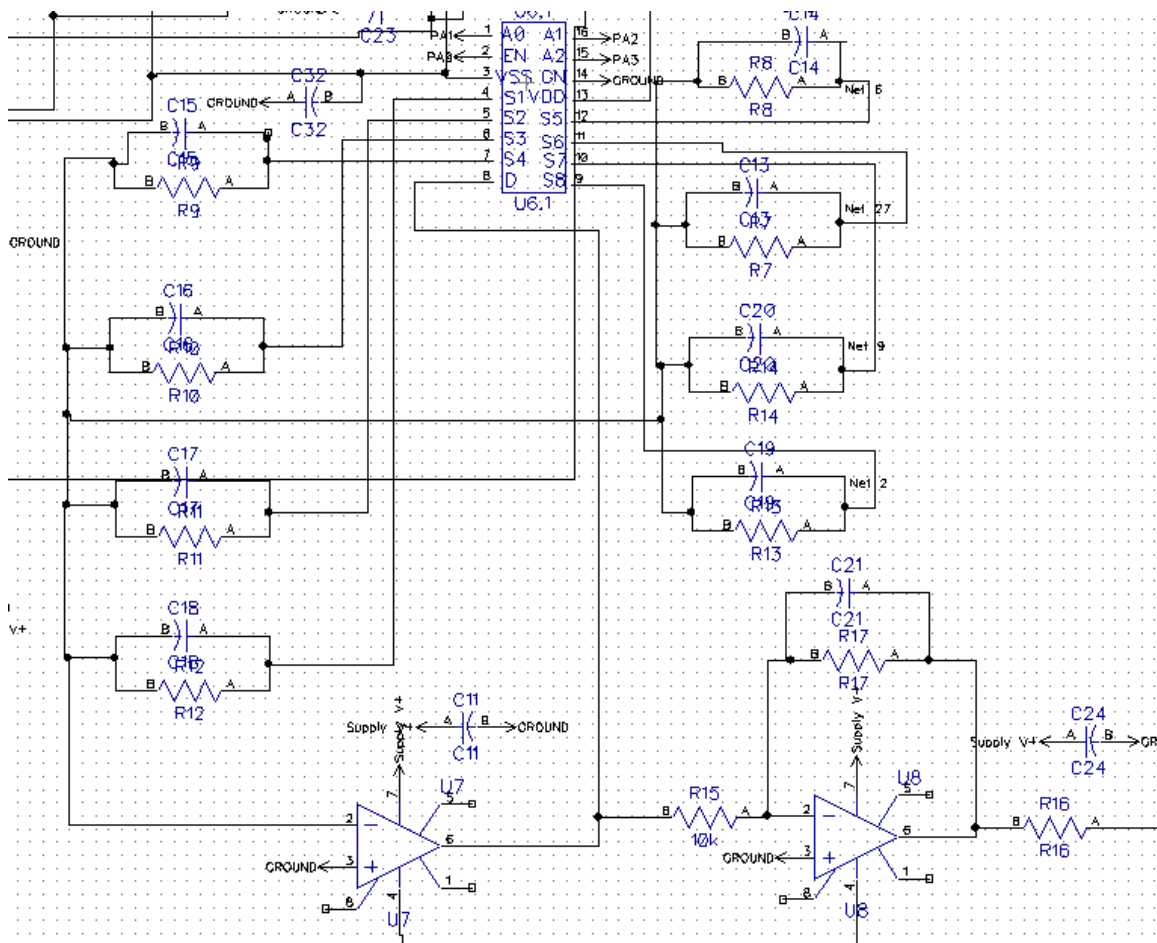


Figure 5.2.6 Schematic of a multiplexer (ADG1208) U6.1 that selects different gain from different resistor. Each set of resistor and capacitor is connected to a different terminal from S1 to S8. All sources share on drain represented by D.

EN represents enable bit that enable this device and A0, A1, and A2 are bits that are controlled by 5 VDC digital logic of the data acquisition card. The truth table for digital output bits from the data acquisition card is shown in Table 5.2.2.

**Table 5.2.2 Truth table of digital output bits**

	A2	A1	A0	Enable bit	Decimal number
Gain	PORT B bit3	PORT B bit2	PORT B bit1	PORT B bit0	
1	0	0	0	1	1
2	0	0	1	1	3
3	0	1	0	1	5
4	0	1	1	1	7
5	1	0	0	1	9
6	1	0	1	1	11
7	1	1	0	1	13
8	1	1	1	1	15

Each set of resistor and capacitor in each net has the uniform 10 ms time constant. The voltage gain we obtain from a set of feed resistor circuit is just current times the resistor. The current to voltage amplifier is also transimpedance amplifier configuration in that current is multiplied by the resistance on the feedback circuit and the output is voltage obtained from this operation, i.e.  $V_{out} = -IR$  where  $V_{out}$  is the output voltage and  $I$  is the signal current and  $R$  is the resistor on the feedback circuit. Depending on which resistor is selected, one can get different amplification. For example, if anodic current, 1  $\mu\text{A}$  is flowing from the working electrode and one selects 1  $\text{M}\Omega$  through the multiplexer,  $V_{out}$  is 1 V. Then one can convert the voltage output to current by dividing the measured voltage by the value of the feed resistor. The table shows resistor and capacitor connected to each level of gain.

**Table 5.2.3 Gain settings of feedback resistors.**

Gain	R,	C	Time constant	Decimal numbers	Hexadecimal numbers	Binary numbers
1	1k,R12	1 $\mu$ F	1 ms	<b>1</b>	01	0001
2	10k,R11	0.1 $\mu$ F	1 ms	<b>3</b>	03	0011
3	100k,R10	10pF	1 ms	<b>5</b>	05	0101
4	1M,R9	1pF	1 ms	<b>7</b>	07	0111
5	10M,R8	0.1pF	1 ms	<b>9</b>	09	1001
6	R7	C13	1 ms	<b>11</b>	0B	1011
7	R14	C20	1 ms	<b>13</b>	0D	1101
8	R13	C19	1 ms	<b>15</b>	0F	1111

### 5.3. Appendix C: Diffusion equation of iodide on a filter paper

We represent the faradaic background current,  $K$  as a constant value in section 4.5.1. Specifically, Equation 4.5.8 indicates that the baseline current is the sum of capacitance current and faradaic current from a straight line gradient of iodide. i.e.,

Equation 5.3.1

$$i_{\text{nonspecific}} = \frac{E}{R} \exp(-t / \tau) + i_{\text{cathode}}$$

The equation was derived by Crank and we introduced the work<sup>58</sup>.

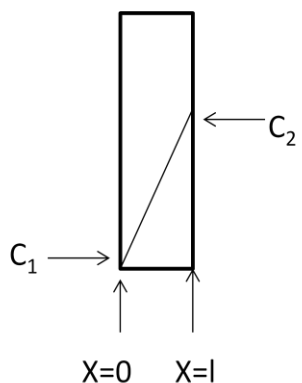


Figure 5.3.1 Concentration gradient of the thin layer cell.

Here we focus on  $i_{\text{cathode}}$  and derive an equation. We consider the case of diffusion through a filter paper with thickness  $l$  and diffusion coefficient  $D$ . At  $x = 0$  and  $x = l$ , we have constant concentration  $C_1$  and  $C_2$ , respectively as shown in Figure 5.3.1. In steady state, there was no change in concentration of  $I^-$  inside the filter paper. Therefore, it is  $d^2C/dx^2 = dC/dt = 0$ . Then  $dC/dx = \text{constant}$ . Integrating both sides yields, the following equation.

---

<sup>58</sup> Crank, J. The Mathematics of Diffusion; Oxford: London, 1956, pp 42-47.

**Equation 5.3.2**

$$\frac{C - C_1}{C_2 - C_1} = \frac{x}{l}$$

This is a straight line equation. Let's consider non-equilibrium state when gradient of  $\Gamma$  keeps changing. We denote  $f(x)$  as a initial distribution function of  $\Gamma$  and consider boundary value problem. We assume that  $\Gamma$  is distributed uniformly and one face,  $x = 0$  of the filter paper is at a constant concentration  $C_1$  and the other,  $x = l$  at  $C_2$  and the  $\Gamma$  is initially at a uniform concentration  $C_0$ .

**Equation 5.3.3**

$$C = C_1, \quad x = 0, \quad t \geq 0,$$

**Equation 5.3.4**

$$C = C_2, \quad x = l, \quad t \geq 0,$$

**Equation 5.3.5**

$$C = C_0, \quad 0 < x < l, \quad t = 0.$$

There is a certain period of time before steady state is reached and during this time, the concentration changes according to

**Equation 5.3.6**

$$C = C_1 + (C_2 - C_1) \frac{x}{l} + \frac{2}{\pi} \sum_{n=1}^{\infty} \frac{C_2 \cos n\pi - C_1}{n} \sin \frac{n\pi x}{l} \exp(-Dn^2\pi^2 t / l^2) + \frac{4C_0}{\pi} \sum_{m=0}^{\infty} \frac{1}{2m+1} \sin \frac{(2m+1)\pi x}{l} \exp(-D(2m+1)^2\pi^2 t / l^2).$$

As  $t$  approaches infinity, the exponentials vanishes and the system reaches the steady state. we obtain Equation 5.3.2. Experimentally, we observed that the current did not decay exponentially for initial 30 s. The initial current was higher than exponentially decaying function, and therefore, we did not include this initial current in our model.

## INDEX

- amperometric gas sensor, 123
- arsenic, iii, iv, xvii, 1, 2, 3, 4, 5, 6, 7, 8, 9, 11, 13, 16, 17, 24, 26, 27, 30, 31, 34, 36, 37, 38, 40, 41, 47, 48, 50, 51, 52, 53, 56, 57, 78, 103, 111, 113, 114, 131, 134, 148, 151, 153, 158, 164, 170, 180, 186, 188, 191, 204, 205, 206, 208
- arsine, viii, xv, xvii, 5, 6, 8, 14, 15, 16, 17, 22, 24, 27, 28, 29, 30, 31, 32, 33, 34, 35, 37, 38, 39, 40, 43, 45, 47, 48, 49, 50, 51, 52, 54, 55, 56, 57, 58, 59, 65, 72, 76, 80, 81, 82, 83, 84, 86, 88, 89, 93, 94, 95, 97, 98, 99, 100, 101, 102, 103, 104, 105, □106, 108, 109, 110, 112, 113, 114, 115, 116, 117, 118, 119, 120, 122, 123, 124, 127, 128, 129, 130, 131, 132, 134, 135, 136, 138, 144, 147, 158, 160, 163, 164, 165, 167, 169, 170, 172, 175, 176, 179, 184, 185, 188, 189, 190, 205, 206, 208
- arsine gas sensor, v, 9, 26, 48
- carbon fiber, xviii, 56, 164, 165, 166, 169, 171, 175, 177, 184, 189, 191
- chronoamperometry, xv, xvi, 19, 34, 44, 55, 65, 81, 83, 86, 87, 91, 96, 99, 106, 110, 143
- Cottrell equation, 95, 101
- cyclic voltammetry, 44, 55, 65, 85, 144

## REFERENCES

## REFERENCES

1. Bagla, P. Arsenic-Laced Well Water Poisoning Bangladeshis, **2003**, *National Geographic News*, June 5.
2. Feeney, R.; Kounaves, S.P., Voltammetric Measurement of Arsenic in Natural Waters. *Talanta*, **2002**, 58, 23.
3. Kinniburgh D.G.; Kosmus W. Arsenic Contamination in Ground Water: some analytical considerations. *Talanta*, **2002**, 58, 165-180.
4. Anderson R.D.; McNeil, L.S.; ASCE, A.M.; Edwards, M.; Morton S.C, Evaluation of a New Field Measurement Method for Arsenic in Drinking Water Samples, *Journal of environmental engineering*, **2008**, May, 382-388.
5. <http://consumerreports.org/cro/arsenicinfood.htm>.
6. Ahuja, S. Mechanism of arsenic contamination of water, Chapter 2: Delineation of a major worldwide problem of arsenic-contaminated groundwater, Handbook of Water Purity and Quality, **2009**, 24-27.
7. Mandal, B. K.; Suzuki, K.T. Arsenic round the world: a review, *Talanta*, **2002**, 201-235.
8. Gutzeit, H., *Pharmaz. Zeitung*. **1879**, 24, 263. cited in Vangreen, A.; Cheng, Z.; Seddiquie, A.A.; Hoque, M.A.; Geman, A.; Graziano, J.H.; Ahsan, H.; Parvez, F.; Ahmed, K.H. Reliability of a commercial kit to test groundwater for Arsenic in Bangladesh, *Environmental Science and Technology*. **2005**, 39, 299-303.
9. Feldmann, J., Salaun, P, Field test kits for arsenic: evaluation in terms of sensitivity, reliability, applicability, and cost. In *Arsenic contamination of Groundwater, Mechanism, Analysis, and remediation*; Ahuja, S. Ed.; John Wiley & Sons: New Jersey, U.S.A., **2008**, pp 183-188.
10. Anderson R.D.; McNeil, L.S.; ASCE, A.M.; Edwards, M.; Morton S.C, Evaluation of a new field measurement method for arsenic in drinking water samples, *Journal of environmental engineering*, **2008**, May, 382-388.
11. Samanta, G.; Chowdhury, T. R. ; Mandal, B. K.; Biswas, B.K.; Chowdhury, U.K.; Basu, G.K.; Chanda, C.R.; Lodh, D.; Chakraborti, D. Flow injection hydride generation atomic absorption spectrometry for determination of arsenic

in water and biological samples from arsenic-affected districts of west bengal, india, and Bangladesh, *Microchemical Journal* , **1999**, **62**, 174–191.

12. Featherstone, A. M.; Butler, E.C.V; O'Grady, B. V.; Michel, P. Determination of arsenic species in sea-water by hydride generation atomic fluorescence spectroscopy. *Journal of Analytical Atomic Spectroscopy*, **1998**, **13**, 1355–1360.
13. Tanaka, T; Nakamura, Y.; Mizuike, A.; Ono, A. Simultaneous Determination of phosphorous, Sulfur, and arsenic in steel by hydride generation and gas chromatography, *Analytical Sciences*, **1996**, **12**, February 77-80.
14. [www.wolfsense.com](http://www.wolfsense.com)
15. Rasul, S.B.; Munir, A.K.M.; Hossain, Z.A.; Khan A.H.; Alauddin, M; Hussam, A. Electrochemical measurement and speciation of inorganic arsenic in ground water of Bangladesh, *Talanta*, **2002**, **58**, 33-43.
16. Yamada D.; Ivandini, T.A.; Komatsu, M; Fujishima, A.; Einaga, Y. Anodic stripping voltammetry of inorganic species of As(III) and As(V) at gold modified boron doped diamond electrodes, *J. Electroanal. Chem.*, **2008**, **615**, 2, 145-153.
17. Simm, A.O.; Banks, C.E.; Compton, R.G. The Electrochemical detection of arsenic(III) at a silver electrode, *Electroanalysis*, **2005**, **19**, 1727-1733.
18. Ivandini, T.A.; Daisuke Yamada, D.; Watanabe, T.; Matsuura, H.; Nakano N.; Fujishima, A.; Einaga, Y. Development of amperometric arsine gas sensor using gold-modified diamond electrodes, *J. Electroanal. Chem.*, **2010**, **645**, 58–63.
19. Mays, D.E.; Hussam, A. Voltammetric methods for determination and speciation of inorganic arsenic in the environment-A review, *Anal. Chim. Acta*, 2009, **646**, 6-16.
20. Huang, H.; Dasgupta, P. K. Electrochemical Sensing of Gases Based on Liquid Collection Interfaces, *Electroanalysis*, **1997**, **9** (8), 585-591.
21. Stetter, J.; Li, J. Amperometric gas sensors-a review, *Chemical Reviews*, **2008**, **108**, 352-366.
22. Bard, A.J.; Faulkner, L.R. *Electrochemical Methods, fundamentals and applications*, 2nd ed.; John Wiley & Sons: New Jersey, **1994**, pp 92-107.
23. Planje, W.G.; Jassen, G.J.M.; . de Heer, M.P. A two-electrode sensor cell for CO detection in a H<sub>2</sub>-rich gas, *Sensors and Actuators B*, **2004**, **99**, 544-555.

24. Farrel, J.R.; Iles, P.J.; Yuan, Y.J., Determination of arsenic by hydride generation gas diffusion flow injection analysis with electrochemical detection, *Ana. Chim. Acta* , **1996**, 334, 193-197.
25. Lolic, A.; Nikolic, S.; Mutic, J. Optimization of a Flow Injection System with Amperometric Detection for Arsenic Determination, *Analytical Sciences*, **2008**, 24, July, 877-880.
26. Gifford, P.R.; Brukenstein, S. Pneumatoamperometric Determination of parts per billion dissolved gas by Gas evolving reactions. *Analytical Chemistry*, **1980**, 52, 1024-1028.
27. Gifford, P.R.; Brukenstein, S. Separation and Determination of Volatile Hydrides by Gas Chromatography with Gold Gas-Porous Electrode detector. *Analytical chemistry*, **1980**, 52, 1028-1031
28. Kumar , M. B.; Suzuki, K. T. Arsenic round the world: a review. *Talanta*, **2002**, 58, 201-235.
29. Tanaka, T.; Nakamura, Y.; Mizuike, A.; Ono, A.. Simultaneous Determination of phosphorous, Sulfur, and arsenic in steel by hydride generation and gas chromatography, *Analytical Sciences*, **1996**, 12, February, 77-80.
30. Funazaki, N.; Satoshi, K.; Hemme, A.; Ito, S.; Asano, Y. Development of catalytic electrochemical gas sensor for arsine. *Sensors and Actuators B*, **1993**, 13, 466-469.
31. Washburn, E.W. The Theory and Practice of the Iodometric Determination of Arsenious Acid. *J. Amer. Chem. Soc.*, **1908**, 31-46.
32. Wiley R.C. et al. Determination of Arsenic: Iodometric Acidimetric Method, *Industrial and Engineering Chemistry*, **1932**, 4(4), 396-397.
33. Rupasinghe, T.W.; Cardwell T. J.; Cattrall. R.W.; Kolevb. S. D. Determination of Arsenic by pervaporation-flow injection hydride generation and permanganate spectrophotometric detection, *Anal. Chim. Acta*, **2004**, 510, 225-230.
34. Tomcik, P.; Jursa, S.; Mesaros, S.; Bustin, D. Titration of As(III) with electrogenerated iodide in the diffusion layer of an interdigitated microelectroarray, *J. Electroanal. Chem.*, **1997**, 423, 115-118.
35. Hignett, G.; Wadhawan, J.D.; Lawrence, N.S.; Hung, D. Q.; Prado C.; Marken, F.; Compton, R.G. Electrochemical Detection of As(III) via Iodine Electrogenerated at Pt, Gold, Diamond or Carbon-Based Electrodes. *Electroanalysis*, **2004**, 16 (11), 897-903.

36. Ji, X.; Banks, C.E.; Compton, R.G. The direct electrochemical oxidation of ammonia in Propylene Carbonate: A Generic Approach to Amperometric Gas Sensors, *Electroanalysis*, **2006**, 18 (5), 449 – 455.
37. Wang, R.; Okajima, T.; Kitamura, F.; Ohsaka, T. A novel Amperometric O<sub>2</sub> sensor based on Supported room temperature Ionic Liquid Polyethylene membrane-Coated Electrodes. *Electroanalysis*, **2004**, 16, 66-72.
38. Ji, X.; Banks C.E.; Silvester D.S.; Aldous L; Hardacre, C.; Compton, R.G.. Electrochemical Ammonia Gas Sensing in Nonaqueous Systems: A Comparison of Propylene Carbonate with Room Temperature Ionic Liquids. *Electroanalysis*, **2007**, 19(21), 2194-2201.
39. Mishima, B.A.; Mishima H.T. Ammonia sensor based on propylene carbonate, *Sens. Actuators, B*, **2008**, 131, 236-240.
40. <http://www.jamestowndistributors.com/> (accessed November 29, 2012).
41. <http://lessemf.com/> (accessed November 29, 2012).
42. CRC Handbook of chemistry and physics, 93 edition, Hayes, W.M. table of electrochemical series, **2012-2013**, 5-80.
43. Schmid, G.M.; Curley-Fiorino, M.E., Chapter IV: Gold In *Encyclopedia of electrochemistry of the elements*; Bard, A. J. Ed.; M. Dekker: New York, U.S.A., **1973**, p 94.
44. Burke, L.D.; Moran, J. M.; Nugent, P. F. Cyclic voltammetry responses of metastable gold electrodes in aqueous media. *Journal of Solid State electrochemistry*, **2003**, 7, 529-538.
45. Kraichman, M, B.; Hogge, E. A. The limiting current on a rotating-disk electrode in silver nitrate-potassium nitrate solutions. The diffusion coefficient of silver ion. *Journal of Physical Chemistry*, **1955**, 59, 986-987.
46. Bard, A.J.; Faulkner, L.R. *Electrochemical Methods, fundamentals and applications*, 2nd ed.; John Wiley & Sons: New Jersey, **1994**, pp 146-147.
47. Sime, R.J. *Physical Chemistry*, **1990**, Saunders College Publishing, a division of Holt, Rinehart and Winston, Inc. p 558-566.
48. Johnson, D.E.; Enke, C. G. *Analytical Chemistry*, **1970**, 42(3), 329.
49. Atkins, P.W. *Physical Chemistry*; Oxford University Press: Oxford, **1990**; P 752.

50. Bard, A.J.; Faulkner, L.R. *Electrochemical Methods, fundamentals and applications*, 2nd ed.; John Wiley & Sons: New Jersey, **1994**, pp 148-151.
51. Bard, A.J.; Faulkner, L.R. *Electrochemical Methods, fundamentals and applications*, 2nd ed.; John Wiley & Sons: New Jersey, **1994**, p 9.
52. Van Wagenen. S.;Carter. D.E. Kinetic control of peak shapes in atomic absorption arsenic determinations by arsine generation, *Analytical Chemistry*, **1987**, 57, 891-896.
53. Kumar, R.; Ryazuddin, P. Mechanism of volatile hydride formation and their atomization in hydride generation atomic absorption spectroscopy, *Analytical Sciences*, **2005**, 21, 1401-1410.
54. Rogers, E.I.; Silvester, D. S.; Aldous, L.; Hardacre, C.; Compton, R. G. Electrooxidation of the iodides [C4mim]I, LiI, NaI, KI, RbI, and CsI in the room temperature ionic liquid [C4mim][NTf2]. *J. Phys. Chem. C* 2008, 112, 6551-6557.
55. Wonsawat. W. et al. Highly Sensitive Determination of Cadmium and Lead Using a Low-cost Electrochemical Flow-through Cell Based on a Carbon Paste Electrode.
56. Maixnerova, L. et al. Thin-Layer and Wall-Jet Arrangement of Amperometric Dectector with Boron-Doped Diamond Electrode, *Electroanalysis*, **2012**, 24(3), 649-658.
57. Datasheet of ADG1208/ADG1209, Analog Devices, Rev. B, 3.
58. Crank, J. *The Mathematics of Diffusion*; Oxford: London, **1956**, pp 42-47.

## CURRICULUM VITAE

Jinsoo Hong was born in Cheongsan Li 406 Ho, Namyee Myun, Chungcheongbukdo, South Korea in 1964. He graduated from Jungang University affiliated high school in 1983. He received his Bachelor of Science from the department of chemistry, Seoul National University, Seoul, South Korea in February, 1992. He received his Master of Science in Chemistry from George Mason University in August, 1999. He worked as an organic chemist for Life technologies Inc. in Rockville, Maryland since August, 1999 until March, 2012. He has been employed by the U.S. department of Health and Human Services, National Institute of Health as a radiochemist at Molecular Imaging Branch, Positron Emission Tomography, Radiochemistry in National Institute of Mental Health since March 1999 until now.

### Publications

- 1) Abe, K (Abe, Kohji); Zoghbi, SS (Zoghbi, S. S.); Inoue, O (Inoue, O.); Itoh, T (Itoh, T.); Hong, J (**Hong, Jinsoo**); Pike, VW (Pike, V. W.); Innis, RB (Innis, R. B.); Fujita, M (Fujita, M.) In vivo density and affinity of [C-11](R)-rolipram binding to phosphodiesterase 4 in rat measured with and without anesthesia  
NEUROIMAGE Volume: 41 Supplement: 2 Pages: T48-T48 DOI: 10.1016/j.neuroimage.2008.04.222 Published: 2008
- 2) Briard, E (Briard, Emmanuelle); Zoghbi, SS (Zoghbi, Sami S.); Imaizumi, M (Imaizumi, Masao); Gourley, JP (Gourley, Jonathan P.); Shetty, HU (Shetty, H. Umesha); Hong, J (**Hong, Jinsoo**); Cropley, V (Cropley, Vanessa); Fujita, M (Fujita, Masahiro); Innis, RB (Innis, Robert B.); Pike, VW (Pike, Victor W.) Synthesis and evaluation in monkey of two sensitive C-11-labeled aryloxyanilide ligands for imaging brain peripheral benzodiazepine receptors in vivo Source: JOURNAL OF MEDICINAL CHEMISTRY Volume: 51 Issue: 1 Pages: 17-30 DOI: 10.1021/jm0707370 Published: JAN 10 2008
- 3) Briard, E (Briard, Emmanuelle); Zoghbi, SS (Zoghbi, Sami S.); Imaizumi, M (Imaizumi, Masao); Gourley, JP (Gourley, Jonathan P.); Shetty, HU (Shetty, H. Umesha); Hong, J (**Hong, Jinsoo**); Cropley, V (Cropley, Vanessa); Fujita, M (Fujita, Masahiro); Innis, RB (Innis, Robert B.); Pike, VW (Pike, Victor W.) Synthesis and evaluation in monkey of two sensitive C-11-labeled aryloxyanilide ligands for imaging brain peripheral benzodiazepine receptors in vivo. JOURNAL OF

MEDICINAL CHEMISTRY Volume: 51 Issue: 1 Pages: 17-30 DOI:  
10.1021/jm0707370 Published: JAN 10 2008

- 4) Brown, AK (Brown, Amira K.); Fujita, M (Fujita, Masahiro); Fujimura, Y (Fujimura, Yota); Liow, JS (Liow, Jeh-San); Stabin, M (Stabin, Michael); Ryu, YH (Ryu, Yong H.); Imaizumi, M (Imaizumi, Masao); Hong, J (**Hong, Jinsoo**); Pike, VW (Pike, Victor W.); Innis, RB (Innis, Robert B.) Radiation dosimetry and biodistribution in monkey and man of C-11-PBR28: A PET radioligand to image inflammation JOURNAL OF NUCLEAR MEDICINE Volume: 48 Issue: 12 Pages: 2072-2079 DOI: 10.2967/jnumed.107.044842 Published: DEC 2007
- 5) Cropley, VL (Cropley, VL); Fujita, M (Fujita, M); Musachio, JL (Musachio, JL); Hong, J (**Hong, Jinsoo**); Ghose, S (Ghose, S); Sangare, J (Sangare, J); Nathan, PJ (Nathan, PJ); Pike, VW (Pike, VW); Innis, RB (Innis, RB) Whole-body biodistribution and estimation of radiation-absorbed doses of the dopamine D-1 receptor radioligand C-11-NNC 112 in humans. JOURNAL OF NUCLEAR MEDICINE Volume: 47 Issue: 1 Pages: 100-104 Published: JAN 2006
- 6) Cai, LS (Cai, Lisheng); Ye, D (Ye, D.); Liow, JS (Liow, J. -S.); Hong, J (**Hong, Jinsoo**); Cohen, RM (Cohen, R. M.); Pike, VW (Pike, V. W.); Innis, RB (Innis, R. B.) PET imaging of transgenic mice TG2576 using the beta-amyloid radioligand, [C-11]PIB. NEUROIMAGE Volume: 31 Supplement: 2 Pages: T141-T142 DOI: 10.1016/j.neuroimage.2006.04.125 Published: 2006.
- 7) Donohue, S (Donohue, S.); Halldin, C (Halldin, C.); Brown, A (Brown, A.); Hong, J (**Hong, Jinsoo**); Musachio, JL (Musachio, J. L.); Bacher, J (Bacher, J.); Innis, RB (Innis, R. B.); Pike, VW (Pike, V. W.) Synthesis, radiosynthesis and initial biological evaluation of a new class of candidate brain cannabinoid type-1 (cb1) receptor radioligand. JOURNAL OF LABELLED COMPOUNDS & RADIOPHARMACEUTICALS Volume: 48 Supplement: 1 Pages: S185-S185 Published: JUN 2005
- 8) Fabrice, G. S.; Liow, J.S.; Zhang, Y.; Hong, J. (**Hong, Jinsoo**); Gladding, R. L.; Zoghbi S. S.; Innis, R. B.; Pike, V. W. Synthesis and characterization in monkey of [<sup>11</sup>C]SP203 as a radioligand for imaging brain metabotropic glutamate 5 receptors, *Eur. J. Nucl. Med. Mol. Imaging.*, 2012, 39(12), 1949-1958.
- 9) Fujita, M (Fujita, M); Zoghbi, SS (Zoghbi, SS); Cresezenzo, MS (Cresezenzo, MS); Hong, J (**Hong, Jinsoo**); Musachio, JL (Musachio, JL); Lu, JQ (Lu, JQ); Liow, JS (Liow, JS); Seneca, N (Seneca, N); Tipre, DN (Tipre, DN); Cropley, VL (Cropley, VL); Imaizumi, M (Imaizumi, M); Gee, AD (Gee, AD); Seidel, J (Seidel, J); Green, MV (Green, MV); Pike, VW (Pike, VW); Innis, RB (Innis, RB) Quantification of brain phosphodiesterase 4 in rat with (R)-[C-11]Rolipram-PET NEUROIMAGE Volume: 26 Issue: 4 Pages: 1201-1210 DOI: 10.1016/j.neuroimage.2005.03.017 Published: JUL 15 2005
- 10) Fujita, M (Fujita, Masahiro); Imaizumi, M (Imaizumi, M.); Zoghbi, SS (Zoghbi, S.

- S.); Fujimura, Y (Fujimura, Y.); Farris, AG (Farris, A. G.); Suhara, T (Suhara, T.); Hong, J (**Hong, Jinsoo**); Pike, VW (Pike, V. W.); Innis, RB (Innis, R. B.) Kinetic analysis in healthy humans of [C-11]PBR28, a new positron emission tomography radioligand to image the peripheral benzodiazepine receptor Source: NEUROIMAGE Volume: 41 Supplement: 2 Pages: T34-T34 DOI: 10.1016/j.neuroimage.2008.04.208 Published: 2008
- 11) Fujita, M (Fujita, Masahiro); Imaizumi, M (Imaizumi, Masao); D'Sa, C (D'Sa, Carrol); Zoghbi, SS (Zoghbi, Sami S.); Crescenzo, MS (Crescenzo, Matthew S.); Hong, JS (**Hong, Jinsoo**); Musachio, JL (Musachio, John L.); Gee, AD (Gee, Antony D.); Seidel, J (Seidel, Jurgen); Green, MV (Green, Michael V.); Pike, VW (Pike, Victor W.); Duman, RS (Duman, Ronald S.); Innis, RB (Innis, Robert B.) In vivo and in vitro measurement of brain phosphodiesterase 4 in rats after antidepressant administration SYNAPSE Volume: 61 Issue: 2 Pages: 78-86 DOI: 10.1002/syn.20347 Published: FEB 2007
- 12) Fujita, M (Fujita, Masahiro); Zoghbi, SS (Zoghbi, S. S.); Irnaizurni, M (Irnaizurni, M.); Hong, J. (**Hong, Jinsoo**); Gladding, RL (Gladding, R. L.); Pike, VW (Pike, V. W.); Innis, RB (Innis, R. B.) Species differences in brain phosphodiesterase levels measured with [C-11](R)-Rolipram PET NEUROIMAGE Volume: 41 Supplement: 2 Pages: T185-T185 DOI: 10.1016/j.neuroimage.2008.04.152 Published: 2008
- 13) Fujita, M (Fujita, Masahiro); Zoghbi, SS (Zoghbi, Sami S.); Crescenzo, MS (Crescenzo, Matthew S.); Hong, JS (**Hong, Jinsoo**); Musachio, JL (Musachio, John L.); Lu, JQ (Lu, Jian-Qiang); Liow, JS (Liow, Jeh-San); Seneca, N (Seneca, Nicholas); Tipre, DN (Tipre, Dnyanesh N.); Cropley, VL (Cropley, Vanessa L.); Imaizumi, M (Imaizumi, Masao); Gee, AD (Gee, Antony D.); Seidel, J (Seidel, Jurgen); Green, MV (Green, Michael V.); Pike, VW (Pike, Victor W.); Innis, RB (Innis, Robert B.) Quantification of brain phosphodiesterase 4 in rat with (R)-[C-11]rolipram-PET" (vol 26, pg 1201, 2005) NEUROIMAGE Volume: 36 Issue: 4 Pages: 1399-1399 DOI: 10.1016/j.neuroimage.2007.04.020 Published: JUL 15 2007
- 14) Fujita, M (Fujita, Masahiro)1; Imaizumi, M (Imaizumi, Masao)1; Zoghbia, SS (Zoghbia, Sami S.)1; Fujimura, Y (Fujimura, Yota)1; Farris, AG (Farris, Amanda G.)1; Suhara, T (Suhara, Tetsuya)2; Hong, J. (**Hong, Jinsoo**)1; Pike, VW (Pike, Victor W.)1; Nnisa, RB (Nnisa, Robert B.) Kinetic analysis in healthy humans of a novel positron emission tomography radioligand to image the peripheral benzodiazepine receptor, a potential biomarker for inflammation NEUROIMAGE Volume: 40 Issue: 1 Pages: 43-52 DOI: 10.1016/j.neuroimage.2007.11.011 Published: MAR 1 2008
- 15) Imaizumi, M (Imaizumi, Masao); Briard, E (Briard, Emmanuelle); Zoghbi, SS (Zoghbi, Sami S.); Gourley, JP (Gourley, Jonathan P.); Hong, J. (**Hong, Jinsoo**); Fujimura, Y (Fujimura, Yota); Pike, VW (Pike, Victor W.); Innis, RB (Innis, Robert

- B.); Fujita, M (Fujita, Masahiro), Brain and whole-body imaging in nonhuman primates of [C-11]PBR28, a promising PET radioligand for peripheral benzodiazepine receptors. Source: NEUROIMAGE Volume: 39 Issue: 3 Pages: 1289-1298 DOI: 10.1016/j.neuroimage.2007.09.063 Published: FEB 1 2008. *Journal of Medicinal Chemistry*, 2011, 54(8), 2687-2700
- 16) Imaizumi, M (Imaizumi, Masao); Briard, E (Briard, Emmanuelle); Zoghbi, SS (Zoghbi, Sami S.); Gourley, JP (Gourley, Jonathan P.); Hong, J. (**Hong, Jinsoo**); Musachio, JL (Musachio, John L.); Gladding, R (Gladding, Robert); Pike, VW (Pike, Victor W.); Innis, RB (Innis, Robert B.); Fujita, M (Fujita, Masahiro) Kinetic evaluation in nonhuman primates of two new PET ligands for peripheral benzodiazepine receptors in brain SYNAPSE Volume: 61 Issue: 8 Pages: 595-605 DOI: 10.1002/syn.20394 Published: AUG 2007
- 17) Imaizumi, M (Imaizumi, Masao); Kim, HJ (Kim, Hyun-Ju); Zoghbi, SS (Zoghbi, Sami S.); Briard, E (Briard, Ernmanuelle); Hong, J. (**Hong, Jinsoo**); Musachio, JL (Musachio, John L.); Ruetzler, C (Ruetzler, Christl); Chuang, DM (Chuang, De-Maw); Pike, VW (Pike, Victor W.); Innis, RB (Innis, Robert B.); Fujita, M (Fujita, Masahiro) PET imaging with [C-11]PBR28 can localize and quantify upregulated peripheral benzodiazepine receptors associated with cerebral ischemia in rat NEUROSCIENCE LETTERS Volume: 411 Issue: 3 Pages: 200-205 DOI: 10.1016/j.neulet.2006.09.093 Published: JAN 16 2007
- 18) Imaizumi, M (Imaizumi, Masao); Briard, E (Briard, Emmanuelle); Zoghbi, SS (Zoghbi, Sami S.); Gourley, JP (Gourley, Jonathan P.); Hong, J (**Hong, Jinsoo**); Musachio, JL (Musachio, John L.); Gladding, R (Gladding, Robert); Pike, VW (Pike, Victor W.); Innis, RB (Innis, Robert B.); Fujita, M (Fujita, Masahiro) Kinetic evaluation in nonhuman primates of two new PET ligands for peripheral benzodiazepine receptors in brain, SYNAPSE Volume: 61 Issue: 8 Pages: 595-605 DOI: 10.1002/syn.20394 Published: AUG 2007
- 19) Itoh, T (Itoh, T.); Abe, K (Abe, K.); Inoue, O (Inoue, O.); Hong, J. (**Hong, Jinsoo**); Pike, VW (Pike, V. W.); Innis, RB (Innis, R. B.); Fujita, M (Fujita, M.) The effect of cAMP dependent protein kinase activator and inhibitor on [C-11]rolipram binding to phosphodiesterase 4 in conscious rats JOURNAL OF CEREBRAL BLOOD FLOW AND METABOLISM Volume: 29 Supplement: S1 Pages: S13-S14 Published: OCT 2009
- 20) Itoh, T (Itoh, Tetsuji); Abe, K (Abe, Kohji); Hong, J.S. (**Hong, Jinsoo**); Inoue, O (Inoue, Osamu); Pike, VW (Pike, Victor W.); Innis, RB (Innis, Robert B.); Fujita, M (Fujita, Masahiro) Effects of cAMP-Dependent Protein Kinase Activator and Inhibitor on In Vivo Rolipram Binding to Phosphodiesterase 4 in Conscious Rats

- 21) Itoh, T (Itoh, Tetsuji); Abe, K (Abe, Kohji); Zoghbi, SS (Zoghbi, Sami S.); Inoue, O (Inoue, Osamu); Hong, J.S. (**Hong, Jinsoo**); Imaizumi, M (Imaizumi, Masao); Pike, VW (Pike, Victor W.); Innis, RB (Innis, Robert B.); Fujita, M (Fujita, Masahiro) PET Measurement of the In Vivo Affinity of C-11-(R)-Rolipram and the Density of Its Target, Phosphodiesterase-4, in the Brains of Conscious and Anesthetized Rats JOURNAL OF NUCLEAR MEDICINE Volume: 50 Issue: 5 Pages: 749-756 DOI: 10.2967/jnumed.108.058305 Published: MAY 1 2009
- 22) Kimura, Y (Kimura, Yasuyuki); Fujita, M (Fujita, Masahiro); Hong, J.S. (**Hong, Jinsoo**); Lohith, TG (Lohith, Talakad G.); Gladding, RL (Gladding, Robert L.); Zoghbi, SS (Zoghbi, Sami S.); Tauscher, JA (Tauscher, Johannes A.); Goebel, N (Goebel, Nancy); Rash, KS (Rash, Karen S.); Chen, ZG (Chen, Zhaogen); Pedregal, C (Pedregal, Concepcion); Barth, VN (Barth, Vanessa N.); Pike, VW (Pike, Victor W.); Innis, RB (Innis, Robert B.) Brain and Whole-Body Imaging in Rhesus Monkeys of C-11-NOP-1A, a Promising PET Radioligand for Nociceptin/Orphanin FQ Peptide Receptors, JOURNAL OF NUCLEAR MEDICINE Volume: 52 Issue: 10 Pages: 1638-1645 DOI: 10.2967/jnumed.111.091181 Published: OCT 1 2011
- 23) Kimura, Y; Fujita, M; Hong, J. (**Hong, Jinsoo**); Lohith, T. G.; Gladding, R. L. ; Zoghbi, S. S.; Tauscher, J. A.; Goebel, N.; Rash, K. S.; Chen, Z. G.; Pedregal, C.; Barth, V.N.; Pike, V. W.; Innis, R. B. Brain and Whole-Body Imaging in Rhesus Monkeys of [C-11] NOP-1A, a Promising PET Radioligand for Nociceptin/Orphanin FQ Peptide Receptors . *Journal of Nuclear Medicine*, 2011, 52(10), 1638-1645.
- 24) Kinetic analysis in healthy humans of [C-11]PBR28, a new positron emission tomography radioligand to image the peripheral benzodiazepine receptor Fujita, M (Fujita, Masahiro); Imaizumi, M (Imaizumi, M.); Zoghbi, SS (Zoghbi, S. S.); Fujimura, Y (Fujimura, Y.); Farris, AG (Farris, A. G.); Suhara, T (Suhara, T.); Hong, J. (**Hong, Jinsoo**); Pike, VW (Pike, V. W.); Innis, RB (Innis, R. B.) NEUROIMAGE Volume: 41 Supplement: 2 Pages: T34-T34 DOI: 10.1016/j.neuroimage.2008.04.208 Published: 2008
- 25) Kreisl, W.C.; Fujita, M.; Fujimura, Y.; Kimura, N.; Jenko, K. J.; Kannan, P. ; Hong, J. (**Hong, Jinsoo**); Morse, C. L.; Zoghbi, S. S.; Gladding, R. L. ; Jacobson, S. ; Oh, U.; Pike, V. W.; Innis, R. B. Comparison of [C-11]-(R)-PK 11195 and [C-11]PBR28, two radioligands for translocator protein (18 kDa) in human and monkey: Implications for positron emission tomographic imaging of this inflammation biomarker, NEUROIMAGE, 2010, 49 (4), 2924-2932.
- 26) Lazarova, N (Lazarova, Neva); Zoghbi, SS (Zoghbi, Sami S.); Hong, J (**Hong, Jinsoo**); Seneca, N (Seneca, Nicholas); Tuan, E (Tuan, Ed)<sup>1</sup>; Gladding, RL (Gladding, Robert L.); Liow, JS (Liow, Jieh-San)<sup>1</sup>; Taku, A (Taku, Andrew); Innis, RB (Innis, Robert B.); Pike, VW (Pike, Victor W.)<sup>1</sup> Synthesis and evaluation of [N-methyl-C-11]N-desmethyl-loperamide as a new and improved PET radiotracer for

- imaging P-gp function. *JOURNAL OF MEDICINAL CHEMISTRY* Volume: 51  
Issue: 19 Pages: 6034-6043 DOI: 10.1021/jm800510m Published: OCT 9 2008
- 27) Liow, JS (Liow, Jieh-San); Lu, SY (Lu, Shuiyu); McCarron, JA (McCarron, Julie A.); Hong, JS (**Hong, Jinsoo**); Musachio, JL (Musachio, John L.); Pike, VW (Pike, Victor W.); Innis, RB (Innis, Robert B.); Zoghbi, SS (Zoghbi, Sami S.) Effect of a P-glycoprotein inhibitor, cyclosporin A, on the disposition in rodent brain and blood of the 5-HT<sub>1A</sub> receptor radioligand, [C-11](R)-(-)-RWAYSYNAPSE Volume: 61  
Issue: 2 Pages: 96-105 DOI: 10.1002/syn.20348 Published: FEB 2007
- 28) Lu, S. Y.; Watts, P.; Chin, F. T.; Hong, J. (**Hong, Jinsoo**); Musachio, J. L.; Haswell, S. J.; Pike, V. W. Exploration of a micro-reactor for the synthesis of NCA <sup>11</sup>C- and <sup>18</sup>F-labeled carboxylic esters. *European journal of nuclear medicine and molecular imaging*, 2004, 31, Supplement: 2, S248-S248.
- 29) Lu, SY ; Hong, J. (**Hong, Jinsoo**); Musachio, J. L.; Pike, V. W. Synthesis of two NCA [carbonyl-<sup>11</sup>C]-labeled 5-HT<sub>1A</sub> receptor agonists based on reactions of in situ generated [<sup>11</sup>C]organocarboxymagnesium halides with amine precursors under microwave-enhanced conditions, *European journal of nuclear medicine and molecular imaging*, 2004, 31, Supplement: 2, S249-S249.
- 30) Lu, SY (Lu, Shuiyu); Hong, J (**Hong, Jinsoo**); Itoh, T (Itoh, Tetsuji); Fujita, M (Fujita, Masahiro); Inoue, O (Inoue, Osamu); Innis, RB (Innis, Robert B.); Pike, VW (Pike, Victor W.) [carbonyl-C-11]Benzyl acetate: Automated radiosynthesis via Pd-mediated [C-11]carbon monoxide chemistry and PET measurement of brain uptake in monkey, *JOURNAL OF LABELLED COMPOUNDS & RADIOPHARMACEUTICALS* Volume: 53 Issue: 7-8 Pages: 548-551 DOI: 10.1002/jlcr.1779 Published: JUN 15 2010
- 31) Lu, SY (Lu, SY); Hong, J (**Hong, Jinsoo**); Musachio, JL (Musachio, JL); Chin, FT (Chin, FT); Vermeulen, ES (Vermeulen, ES); Wikstrom, HV (Wikstrom, HV); Pike, VW (Pike, VW) Alternative methods for labeling the 5-HT<sub>1A</sub> receptor agonist, 1-[2-(4-fluorobenzoylamino)ethyl]-4-(7-methoxynaphthyl)piperazine (S14506), with carbon-11 or fluorine-18. *JOURNAL OF LABELLED COMPOUNDS & RADIOPHARMACEUTICALS* Volume: 48 Issue: 13 Pages: 971-981 DOI: 10.1002/jlcr.1009 Published: NOV 200
- 32) Lu, SY (Lu, S. Y.); Liow, JS (Liow, J. S.); Ichise, M (Ichise, M.); Hong, J (**Hong, Jinsoo**); Musachio, JL (Musachio, J. L.); Zoghbi, SS (Zoghbi, S. S.); Nichols, L (Nichols, L.); Seidel, J (Seidel, J.); Vermeulen, ES (Vermeulen, E. S.); Wikstrom, HV (Wikstrom, H. V.); Innis, RB (Innis, R. B.); Pike, VW (Pike, V. W.). Evaluation of [<sup>11</sup>C]S14506 as an agonist radioligand for brain 5-HT<sub>1A</sub> receptors in rat and monkey. *JOURNAL OF LABELLED COMPOUNDS & RADIOPHARMACEUTICALS* Volume: 48 Supplement: 1 Pages: S72-S72  
Published: JUN 2005
- 33) Lu, SY (Lu, S. Y.); Hong, J (**Hong, Jinsoo**); Musachio, JL (Musachio, J. L.); Chin, FT (Chin, F. T.); Vermeulen, ES (Vermeulen, E. S.); Wikstrom, HV (Wikstrom, H.

- V.); Pike, VW (Pike, V. W.) Methods for labeling the 5-HT<sub>1A</sub> receptor agonist, s14506, with a positron-emitter at any of three alternative positions JOURNAL OF LABELLED COMPOUNDS & RADIOPHARMACEUTICALS Volume: 48 Supplement: 1 Pages: S146-S146 Published: JUN 2005
- 34) McCarron, JA (McCarron, JA); Chin, FT (Chin, FT); Pike, VW (Pike, VW); Hong, J (**Hong, Jinsoo**); Musachio, JL (Musachio, JL); Ichise, M (Ichise, M); Zoghbi, SS (Zoghbi, SS); Vines, DC (Vines, DC); Vermeulen, ES (Vermeulen, ES); Wikstrom, HV (Wikstrom, HV); Halldin, C (Halldin, C); Innis, RB (Innis, RB) New candidate PET radioligands for brain 5-HT<sub>1A</sub> receptors based on 2,3,4,5,6,7-hexahydro-1-[4-[1[4-(2-methoxyphenyl)-piperazinyl]]-2-phenylbutyryl]-m-azepine (RWAY) NEUROIMAGE Volume: 22 Supplement: 2 Pages: T34-T35 Published: 2004
- 35) Musachio, JL (Musachio, JL); Hong, J (**Hong, Jinsoo**); Ichise, M (Ichise, M); Seneca, N (Seneca, N); Brown, AK (Brown, AK); Liow, JS (Liow, JS); Halldin, C (Halldin, C); Innis, RB (Innis, RB); Pike, VW (Pike, VW); He, R (He, R); Zhou, J (Zhou, J); Kozikowski, AP (Kozikowski, AP) Development of new brain imaging agents based upon cocaine-modafinil hybrid monoamine transporter inhibitors BIOORGANIC & MEDICINAL CHEMISTRY LETTERS Volume: 16 Issue: 12 Pages: 3101-3104 DOI: 10.1016/j.bmcl.2006.03.066 Published: JUN 15 2006
- 36) Ozaki, H.; Zoghbi, S. S.; Hong, J. (**Hong, Jinsoo**); Verma, A. ; Pike, V. W.; Innis, R. B.; Fujita, M. In Vivo Binding of Protoporphyrin IX to Rat Translocator Protein Imaged With Positron Emission Tomography, *Synapse*, 2010, 64(8), 649-658.
- 37) Pike, V. W. ; Taliani, S; Lohith, T. G. ; Owen, D. R. J. ; Pugliesi, I. ; Da Pozzo, E.; Hong, J. (**Hong, Jinsoo**) ; Zoghbi, S. S.; Gunn, R. N.; Parker, C. A.; Rabiner, E. A.; Fujita, M.; Innis, R. B.; Martini, C.; Da Settimo, F. Evaluation of Novel N-1-Methyl-2-phenylindol-3-ylglyoxylamides as a New Chemotype of 18 kDa Translocator Protein-Selective Ligand Suitable for the Development of Positron Emission Tomography Radioligands, *Journal of Medicinal Chemistry*, 2011,54(1), 366-373.
- 38) Pike, V. W.; Rash, K. S.; Chen, Z. G.; Pedregal, C. ; Statnick, M. A.; Kimura, Y; Hong, J. (**Hong, Jinsoo**) ; Zoghbi, S. S.; Fujita, M.; Toledo, M. A.; Diaz, N. ; Gackenheimer, S. L.; Tauscher, J. T.; Barth, V. N. ; Innis, R. B. Synthesis and Evaluation of Radioligands for Imaging Brain Nociceptin/Orphanin FQ Peptide (NOP) Receptors with Positron Emission Tomography
- 39) Schou, M (Schou, M.); Zoghbi, SS (Zoghbi, S. S.); Shetty, H (Shetty, H.); Shchukin, E (Shchukin, E.); Liow, J (Liow, J.); Hong, J. (**Hong, Jinsoo**); Andree, A (Andree, A.); Gulyas, B (Gulyas, B.); Farde, L (Farde, L.); Innis, RB (Innis, R. B.); Pike, VW (Pike, V. W.); Halldin, C (Halldin, C.) Investigation of the metabolites of (S, S)-[11C] MeNER in humans, monkeys and rats. EUROPEAN JOURNAL OF NUCLEAR MEDICINE AND MOLECULAR IMAGING Volume: 33 Supplement: 2 Pages: S212-S212 Published: SEP 2006
- 40) Seneca, N (Seneca, Nicholas); Liow, JS (Liow, J. S.); Zoghbi, S (Zoghbi, S.); Musachio, JL (Musachio, J. L.); Hong, J (**Hong, Jinsoo**); Pike, VW (Pike, V. W.);

- Halldin, C (Halldin, C.); Innis, RB (Innis, R. B.) Imaging endogenous dopamine occupancy of the D2 receptor in rat brain with [<sup>11</sup>C]MNPA  
NEUROIMAGE Volume: 31 Supplement: 2 Pages: T119-T119 DOI:  
10.1016/j.neuroimage.2006.04.105 Published: 2006
- 41) Skinbjerg, M (Skinbjerg, Mette); Seneca, N (Seneca, Nicholas); Liow, JS (Liow, Jeih-San); Hong, J.S. (**Hong, Jinsoo**); Weinshenker, D (Weinshenker, David); Pike, VW (Pike, Victor W.); Halldin, C (Halldin, Christer); Sibley, DR (Sibley, David R.); Innis, RB (Innis, Robert B.) Dopamine beta-Hydroxylase-Deficient Mice Have Normal Densities of D-2 Dopamine Receptors in the High-Affinity State Based on In Vivo PET Imaging and In Vitro Radioligand Binding, SYNAPSE Volume: 64 Issue: 9 Pages: 699-703 DOI: 10.1002/syn.20781 Published: SEP 2010
- 42) Toyama, H (Toyama, H); Ye, D (Ye, D); Ichise, M (Ichise, M); Liow, JS (Liow, JS); Cai, LS (Cai, LS); Jacobowitz, D (Jacobowitz, D); Musachio, JL (Musachio, JL); Hong, J. (**Hong, Jinsoo**); Crescenzo, M (Crescenzo, M); Tipre, D (Tipre, D); Lu, JQ (Lu, JQ); Zoghbi, S (Zoghbi, S); Vines, DC (Vines, DC); Seidel, J (Seidel, J); Katada, K (Katada, K); Green, MV (Green, MV); Pike, VW (Pike, VW); Cohen, RM (Cohen, RM); Innis, RB (Innis, RB) PET imaging of brain with the beta-amyloid probe, [<sup>11</sup>C-11]6-OH-BTA-1, in a transgenic mouse model of Alzheimer's disease EUROPEAN JOURNAL OF NUCLEAR MEDICINE AND MOLECULAR IMAGING Volume: 32 Issue: 5 Pages: 593-600 DOI: 10.1007/s00259-005-1780-5 Published: APR 2005
- 43) Tsujikawa, Tetsuya; Zoghbi, Sami; Hong, J. (**Hong, Jinsoo**), Quantification of human brain cannabinoid CB1 receptors using a novel PET radioligand, [<sup>11</sup>C]SD5024, 2012, JOURNAL OF CEREBRAL BLOOD FLOW AND METABOLISM Volume: 32 Supplement: 1 Pages: S133-S134 Published: AUG 2012
- 44) Shetty, HU (Shetty, H. Umesha); Zoghbi, SS (Zoghbi, Sami S.); Liow, JS (Liow, Jeih-San); Ichise, M (Ichise, Masanori); Hong, J (**Hong, Jinsoo**); Musachio, JL (Musachio, John L.); Halldin, C (Halldin, Christer); Seidel, J (Seidel, Jurgén); Innis, RB (Innis, Robert B.); Pike, VW (Pike, Victor W.) Identification and regional distribution in rat brain of radiometabolites of the dopamine transporter PET radioligand [<sup>11</sup>C-11]PE2I. EUROPEAN JOURNAL OF NUCLEAR MEDICINE AND MOLECULAR IMAGING Volume: 34 Issue: 5 Pages: 667-678 DOI: 10.1007/s00259-006-0277-1 Published: MAY 2007
- 45) Xu, R (Xu, Rong); Hong, J. (**Hong, Jinsoo**); Morse, CL (Morse, Cheryl L.); Pike, VW (Pike, Victor W.) Synthesis, Structure-Affinity Relationships, and Radiolabeling of Selective High-Affinity 5-HT<sub>4</sub> Receptor Ligands as Prospective Imaging Probes for Positron Emission Tomography, JOURNAL OF MEDICINAL CHEMISTRY Volume: 53 Issue: 19 Pages: 7035-7047 DOI: 10.1021/jm100668r Published: OCT 14 2010
- 46) Yasuno, F (Yasuno, Fumihiko); Brown, AK (Brown, Amira K.); Zoghbi, SS (Zoghbi, Sami S.); Krushinski, JH (Krushinski, Joseph H.); Chernet, E (Chernet, Eyassu);

- Tauscher, J (Tauscher, Johannes); Schaus, JM (Schaus, John M.); Phebus, LA (Phebus, Lee A.); Chesterfield, AK (Chesterfield, Amy K.); Felder, CC (Felder, Christian C.); Gladding, RL (Gladding, Robert L.); Hong, J. (**Hong, Jinsoo**); Halldin, C (Halldin, Christer); Pike, VW (Pike, Victor W.); Innis, RB (Innis, Robert B.) The PET radioligand [C-11]MePPEP binds reversibly and with high specific signal to cannabinoid CB1 receptors in nonhuman primate brain  
 NEUROPSYCHOPHARMACOLOGY Volume: 33 Issue: 2 Pages: 259-269  
 DOI: 10.1038/sj.npp.1301402 Published: JAN 2008 Times Cited: 30 (from Web of Science)
- 47) Yasuno, F.; Brown, A. K. ; Zoghbi, S. S.; Krushinski, J. H. ; Chernet, E. ; Tauscher, J.; Schaus, J. M.; Phebus, L. A.; Chesterfield, A. K. ; Felder, C. C.; Gladding, R. L.; Hong, J. (**Hong, Jinsoo**); Halldin, C.; Pike, V. W.; Innis, R. B. The PET radioligand [C-11]MePPEP binds reversibly and with high specific signal to cannabinoid CB1 receptors in nonhuman primate brain, *Neuropsychopharmacology*, 2008, 33(2) 259-269.
- 48) Zanotti-Fregonara, P (Zanotti-Fregonara, Paolo); Zoghbi, SS (Zoghbi, Sami S.); Liow, JS (Liow, Jeh-San); Hong, J. (**Hong, Jinsoo**); Boellaard, R (Boellaard, Ronald); Pike, VW (Pike, Victor W.); Innis, RB (Innis, Robert B.); Fujita, M (Fujita, Masahiro) Quantification and test-retest study of C-11-(R)-rolipram, a PET tracer of the cAMP cascade, using an arterial input function and an image-derived input function NEUROIMAGE Volume: 52 Supplement: 1 Pages: S161-S161 DOI: 10.1016/j.neuroimage.2010.04.131 Published: AUG 2010
- 49) Zhang, X (Zhang, X.); Yasuno, F (Yasuno, F.); Zoghbi, S (Zoghbi, S.); Liow, J (Liow, J.); Hong, J. (**Hong, Jinsoo**); McCarron, J (McCarron, J.); Pike, V (Pike, V.); Innis, R (Innis, R.) Quantification of serotonin 5-HT1A receptors in humans with [11C](R)-(-)-RWAY: Radiometabolite(s) likely confound brain measurements. CLINICAL PHARMACOLOGY & THERAPEUTICS Volume: 81 Supplement: 1 Pages: S119-S119 Published: MAR 2007
- 50) Zoghbi, SS (Zoghbi, S. S.); Shetty, UH (Shetty, U. H.); Liow, JS (Liow, J. -S.); Ichise, M (Ichise, M.); Hong, J (**Hong, Jinsoo**); Musachio, JL (Musachio, J. L.); Seneca, N (Seneca, N.); Halldin, C (Halldin, C.); Seidel, JL (Seidel, J. L.); Pike, VW (Pike, V. W.); Innis, RB (Innis, R. B.) The dopamine transporter probe [c-11]pe2i shows active and inactive radioactive metabolites in rat brain. JOURNAL OF LABELLED COMPOUNDS & RADIOPHARMACEUTICALS Volume: 48 Supplement: 1 Pages: S98-S98 Published: JUN 2005
- 51) Zoghbi, SS (Zoghbi, Sami S.); Liow, JS (Liow, Jeh-San); Yasuno, F (Yasuno, Furnihiko); Hong, J (**Hong, Jinsoo**); Tuan, E (Tuan, Edward); Lazarova, N (Lazarova, Neva)<sup>1</sup>; Gladding, RL (Gladding, Robert L.)<sup>1</sup>; Pike, VW (Pike, Victor W.)<sup>1</sup>; Innis, RB (Innis, Robert B.) C-11-loperamide and its N-desmethyl radiometabolite are avid substrates for brain permeability-glycoprotein efflux. JOURNAL OF NUCLEAR MEDICINE Volume: 49 Issue: 4 Pages: 649-656  
 DOI: 10.2967/jnumed.107.047308 Published: APR 2008.